



The
University
Of
Sheffield.

Investigating the role of CHMP7 and ESCRT-III in nuclear envelope integrity and genomic stability

Jessica Willan

**A thesis submitted in partial fulfilment of the requirements
for the degree of Doctor of Philosophy**

**The University of Sheffield
Faculty of Science
Department of Chemistry**

April 2017

Abstract

The ESCRT-III (endosomal sorting complex required for transport-3) machinery plays a role in a wide variety of cellular processes involving membrane remodelling and scission, including cytokinesis, viral budding, multivesicular body biogenesis and plasma membrane repair. Mammalian ESCRT-III is assembled from subunits of the CHMP (charged multivesicular body/chromatin modifying protein) family, and forms a helical, membrane-associated polymer which constricts and cuts the membrane neck. The ESCRT-III-associated ATPase VPS4 catalyses systematic disassembly of the CHMP polymer.

CHMP7 is a poorly characterised member of the CHMP family, which shares the common CHMP domain, but is twice the length of other family members, containing an N-terminal domain of uncharacterised function. We have previously shown that VPS4 depletion prevents ESCRT-III disassembly, revealing a subset of CHMP proteins at the interphase nucleus, where they form large nuclear foci whose formation is dependent on the presence of CHMP7.

This work shows that ESCRT-III foci marks holes in the nuclear lamina and strongly associate with the inner nuclear membrane protein LAP2, as well as inducing a local DNA damage response and recruitment of PML bodies. Moreover, endogenous CHMP7 localises to the nuclear rim in interphase as revealed by detergent pre-extraction of soluble proteins.

Accordingly, this work shows that CHMP7 depletion results in a loss of nuclear envelope integrity, organisation, and compartmentalisation, leading to increased DNA damage and loss of genomic integrity. This wide variety of aberrant cellular phenotypes results in significantly decreased cell viability and reduced proliferation in HeLa, HeLa M and U2OS cell lines.

CHMP7-dependent nuclear ESCRT-III recruitment was also observed at mitotic chromatin. CHMP7, CHMP4B and CHMP1B were found to localise transiently to the nuclear rim in a specific period of mitosis, corresponding to nuclear envelope reformation in late anaphase and telophase. Moreover, a HA-tagged, truncated form of CHMP7, consisting of the uncharacterised N-terminal domain only, was able to localise to chromatin in telophase, suggesting a role for this domain in nuclear targeting.

Interestingly, the CHMP7-nucleated ESCRT-III complex was found to localise specifically to aberrant nuclear structures caused by DNA damage or mitotic defects, which also demonstrate a lack of lamin proteins and enrichment of LAP2. These structures include micronuclei which have lost nucleocytoplasmic compartmentalisation and ultrafine internuclear bridges, suggesting a potential function of CHMP7 and ESCRT-III at the nuclear envelope of such markers of genomic instability.

In summary, this thesis outlines a role for CHMP7 as adaptor molecule between nuclear membranes and ESCRT-III, targeting ESCRT-III to carry out membrane remodelling functions at the nuclear envelope at nuclei and aberrant nuclear structures in order to preserve nuclear integrity and genomic stability.

Acknowledgements

Firstly, I would like to thank my supervisor, Dr Barbara Ciani, for giving me the opportunity to undertake this project. I am grateful for all of her enthusiasm, patience, and support throughout these past four years.

I would like to thank Dr Helen Bryant, for being a second supervisor to me, letting me be part of her group, and allowing me to work in her lab all hours of the day and night.

Thanks go to Jim Reid for his help and guidance as my independent advisor, and to Professor Jane Grasby for her patience, and helping and encouraging me through presentations and out the other side. I would like to thank Professor Phil Woodman for his feedback on results and for welcoming me into his lab. I'm also grateful to Dr Alexa Cleasby for getting me started on the project, Dr Flavia Stefani for immunofluorescence and Dr Neftali Flores-Rodriguez for live cell imaging.

Thanks to everyone I have worked alongside in the Bryant, Collis and Ciani labs, for both scientific advice and cakes. Special mentions go to Charlotte, Natasha, Caroline, Clair, Katie, Ryan, Abhijit, Karl, Tom, Spencer, Chris Staples, Dan, and Liam. Dr Chris Marklew has been a star during writing up, always ready with a word of encouragement and sage advice. Luke McKenzie, for keeping me company in both the Medical School and Chemistry, long chats and a cool and calm outlook on everything – you'll go far. And also Mehul Makwana, for being equally a help and a hindrance, and an inexhaustible source of food.

Thank you to Koutetsu students, present and past, for punches exchanged, and long nights in the pub, especially Chris Gowlett, Matt Bailey, Tom Brooks, Hannah Lamb and Matt Mullin.

I'd like to thank my Mum and my Gran for their love and support when I needed it the most, and my Dad, although you never got to see me reach this point, I know you'd be proud.

Last but not least, thanks to Chris, for everything.

Abbreviations

A-498	human kidney carcinoma cell line
AAA	ATPases associated with diverse cellular activities
ALG-2	apoptosis linked gene 2
ALIX	ALG-2-interacting protein X
ALT	alternative lengthening of telomeres
AMSH	associated molecule with SH3 domain of STAM
APS	ammonium persulphate
ARF	ADP-ribosylation factor
ATM	ataxia-telangiectasia mutated
ATP	adenosine triphosphate
ATR	ATM- and Rad3-related
BABAM1	BRISC and BRCA1 A complex member 1
BAF	barrier-to-autointegration factor
BLM	Bloom's syndrome protein
BMI1	B lymphoma Mo-MLV insertion region 1
bp	base pairs
BRCA1	breast cancer 1
BRISC	Brcc36-containing isopeptidase complex
Bro1	BCK1-like resistance to osmotic shock
BSA	bovine serum albumin
CC	coiled-coil
CDK	cyclin-dependent kinase
cDNA	complementary DNA
CDNK2A	cyclin-dependent kinase inhibitor 2A
Cdv	cell division
CENP-A	centromere protein A
CEP55	centrosomal protein 55kDa
ChIP	chromatin immunoprecipitation
Chk1	checkpoint kinase 1
CHMP	charged multivesicular-body protein or chromatin-modifying protein
CPC	chromosomal passenger complex
CTD	C-terminal domain
CyPNs	cytoplasmic assemblies of PML and nucleoporins
DAPI	4',6-diamidino-2-phenylindole
DDR	DNA damage response
Did2	DOA4-independent degradation protein 2
DMEM	Dulbecco's modified eagle medium
DMSO	dimethyl sulphoxide
DNA	deoxyribonucleic acid
DNA-PK	DNA-dependent protein kinase
DSB	double strand break
DUB	deubiquitinase

<i>E. coli</i>	<i>Escherichia coli</i>
EABR	ESCRT and ALIX-binding region
EAP	ELL-associated protein
ECL	enhanced chemiluminescence
ECV	endosomal carrier vesicle
EDTA	ethylenediaminetetraacetic acid
EGF	epidermal growth factor
EGFR	epidermal growth factor receptor
EGTA	ethyleneglycoltetraacetic acid
ELC	endosomal-like compartment
ELYC	domain containing ELYC tetrapeptide sequence
EPR	electron paramagnetic resonance
ER	endoplasmic reticulum
ESCRT	endosomal sorting complex required for transport
FACS	fluorescence-assisted cell sorting
FBS	foetal bovine serum
FCS	foetal calf serum
FYVE	Fab1, YOTB, Vac1 and EEA1
G1	growth or gap phase 1 (of the cell cycle)
G2	growth or gap phase 2 (of the cell cycle)
GFP	green fluorescent protein
GLUE	GRAM-like ubiquitin binding in EAP45
GRAM	glucosyltransferases, Rab-like GTPase activators and myotubularins
GST	glutathione S-transferase
GWAS	genome wide association study
HA	haemagglutinin
HAV	hepatitis A virus
HD-PTP	his domain-containing protein tyrosine phosphatase
HEK	human embryonic kidney cell line
HeLa	human cervix carcinoma cell line
HeLa M	human cervix carcinoma cell line – monolayer (M) subtype
HEPES	4-(2-hydroxyethyl)-1-piperazineethanesulfonic acid
HIV-1	h+C81human immunodeficiency virus type 1
HP1	heterochromatin protein 1
HRP	horseradish peroxidase
Hrs	hepatocyte growth factor-regulated tyrosine kinase substrate
HSPC	haematopoietic stem/progenitor cells
ICF	immunodeficiency, centromeric instability, and facial dysmorphism
IF	immunofluorescence
ILV	intraluminal vesicle
INCENP	inner centromere protein
INK4A	inhibitor of CDK4
INM	inner nuclear membrane
IP	immunoprecipitation

IPTG	isopropyl β -D-1-thiogalactopyranoside
IR	ionising radiation
IST1	increased sodium tolerance 1
kDa	kilodalton
LAMP	lysosome-associated membrane protein
LAP2	lamin associated protein 2
Lap2	lamin associated protein 2
LB	Luria-Bertani medium/lysogeny broth
LBR	Lamin B receptor
LC3	microtubule-associated protein 1A/1B-light chain 3
LEM	LAP2, Emerin and MAN1
LINC	linker of nucleoskeleton and cytoskeleton
LIP5	LYST-interacting protein 5
LYST	lysosomal trafficking regulator
MAN1	MAN antigen 1
MHC	major histocompatibility complex
MIM	MIT-interacting motif
MIT	microtubule-interacting and transport
MKLP1	mitotic kinesin-like protein 1
M-phase	mitotic phase (of the cell cycle)
MRE11	mitotic recombination 11
mRNA	messenger RNA
mRNP	messenger ribonucleoprotein
MTOR	mechanistic target of rapamycin
MTT	3-(4,5-dimethylthiazol-2-yl)-2,5-diphenyltetrazolium bromide
MVB	multivesicular body
NAT10	N-acetyltransferase 10
NE	nuclear envelope
NEAA	non-essential amino acids
NERDI	nuclear envelope rupture during interphase
NES	nuclear export signal
NIH-3T3	mouse embryo fibroblast cell line
NLS	nuclear localisation signal
NPC	nuclear pore complexes
NPL4	nuclear protein localization 4
NSF	N-ethylmaleimide-sensitive factor
nt	nucleotides
NTD	N-terminal domain
NTH	N-terminal helix
Nup	nucleoporin
NZF	Npl4 zinc finger
OD	optical density
ONM	outer nuclear membrane
ORC2	origin recognition complex 2

PanC1	human pancreatic ductal tumour cell line
pAuk	phosphorylated aurora kinase
PBS	phosphate-buffered saline
PBST	phosphate-buffered saline + Tween-20
PBStx	phosphate-buffered saline + Triton X-100
PcG	polycomb group
Pcl	Polycomblike
PCM	pericentriolar material
PCR	polymerase chain reaction
PDB	protein data bank
PDI	protein disulphide isomerase
PFA	paraformaldehyde
Phyre2	Protein Homology/Analogy Recognition Engine v2.0
PI	propidium iodide
PI3P	phosphatidylinositol 3-phosphate
PICH	Plk1-interacting checkpoint helicase
PIKK	phosphatidylinositol 3-kinase-related kinase
PIPES	piperazine-N,N'-bis(2-ethanesulfonic acid)
PLK	polo-like kinase
PML	promyelocytic leukaemia protein
POM	pore membrane proteins
PRC	polycomb repressive complex
PRD	proline-rich domain
PSAP	Pro-Ser/Thr-X-Pro motif
PtdIns(3)P	phosphatidylinositol 3-phosphate
RAN	RAs-related Nuclear protein
RANBP2	RAN binding protein 2
RAP80	receptor-associated protein 80
REEP	Receptor Expression Enhancing Protein
RING	really interesting new gene
RIPA	radioimmunoprecipitation assay
RNA	ribonucleic acid
RNAi	RNA interference
RNAse	ribonuclease
ROS	reactive oxygen species
RPA	replication protein A
rpm	revolutions per minute
SAC	spindle assembly checkpoint
SAXS	small-angle X-ray scattering
SDS	sodium dodecyl sulphate
SDS-PAGE	SDS-polyacrylamide gel electrophoresis
SIM	SUMO-interacting motif
SINC	storage of improperly assembled nuclear pore complexes compartment
siRNA	small interfering RNA

SMART	simple modular architecture research tool
SNARE	SNAP (soluble NSF attachment protein) receptor
Snf7	sucrose non-fermenting 7
SNP	single-nucleotide polymorphism
S-phase	synthesis phase (of the cell cycle)
ssDNA	single stranded DNA
STAM	signal transducing adaptor molecule
SUMO	small ubiquitin-like modifier
TAE	tris-acetate-EDTA
TBS	tris-buffered saline
TEMED	tetramethylethylenediamine
TREX1	Three prime repair exonuclease 1
TSG101	tumour susceptibility gene 101
U2OS	human bone osteosarcoma cell line
UBC9	ubiquitin-conjugating enzyme 9
UBD	ubiquitin binding domain
UBPY	ubiquitin-specific protease Y
UEV	ubiquitin E2 variant
UFD1	Ubiquitin fusion degradation protein 1
UIM	ubiquitin interacting motif
ULK	Unc51-like autophagy activating kinase
USP8	ubiquitin specific peptidase 8
UV	ultraviolet radiation
VHS	Vps27/Hrs/STAM
VPS	vacuolar protein sorting
VSE	VPS4 stimulatory element
VSL	Vta1/SBP1/LIP5
Vta1	VPS20-associated 1
WB	Western blot
WH	winged-helix
YFP	yellow fluorescent protein
γH2AX	phosphorylated histone H2AX

Table of Contents

	Page
Abstract	i
Acknowledgements	ii
Abbreviations	iii
Table of Contents	viii
List of Figures	ix
Chapter 1 Introduction	1
1.1 An overview of the ESCRT-III machinery	4
1.2 Roles for the ESCRT-III complex	18
1.3 ESCRTs in cytokinesis	23
1.4 Nuclear roles for CHMP proteins	31
1.5 Project Aims	38
Chapter 2 Materials and Methods	39
2.1 Human tissue culture	41
2.2 Bacterial cell culture and DNA manipulation	54
Chapter 3 CHMP7 depletion impairs nuclear envelope organisation and integrity	57
3.1 Introduction	60
3.2 Results	65
3.3 Discussion	97
Chapter 4 The role of CHMP7 and the ESCRT-III complex at the nuclear envelope	109
4.1 Introduction	113
4.2 Results	120
4.3 Discussion	167
Chapter 5 CHMP7 and ESCRT-III associate with the nuclear envelope of structures characteristic of genomic instability	177
5.1 Introduction	181
5.2 Results	189
5.3 Discussion	228
Chapter 6 Discussion	240
6.1 Key findings	242
6.2 Recent research into CHMP7 and ESCRT-III	245
6.3 Future work	250
Appendices	252
References	258

List of Figures

Figure	Title	Page
Chapter 1		
1.1	Multiple cellular roles for the ESCRT-III complex	4
1.2	The role of ESCRTs in multivesicular body biogenesis	6
1.3	Structure of the CHMP family of proteins	8
1.4	The mechanism of CHMP domain autoinhibition	10
1.5	ESCRT-III complex nucleation and polymerisation	13
1.6	Recruitment of VPS4 to the ESCRT-III complex for disassembly	15
1.7	The chromosomal passenger complex interaction with CHMP4C.	26
1.8	ESCRT-III recruitment and formation at the cytokinetic midbody	29
1.9	Structural prediction of the CHMP7 N-terminal domain	37
Chapter 3		
3.1	A diagram of the nuclear envelope and associated cellular components	61
3.2	Cell cycle progression, regulatory checkpoints, and centrosome maturation	61
3.3	Confirmation and optimisation of CHMP7 and VPS4 depletion by siRNA using Western blots	65
3.4	CHMP7 depletion results in decreased cell viability and proliferation rates in HeLa, HeLa M and U2OS cells	68
3.5	CHMP7 depletion causes a decrease in mitotic cells and some accumulation in G1	71
3.6	Depletion of CHMP7 results in an increase in apoptotic cells as observed by immunofluorescence	73
3.7	Depletion of CHMP7 results in an increase in multinucleated cells as observed by immunofluorescence	75
3.8	CHMP7 depletion causes abnormalities of nuclear morphology	77
3.9	CHMP7 depletion causes nuclear lamina defects	79
3.10	The relationship of nuclear pore complexes to nuclear envelope abnormalities in HeLa cells	82
3.11	CHMP7-depleted HeLa M cells display a dramatic loss of nuclear envelope integrity and organisation not observed in other cell lines	83
3.12	Nuclear pore complex proteins are found in cytoplasmic accumulations following CHMP7 knockdowns	87
3.13	The effect of CHMP7 knockdown on DNA damage as marked by γ H2AX foci	89
3.14	Changes in centrosome positioning and separation in interphase cells following CHMP7 knockdown	91
3.15	The percentage of cells in which PML is mislocalised into the cytoplasm in HeLa and U2OS cell lines	94
3.16	A model of the cell cycle progression of CHMP7-depleted cells	98
3.17	A model of the defects caused by depletion of CHMP7	99

3.18	A model to show development of nuclear defects in CHMP7-depleted cells	101
Chapter 4		
4.1	Formation of the nuclear envelope from ER membrane during mitosis	114
4.2	ER membrane recruitment and nuclear envelope sealing in telophase	115
4.3	Subcellular localisation of CHMP7 throughout the cell cycle	120
4.4	VPS4 knockdown causes nuclear accumulation of CHMP7 into foci	123
4.5	CHMP7 nuclear foci in VPS4-depleted cells also contain CHMP4B and CHMP1B	125
4.6	CHMP7 and VPS4 knockdown affect PML body number, size, and shape	127
4.7	Large CHMP7 nuclear foci associate with or are encircled by PML protein	129
4.8	CHMP7 nuclear foci associate with various DNA damage and repair proteins	131
4.9	CHMP7 does not form nuclear foci upon induction of DNA damage with UVC radiation	133
4.10	Large CHMP7 foci show strong LAP2 colocalisation	135
4.11	Large CHMP7 foci correspond with gaps in the nuclear lamina	136
4.12	CHMP7 foci localise at the periphery of the nucleus	138
4.13	CHMP7 displays a novel, chromatin-associated pattern of accumulation into puncta in VPS4-depleted cells	139
4.14	Features of CHMP7 localisation in mitosis	142
4.15	CHMP4B and CHMP1B colocalise with CHMP7 at late anaphase/early telophase	143
4.16	CHMP7 occasionally shows localisation near centromeres in telophase cells	147
4.17	Optimisation of ER membrane staining	149
4.18	CHMP7 localises to telophase chromatin with ER membranes	151
4.19	CHMP7 colocalises with LAP2 at the reforming nuclear envelope	153
4.20	CHMP7 localises adjacent to Lamin B at the reforming nuclear envelope	156
4.21	CHMP7 knockdown does not affect recruitment of LAP2, Lamin B or NPCs to the nascent nuclei	159
4.22	Overexpressed full length and N-terminal CHMP7 in HeLa cells	161
4.23	Endogenous CHMP7 and CHMP4B are found on the nuclear rim following detergent pre-extraction	165
4.24	A nuclear role for the ESCRT-III complex	168
4.25	A model for nuclear envelope sealing in CHMP7 and VPS4-depleted cells	170
4.26	Perturbation of ESCRT-III activity results in DNA damage	172
Chapter 5		
5.1	Generation and fate of micronuclei	181
5.2	Generation and resolution of chromosome bridges	184
5.3	CHMP7 localises to micronuclei in various cell lines in control and VPS4-depleted cells	189
5.4	ESCRT-III localises to micronuclei in the presence of CHMP7	190

5.5	CHMP7 localises more frequently to smaller micronuclei containing chromosome fragments	192
5.6	CHMP7 preferentially localises to micronuclei lacking an intact nuclear lamina	195
5.7	CHMP7 preferentially localises to micronuclei lacking nuclear pore complexes	196
5.8	CHMP7-positive micronuclei retain LAP2 staining, but show loss of soluble nuclear protein	198
5.9	CHMP7-positive micronuclei show ER membrane invasion into chromatin	200
5.10	Impairment of ESCRT-III function increases multinucleation of HeLa cells	202
5.11	Impairment of ESCRT-III function decreases micronuclear integrity and increases loss of compartmentalisation	204
5.12	Scoring of HeLa cells for CHMP7 and γ H2AX micronuclear foci	207
5.13	CHMP7 forms filamentous structures in various cell lines in control and VPS4-depleted cells	210
5.14	ESCRT-III components localise at bridge structures when CHMP7 is present	211
5.15	CHMP7 bridges connect nuclear structures	213
5.16	CHMP7 bridges do not correspond to anaphase BLM bridges, but appear later in mitosis	216
5.17	Occurrence of CHMP7 bridges at different cell stages	218
5.18	Nuclear envelope assembly around CHMP7 internuclear bridges	221
5.19	Lamin B and mab414 are absent from CHMP7 nuclear bridges	223
5.20	The effect of ESCRT-III impairment on the prevalence of internuclear bridges	225
5.21	Model for the relationship between CHMP7/ESCRT-III and micronuclei	230
5.22	Model for the relationship between CHMP7/ESCRT-III and chromosome bridges	235

Chapter One

Introduction

Contents

	Page
1.1 An overview of the ESCRT-III machinery	4
1.1.1 The ESCRT complexes	4
1.1.2 Class E vacuolar protein sorting (VPS) proteins	5
1.1.3 The ESCRT-III complex	7
1.1.4 The CHMP family	7
1.1.5 CHMP autoinhibition	9
1.1.6 Insights into ESCRT-III polymerisation	11
1.1.7 Assembly of ESCRT-III in multivesicular body biogenesis	12
1.1.8 The role of VPS4 in ESCRT-III disassembly	14
1.1.9 VPS4 structure and function	15
1.2 Roles for the ESCRT-III complex	18
1.2.1 The ancestral function of the ESCRT-III complex	18
1.2.2 ESCRTs in viral budding	19
1.2.3 ESCRTs in autophagic degradation	20
1.2.4 A role for ESCRT-III in plasma membrane repair	22
1.3 ESCRTs in cytokinesis	23
1.3.1 Cytokinesis	23
1.3.2 Entry into mitosis	24
1.3.3 Intercellular bridge and midbody formation	24
1.3.4 The chromosomal passenger complex (CPC)	25
1.3.5 CHMP4C can delay cytokinesis to promote genome stability	25
1.3.6 Recruitment of the ESCRT-III complex and abscission	27
1.3.7 ESCRTs in centrosome duplication and spindle formation	30
1.4 Nuclear roles for CHMP proteins	31
1.4.1 CHMP1	31
1.4.2 CHMP1A overexpression and chromatin condensation	32
1.4.3 CHMP1A is a predicted tumour suppressor	33
1.4.4 CHMP4	34
1.4.5 CHMP7	35
1.4.6 Structural prediction of the CHMP7 N-terminal domain	36
1.5 Project Aims	38

List of Figures

Figure	Title	Page
1.1	Multiple cellular roles for the ESCRT-III complex	4
1.2	The role of ESCRTs in multivesicular body biogenesis	6
1.3	Structure of the CHMP family of proteins	8
1.4	The mechanism of CHMP domain autoinhibition	10
1.5	ESCRT-III complex nucleation and polymerisation	13
1.6	Recruitment of VPS4 to the ESCRT-III complex for disassembly	15
1.7	The chromosomal passenger complex interaction with CHMP4C	26
1.8	ESCRT-III recruitment and formation at the cytokinetic midbody	29
1.9	Structural prediction of the CHMP7 N-terminal domain	37

1.1 An overview of the ESCRT-III machinery

1.1.1 The ESCRT complexes

The ESCRT (endosomal sorting complex required for transport) family of four complexes (ESCRT-0, -I, -II and -III) function in the sorting of receptor proteins tagged for destruction through the endosomal (vacuolar in yeast) pathway, through the generation of multivesicular bodies (MVBs). Here we focus on the ESCRT-III complex, which has been singled out as the agent of membrane scission in viral budding, cytokinesis, and cell membrane repair alongside multivesicular body biogenesis (Figure 1.1).

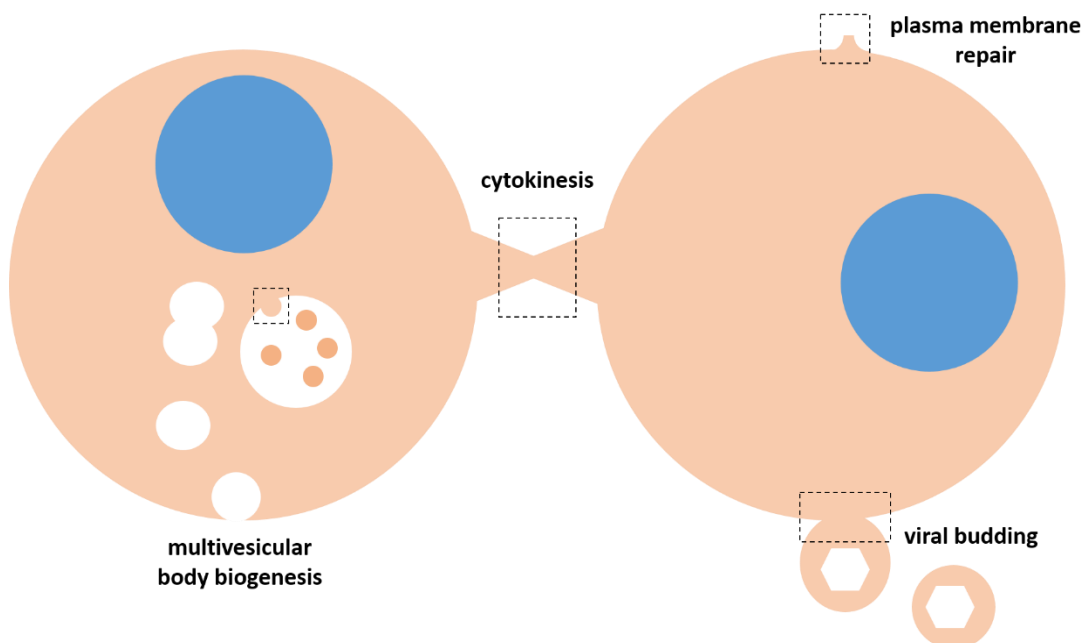


Figure 1.1 – Multiple cellular roles for the ESCRT-III complex

ESCRTs are known to perform roles in many membrane remodelling and cutting processes. All of the ESCRT complexes are involved in multivesicular body biogenesis, however ESCRT-III, along with various subsets of ESCRTs is also involved in membrane scission in viral budding, cytokinesis, and removal of damaged areas of plasma membrane. A role in autophagy is also predicted, however its exact function in this process is not known.

The ESCRT machinery consists of four complexes, ESCRT-0, -I, -II, and -III, which are broadly conserved across all eukaryotes. All four complexes work in sequence to recognise, sort and sequester ubiquitinated membrane proteins in endosomes, directing them for lysosomal degradation (Figure 1.2). All endocytosed surface receptors are collected on the membrane

of early endosomes, where those to be recycled back to the cell surface are segregated from those which are to be downregulated, marked out by ubiquitination. As part of this process, ESCRTs and their accessory proteins catalyse the budding and formation of intraluminal vesicles which incorporate and sequester ubiquitin-tagged receptors away from the outer endosomal membrane. The term multivesicular body (MVB) is used to describe either an intermediary, endosomal carrier vesicle (ECV) between early and late endosomes, or a late endosome itself, which contains many of these intraluminal vesicles destined for the lysosome.

1.1.2 Class E vacuolar protein sorting (VPS) proteins

Classification of the various vacuolar mutant phenotypes in *Saccharomyces cerevisiae* by Raymond *et al.* (1992) identified a group of *vps* (vacuolar protein sorting) proteins, which produce a large abnormal early endosome, defined as a class E compartment. These Class E *vps* genes are highly conserved throughout eukaryotes, also indicating a conserved MVB pathway (Bishop and Woodman, 2001), and components have been shown to be present in a common ancestor before the divergence of the animal and plant kingdoms (Slater and Bishop, 2006).

The majority of Class E *vps* proteins function as subunits of ESCRT-I, II and III, with a fourth (ESCRT-0) defined in both fungi and metazoans. ESCRT-I and II do not even appear to be absolutely essential for MVB biogenesis, being lost in some organisms, including the parasites *Plasmodium falciparum* and *Toxoplasma gondii*, which still form intraluminal vesicles using their ESCRT-III and VPS4 homologues (Yang *et al.*, 2004). However, ESCRT-III, and its accessory protein VPS4, are fundamental to all ESCRT-mediated cellular functions, and all sequenced eukaryotes have been found to possess ESCRT-III homologues. Humans possess an expanded subset of ESCRT-III-related components compared to yeast.

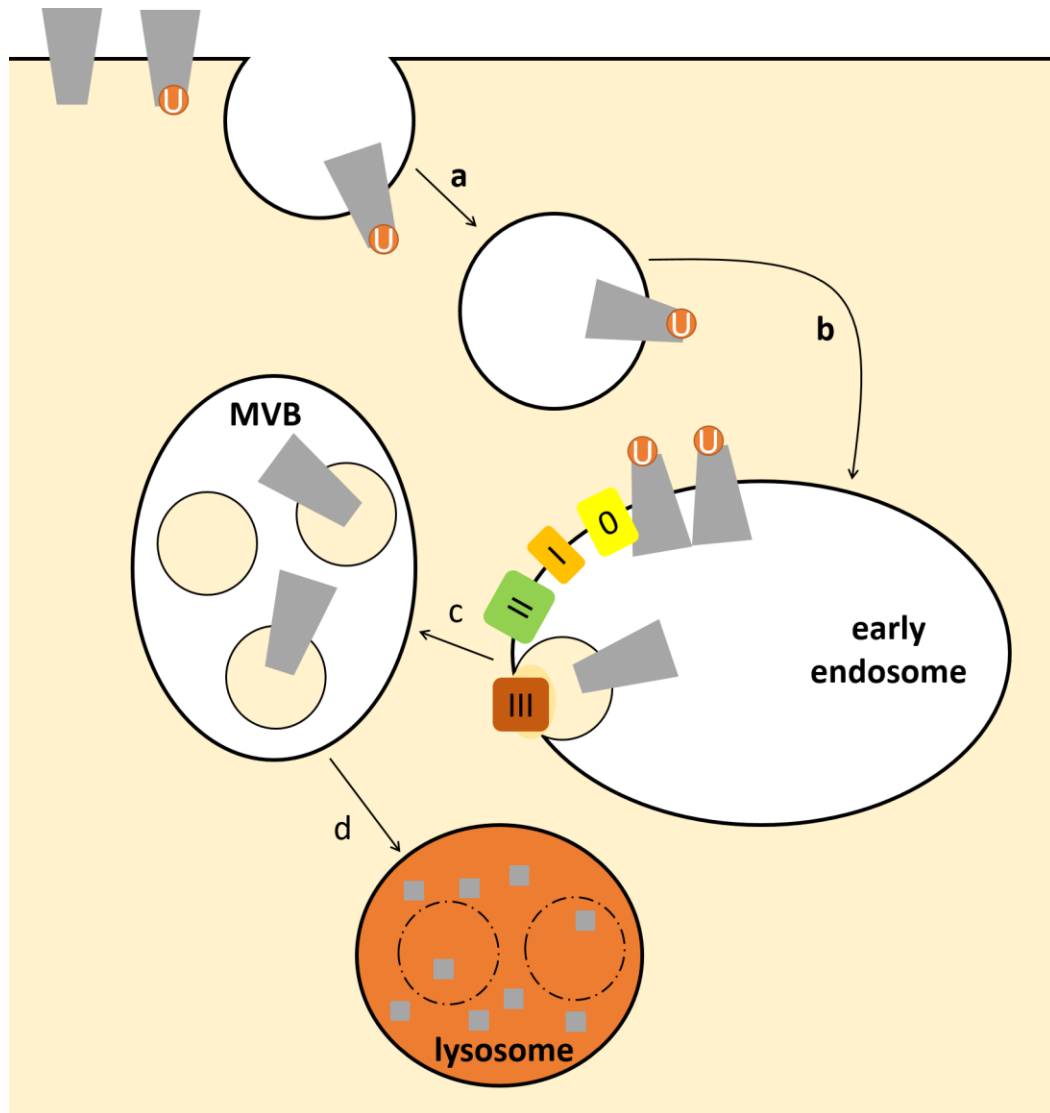


Figure 1.2 – The role of ESCRTs in multivesicular body biogenesis

a) Ubiquitin-tagged receptors destined for degradation in lysosomes are endocytosed and internalised in vesicles. **b)** Vesicles fuse to form an endosome, in which proteins are sorted for degradation or recycling. **c)** Ubiquitinated receptors are recognised, bound, and sorted by the early ESCRT machinery, and receptors accumulated on the endosomal membrane and deubiquitinated. Sequential action of ESCRTs cause invagination of the endosomal membrane, ending with abscission carried out by the ESCRT-III complex, creating discrete intraendosomal vesicles. The resulting late endosomal structures are known as multivesicular bodies (MVBs). **d)** MVBs fuse with lysosomes and all contents of the MVB are degraded.

1.1.3 The ESCRT-III complex

The ESCRT-III complex coordinates and carries out the final and most important step of the ESCRT pathway, the deformation, constriction and scission of the membrane, resulting in discrete intraluminal vesicles, daughter cells or virions, depending on its site of recruitment and action (Wollert *et al.*, 2009a; Figure 1.1). The large oligomeric membrane-associated ESCRT-III complex is built from highly-charged, normally soluble, autoinhibited subunits, in humans known as the CHMP family. Essential for ESCRT-III function is the accessory AAA-ATPase enzyme VPS4, which catalyses the systematic disassembly of the ESCRT-III complex, thought to be an ingredient of the driving force of membrane deformation (Adell *et al.*, 2014), as well as performing a recycling function of returning the CHMP subunits to the cytosolic pool, ready for further rounds of assembly and action.

1.1.4 The CHMP family

The CHMP family was simultaneously named after two predicted functions of the newly discovered protein, CHMP1 (now known as CHMP1A) as published in two related papers from the Hollenberg group (Howard *et al.*, 2001; Stauffer *et al.*, 2001). Both 'chromatin-modifying protein' and 'charged multivesicular-body protein' were used, with the latter becoming more common in the literature due to the greater prevalence of studies investigating the role played by the CHMPs in multivesicular body biogenesis. Eleven CHMP proteins are found in humans, falling into 7 types, CHMP1-7. Of these, CHMP1-6 each correspond to a member of the well-studied yeast ESCRT-III complex. Humans possess multiple isoforms of CHMP1 and CHMP2, with A and B isoforms; CHMP4, which has A, B, and C isoforms, and VPS4, which has A and B isoforms.

The defining feature of the CHMP family is a shared basic structure (Figure 1.3a) which has been determined by X-ray crystallography for the CHMP3 subunit (Muzioł *et al.*, 2006), and extrapolated to the rest of the CHMP family. The CHMP domain consists of a core four-helix bundle, with helices 1 and 2 forming a central coiled coil of 70Å length, along with two

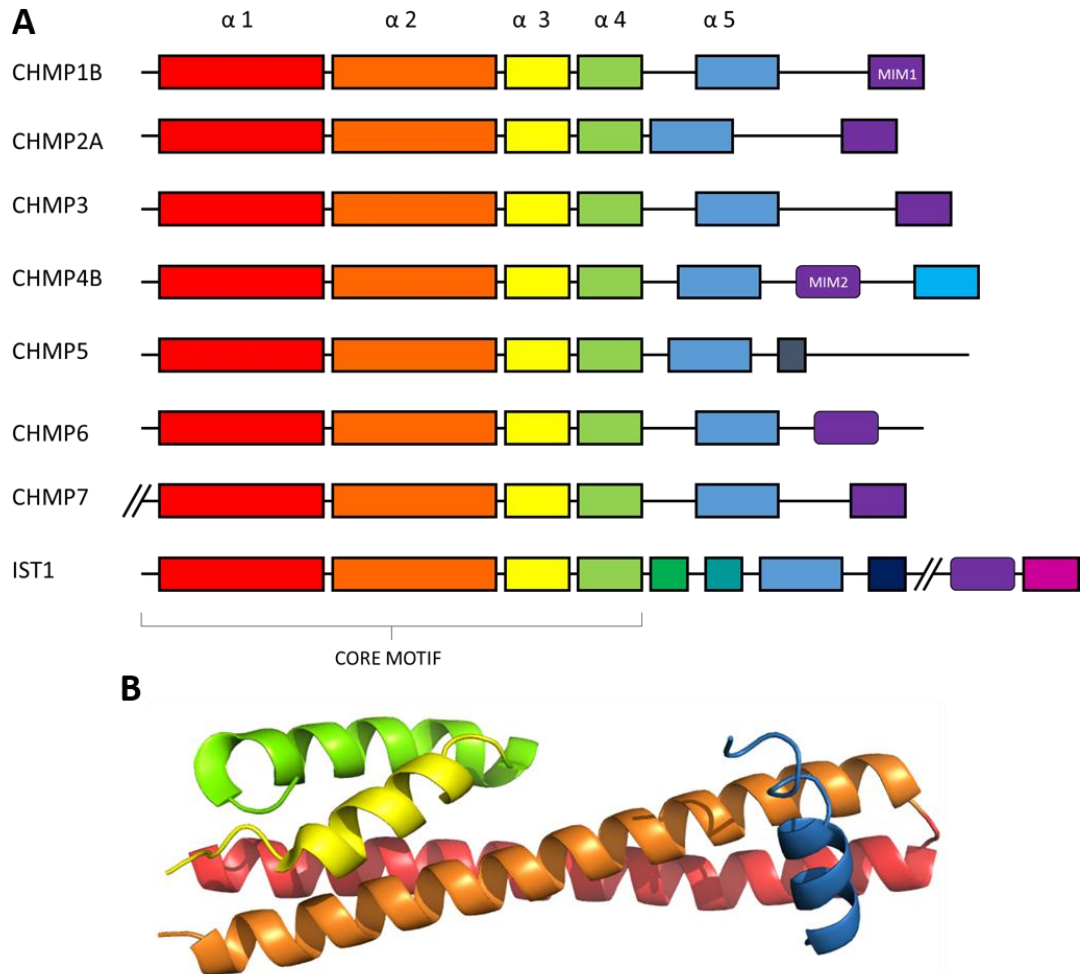


Figure 1.3 – Structure of the CHMP family of proteins

a) CHMPs share a common central coiled-coil motif, consisting of 5 α -helices. In all CHMPs except CHMP7, this motif forms the N-terminal region of the protein, with the C-terminal half varying and providing a diversity of binding partners and functions. Many of these C-terminal interactions are mediated by MIM domains. IST1 shares a number of similarities with the CHMPs, however is not considered a member of the CHMP family. **b)** Structure of the core motif of the CHMP family, based on a crystal structure of Homo sapiens CHMP3 α -helices 1-5 in an autoinhibited state. Helices 1 and 2 form a central coiled coil, which is inhibited from making interactions by the presence of helix 5, which is separated from the core by a flexible linker which allows it to move to reveal the binding site. Helices 3 and 4 form a second, smaller coiled coil, forming a region with a four-helix bundle at one end of the protein. (Based on PDB coordinates 3FRT, Bajorek *et al.*, 2009).

shorter helices, 3 and 4, and a fifth helix distanced from the core by a 20-amino acid flexible linker region (Figure 1.3b). In a number of CHMPs this is followed by a sixth helix containing a C-terminal MIM (microtubule interacting and trafficking (MIT)-interacting motif), which is disordered in the crystal structure. CHMP1-6 are small, between 190-240 amino acids, and are characterised by an uneven charge across the structure – N-terminally basic and C-terminally acidic.

The most recently discovered member of the family, CHMP7, differs from CHMP1-6 by being approximately twice the length, at 450 amino acids. CHMP7 retains the CHMP motif as its N-terminal half, while the structure and function of its C-terminal region remain inconclusively determined (Horii *et al.*, 2006). Interestingly, the 363 residue protein IST1 (increased sodium tolerance 1), known to be an accessory protein to the ESCRT-III complex, has also been shown to share the core four-helix bundle characteristic of the CHMPs (Bajorek *et al.*, 2010). Therefore, IST1 could be considered as a member of the CHMP family, however it is commonly referred to in the literature as a ‘regulator’ of ESCRT-III, as opposed to a family member.

The helical hairpin created by helices 1 and 2 is the region thought to be key to oligomerisation (CHMP-CHMP interactions) and membrane binding. This is supported in a number of ways, including the ability of a truncated form of CHMP4A (residues 1-116) which comprises helices 1 and 2 as a constitutively exposed coiled-coil, to associate with membranes in a polymeric structure (Lini *et al.*, 2005) and cause bud-like deformation of membranes (Hanson *et al.*, 2008).

1.1.5 CHMP autoinhibition

Structural determination of CHMP3 also elucidates the mechanism by which the monomers exist in inactive soluble and active binding states (Figure 1.4; Lata *et al.*, 2008). The bipartite charged nature of the CHMP proteins allows the mainly acidic fifth helix to interact with the

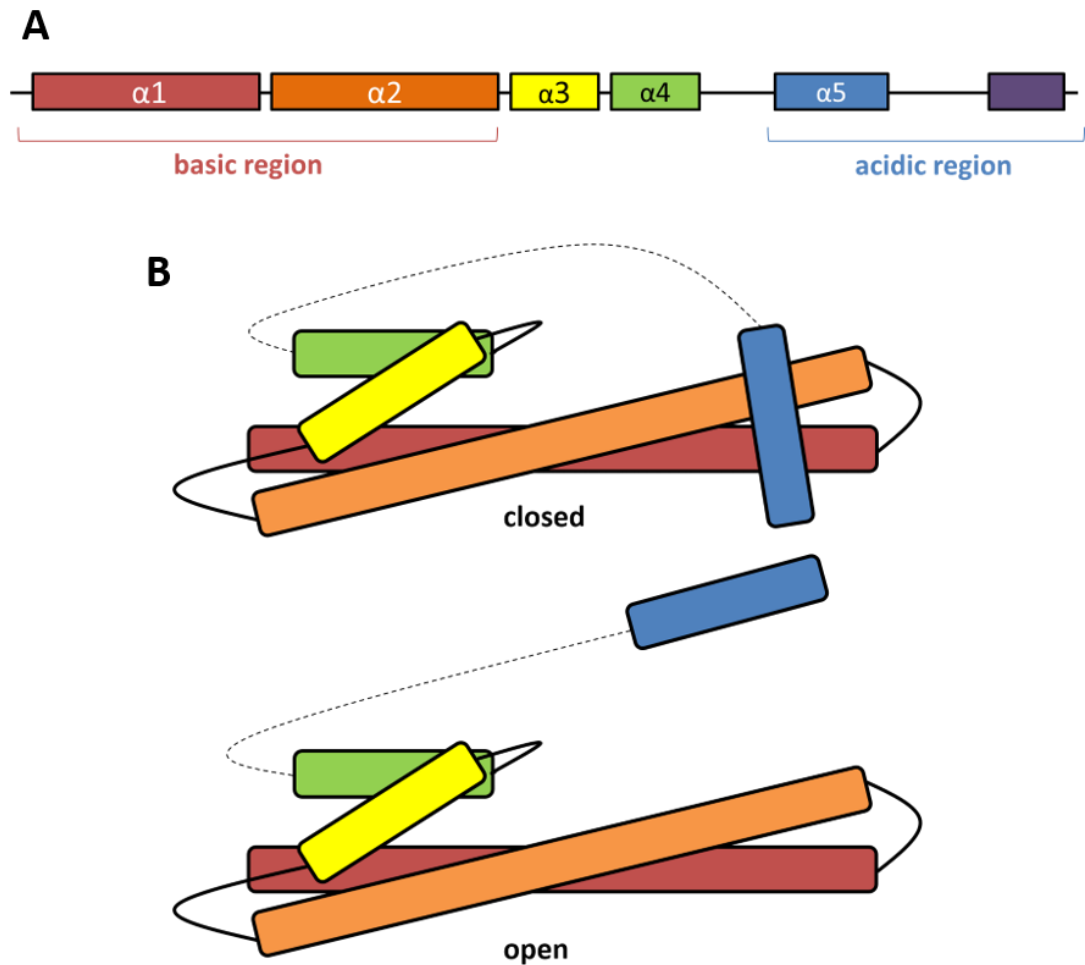


Figure 1.4 – The mechanism of CHMP domain autoinhibition

a) The general structure of CHMP proteins. The CHMP domain has a biased distribution of charged residues, basic towards the N-terminus, across the two core α -helices, and acidic towards the C-terminus, particularly in the fifth α -helix. **b)** Soluble monomeric CHMPs in the cytoplasm are autoinhibited, in a closed conformation which is unable to interact with other proteins through the core coiled-coil consisting of α -helices 1 and 2. Autoinhibition is mediated by the fifth α -helix, which is connected to the core bundle by a flexible linker region and interacts across both helices 1 and 2, blocking them from forming CHMP-CHMP interactions. Upon activation, a conformational change results in the displacement of helix 5 from its interactions with helices 1 and 2, revealing the open conformation through which CHMP-CHMP binding and polymerisation can occur.

loop region of the basic coiled coil formed from helix 1 and 2, shielding it from forming other interactions (Shim *et al.*, 2007). The mechanism by which the CHMPs are conformationally switched into an oligomerising state upon recruitment to the target membrane has not been conclusively determined, however a number of mechanisms have been proposed.

Zamborlini *et al.* (2006) propose that autoinhibition of CHMP3 is alleviated by binding of the deubiquitinase AMSH to its C-terminus, disturbing the autoinhibitory interaction within the protein. Though this does not provide a general theory for CHMP interaction, it is possible that accessory proteins binding to the C-termini of CHMPs could cause disruptions leading to exposure of the CHMP-CHMP interaction module (Shim *et al.*, 2007). Yorikawa *et al.* (2005) suggest that Vps20/CHMP6 interaction with either the lipid membrane or the ESCRT-II component Vps25/EAP20 upon its recruitment causes exposure of its N-terminal coiled coil. It is suggested that this initial uninhibited subunit could nucleate CHMP polymer, with displacement of autoinhibition caused by the CHMP-CHMP interactions (Fyfe *et al.*, 2011).

1.1.6 Insights into ESCRT-III polymerisation

CHMP4 filaments were first demonstrated to form rings by Hanson *et al.* (2008) who overexpressed CHMP4A and CHMP4B and observed using electron microscopy the structures which formed as a result. The subunits accumulated on endosomal and plasma membranes, forming curved and spiralling oligomeric filaments which deform the membranes to which they associated. A catalytically-deficient (E235Q) mutant of VPS4B was also found to associate with these membrane-bound filaments, and caused the formation of significant buds or longer tubules of between 100-120nm in diameter.

In vitro experiments using purified ESCRT-III components demonstrate that Snf7 (CHMP4) and Vps24 (CHMP3) are able to automatically homopolymerise (Ghazi-Tabatabai *et al.*, 2008). Snf7 was observed forming filaments, lattice-like sheets, and ring structures, with variability of order and interaction between subunits. In comparison, Vps24 forms regular

double-stranded helical filaments, with three contact points of subunit-subunit interaction: between $\alpha 3/\alpha 4$ loop and $\alpha 4$, $\alpha 1/\alpha 2$ loop and $\alpha 2$ and $\alpha 1/\alpha 2$ hairpin contacts. Despite the importance of the central coiled-coil element of ESCRT-III subunits, Shim *et al.* (2007) demonstrate that the loss of CHMP4 helix 4-6 decreases oligomerisation efficiency when compared to a CHMP4 helix 1-4 construct.

In vitro mixtures of CHMP2A and CHMP3, truncated at the C-terminus to remove autoinhibition, form helical tubes primarily of 40-50nm diameter with a 1:1 stoichiometry (Lata *et al.*, 2008). Incubation of VPS4B with tubules formed from truncated CHMP2A and full length CHMP3 catalysed region on the outer face, and inner interaction with VPS4 could show the arrangement whereby defined helical CHMP structures can form inside a membrane neck, with subsequent VPS4 disassembly. Changes in lipid composition of large unimellar vesicles in the study resulted in morphological changes on the CHMP2A-CHMP3 subcomplex, including induction of tubes which narrow to a closed, domed end – demonstrating a potential effect of membrane lipids on construction of the CHMP complex.

Bajorek *et al.* (2009), also demonstrated the formation of similar homo-oligomeric helical tubular structures upon enrichment of pure CHMP1B, of approximately 230nm in diameter. A construct of residues 1-189 of IST1, which corresponds to its core CHMP-like domain also spontaneously self-assembled into very large (approximately 700nm in diameter) tubular formations. This shows the many ESCRT-III components naturally tend towards this arrangement, and CHMP polymerisation occurs spontaneously (shown both *in vitro* and *in vivo*) when sufficient concentrations of subunit are present.

1.1.7 Assembly of ESCRT-III in multivesicular body biogenesis

Assembly of the ESCRT-III complex has been thoroughly studied, and a basic model of assembly in multivesicular body biogenesis is shown in Figure 1.5). Both yeast Vps20 and its homologue CHMP6 have been shown to undergo a myristoylation event of an N-terminal

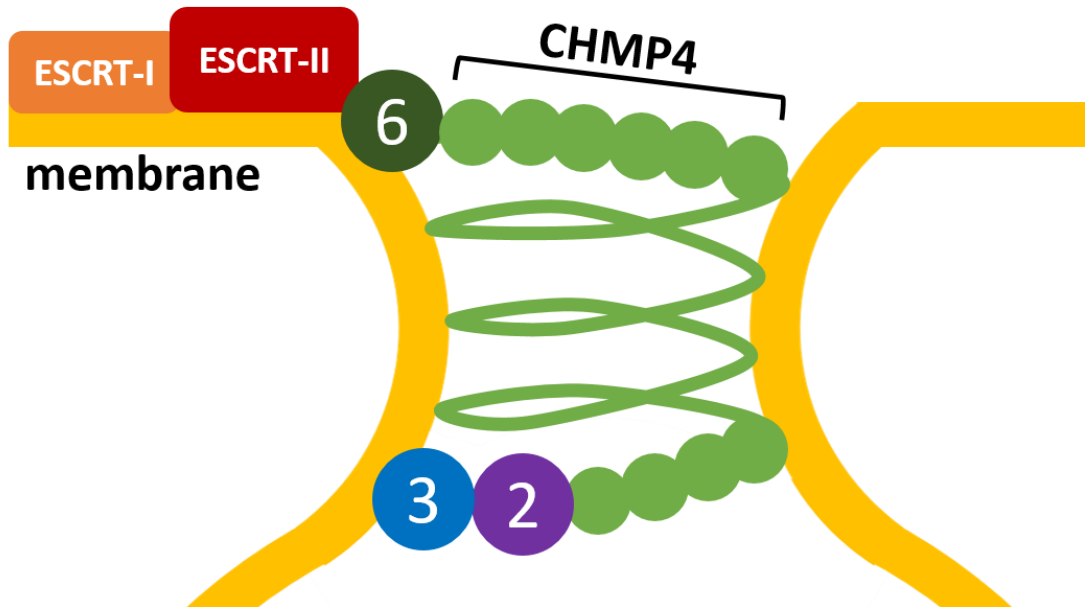


Figure 1.5 – ESCRT-III complex nucleation and polymerisation

ESCRT-III formation is nucleated by the EAP20 subunits of ESCRT-III, which interacts with CHMP6. From this point, a polymer of CHMP4 subunits associates in a helical pattern on the membrane, causing deformation and confining membrane-bound cargo into a bud. The cargo is subsequently deubiquitinated by deubiquitinase enzymes recruited by the ESCRT-III complex. The polymer is capped by a CHMP2/3 subcomplex, which contains high affinity MIMs for the recruitment of VPS4.

glycine residue (Babst *et al.*, 2002b; Yorikawa *et al.*, 2005). This modification and the positively-charged region around it seem to be a likely candidate for targeting of Vps20/CHMP6 to endosomes, through an interaction which has been demonstrated with ESCRT-II component Vps25/EAP20 (Saksena *et al.*, 2009). Exactly how autoinhibition is alleviated is unclear; however, association with either the membrane or ESCRT-II components may allow this to occur.

The newly exposed helix 2 coiled-coil face of Vps20/CHMP6 then provides a nucleation site for ESCRT-III filament assembly. While the stoichiometry of the ESCRT-III complex is difficult to determine, by far the most abundant element of these filaments is Snf7/CHMP4. Teis *et al.* (2008) speculate an ESCRT-III complex (filament), at a molecular weight of 450kDa, contains between 10-15 Snf7 components, nucleated from a single Vps20 molecule. Upon overexpression of Snf7/CHMP4, or abrogation of disassembly by VPS4, longer filaments

form, resulting in the formation of larger vesicles (Dudek *et al.*, 2010). Snf7/CHMP4 oligomerisation is terminated by the addition of a Vps24-Vps2 (CHMP3-CHMP2A) heterodimer, which exists as a subcomplex prior to recruitment (Babst *et al.*, 2002a). This subcomplex contains the high-affinity MIM domains which facilitate subsequent recruitment of Vps4 (Saksena *et al.*, 2009).

The role of Did2 (CHMP1) is that of an accessory protein, without which intraluminal vesicles can still form, but ESCRT-III remains associated to endosomal membranes, and cargo is improperly sorted into the appropriate vesicles (Chen *et al.*, 2007). Did2 is recruited by the Vps24-Vps2 subcomplex, as demonstrated by Nickerson *et al.* (2006); upon depletion of both Vps24 and Vps2, Did2 remains cytosolic. The N-terminal core region of Did2 associates with Vps24, while the C-terminal, MIM containing region binds Vps4, recruiting it to the ESCRT-III complex. Lottridge *et al.* (2006) showed that the interaction between Vta1 (LIP5) and Snf7 (CHMP4) requires the presence of Did2 (CHMP1). VPS4 and AMSH (a deubiquitinating enzyme discussed below) compete for binding to the MIT domains of CHMP1A and CHMP1B, suggesting that they play role in the regulation of cargo deubiquitination (Agromayor and Martin-Serrano, 2006).

1.1.8 The role of VPS4 in ESCRT-III disassembly

VPS4 is a member of the AAA (ATPases associated with diverse cellular activity) family of proteins which share a common ATPase domain and mechanism, by which they transduce energy from hydrolysis of ATP to a conformational change in the target protein (White and Lauring, 2007). AAA enzymes have been found in all organisms to carry out a vast range of processes, including disruption of DNA-protein and protein-protein interactions, unfolding protein substrates and powering cargo transport along microtubules. Their structure typically consists of C-terminal ATPase cassettes, type I and type II AAA ATPases respectively

containing one and two of these cassettes, and a specific N-terminal substrate recognition and binding domain.

VPS4 is fundamental to the activity of ESCRT-III, catalysing the disassembly of the complex coupled to membrane deformation and scission events, and recycling the CHMP subunits into the cytoplasm (Babst *et al.*, 1998; Scott *et al.*, 2005). The machinery of ESCRT-III and VPS4 is evolutionarily conserved in archaea alongside eukaryotes, as detailed in section 1.2.1.

1.1.9 VPS4 structure and function

In higher eukaryotes, VPS4 exists as two isoforms, VPS4A and VPS4B (Scheuring *et al.*, 2001), 2001), which share 80% sequence identity with each other and 59% and 60% respectively with yeast Vps4. The core ATPase cassette is connected via a 45-residue flexible linker to an N-terminal microtubule interacting and trafficking (MIT) domain (Figure 1.6). The MIT domain forms a three-helix bundle structure, which is required for recognition and interaction of ESCRT-III substrates, through their MIT-interacting motifs (MIM1 and MIM2).

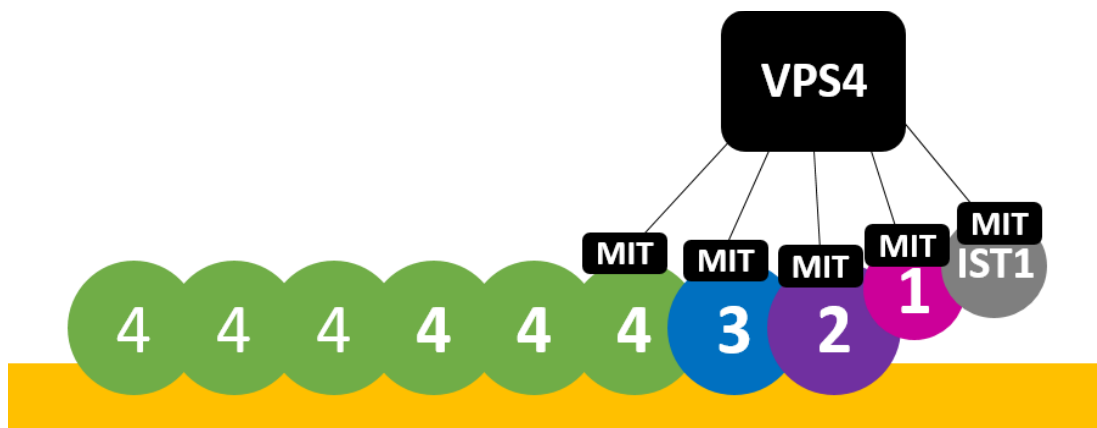


Figure 1.6 – Recruitment of VPS4 to the ESCRT-III complex for disassembly

VPS4 complexes consist of a ringed structure, with each monomer providing a MIT domain connected to the core complex via a flexible linker. IST1 and CHMP1 form a subcomplex, and work together to regulate and recruit VPS4. Both have C-terminal MIM domains which interact with MIT domains of VPS4. Through these interactions, VPS4 causes disassembly of the ESCRT-III filaments, removing CHMP components from the complex and releasing them back into the cytoplasm as soluble monomers.

The VPS4 ATPase cassette comprises a large and small domain, shared by all AAA proteins, and particularly resembles those of spastin (Roll-Mecak and Vale, 2008) and p97 (Zhang *et al.*, 2000). These domains provide the architecture for ATP binding and hydrolysis. The beta domain is unique to eukaryotic VPS4, inserted next to a proline residue, allowing for its projection away from the rest of the cassette. This three-stranded beta sheet binds the accessory protein known as LIP5, or Vta1 in yeast (Azmi *et al.*, 2006). The C-terminal helix is also particular to eukaryotic VPS4, being important in the assembly of the active VPS4 (Vajjhala *et al.*, 2008).

The mechanism by which VPS4 carries out disassembly of the ESCRT-III complex has not been unequivocally determined. This is due, in part, to the difficulty in ascertaining the nature of the quaternary structure of the complete VPS4 ATPase. Type I AAA ATPases, such as spastin, typically consist of a hexameric ring of subunits forming a hydrophobic pore. However, the prevailing prediction in the literature is that of a double ringed structure, consisting of either ten (Babst *et al.*, 1998), twelve (Yu *et al.*, 2008; Landsberg *et al.*, 2009), or fourteen (Hartmann *et al.*, 2008) subunits. The latter three, being independent EM models, conclude a double-ring conformation, however differ significantly in the structural detail. VPS4 purifies as a monomer or dimer in its wild type form, and higher order structural analysis necessitates the use of an enzymatically deficient mutant, most commonly Vps4-E233Q. It has generally been assumed that such a mutation would not affect the assembly of the quaternary structure, however this has recently been challenged by Monroe *et al.* (2014), who demonstrate that wild-type VPS4 universally (in eukaryotes and archaea) forms an active, hexameric complex in the presence of ATP. This corresponds to a single-ring model, and purports to dismiss any double-ring arrangements as non-physiological.

A model for the disassembly of ESCRT-III begins with the interaction of VPS4 MIT domains with CHMP MIM domains (Figure 1.6). Following this it is proposed that CHMPs are pulled

through the central hydrophobic pore of the complex, using the energy from ATP hydrolysis to induce a conformational change in the CHMP protein and causing it to dissociate from the complex (Hill and Babst, 2012). This is a similar mechanism to those used by other AAA ATPase enzymes. However, an interaction between CHMPs and the pore of the VPS4 complex has not been observed, and this model is unsubstantiated.

1.2 Roles for the ESCRT-III complex

1.2.1 The ancestral function of the ESCRT-III complex

The structure and role of VPS4 is widely conserved, as ESCRT-III has an ancestral function in cell division. This has been studied in the Crenarchaea, a subdomain of Archaea of which the most well characterised are *Sulfolobus*, hyperthermophiles which thrive at high temperatures and low pH. *Sulfolobus* possess CHMP homologues and a VPS4 protein, the transcripts of which are enriched in dividing cells, localise to a midbody equivalent, and prevent normal cell division upon mutagenesis causing loss of VPS4 function (Samson and Bell, 2009). The core of this machinery is found in one operon, designated *cdv* (cell division), and of three genes, *CdvA*, *CdvB* and *CdvC* (Lindås *et al.*, 2008). *CdvA* appears to be specific to Crenarchaea, showing distant homology based on coiled-coil and filament elements, to the precursors of nuclear envelope and cytoskeleton proteins in eukaryotes, e.g. lamins. *CdvB* is homologous to the CHMP proteins, sharing the highly-charged coiled-coil motif, and interestingly, a predicted C-terminal helix-turn-helix domain which could potentially confer a DNA-binding ability. Further CHMP homologues, between 2 and 4, are found in all Crenarchaeal genomes which possess this ESCRT-III like machinery. *CdvC* is a homologue of VPS4, being an AAA-ATPase protein which functions in disassembly of the cell division complex (Härtel and Schwille, 2014). However, the mechanism by which *CdvC* recognises *CdvB* and other CHMP-like proteins is unknown, given that *CdvB* does not possess the MIM motif responsible for recognition of VPS4 in ESCRT-III.

There are two interesting features of the machinery in *Sulfolobus*. First, the ESCRT-III protein located proximal to VPS4 within their operon is notably longer than the other homologues, and contains a predicted C-terminal winged helix domain, making it analogous to human CHMP7. Speculation by Samson and Bell (2009) attributes this domain to the winged helix domain in ESCRT-II member Vps25, suggesting a separation of function related to increasing

complexity during evolution. However, the presence of this domain prior to the evolution of ESCRT-II, and therefore the need for this winged helix domain to interact with ESCRT-III Vps20, suggests an alternative function for this domain.

All of this points to ESCRT-III components, the precursors of the CHMP family and VPS4, predating the divergence of Crenarchaea and Eukaryotes - indicating that cytokinesis was the original function of this machinery.

1.2.2 ESCRTs in viral budding

ESCRT-III is appropriated by the majority of enveloped viruses, including well-studied retroviruses such as HIV-1, in their terminal step of bud scission from the plasma membrane, producing enveloped virions independent of the infected host cell. This budding process differs from that of intraendosomal vesicles in that membrane reformation to generate the bud is mediated by viral proteins, and not by the full complement of preceding ESCRT complexes. In HIV-1, the self-assembly of capsid molecules derived from the viral Gag protein is a highly energetically favourable budding mechanism, and ESCRT-III is simply required for the final abscission step.

Viral L-domains (late domains) are motifs on proteins expressed in the later phase of the infectious cycle, which allow the viral machinery to recruit the host machinery they require for exit from the cell. P(S/T)AP L-domain motifs engage the UEV domain of ESCRT-I component TSG101 by mimicking the same motif found in the ESCRT-0 component Hrs (Pornillos *et al.*, 2003). PPXY L-domains associate with WW domains, a domain found in approximately 100 human proteins (Hu *et al.*, 2004).

Recently, the hepatitis A virus (HAV), which is a picornavirus - a positive stranded RNA virus which lacks a membrane envelope - was shown to require ESCRT-related proteins for proliferation (Feng *et al.*, 2013). Specifically, VPS4B and ALIX knockdown caused an inhibition of viral release, whereas TSG101 and CHMP4 knockdown caused minimal to

no inhibition. This strange arrangement, whereby a non-enveloped virus is partially dependent upon ESCRT proteins, led to the discovery of a method used by HAV to avoid the host immune system. The majority of HAV virions appropriate host membrane as a defence against antibody-mediated recognition by the immune system, termed 'membrane hijacking'.

1.2.3 A potential role for ESCRTs in exosome generation

Multivesicular bodies, in addition to the fusion with lysosomes, can fuse with the plasma membrane, releasing the intraluminal vesicles into the extracellular environment. Such released vesicles are termed exosomes. Exosomes and their content (including microRNAs) are proposed to mediate cell-to-cell communication within the local environment and the immune system and production is stimulated upon activation of the p53-mediated stress response (Yu *et al.*, 2006). ESCRT-I proteins ALIX and TSG101 are found within exosomes, such that they are commonly used as markers by which to distinguish exosomes from other multivesicular structure (Bobrie *et al.*, 2012). CHMP4C siRNA knockdown has been shown to cause inhibition of exosome production, which could be subsequently rescued by CHMP4C overexpression (Yu *et al.*, 2009). Colombo *et al.* (2013) also studied the effects of various ESCRT proteins on exosome secretion, and unexpectedly found that VPS4B depletion resulted in an increase in number of exosomes and proteins secreted. The role of ESCRTs in exosomes production is still very unclear.

1.2.3 ESCRTs in autophagic degradation

Autophagy is a cellular self-digestion mechanism by which intracellular components are identified and lysosomally degraded (Mizushima *et al.*, 2008). Microautophagy, sometimes known as endosomal microautophagy, refers to the sorting of proteins for degradation in multivesicular bodies for degradation in lysosomes. The term "autophagy" is used here in its commonly used sense to describe macroautophagy, in which cellular components are

engulfed in a double-membraned vesicle known as a phagophore, forming an autophagosome structure. These organelles then fuse with lysosomes, forming an autolysosome in which hydrolytic enzymes digest the contents.

Targets for autophagic destruction include threats such as pathogens, harmful organelle remnants and protein aggregates, with impairments to this process implicated in human disease through cell dysfunction and death. Under starvation or stress conditions, recycling of macromolecules can provide a valuable source of cellular resources such as amino acids, and cell or tissue remodelling also requires the redistribution of such constituents.

A link between ESCRT-III and autophagy was first observed upon knockdown of CHMP4B in cultured mouse neuronal cells, which causes autophagosomes to accumulate within cells (Lee *et al.*, 2009b). Expression of mutant CHMP2B also generated the same phenotype, which leads to neurodegenerative processes consistent with previous observations that CHMP2B mutations are implicated in clinical cases of frontotemporal dementia (Skibinski *et al.*, 2005) and motor neurone disease (Parkinson *et al.*, 2006). Recently, ESCRT-0/Hrs depletion in neuronal cells has been shown to impair autophagic degradation, leading to accumulation of harmful ubiquitinated protein, ER stress and compromised cell viability (Oshima *et al.*, 2016)

Rusten and Stenmark (2009) have outlined the possible stages at which CHMPs may be important to completion of the autophagic pathway. There are a number of parallels between the autophagic and multivesicular body machinery. Both pathways are initiated alongside phospholipid PtdIns3P synthesis (Nakatogawa *et al.*, 2009) and the target for degradation can be marked out by a ubiquitination signal (Kirkin *et al.*, 2009)). The engulfment of the target involves the fusion of the phagophore membrane with itself, forming a double-membraned autophagosome. This phagophore neck fusion event is mechanistically equivalent to the scission carried out by ESCRT-III in multivesicular body

biogenesis. Also, the autophagosome itself is structurally equivalent to an endosome containing one intraluminal vesicle, which subsequently merges with a lysosome in a similar manner to multivesicular bodies. The autophagic and endosomal pathways have also been shown to converge at the fusion of autophagosomes with multivesicular endosomes, forming structures termed amphisomes prior to lysosomal fusion (Berg *et al.*, 1998).

1.2.4 A role for ESCRT-III in plasma membrane repair

ESCRT-III has been shown to have a role in the repair of the plasma cell membrane (Scheffer *et al.*, 2014). Damage to cell membranes occurs most notably in mechanically active tissues, such as muscle cells, which sustain relatively large tears while being placed under strain. Ionomycin is an ionophore, which is used to increase the levels of intracellular Ca^{2+} , a state which was known to be key to the repair of these membrane tears. A screen for proteins found to be upregulated by ionomycin treatment included proteins related to endosomal function, with CHMP4B and CHMP1A showing particularly high upregulation. Other proteins which were identified included CHMP6, ALIX, TSG-101 and VPS4, however, proteins from the ESCRT-0 and II families were not identified.

Immunofluorescence revealed the formation of VPS4, CHMP4B, TSG101 and CHMP1A puncta at the cell surface in response to ionomycin treatment, and at the site of repair upon deliberate injury inflicted by a pulsed laser on the cell membrane. The proteins were sequentially recruited in a specific order, initially (ALG-2 then) ALIX, followed by CHMPs, and then VPS4B. This response was determined to be activated independently of cell type, and functioned similarly in HeLa cells. Stable knockdown of VPS4B in a HeLa cell line had no effect on the accumulation of ALG-2 or CHMP4B, said by Scheffer *et al.* (2014) to indicate the dispensability of VPS4B in this accumulation process. This seems a likely conclusion, however the potential role for VPS4A to compensate for the depletion of VPS4B was not considered.

1.3 ESCRTs in cytokinesis

1.3.1 Cytokinesis

Cytokinesis is the mechanism by which a eukaryotic cell is divided into two separate daughter cells following the replication and segregation of the genetic material. Each daughter cell also contains approximately half of the cytoplasmic material of the original cell. The division process is initiated once the sister chromatids have been segregated at opposite poles of the cell, in late anaphase to early telophase. Cytokinesis can be summarised in four stages: determination of the division site; membrane furrowing driven by an acto-myosin ring; formation of an intercellular bridge and midbody structure in late telophase; and resolution of the midbody by abscission, severing the membrane and resulting in two discrete cells. Successful cytokinesis relies on the tightly controlled orchestration of the spatial and temporal movement of the chromosomes, cytoskeleton, and spindle structures. The cyclin-dependent kinase (CDK), polo-like kinase (PLK) and aurora kinase (pAuk) families regulate overall coordination and progression through mitosis and cytokinesis. Failed or faulty cytokinesis can compromise genetic integrity, resulting in cellular instabilities such as mis-segregation, chromosomal breakage, centrosome amplification and multinucleation, and potential carcinogenesis.

A link between the ESCRTs and completion of cell division was first hinted at through a mutation in *Arabidopsis* of the TSG101 plant homologue (known as ELC). Spitzer *et al.*, (2006) found plant counterparts to ESCRT-I-III components, and noted that a mutation in ELC resulted in multinucleated cells. A similar phenotype, resulting in cytokinetic defects and multinucleation, was subsequently observed upon depletion of human ESCRT-I proteins ALIX and TSG101 (Carlton and Martin-Serrano, 2007; Morita *et al.*, 2007).

Furthermore, a novel archaeal cell division system, which performs cytokinesis independently of the actomyosin-homologous mechanism found in many bacteria and

archaea was found to rely on ESCRT-III and VPS4 homologues encoded by the three genes of the *cdv* operon (Lindås *et al.*, 2008; Samson *et al.*, 2014). Given that Archaea lack components of the other three ESCRT complexes, as well as an endomembrane system, it is hypothesised that cell division is the original purpose of the ESCRT machinery.

1.3.2 Entry into mitosis

At the G2/M border of the cell cycle, a checkpoint controls entry into mitosis, dependent on the resolution of genomic damage. Cdc2 activation is regulated based on the signals received from DNA damage through p53, aurora A and PLK1 pathways, and formation of the CyclinB-cdc2 (CDK1) complex drives the beginning of mitosis, consisting of chromosome condensation and spindle formation.

The next checkpoint is the spindle checkpoint – ensuring sister chromatids are correctly attached through microtubules to opposite ends of the mitotic spindle (Musacchio and Hardwick, 2002). Fulfilment of the checkpoint requirements initiates anaphase, whereby the spindle elongates in order to pull the sister chromatids apart (kinetochore). The site of furrow ingression and positioning of cytokinesis is determined by the location of the spindle midzone, a central region at which the ends of antiparallel microtubules emanating from each spindle pole overlap, forming a bundled structure to which cytokinesis-related proteins can localise, and around which a cleavage plane can be developed (Glotzer, 2004). The spindle midzone is stabilised by the chromosomal passenger complex (CPC), a master complex which regulates cytokinesis and shows a link with ESCRT proteins.

1.3.3 Intercellular bridge and midbody formation

The midbody is organised around the interdigitating microtubules originating from both spindle poles. Organisation is mediated by a set of microtubule interacting proteins that localise to the midzone. The ingression of the cleavage furrow eventually leads to the formation of a thin 20-100 nm intercellular bridge connecting the two daughter cells, with

CPC proteins located either side of the midbody. During compaction, a bulge that develops at the centre of midbody is called the stem body.

1.3.4 The chromosomal passenger complex (CPC)

Aurora B kinase is the enzymatically active component of the CPC (chromosomal passenger complex, a serine/threonine kinase key to the regulation of chromosome segregation and cytokinesis. The CPC consists of Aurora B, INCENP (inner centromere protein), survivin and borealin. The N-terminus of INCENP provides a platform for CPC formation, forming a triple helix bundle with survivin and the N-terminal domain of borealin.

During interphase, CPC has been seen to be targeted to heterochromatin via INCENP-HP1 binding. In early mitosis, this complex is enriched on centromeres, binding through the C-terminal domain of borealin. Aurora B kinases phosphorylate condensin, promoting heterochromatin formation through condensin-H2A interactions (Tada *et al.*, 2011). At the onset of anaphase the CPC is translocated to the spindle midzone, where it stabilises the structure and allows progression of cytokinesis, through recruitment of factors such as the centralspindlin complex. A number of CHMP proteins have been shown to interact in yeast two-hybrid assays with Borealin of the CPC, specifically CHMP2A, CHMP4B, CHMP4C and CHMP6, with CHMP4C demonstrating the strongest interaction, and co-precipitation (Carlton *et al.*, 2012). In the presence of lagging chromosomes, the CPC activates the abscission (NoCut) checkpoint whereby CHMP4C is recruited (Figure 1.7).

1.3.5 CHMP4C can delay cytokinesis to promote genome stability

The NoCut checkpoint, discovered in yeast (Norden *et al.*, 2006), links the terminal abscission step of cytokinesis to completion of chromosome segregation safely into each of the daughter cells. The action of this checkpoint delays ESCRT-III-mediated scission until all chromatin has been retracted fully from the plane of cleavage. This is a key mechanism for maintenance of genomic stability, preventing chromosome breakage or uneven genomic

segregation caused by premature abscission. Segregation defects such as lagging chromosomes or anaphase/chromatin bridges occur in an estimated 1% of somatic cell divisions, and with increasing incidence dependent on telomere dysfunction or levels of double strand breaks (Cimini *et al.*, 2003).

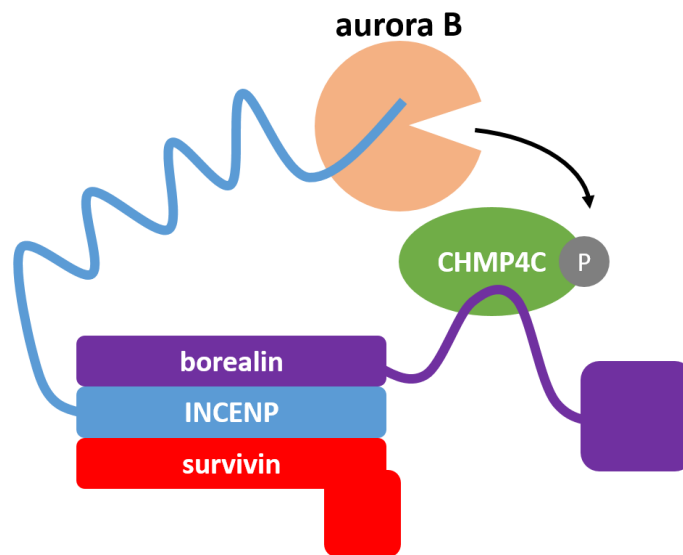


Figure 1.7 - The chromosomal passenger complex interaction with CHMP4C.

INCENP acts as a platform for CPC assembly and HP1 interaction. Aurora B kinase is a master regulator of mitosis, and while it is active phosphorylates CHMP4C, preventing onset of abscission until the conditions of the NoCut checkpoint have been met.

The loss of a telomere from such a breakage event can initiate a breakage-fusion-bridge (BFB) cycle, known to cause repeated translocations and chromosomal instability at each cell division through chromosome fusion leading to chromosome bridges broken at each cytokinetic event, leading to potentially cancerous cells, and generating extensive heterogeneity within tumour tissues (Gisselsson *et al.*, 2000).

The first evidence that such a checkpoint existed in animal cells demonstrated an Aurora-B dependent mechanism, and showed that the NoCut pathway was conserved across eukaryotic cells (Steigemann *et al.*, 2009). The interaction of the CPC complex with acetylated chromatin, if it found at the midbody, is sufficient to trigger the NoCut response and impede scission (Norden *et al.*, 2006).

Carlton *et al.* (2012) investigated the role of all three isoforms of CHMP4 in cytokinetic abscission. While RNAi-mediated depletion of CHMP4A and CHMP4C was found to present no hindrance to the completion of cytokinesis, CHMP4B being the only essential isoform, CHMP4C depletion resulted in a faster resolution of the midbody, alongside increased levels of H2AX phosphorylation. Together, this suggests the absence of CHMP4C leads to a faulty checkpoint, premature abscission, and accumulation of DNA damage. CHMP4C contains an insertion relative to the other CHMP4 isoforms, in the region 201-217 in which Aurora B specifically phosphorylates CHMP4C on S210 in a cell cycle dependent manner (Figure 1.7). At commencement of mitosis, phosphorylation of CHMP4C is initiated, with dephosphorylation occurring throughout mitotic progression.

This phosphorylation directs CHMP4C to the Flemming body, the central region of the midbody. The precise mechanism of inhibition of cytokinesis by CHMP4C in this region is unknown, however it may be able to prevent the assembly of a productive ESCRT-III complex. This role of CHMP4C suggests a role in protection of genome stability and prevention against accumulation DNA damage. In addition, a physical interaction between CHMPs and the lagging chromatin may be required to trigger such a checkpoint in an as yet unknown manner. Persistent chromatin bridges such as those that would initiate the delay of cytokinesis are targeted by condensin complexes, driven by Aurora B phosphorylation, in order to effect chromatin compaction to aid evacuation of chromosomes from the cleavage plane (Mora-Bermúdez *et al.*, 2007). This may correlate with the suggested role of CHMPs in ensuring proper chromosome segregation and in chromatin condensation.

1.3.6 Recruitment of the ESCRT-III complex and abscission

Following telophase, the separation of daughter nuclei and the formation of an intercellular bridge, assembly of an ESCRT-III complex at the midbody is triggered by the release of tension

in the intercellular bridge, thought to indicate that the daughter cells are in an appropriate final location (Lafaurie-Janvore *et al.*, 2013).

CEP55 (centrosomal protein 55kDa) localises as a dimer to intercellular bridge by associating with MKLP1 of the centralspindlin complex (Figure 1.8). Plk1 prevents premature onset of cytokinesis by phosphorylating MKLP1, preventing its interaction with CEP55 (Bastos and Barr, 2010). CEP55 is a coiled-coil protein containing a 57 residue 'hinge' region between the alpha helices, known as EABR (ESCRT and ALIX-binding region; (Lee *et al.*, 2009a). This region can bind either ALIX or TSG101 via their GPPX₃Y motifs, recruiting them to rings on either side of the midbody. The BRO1 domain of ALIX binds CHMP4 (McCullough *et al.*, 2008), and is proposed to relieve the autoinhibition and nucleate the assembly of CHMP4 polymers. CHMPs are then sequentially recruited to the midbody, as in formation of the ESCRT-III complex on the endosomal membrane, forming filaments which spiral and extend into the constriction zone.

Spastin, the AAA-ATPase enzyme which cuts microtubules spanning the midbody, is recruited to this site through a high-affinity interaction of its MIT domain with the C-terminal region of CHMP1B (Yang *et al.*, 2008). Mutations in the spastin-binding region of CHMP1B, or CHMP1B depletion result in cytokinetic impairments due to the inability to sever this obstruction to proper abscission. IST1, while dispensable for multivesicular body biogenesis and viral budding, plays an essential role in cytokinesis (Bajorek *et al.*, 2009a). IST1 and CHMP1 form a subcomplex important for the recruitment of VPS4 to the ESCRT-III complex at the midbody. Depletion of either IST1 or CHMP1 results in low levels of VPS4 localisation at the midbody. Depletion of IST1 in HeLa cells resulted in a reduction of successful cell division from 90% of control cells to 9% of treated cells, which formed intercellular bridges, however failed to perform the abscission step (Bajorek *et al.*, 2009a).

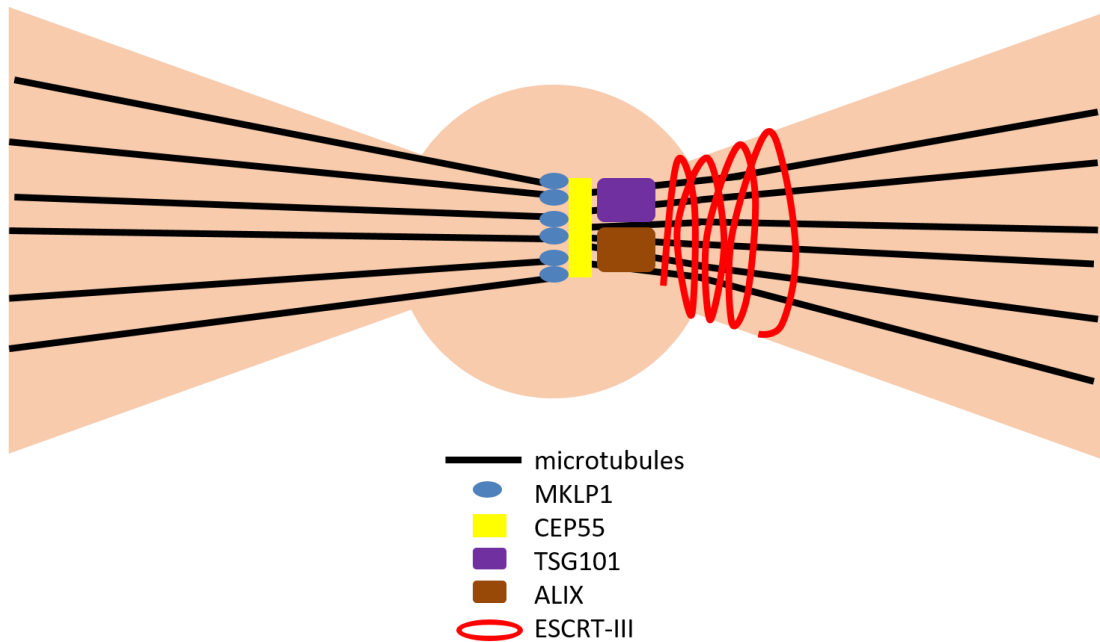


Figure 1.8 – ESCRT-III recruitment and formation at the cytokinetic midbody

CEP55 is recruited to the midbody by MKLP1 at the onset of cytokinesis, and drives progression through cytokinesis through recruitment of ESCRT-III. Through its EABR region, TSG101 and ALIX compete for binding of CEP55. Both TSG101 and ALIX are capable of recruiting CHMP4, nucleating the formation of helical ESCRT-III on one side of the midbody structure.

ESCRT-III helices on the membrane cause constriction at the midbody, and its abscission is thought to be driven by remodelling of the complex by VPS4 enzymes (Elia *et al.*, 2012). VPS4 is essential for successful abscission at the midbody. The recent observations that ESCRT-III plays a role in wound healing at the plasma membrane (Jimenez *et al.*, 2014) may suggest a mechanism whereby the membrane is broken and then sealed through the actions of the ESCRT-III complex. Despite the lack of clarity of the moment of abscission, the ESCRT-III complex provides the membrane-remodelling required for cytokinesis to occur.

1.3.7 ESCRTs in centrosome duplication and spindle formation

Depletion of CHMP2A or CHMP5 has been shown to result in the formation of monopolar spindles, due to the presence in the cell of only one centrosome. Conversely, depletion of CHMP1A, CHMP2B, CHMP4B, CHMP4C or VPS4 resulted in high numbers of centrosomes within each cell, producing multipolar spindles in mitosis (Morita *et al.*, 2010). A number of

ESCRTs have been seen to concentrate at centrosomes, including TSG101 (Xie *et al.*, 1998), ALIX (Morita *et al.*, 2007), EAP20 (Langelier *et al.*, 2006) and IST1 (Bajorek *et al.*, 2009a).

Together with the results from this study, these observations collectively suggest that the entire ESCRT pathway probably exerts centrosomal and possibly other functions that are conserved across fission yeast, plants, and mammals. The late-acting ESCRT-III/VPS4 proteins appear to play the most critical roles in centrosome maintenance, however, because their depletion induced stronger mitotic defects than did depletion of early-acting ESCRT factors such as TSG101 and ALIX.

Maintenance and duplication of the centrosomal machinery in each cell is vital to cell cycle progression and successful mitosis, due to their key role in spindle formation and cell division. The centrosome is duplicated during S-phase, and separate in prophase to opposite ends of the nucleus, associated with the nuclear envelope. Centrosomes act as centres of microtubule growth, and upon disintegration of the nuclear membrane, these microtubules can associate with chromosomes through the kinetochores, founded on the centromeric regions of DNA. This forms the mitotic spindle, as monitored by the spindle assembly checkpoint (SAC) which ensures that all chromosomes are amphitelically attached to the spindle – meaning that sister chromatids are attached to opposite centrosomal poles. Upon cytokinesis, one centrosome is incorporated into each daughter cell.

Aberrant centrosome duplication or cell division can result in an aberrant number of centrosomes at the point of spindle formation, causing dramatic faults in the formation of a bipolar spindle, including unipolar and multipolar spindles. This causes severe consequences for chromosome segregation and success of cytokinesis, and the viability of any resulting daughter cells. Aberrant centrosome number is correlated with aberrant chromosome content, responsible for chromosomal instability cell death or carcinogenesis.

1.4 Nuclear roles for CHMP proteins

The roles of CHMPs in cytokinesis is clear, however CHMPs appear to be present in the nucleus throughout the cell cycle, especially upon VPS4 knockdown. However, the functions of ESCRTs and CHMPs in the nucleus are poorly understood. A number of observations have been made regarding individual CHMPs performing roles in the nucleus, however a comprehensive theory as to how multiple components may function together in a complex fashion has not yet been determined.

1.4.1 CHMP1

CHMP1 exists as two isoforms in the human proteome, CHMP1A and CHMP1B, which share approximately 60% sequence identity, and 82% amino acid similarity. This difference in sequence results in differential roles for the two proteins, for example, CHMP1B is capable of binding and recruiting spastin however CHMP1A cannot (Wollert *et al.*, 2009b), despite the presence of MIT domains in both proteins. The two isoforms are also thought to have individual roles in other cellular processes, with CHMP1A indicated in various nuclear roles in several studies. The potential role of CHMP1B in the nucleus and in other cellular functions is less well researched.

The subcellular localisation of CHMP1A in a number of different human cell lines is documented by the Human Protein Atlas (Uhlen *et al.*, 2015). These findings show CHMP1A to be primarily cytoplasmic, but also significantly nuclear, and excluded in from nucleoli. Mochida *et al.* (2012) also observed almost total CHMP1A exclusion from the nucleus in NIH 3T3 cells, which are derived from mouse embryonic fibroblasts. CHMP1 isoforms contain predicted nuclear localisation sequences, which suggest a role within the nucleus alongside other functions with ESCRT-III.

1.4.2 CHMP1A overexpression and chromatin condensation

CHMP1A was first discovered in a study looking for binding partners of the PcG family member Pcl (Polycomblike), through a yeast two-hybrid method (Stauffer *et al.*, 2001). Polycomb proteins modulate gene silencing through patterns of chromatin remodelling. Transcriptional repression is achieved through histone modifications, including trimethylation and ubiquitination, which promote chromatin compaction (Francis *et al.*, 2004). The patterns of histone modification in specific regions of genome can be maintained through cell divisions in an epigenetic fashion.

Features of CHMP1A as determined by Stauffer *et al.* (2001) included the existence of CHMP1A as two differentially sized forms, localising within the cytoplasm and the nuclear matrix distinctly, suggesting a post-translational modification of the protein related to a relocalisation. Also predicted is a nuclear localisation signal contained within the protein. Upon dissolution of the nuclear matrix in mitosis, Stauffer *et al.*, observed CHMP1A remaining associated with the axial chromosome scaffold region, suggesting, in these HEK293 (human embryonic kidney) cells at least, a role with chromatin throughout the cell cycle. Additionally, induced overexpression of CHMP1A caused cell cycle arrest in S-phase.

Immunofluorescence experiments documenting the effects of CHMP1A overexpression showed the formation of large, stable nuclear structures which are nuclease-resistant and stain strongly for CHMP1A. The presence of these structures was found to be associated with the alteration of histone modification status and increased local levels of chromatin condensation. Closer observation revealed that CHMP1A is found to surround areas of heavily condensed chromatin, with increased phosphorylated and acetylated histone H3 at the periphery of the condensed region.

Associated with the CHMP1 structures are the Polycomb complex proteins, with CHMP1 showing the ability to recruit BMI1, a Polycomb transcriptional repressor, to the condensed

chromatin, with staining for BMI1 found to be entirely contained within the CHMP1A domains. A link between BMI1 and CHMP1A is supported by an experiment in *Xenopus* embryos in which misexpressed CHMP1 causes the same phenotype previously seen upon misexpression of polycomb group protein (Yoshitake *et al.*, 1999). This phenotype is one of altered neural development due to misregulation of the genes responsible for embryonic development of the nervous system.

Taken together, the work of Stauffer *et al.* shows that in effect, overexpression of CHMP1 promotes chromatin condensation, potentially associated with gene silencing regulation, and demonstrates a role spatially and functionally distinct from its role in the ESCRT-III complex.

1.4.3 CHMP1A is a predicted tumour suppressor

A number of studies propose a tumour suppressor role for CHMP1A, with the protein found to be differentially expressed in a variety of different cancer tissues (Human Protein Atlas; Uhlén *et al.*, 2015). Knockdown of CHMP1A in non-cancerous human embryonic kidney cells (HEK293) resulted in tumour formation when introduced to an *in vivo* nude mouse model (Li *et al.*, 2008). The cancerous cells demonstrated many abnormalities, including multiple nuclei, defective mitosis, and a high ratio of nuclear to cytoplasmic content. Overexpression of CHMP1A in PanC-1 (human pancreatic ductal tumour cells) in a xenograft mouse model resulted in smaller tumours *in vivo* compared to control PanC-1 cells, showing a correlation between increased levels CHMP1A and inhibited tumour growth (Li *et al.*, 2008). You *et al.* (2012) demonstrated a similar effect in renal cell carcinoma, through comparison of tissue samples, and knockdown or overexpression of CHMP1A in A-498 human kidney carcinoma cell line *in vitro* and introduced to *in vivo* mouse models.

Correlated with CHMP1A overexpression is increased levels of both p53 and phosphorylated-p53, and assumes that CHMP1A positively regulates p53 expression (Li *et al.*, 2008). Manohar

et al. (2011) take this further, to propose a role for CHMP1A in ATM regulation through p53, and show immunofluorescent colocalisation of CHMP1A and phosphorylated ATM upon overexpression of CHMP1A.

While these studies into CHMP1A demonstrate a potential role for CHMP1A in tumour suppression and cell growth inhibition, no biochemical evidence or mechanism of action has been provided for the proposed interactions and effects of CHMP1A within the cell. In particular, the correlation with p53 and ATM activity could be caused by a number of things, including cellular stress. Overexpression of CHMP1A has previously been shown to cause cellular arrest in S-phase (Stauffer *et al.*, 2001), an event which would cause problems. CHMP1A is also involved in cytokinesis, which may be affected by overexpression.

1.4.4 CHMP4

The three human isoforms of CHMP4, CHMP4A-C, share very similar N-terminal regions, and are distinguished primarily by differences in the C-terminal regions. This is exemplified by the 17 amino acid insert in CHMP4C, which provides a phosphorylation site for targeting by Aurora B kinase, allowing it to be regulated in line with the cell cycle and play a distinct role at the midbody in mitosis (Carlton *et al.*, 2012). CHMP4B is the most abundant isoform, being the core component of the ESCRT-III assembly and essential to all functions of the complex, and capable of interacting with all other CHMP subunits. In yeast, the CHMP4 homologue SNF7 is the only ESCRT-III subunit absolutely required for severing of the ILVs from the membrane (Peck *et al.*, 2004). CHMP4 isoforms have been implicated in several cancers, cataract formation and response to cell stresses such as hypoxia.

A large GWAS analysing SNPs for association with epithelial ovarian cancer (EOC), identified SNPs in CHMP4C as its primary candidate for susceptibility to EOC (Pharoah *et al.*, 2013). Additionally, a microarray study by Nikolova *et al.* (2009) specifically identify CHMP4C as a potential treatment target and diagnostic marker for this cancer, finding it to be routinely

overexpressed in cancerous tissue, and not in healthy controls. Based on the knowledge of the role CHMP4C plays in the regulation of cell division, in which it delays cytokinesis in order to protect genomic integrity (Section 1.3.5; Carlton *et al.*, 2012), and its transcriptional regulation by p53.

CHMP4A has been found to be differentially expressed in patients with advanced-stage ovarian cancer (Barlin *et al.*, 2013). In a potentially related function, CHMP4A is thought to be involved in the regulation of hypoxia-inducible factor 1 (Shi *et al.*, 2010), in a screen of genes which affected expression of the protein. CHMP4A is postulated to upregulate the expression of this hypoxia related protein under both normal and hypoxic conditions.

Mutations in CHMP4B have also been linked to the formation of cataracts in studied cases of inherited predisposition to childhood onset of the disease in an autosomal dominant fashion (Shiels *et al.*, 2007). Multiple mutations have been observed, resulting in protein truncations, however the precise mechanism by which this results in problems with lens development and visual impairment is unclear.

1.4.5 CHMP7

CHMP7 is the most recently classified member of the CHMP family (Horii *et al.*, 2006), and unique among them due to its length of 453 amino acids, approximately twice as long as CHMPs 1-6. The C-terminal half (220-453) contains the canonical CHMP (Figure 1.9), while N-terminal domain is of unknown structure and function, however Horii *et al.* suggest that it may be related to the Snf7 domain.

Determination of the subcellular localisation of CHMP7 shows conflicting reports, with Horii *et al.* identifying CHMP7 as being cytoplasmic and primarily perinuclear. However, only CHMP7 constructs involving either a GFP or FLAG tag were used in these immunofluorescence studies, and subsequent work using direct antibody targeting of native CHMP7 shows it to be principally nuclear (but excluded from nucleoli), with some diffuse

cytoplasmic staining (Human Protein Atlas; Cleasby, PhD thesis 2013). This pattern of localisation makes CHMP7 unique among the ESCRT-III components, which are found most significantly in the cytoplasm.

A role for CHMP7 in the ESCRT-III complex has not been determined, but interaction studies between CHMP7 and CHMP1-4 and 6 have been carried out. Yeast two-hybrid assays have demonstrated interaction between the C-terminal half of CHMP7 and CHMP4A, 4B and 4C with approximately equal affinities, and these findings were confirmed by pull-down assays (Horii *et al.*, 2006). In the same study, overexpression of GFP-CHMP7 caused a slight increase in the levels of ubiquitin present in the cytoplasm, suggesting that CHMP7 has a role in the endocytic pathway. Despite this, ubiquitin and CHMP7 colocalisation were not observed. In addition, they saw a reduced degradation rate of the EGF receptor targeted by the ESCRT system, a phenotype previously observed upon overexpression of CHMP4B (Kato *et al.*, 2004). These findings must be considered in the light of potentially unnatural localisation or function of CHMP7 caused by the fusion of a GFP tag throughout the experiments.

1.4.6 Structural prediction of the CHMP7 N-terminal domain

The structure and nature of the N-terminal half of the protein is undetermined, and therefore structural prediction software is a useful tool for its study. Phyre2 (Protein Homology/Analogy Recognition Engine v2.0; Kelley and Sternberg, 2009) is a computational tool which uses sequence alignment and homology detection modelling against structures already stored in the PDB (protein data bank) database, taking into account secondary structure predictions and statistical scoring, and producing a series of predicted models in order of likelihood.

An input of N-terminal half of the protein (residues 1-230) - the top 5 hits match templates relating to structures of EAP20/Vps25, a subunit of the ESCRT-II complex (Wernimont and Weissenhorn, 2004; PDB 1XB4). While the percentage sequence identity of the top hit is only

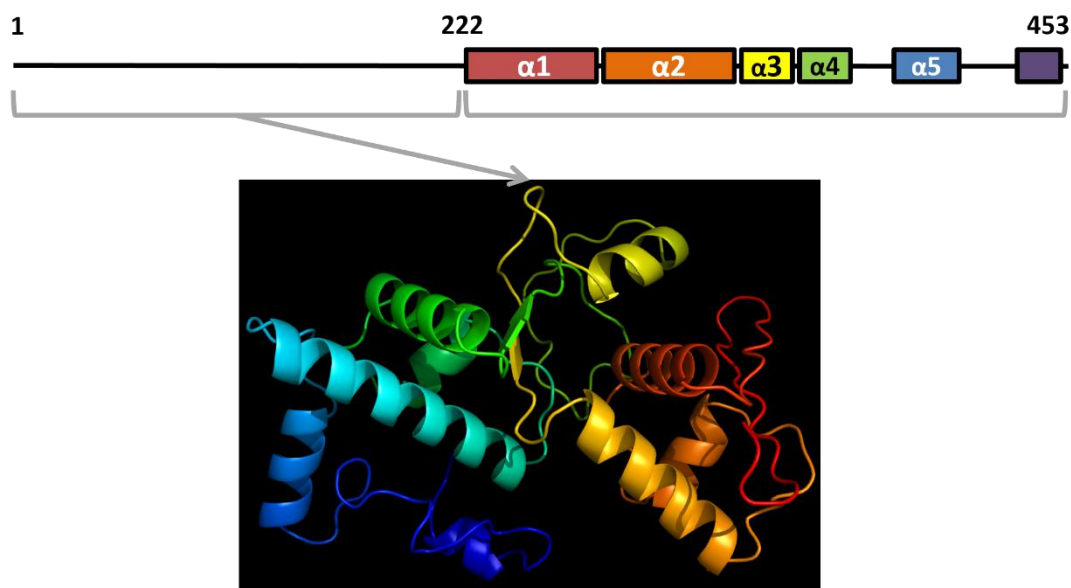


Figure 1.9 –Structural prediction of the CHMP7 N-terminal domain

CHMP7 contains the five α -helices and core domain of the CHMP family in its C-terminal half. The structure and function of the N-terminal domain is undetermined, however a Phyre2 structural prediction obtained using the threading method estimates a double winged-helix domain with 98.7% confidence. The winged-helix is a common nucleic acid binding domain.

25%, the confidence level for the overall protein fold match is high, at 98.7% (Figure 1.9). In addition, that the closest structural match resembles another member of the ESCRT family is a positive indication of the likelihood of the match. The fold which has been recognised is a double occurrence of the approximately 110-residue winged-helix motif. This sub-class of helix-turn-helix domains is commonly found in transcription factors, acting as a nucleic acid or protein interaction module (Teichmann *et al.*, 2012). Interaction of CHMP7 with EAP20 was tested and found not to occur by Horii *et al.* (2006). It has not been demonstrated whether the winged-helices of Vps25 bind to nucleic acids *in vivo* or *in vitro*, however interactions between the N-terminal repeat and ESCRT-II proteins Vps22 and Vps35 have been shown (Im and Hurley, 2009). It remains to be seen whether this distinguishing feature of CHMP7 among CHMP proteins is related to its nuclear localisation and potential function.

1.5 Project aims

Previous work by Cleasby (PhD thesis, 2013) showed the existence of ESCRT-III complexes at nuclear foci in interphase cells, a phenotype observed exclusively following VPS4 depletion, which prevents ESCRT-III disassembly. These nuclear ESCRT-III foci have been observed to be dependent on the presence of CHMP7 and associate with various markers of DNA damage: PML bodies, γ H2AX and BRCA1, leading us to hypothesise a specific role for this complex in genomic stability. This thesis aims to dissect the role of the poorly characterised ESCRT-III-related protein CHMP7 in relation to the nuclear ESCRT-III complex by investigating the relationship with DNA damage and nuclear structures associated with genomic instability.

In Chapter 3, depletion of CHMP7 by RNAi is used to investigate the effects on HeLa, HeLa M and U2OS cancer cell lines of the loss of CHMP7. This will allow for an initial characterisation of the importance and role of the protein across these cell lines and observation of the consequences of CHMP7 loss on genomic stability and nuclear function. In Chapter 4, immunofluorescent techniques are used to visualise CHMP distribution throughout the cell as it proceeds through the cell cycle. The relationship of ESCRT-III with various nuclear proteins are examined, focusing particularly on their localisation during mitosis and the nature of ESCRT-III nuclear accumulations which form following VPS4 depletion. Chapter 5 explores the association of ESCRT-III with nuclear material, in particular, aberrant structures formed from improper nuclear segregation – micronuclei and chromosome bridges.

Chapter Two

Materials and Methods

Contents

	Page
2.1 Human tissue culture	41
2.1.1 Antibodies	41
2.1.2 Human cell lines	42
2.1.3 Preparation of cell culture reagents	42
2.1.4 Passage and maintenance of cell lines	43
2.1.5 Long-term storage of cell lines	43
2.1.6 RNA interference (RNAi)	44
2.1.7 Transient DNA transfection of human cells	45
2.1.8 UV irradiation of cells	45
2.1.9 Preparation of cell lysate for Western blot	45
2.1.10 Immunoprecipitation	46
2.1.11 SDS-PAGE	47
2.1.12 Western blotting	48
2.1.13 Immunofluorescence	49
2.1.14 <i>In situ</i> protein pre-extraction of adherent cells	50
2.1.15 Criteria for micronuclei scoring	51
2.1.16 MTT assay	51
2.1.17 Fluorescence-activated cell sorting (FACS)	52
2.1.18 Subcellular fractionation	53
2.2 Bacterial cell culture and DNA manipulation	54
2.2.1 Generation of HA-tagged CHMP7 plasmids	54
2.2.2 Agarose DNA gels	55
2.2.3 Bacterial cell strains	55
2.2.4 Bacterial media and agar	55
2.2.5 Bacterial transformation, culture, and plasmid purification	56

2.1 Mammalian tissue culture

2.1.1 Antibodies

Primary antibodies used in this study					
Antibody (α -Hu)	Host Species	Source	Code	Dilution	
				WB	IF
α -p-Aurora kinase	rabbit	Cell Signaling Tech	#2914	1:2000	1:100
α - β -actin	mouse	Proteintech	66009-1-IG	1:10000	1:100
α - β -tubulin	mouse	Sigma	T8328	1:1000	1:200
α -BLM	goat	Santa Cruz	SC-7790	X	1:100
α -calnexin	rabbit	Cell Signaling Tech	#2679	1:5000	1:500
α -CHMP1B	rabbit	Proteintech	14639-1-AP	1:1000	1:200
α -CHMP4B	rabbit	Proteintech	13683-1-AP	1:1000	1:200
α -CHMP7	mouse	Santa Cruz	SC-271805	1:1000	1:250
α -CHMP7	rabbit	Proteintech	16424-1-AP	1:1000	1:200
α -CHMP7	sheep	house-generated	N/A	1:2500	1:800
α -CREST	human	Antibodies Inc	15-234-0001	X	1:50
α - γ H2AX	mouse	Abcam	ab11174	1:5000	1:1000
α - γ H2AX	rabbit	Cell Signaling Tech	#9718	1:1000	1:400
α -HA	mouse	Pierce	26183	1:1000	1:500
α -Lamin A/C	goat	Santa Cruz	SC-6215	1:1000	1:500
α -Lamin B1	rabbit	Proteintech	12987-1-AP	1:2500	1:300
α -LAP2	rabbit	Proteintech	14651-1-AP	1:2000	1:1000
α -PARP1	mouse	Calbiochem	AM30	1:1000	1:500
α -PDI	rabbit	Cell Signaling Tech	#2446	1:1000	1:500
α -pericentrin	rabbit	Abcam	ab4448	X	1:1000
α -PML	rabbit	Abcam	Ab53773	1:1000	1:200
α -RAD51	rabbit	Santa Cruz	SC-8349	X	1:100
α -RPA34-20	mouse	Calbiochem	NA19L	X	1:200
α -SUMO2/3	rabbit	Proteintech	11251-1-AP	1:500	1:100
α -VPS4A	rabbit	Proteintech	14272-1-AP	1:1000	1:200
Secondary antibodies used in this study					
Target species	Host species	Fluorophore/ Conjugate	Source	Code	Dilution
sheep	donkey	Cy3	Millipore	AP184C	1:1000
mouse	goat	Alexa-488	Life Technologies	R37120	1:2000
mouse	goat	Alexa-594	Life Technologies	R37121	1:2000
rabbit	goat	Alexa-488	Life Technologies	R37116	1:2000
rabbit	goat	Alexa-594	Life Technologies	R37117	1:2000
goat	donkey	Alexa-488	Life Technologies	R37114	1:1000
mouse	horse	HRP	Cell Signaling Tech	#7076	1:5000
rabbit	goat	HRP	Cell Signaling Tech	#7074	1:5000

Three CHMP7-specific antibodies were obtained for detection of CHMP7. The first is a sheep-derived serum antibody obtained from the Scottish National Blood Transfusion Service which is raised against the N-terminal region (amino acids 1-222) of the CHMP7 protein. The second is produced by Proteintech, raised in a rabbit host to the C-terminal region of the CHMP7. The third is a mouse-derived antibody produced by Santa Cruz, raised against residues 1-300 of the protein.

2.1.2 Human cell lines

Cell line	Genotype
HeLa	human cervix carcinoma
HeLa M	human cervix carcinoma – monolayer (M) subtype
U2OS	human bone osteosarcoma

2.1.3 Preparation of cell culture reagents

Dulbecco's Modified Eagle Medium (DMEM; BioWhittaker) - with L-glutamine and 4.5g/L glucose – Stored at 4°C

Foetal Calf Serum (FCS; Sera Lab) – Free of virus, endotoxin and mycoplasma contamination. Filter sterilised prior to use and stored at -20°C

Non-Essential Amino Acid Solution 100x (NEAA; BioWhittaker) – Stored at 4°C

1x PBS (phosphate-buffered saline) is made by dissolving: 8g NaCl, 0.2g KCl, 1.44g Na₂HPO₄ and 0.24g KH₂PO₄ in 1L distilled water. Adjustment of the buffer to pH 7.4 is carried out by addition of HCl, and the buffer is sterilised by autoclaving.

PBST: phosphate-buffered saline, 0.1% Tween-20

PBStx: phosphate-buffered saline, 0.1% Triton X-100

To make the complete supplemented culture medium, 50ml FCS and 5ml NEAA were added to each 500ml bottle of DMEM. DMEM and NEAA were stored at 4°C, FCS at -20°C, and supplemented DMEM ready for use was stored at 4°C.

2.1.4 Passage and maintenance of cell lines

Cell lines were typically maintained in 75cm² treated and vented flasks (Thermo Scientific Nunc EasyFlasks), containing 8-15ml culture medium and incubated in a humidified incubator at 37°C and 5% CO².

Passaging or sub-culturing of cell lines was carried out when cells were approximately 80% confluent, and therefore still in the log phase of growth. Culture medium, trypsin and PBS were warmed to 37°C in a water bath for at least 30 minutes. Within a hood, culture medium is removed from the flask and discarded, and the monolayer is washed twice gently with 10ml warmed PBS. After removal of all PBS, 1ml trypsin is added to the flask, and tilted to that the trypsin makes contact with all cells. The flask is returned to the incubator to allow gentle breakdown of monolayer adhesion. After 5-10 minutes, 9ml fresh, warmed culture medium was added to the flask, and pipetted up and down to ensure even suspension of all cells within the medium. In a new flask, 1ml of the cell suspension was added to 9ml fresh culture medium, and mixed to ensure an even spread of cells across the flask surface. The flask was then returned to the incubator.

The growth rate of healthy HeLa cells resulted in a typical growth period of 2-3 days to reach 80% confluence once again. At 80% confluence, a 75cm² flask will contain approximately 6.7x10⁶ cells. When necessary, cell numbers were quantified using a haemocytometer (Neubauer; depth 0.1mm, 1/400mm²).

2.1.5 Long-term storage of cell lines

Cell line stocks can be maintained indefinitely when frozen and stored at -80°C. Cryopreserved stocks are required in case of contamination, cell line death or cell line dysfunction due to genetic change after many passages.

Freezing medium: supplemented DMEM containing 10% (v/v) DMSO (dimethyl sulphoxide)

Culture medium is removed from a flask of cells at approximately 80% confluence, the cells trypsinised with 1ml trypsin for 5-10 minutes, and 9ml fresh culture medium added to form a cell suspension, as in the passaging of cells. The density of the cells in the suspension was measured by counting using a haemocytometer. The suspension is then spun down in a centrifuge at 1200rpm (4°C) for 5 minutes, and the medium removed from the cell pellet and discarded. Based on the number of cells estimated in the pellet, it is resuspended in enough freezing media to create a suspension of 1×10^6 cells/ml.

2.1.6 RNA interference (RNAi)

Depletion of target proteins in HeLa cells was carried out by transfection of siRNA using INTERFERin (DHARMAFECT) reagent (Polyplus transfection). Stocks of specific-protein targeting siRNA solutions were made at 20 μ M concentration in RNase-free water, with siRNA oligonucleotides obtained as “On-Target Plus” formulations (Dharmacon). As a control for siRNA transfection, ON-TARGETplus non-targeting control siRNA (#1; Dharmacon) was used. Cells were plated 24 hours prior to knockdown, at a density of 50, 000-250, 000 cells per well in a 6-well plate, dependent on the length of the knockdown to be carried out, between 24 and 72 hours. For each well in a 6-well plate, siRNA to the appropriate concentration (usually 1-25nM) was added to 200 μ l serum-free DMEM medium and 4 μ l INTERFERin reagent, mixed thoroughly and incubated for 10 minutes at room temperature. This was then added dropwise to 2ml fresh complete DMEM medium in a well on a 6-well plate, mixed thoroughly and the plate incubated at 37°C for 24-72 hours before harvesting or fixation of the cells.

siRNA target	siRNA oligonucleotide sequences
CHMP7-1	GGGAGAAGAUUGUGAAGUU
CHMP7-2	GAGCAGAGGAGAAGAAUUU
CHMP7-3	GGAGGUGUAUCGUCUGUAU
VPS4A/B (SMARTpool)	CCACAAACAUCCCAUGGGU
	CCGAGAAGCUGAAGGAUUA
	GGGCAAAGUGUACAGAAUA
	CGAUAGAUCUGGCUAGCAA

2.1.7 Transient DNA transfection of human cells

Transfection of cells with DNA for 48 hours was carried out using JetPEI transfection reagent (Polyplus transfection). Cells were plated 24 hours prior to transfection, at a density of 150,000 cells per well of a 6-well plate. For transfection of one well in a 6-well plate, 3µg DNA was diluted to a volume of 100µl in 150mM NaCl solution, and in a separate tube, 6µl JetPEI reagent was diluted to 100µl with 150mM NaCl solution. The JetPEI reagent was added to the DNA, mixed thoroughly and left to incubate at room temperature for 15-30 minutes to allow for complexation of the DNA and reagent. The 200µl solution was added dropwise to 2ml fresh DMEM media in the well of the plate, mixed thoroughly and the plate incubated for 24-72 hours at 37°C.

2.1.8 UV irradiation of cells

Induction of DNA damage through irradiation with UVC light was carried out 24 hours following seeding of cells into a plate or dish. Irradiation was carried out in a CX-2000 Ultraviolet Crosslinker (UVP) which uses an overhead 254nm UV source. Culture medium was removed from the cells, and washed with ice-cold PBS to remove all traces of medium. PBS buffer was fully removed from the cells, and exposure was carried out at 10mJ/cm² in sterile conditions, and fresh culture medium quickly replaced in the plate or dish to prevent cell drying out. Cells were returned to incubation at 37°C. Fixation of cells following UV irradiation was carried out immediately following induction of damage, or at various timepoints between 1-72 hours.

2.1.9 Preparation of cell lysate for Western blot

RIPA buffer (5x): 125mM Tris pH 7.6, 750mM NaCl, 5% NP-40, 5% sodium deoxycholate, 0.5% SDS, 5mM EDTA

Plates containing cells to be harvested for analysis by Western blot were washed twice with 10ml ice-cold PBS (for a 10cm dish) following removal of the media from the cells.

Subsequently, 10ml ice-cold PBS containing protease inhibitors (one Roche cOmplete Protease Inhibitor Cocktail tablet) was added to the plate and cells collected into a 15ml tube using a cell scraper and pipette. The cells were centrifuged for 5 minutes at 1500rpm at 4°C, and the PBS removed. The cell pellet was resuspended in 0.5ml RIPA lysis buffer containing protease inhibitors, and lysed by incubation on ice for 15 minutes with frequent vortexing. Centrifugation at 10000rpm for 10 minutes is carried out to remove the insoluble cell debris, leaving lysate which can be used in immunoprecipitation experiments or analysed directly by Western blot.

2.1.10 Immunoprecipitation

Immunoprecipitation is carried out on clarified cell lysate in RIPA lysis buffer with protease inhibitors. A 10% sample of the initial lysate was taken prior to immunoprecipitation, and the remainder divided evenly between 1.5ml centrifuge tubes in which the IP will be performed. Primary antibody is added to the appropriate samples and incubated overnight at 4°C with constant agitation. A no-antibody, beads-only control was performed alongside each immunoprecipitation experiment. Protein A/G agarose beads were used for the immunoprecipitation step, with 25µl washed beads added to each sample for 2 hours at 4°C with constant agitation. The beads were removed by centrifugation at 5000rpm for 1 minute, the supernatant discarded and the beads washed three times with RIPA buffer with protease inhibitors. The beads were boiled in 25µl 2x protein loading buffer for 15 minutes at 95°C, with frequent mixing. The beads were spun to the bottom of the sample by centrifugation for 2 minutes at 10000rpm, and the supernatant sample analysed via Western blot alongside the input lysate, no-antibody control and samples of supernatant taken from the unbound and wash fractions throughout the experiment.

2.1.11 SDS-PAGE

SDS-PAGE (SDS-polyacrylamide gel electrophoresis) is carried out to separate proteins in a sample based on size, for easier analysis of the proteins present in the sample. Preparation of samples for SDS-PAGE is carried out by addition of 5x protein loading buffer to the solubilised protein and boiling at 95°C for 10 minutes to denature and reduce the proteins in the sample.

SDS-PAGE loading buffer (5x): 250mM Tris, 10% SDS, 30% glycerol, 5% β -mercaptoethanol, 0.05% bromophenol blue. Adjusted to pH 6.8 with HCl.

SDS-PAGE running buffer (10x): 25mM Tris, 192mM glycine, 0.1% SDS.

Resolving gel layer (5ml)	Acrylamide content		
	8%	10%	12%
40% acrylamide	1.3	1.7	2.0
1M Tris HCl pH6.8	1.3	1.3	1.3
ddH ₂ O	2.3	1.9	1.6
10% SDS solution	0.05	0.05	0.05
TEMED	0.05	0.05	0.05
10% APS	0.005	0.005	0.005
Stacking gel layer (5ml)	Acrylamide content		
	6%		
40% acrylamide	0.83		
1M Tris HCl pH8.8	0.63		
ddH ₂ O	3.4		
10% SDS solution	0.05		
TEMED	0.05		
10% APS	0.005		

All volumes given in ml

Gels are cast with a 1.5mm thickness using the Mini-PROTEAN Tetra Cell system (BioRad). The gel is prepared in two layers, firstly an 8-12% acrylamide resolving layer and a 6% acrylamide stacking layer, with the acrylamide content of the resolving gel dependent on the size of the target protein for analysis. Cooled samples are applied to wells in the upper layer of the gel using a pipette, alongside a protein ladder (BioRad Precision Plus Dual Colour

Standard). SDS-PAGE gels are run in a gel tank at between 100-200V for 60-120 minutes under SDS running buffer.

Proteins were visualised using gel stain to observe total protein content, or Western blot to identify specific protein content. For total protein, gels were stained for 1hr with Coomassie Blue Stain (0.1% Coomassie Blue, 40% methanol, 10% acetic acid), after being rinsed in distilled water. Excess stain was removed by rinsing in distilled water, and destaining carried out in 20% methanol and 10% acetic acid solution.

2.1.12 Western blotting

Western blot transfer buffer (1x): 25mM Tris, 192mM glycine, 20% methanol

Western blotting follows separation of proteins on an SDS-PAGE gel. Gels for Western blotting were placed in transfer buffer, along with nitrocellulose membrane (GE Healthcare, 0.45µm pore size) and filter paper. The gel, membrane and filter paper were assembled in a Western blot cartridge using a Bio-Rad Criterion Blotter system, and submerged in transfer buffer. The transfer was carried out at 350mA for 90 minutes. The nitrocellulose membrane was subsequently washed in PBS for 5 minutes, and blocked in PBST buffer containing 5% milk or BSA and 0.5% Tween-20 for 1 hour. Following blocking the membrane was probed using various primary antibodies, in PBST with 1% milk or BSA. The primary antibody was incubated with the membrane overnight at 4°C. Following removal of the primary antibody, the membrane was washed three times for a duration of 5 minutes with PBST. The secondary antibody was added to PBST plus 1% milk or BSA, and incubated with the membrane in the dark. After 1-2 hours, the secondary antibody was removed, and the membrane washed with PBST three times for 5 minutes.

The washed membrane was incubated in 0.5ml ECL Western blot reagent (Amersham) for 60 seconds, and exposed to medical X-ray film (Fujifilm) in a sealed cassette for varying exposure

times. The film was then processed through a Western blot developer to produce the finished blot.

2.1.13 Immunofluorescence

For immunofluorescence, cells were cultured on 22x22mm glass coverslips placed in wells of a 6-well plate prior to seeding of cells. Cells were seeded on the coverslips and grown for 24 hours, treated through siRNA knockdown, transfection, irradiation or left untreated and grown for 24-72 hours to a confluence of approximately 75%. Following removal of culture medium, and three washes of 2ml PBS per well, were fixed by overlaying 1ml 4% PFA (paraformaldehyde) in PBStx on the coverslip in the well for 15 minutes at room temperature. Alternatively, 1ml ice-cold methanol was overlaid on the coverslip, and the cells fixed at -20°C for 15 minutes. The coverslips were subsequently washed for 5 minutes three times with 2ml PBS with constant swirling to remove the fixative from the well.

Cell permeabilisation was carried out through addition of 1.5ml 0.5% Triton X-100 in PBS for 30 minutes, and blocking by addition of 3% BSA in PBStx for 45 minutes, both with constant gentle mixing. Primary antibody was prepared by dilution in PBStx with 1% BSA. Coverslips were overturned onto 100µl primary antibody solution on the lid of the 6-well plate, and incubated from 1 hour to overnight in a humidified chamber at 4°C. The coverslips were then washed three times for 5 minutes in 2ml PBS for thorough removal of excess primary antibody. Secondary antibodies were diluted and applied to the coverslips in the same manner as primary antibodies, however the secondary antibodies were incubated in the dark so as to maintain intensity of the conjugated fluorophore. Incubation with secondary antibody was carried out for 1-2 hours, and followed by three washes of 5 minutes each in 2ml PBStx and a final wash in PBS.

Coverslips were removed from the 6-well plate using tweezers, and overturned onto 25µl VECTASHIELD mounting medium (Vector Laboratories) which contains DAPI stain at a

concentration of 1.5µg/ml. For prolonged storage, coverslips were sealed around the edge with nail varnish, and stored in the dark at 4°C.

Immunofluorescence was observed using a Nikon Eclipse TE200 fluorescence microscope with x20, x60 or x100 objectives. Microscope filters were used isolate emission of fluorescence within a selected wavelength range corresponding to the desired fluorophore, which prevents bleed-through of irrelevant fluorescent signal. Images were recorded using a Hamamatsu C4742-96-12G04 digital CCD camera, which has a cell size of 6.45µm, resulting in 0.0645µm/pixel at x100 objective and 0.1075 µm/pixel at x60 objective. Images were acquired using Volocity cellular imaging and analysis software (Perkin Elmer), and analysed using ImageJ.

Alternatively, an Applied Precision Deltavision deconvolution microscope was used to obtain 3D images. A UplanSApo 100x oil (NA 1.4) objective was used, with a standard filter set of DAPI (360/457); FITC (490/528); Rhodamine-TexasRed-PE (555/617). Images were recorded using a Photometrics CoolsnapHQ CCD camera (1392 x 1040; 6.45µm pixels), resulting in 0.0645µm/pixel at x100 objective. Z-slices were taken at 10µm increments unless otherwise specified. Image acquisition was carried out using softWoRx v6 software, and deconvolution was carried out in Resolve 3D software at recommended settings. Images were subsequently analysed using ImageJ.

Cells were scored after various treatments for various properties by looking at cells in randomly observed field of view across the slide to ensure no cell was scored multiple times. Quantification was repeated on multiple, independently prepared samples and slides.

2.1.14 *In situ* protein pre-extraction of adherent cells

Pre-extraction buffer: 60mM PIPES, 25mM Hepes, 10mM EGTA, 2mM MgCl₂, pH 6.8, with Triton X-100 added to a concentration of 0.5% prior to use.

In order to more accurately determine the fraction of membrane-bound protein by immunofluorescence, *in situ* pre-extraction is carried out on live glass-adherent cells to remove soluble protein prior to fixation and immunofluorescence. Culture medium was aspirated carefully from adherent cells, which were then gently washed twice with ice-cold TBS buffer. Ice-cold pre-extraction buffer was added to cells and incubated on ice for 5 minutes. Pre-extraction buffer was aspirated carefully from cells, which were then washed twice in ice-cold PBS prior to fixation as normal (Section 2.1.12), and subsequent immunofluorescence steps carried out as above.

2.1.15 Criteria for micronuclei scoring

In order to maintain a consistent scoring system, micronuclei were defined by a comprehensive set of criteria based on those used by Fenech *et al.* (2003). The key criteria are:

1. The size (diameter) of the micronucleus should not exceed 1/3 that of the primary nucleus;
2. The boundary of the micronucleus should be distinct from that of the primary nucleus – such that they do not overlap;
3. They micronucleus should not be linked or attached to the primary nucleus;
4. The micronucleus should have a similar intensity of DAPI staining to the primary nucleus;
5. The micronucleus should have a rounded or oval-shaped morphology.

2.1.16 MTT assay

MTT (3-(4,5-dimethylthiazol-2-yl)-2,5-diphenyltetrazolium bromide) is a yellow compound which is reduced to purple insoluble formazan by mitochondrial enzymes present in human cells. The MTT assay uses this reaction as carried out by growing human cells growing in a 96-well plate as a measurement of levels of cell metabolic activity within the well, which correlates to numbers of viable cells present. The amount of viable cells can be calculated

from the intensity of the purple colour following incubation with solvent to dissolve the formazan crystals.

Cells are plated in a 96-well plate 24 hours prior to transfection of siRNA. RNAi-mediated knockdown was allowed to proceed for between 1-6 days before addition of 50µl of 3mg/ml MTT (dissolved in PBS) to each well. Cells were incubated with MTT at 37°C for 3 hours, before removal of culture medium by aspiration. The remaining formazan precipitate was dissolved in 200µl DMSO and mixed to dissolve all purple dye crystals. Optical density (OD) measurements of the resulting solution were read using a Thermo Scientific Multiskan FC plate reader set at 540nm. In each experiment, six replicates of each condition were measured. Survival fractions were calculated by comparison of treatment conditions to non-targeting siRNA controls, and each assay was repeated three times to calculate averages and standard error.

2.1.17 Fluorescence-activated cell sorting (FACS)

Flow cytometry can be used to assess the properties of single cells, identifying cell shape and size as well as density. The use of fluorescent probes can be used to collect further information.

Sorting using propidium iodide staining of cell nuclei uses the stoichiometric nature of the dye-binding to stain the genomic content of the cell. The amount of DNA in a single cell is quantified via the brightness of the fluorescent signal, and used to estimate the phase of the cell cycle. Cells in G1 phase have half the DNA content of G2/M cells, with S-phase cells falling in between the two points. Apoptotic cells feature fragmented and degraded DNA, causing the fluorescence levels to fall in the sub-G1 region.

Cultured cells are transfected with siRNA, grown for 24-72 hours before being collected by mechanical scraping or trypsinisation. Cells floating in the culture medium were collected by centrifugation of the culture medium at 1500rpm for 3 minutes. Cell pellets were washed

three times with PBS, all centrifugation steps carried out at 1500rpm for 3 minutes. Cell pellets were resuspended in 1ml ethanol and left to incubate at -20°C for a minimum of 1 hour and a maximum of 1 week. In order to stain cells with propidium iodide, the ethanol was removed and cells washed with PBS. Cells were left to rehydrate in 1ml PBS for 1 hour at room temperature, before centrifugation and thorough aspiration of PBS. The cell pellet was resuspended in 500µl PI/RNase solution (18µg/ml PI, 8mg/ml RNase A) and incubated at 4°C for 90 minutes in the dark prior to analysis on the BD FACSCalibur.

2.1.18 Subcellular fractionation

Buffer A: 10mM Hepes (pH 7.9), 10mM KCl, 1.5m M MgCl₂, 0.34M sucrose, 10% glycerol. Triton X-100 was added to a final concentration of 0.1%, and one Roche cOmplete Protease Inhibitor Cocktail tablet was added per 10ml buffer prior to use.

Buffer B: 3mM EDTA, 0.2mM EGTA, 1 mM DTT. One Roche cOmplete Protease Inhibitor Cocktail tablet was added per 10ml buffer prior to use.

Subcellular fractionation was used to separate various fractions of a cell pellet, in order for them to be individually analysed and determine the subcellular location of specific proteins. Cells were resuspended in buffer A and incubated for 5 minutes on ice. Cells were then centrifuged at 4°C and 1500rpm for 5 minutes in order to pellet the whole cell nuclei. The supernatant, containing the cytosolic fraction, was removed from the pellet and saved. The whole cell nuclei were washed with ice-cold buffer A twice, each time being resuspended and re-pelleted at 1500rpm. The nuclei were then lysed in buffer B on ice for 5 minutes. The nuclei were centrifuged at 4°C and 1500rpm for 5 minutes to pellet the nuclear matrix, chromatin and associated protein fraction. The supernatant was also collected, containing the soluble nucleoplasmic protein fraction. These fractions were then analysed using SDS-PAGE and Western blotting.

2.2 Bacterial cell culture and DNA manipulation

2.2.1 Generation of HA-tagged CHMP7 plasmids

CHMP7 was cloned from cDNA using PCR to produce fragments for ligation into a pcDNA 3.1+ vector (ThermoFisher), which contains multiple restriction sites, as well as ampicillin/carbenicillin and Geneticin antibiotic resistance. A full vector map, alongside complete DNA and protein sequences for each construct, is included in Appendix 1.

Forward primer for both constructs – containing a BamHI restriction site, start codon, HA-tag, and residues 1-6 of CHMP7

5' – CTC GTC GGA TCC ATG TAT CCG TAT GAT GTG CCG GAT TAT GCG TGG TCC CCG GAG CGG GAG – 3'

Reverse primer for full-length CHMP7 construct – containing an EcoRI restriction site, stop codon, and residues 448-453 of CHMP7

5' – CTC GTC GAA TTC CTA CAA TGG CTT TAG AGT CGG – 3'

Reverse primer for N-terminal CHMP7 construct – containing an EcoRI restriction site, stop codon, and residues 221-226 of CHMP7

5' – CTC GTC GAA TTC CTA CCC TCG GGC AAA CTT CAC – 3'

Vector DNA digestion was carried out using BamHI and EcoRI restriction enzymes in a double digestion reaction in NEBuffer 3.1 (New England Biolabs). Plasmid DNA (1µg) was added to 1x NEBuffer 3.1 up to a volume of 48µl, prior to addition of 1µl EcoRI enzyme (New England Biolabs) and 1µl BamHI enzyme (New England Biolabs). The reaction mixture was incubated for 1 hour. Complete digestion was determined with agarose gel electrophoresis.

Vector and insert ligation was carried out using T4 DNA Ligase (New England Biolabs), with 1µl T4 DNA ligase added to 50ng vector DNA, 37.5ng insert DNA, 2µl T4 DNA ligase buffer (10x), with the reaction made up to 20µl with nuclease-free water. This reaction mixture was incubated for 1 hour at room temperature, prior to heat inactivation at 65°C for 10 minutes.

Ligated DNA was either used directly for bacterial transformation after being chilled on ice, or stored at -20°C for use at a later date.

2.2.2 Agarose DNA gels

TAE buffer (10x): 400mM Tris, 200mM acetic acid, 10mM EDTA.

DNA loading buffer (5x): 60% glycerol, 50mM EDTA, 0.25% bromophenol blue.

To prepare a 1% agarose gel, 1g of agarose powder is added to 100ml 1x TAE buffer, and dissolved by heating and stirring. Following complete dissolving of the agarose powder, 8µl ethidium bromide is added to the mixture, which is poured into a gel mould with a 15-well comb. The gel is left to set for 1 hour at room temperature, before being immersed in 1x TAE buffer in a Geneflow Multi Sub Maxi gel electrophoresis tank. The comb forming the wells in the gel is removed for application of the sample to be run, alongside 5µl HyperLadder DNA size ladder. The plasmid or digested DNA was mixed with 5x DNA loading buffer and ddH₂O to a total volume of 20µl. Gel running is carried out at 100V for 1-2 hours depending on the separation required. The gel was visualised using a UV transilluminator and imaged using the Kodak Electrophoresis Documentation and Analysis System 120, and the Kodak 1D image analysis software.

2.2.3 Bacterial cell strains

E. coli JM109 (DE3) or DH5α (Promega) strains were used for all applications involving cloning and general transformation and growth of plasmids.

2.2.4 Bacterial media and agar

LB medium (1 litre): 10g bacto-tryptone, 10g yeast extract, 5g NaCl.

2xYT medium (1 litre): 16g bacto-tryptone, 10g yeast extract, 5g NaCl.

LB agar (1 litre): LB medium with the addition of 15g agar.

LB medium was used for the growth of bacteria, with the nutritionally richer 2xYT medium used for encouraging a higher cell density in the culture. LB agar was used for growth of

transformed cells on agar plates. All media and agar were autoclaved at 115°C for 15 minutes following preparation, and kept sealed until use. Antibiotics were added to the medium following autoclaving, with ampicillin or carbenicillin used at a working concentration of 100µg/ml. Agar plates are prepared by pipetting of 20ml liquid agar into a Petri dish under sterile conditions, which are left to set in sterile air, under the flame of a Bunsen burner. Antibiotic is added either to the agar prior to pouring of the plates, or applied to the surface of the agar prior to use. For growth of transformed *E. coli*, 100µg/ml ampicillin was incorporated into the agar.

2.2.5 Bacterial transformation, culture, and plasmid purification

Plasmid DNA was transformed into DH5α competent cells by addition of 1-5µl DNA at a concentration of 1pg-100ng to 50µl competent cells thawed for 5 minutes on ice. The plasmid and cells were mixed and incubated on ice for 30 minutes before. The cells were then subjected to heat shock at in a water bath at 42°C for 30 seconds. Cells were returned to the ice for 2 minutes, before being spread on the surface of a prepared, ampicillin-containing LB agar plate. The agar plates were incubated at 37°C for 24 hours to allow growth of successfully transformed cells into colonies.

Starter cultures consisting of 5-10ml LB or 2xYT broth supplemented with antibiotics were inoculated with a single colony, and incubated for 16 hours at 37°C. The culture was centrifuged at 4000rpm to obtain a cell pellet. Plasmid DNA was extracted from cell pellets using a QIAprep Spin Miniprep Kit (QIAGEN), and eluted into 50µl ddH₂O. Concentration of the eluted plasmid was measured using a NanoDrop 2000 spectrophotometer, and sequence verification was carried out by The University of Sheffield Core Genomic Facility.

Chapter Three

CHMP7 depletion impairs nuclear envelope organisation and integrity

Contents

	Page
3.1 Introduction	60
3.1.1 Chapter Summary	60
3.1.2 Human cell lines used in this study	60
3.1.3 An introduction to nuclear structure and function	61
3.1.4 Background to the cell cycle and regulatory checkpoints	63
3.2 Results	65
3.2.1 Optimisation of CHMP7 and VPS4 siRNA knockdown	65
3.2.2 CHMP7 depletion is toxic and causes reduced cell viability and proliferation	68
3.2.3 Investigation of the toxicity of CHMP7 depletion	70
3.2.4 CHMP7 depletion causes a reduction in mitotic cells, specifically those found in cytokinesis	70
3.2.5 CHMP7 depletion results in moderate accumulation of cells in G1 phase	71
3.2.6 CHMP7 depletion results in increased apoptosis	73
3.2.7 CHMP7 depletion results in generation of multinucleated cells	75
3.2.8 CHMP7 depletion causes abnormalities of nuclear shape	77
3.2.9 CHMP7 depletion causes defects of nuclear envelope structure, which do not appear in VPS4-depleted cells	79
3.2.10 Nuclear defects in CHMP7-depleted cells display loss of nuclear envelope organisation	81
3.2.11 HeLa M cells display a unique nuclear fragmentation phenotype upon CHMP7 depletion	83
3.2.12 Large lamina ruptures, protruding chromatin and mislocalised nuclear pore complexes are observed in CHMP7-depleted HeLa M nuclei	86
3.2.13 CHMP7 knockdown causes mislocalisation and accumulation of cytoplasmic NPC proteins	87
3.2.14 CHMP7 knockdown causes an increase in DNA damage	89
3.2.15 CHMP7 depletion compromises centrosomal cohesion and positioning in interphase HeLa, but not U2OS, cells	90
3.2.16 CHMP7-depleted cells demonstrate loss of nuclear compartmentalisation	95
3.3 Discussion	97
3.3.1 Discussion of the mitotic role of CHMP7	98
3.3.2 The effect of CHMP7 knockdown on nuclear envelope organisation and integrity	104
3.3.3 A role for CHMP7 in nuclear pore complex organisation	107

List of Figures

Figure	Title	Page
3.1	A diagram of the nuclear envelope and associated cellular components	62
3.2	Cell cycle progression, regulatory checkpoints, and centrosome maturation	62
3.3	Confirmation and optimisation of CHMP7 and VPS4 depletion by siRNA using Western blots	66
3.4	CHMP7 depletion results in decreased cell viability and proliferation rates in HeLa, HeLa M and U2OS cells	69
3.5	CHMP7 depletion causes a decrease in mitotic cells and some accumulation in G1	72
3.6	Depletion of CHMP7 results in an increase in apoptotic cells as observed by immunofluorescence	74
3.7	Depletion of CHMP7 results in an increase in multinucleated cells as observed by immunofluorescence	76
3.8	CHMP7 depletion causes abnormalities of nuclear morphology	78
3.9	CHMP7 depletion causes nuclear lamina defects	80
3.10	The relationship of nuclear pore complexes to nuclear envelope abnormalities in HeLa cells	83
3.11	CHMP7-depleted HeLa M cells display a dramatic loss of nuclear envelope integrity and organisation not observed in other cell lines	84
3.12	Nuclear pore complex proteins are found in cytoplasmic accumulations following CHMP7 knockdowns	88
3.13	The effect of CHMP7 knockdown on DNA damage as marked by γ H2AX foci	90
3.14	Changes in centrosome positioning and separation in interphase cells following CHMP7 knockdown	92
3.15	The percentage of cells in which PML is mislocalised into the cytoplasm in HeLa and U2OS cell lines	95
3.16	A model of the cell cycle progression of CHMP7-depleted cells	99
3.17	A model of the defects caused by depletion of CHMP7	100
3.18	A model to show development of nuclear defects in CHMP7-depleted cells	102

3.1 - Introduction

3.1.1 Chapter Summary

The association of the CHMP7 protein with the ESCRT-III complex was established by Horii *et al.* (2006), however, little work has since been carried out focused on characterising the role of this subunit. Based on general observations made by Cleasby (PhD thesis, 2013) in the HeLa M cell line, we hypothesise that CHMP7 depletion causes problems with cell viability, resulting in cell dysfunction and death. Cleasby observed that CHMP7 localises to interphase nuclei of HeLa M cells upon depletion of VPS4, in the form of bright, discrete foci, leading us to hypothesise a nuclear role for the CHMP7 protein in conjunction with the ESCRT-III complex.

This chapter focuses on using siRNA-mediated depletion of CHMP7 in various cell lines as a tool to allow investigation of the impact of CHMP7 loss on cell viability, thereby giving an insight into its importance and function. Data is presented on the toxicity of the CHMP7 knockdown, followed by elucidation of the effect on cell cycle progression, cellular and nuclear aberration, nuclear envelope structure and function, and genomic integrity. CHMP7 knockdown was found to be toxic in all tested cell lines, resulting in loss of proliferation and increased apoptosis. Aberrances found to contribute to this lethality include G1 phase cell cycle arrest, multinucleation, an increase in DNA damage, and loss of nucleocytoplasmic compartmentalisation due to nuclear envelope holes and DNA herniation. Further nuclear disorganisation was evident from nuclear pore complex mislocalisation, and centrosomes which displayed both aberrant cohesion and loss of association with the nuclear envelope.

3.1.2 Human cell lines used in this study

The key cell lines used in this study are HeLa, HeLa M and U2OS, all of which are adherent human cancer cell lines. HeLa is a standard, well-characterised cell line used for research, derived from a human cervical tumour. HeLa M is a subclone derived from the original HeLa

line, which displays several differences including an increased size and flattened shape ideal for microscopy and imaging. They also display a tendency to grow closer together and to migrate less across the growth surface, forming a characteristic monolayer from which the “M” designation is derived. U2OS is an osteosarcoma line known for their regular, rounded nuclei and suitability for immunofluorescent microscopy.

3.1.3 An introduction to nuclear structure and function

In order to investigate the effect of CHMP7 depletion on nuclear function, it is important to understand nuclear composition and morphology, and the relationship between various components in the nuclear envelope and the cellular architecture (Figure 3.1). The nuclear membrane which surrounds the nuclear material consists of an inner membrane (INM), which interacts with the nuclear interior and chromatin, and an outer membrane (ONM), which is continuous with the endoplasmic reticulum (ER). The region between the inner and outer membranes is known as the perinuclear space, which is continuous with the ER lumen.

The nuclear lamina is a dense meshwork of lamin proteins which forms within the inner nuclear membrane, which provides structural and mechanical support to the nucleus. B-type lamins are intermediate filament proteins, constitutively expressed in all cell types, which are anchored to the inner nuclear membrane through the Lamin B receptor (LBR). Lamin A/C is derived from two differently spliced isoforms of the developmentally regulated LMNA gene. More than 10 distinct laminopathies are caused by mutations in Lamin A/C (Broers *et al.*, 2006), and deficiency of Lamin A/C causes an increase in misshapen nuclei (Broers *et al.*, 2004). While Lamin B plays a key role in nuclear integrity, with its depletion leading to nuclear rupture and blebbing, work by Lammerding *et al.* (2006) shows that the mechanical stiffness of the nucleus is dependent on the Lamin A/C content of the nuclear lamina.

Nuclear pore complexes (NPCs) are large complexes of formed from multiple copies of approximately 30 nucleoporin subunits, which form a pore channel structure. Approximately

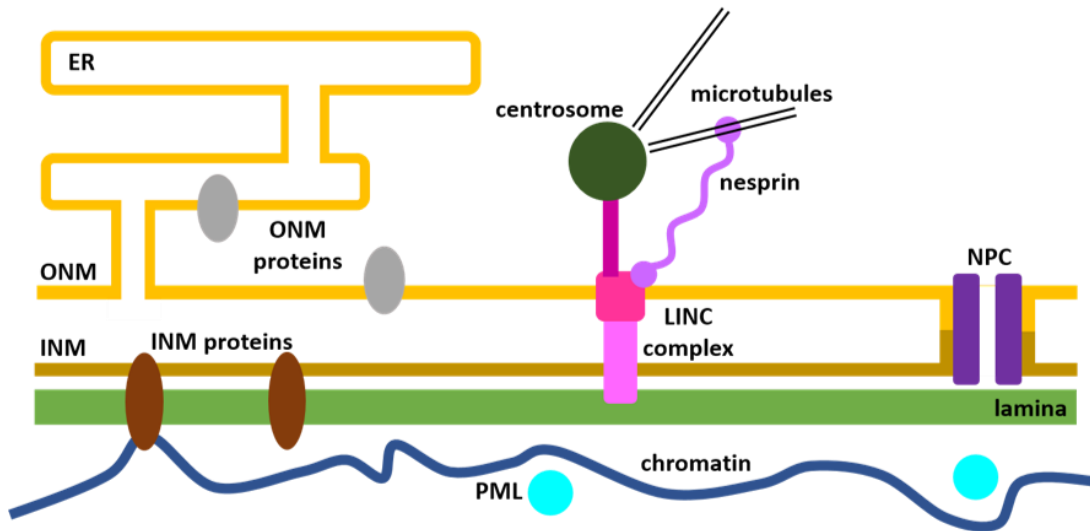


Figure 3.1. A diagram of the nuclear envelope and associated cellular components

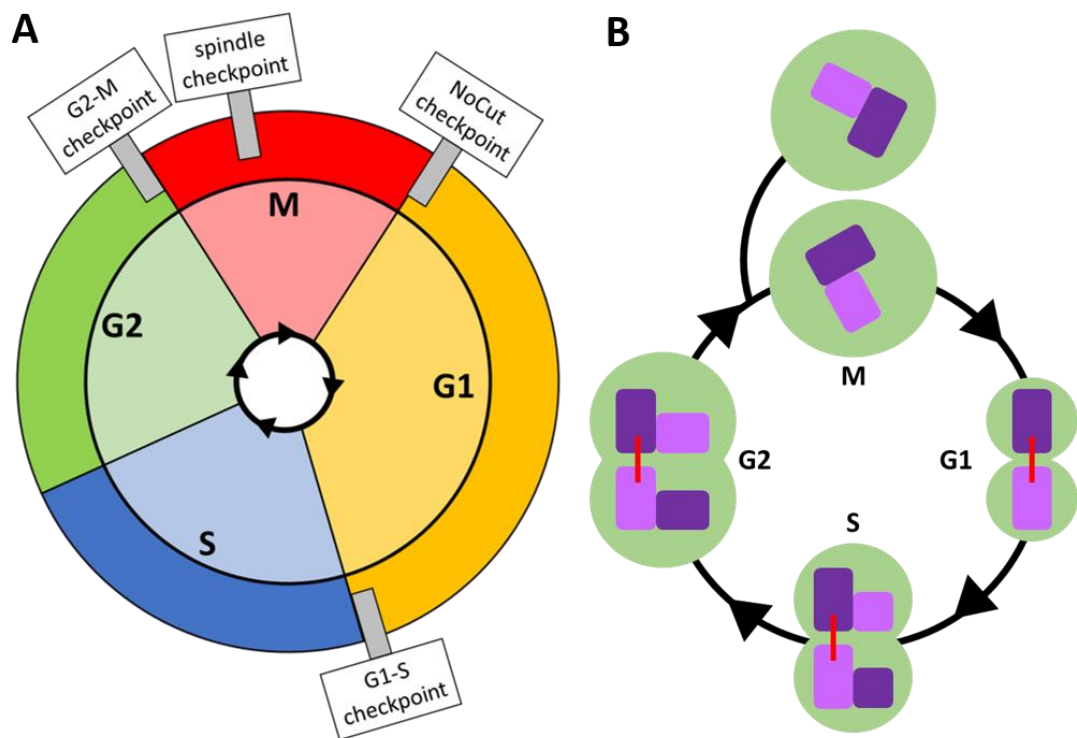


Figure 3.2. Cell cycle progression, regulatory checkpoints, and centrosome maturation

a) A diagram of the cell cycle, showing the location of key regulatory checkpoint events, at which continuation through the cell cycle is dependent on certain conditions. b) Centrosome cohesion, duplication, and separation throughout the cell cycle.

2000-3000 are found per nucleus, anchored in the nuclear lamina, spanning the double nuclear membrane and creating selective channels allowing for bidirectional transport. INM proteins of the LEM family, which include lamin-associated polypeptide 2 (LAP2) and LBR, are integral INM structures which can interact with the nuclear lamina as well as chromatin-associated proteins and DNA itself. A mechanical connection between the cytoskeleton and the nuclear interior is mediated by the nuclear envelope, with the LINC (linker of nucleoskeleton and cytoskeleton) complex forming a nuclear envelope bridge connecting the nuclear lamina to the cytoplasm, where it can interact through a variety of linker proteins to cytoskeletal components – actin, microtubules and centrosomes (Chang *et al.*, 2015).

3.1.4 Background to the cell cycle and regulatory checkpoints

The eukaryotic cell cycle is the process by which cell contents are duplicated and segregated equally between two daughter cells (Figure 3.2a). DNA replication occurs in a specific period of the cell cycle, synthesis or S-phase, with chromosome segregation and cell division occurring in mitosis, also known as M-phase. These key events are separated by two gap phases, G1 and G2, during which cells grow, migrate, and synthesise proteins and RNA in preparation for DNA replication and cell division. The cell cycle is controlled by cyclins and the cyclin-dependent kinases (CDKs), the expression of which are modulated throughout the cell cycle to induce phase-specific phosphorylation events, in order to activate functional proteins in an appropriate order. Eukaryotic cells progress through the cell cycle by passing through tightly regulated transition points to ensure correct temporal and spatial control of events. These checkpoints ensure completion of all necessary processes, and the integrity of cellular components before continuing to the next stage. Key checkpoints exist at the G1-S transition, the G2-M transition, and the spindle checkpoint at the metaphase-anaphase transition in mitosis. For the purposes of this study, the previously discussed NoCut checkpoint (Section 1.3.5), a checkpoint controlling the point of abscission for cell division, is also important due to its relationship to ESCRT-III proteins.

Cells remain in G1 until the transition into S-phase commits the cell to progression through a cell division cycle. G1-S transition requires DNA integrity to be assessed, ensuring any DNA lesions have been repaired prior to entry into the replication phase. Attempts to replicate damaged regions of DNA can lead to stalled replication forks, incompletely replicated DNA or double-stranded DNA breaks, all of which can further compromise genomic integrity (Satyanarayana *et al.*, 2008). The G2-M checkpoint also ensures completion of DNA damage repair prior to initiation of mitosis, to ensure that chromosomes are whole and will be correctly segregated in mitosis, with abrogated G2-M checkpoints leading to genome instability and increased cancer risks (Lobrich and Jeggo, 2007). The spindle checkpoint halts mitosis in metaphase until it has been determined that all chromosomes are correctly attached via their kinetochores to the opposing spindle poles (Lara-Gonzalez *et al.*, 2012). Once this condition has been satisfied, the block is removed and the cell progresses into anaphase, and the separation of chromosomes.

Centrosomes are the centres of microtubule organisation within the cell, and form the basis of the two mitotic spindle poles (reviewed in Conduit *et al.*, 2015). A fully-formed mitotic centrosome consists of two (mother and daughter) centrioles, engaged at right-angles to each other (Figure 3.2b), surrounded by dense proteinaceous pericentriolar material (PCM). Following mitosis, the mother and daughter centrioles disengage, but remain connected by a centrosomal linker. In S-phase, centrosomal duplication occurs, generating new daughter centrioles at a right-angle to the existing mother centrioles. During G2, centrosomes accumulate PCM, until the centrosomal linker is broken upon entry into mitosis, whereupon they segregate to opposite sides of the cell to form the mitotic spindle. Throughout interphase, centrosomes are tethered to the nuclear envelope through the LINC complex until the breakdown of the nuclear envelope and entry into mitosis.

3.2 - Results

3.2.1 Optimisation of CHMP7 and VPS4 siRNA knockdown

Three sequences for siRNA transfection to knockdown CHMP7 were designed, designated CHMP7-1, CHMP7-2 and CHMP7-3 (more details can be found in Section 2.1.6). As a control for siRNA transfection, ON-TARGETplus non-targeting control siRNA (#1; Dharmacon) was used, hereafter referred to as the NT-control. CHMP7-1 and CHMP7-3 were used for the majority of experiments due to their consistency of knockdown across the three used cell lines, HeLa, HeLa M and U2OS.

HeLa cells were transfected with either 5, 10 or 20nM siRNA for 24, 48 or 72 hours, before the cells were collected, lysed, and run on a Western blot. Transfection of the non-targeting control siRNA showed no knockdown effect on CHMP7. All CHMP7 siRNA transfection conditions showed significant, though not complete CHMP7 depletion, even at the greatest level of transfection (Figure 3.3a). However, it was found that the rabbit antibody used for the Western blot in Figure 3.3a detects two very closely-sized bands, one of which is unaffected by cell transfection with CHMP7-targeting siRNA.

This distinction is made in Figure 3.3c, in which the mouse CHMP7 antibody is compared to the rabbit antibody, showing the disparity in band patterns, particularly in blotting of the U2OS cell line. Therefore, this shows that the mouse antibody is the most appropriate for Western blotting to unambiguously detect CHMP7. Transfection of CHMP7-targeting siRNA was also optimised for the U2OS and HeLa M cell lines (Figure 3.3c and Figure 3.3d), with knockdown efficiencies as measured by the mouse antibody between 85 and 100%.

In order to observe the effect of the double knockdown between CHMP7 and VPS4, HeLa cells were transfected simultaneously with 20nM CHMP7-1 or CHMP7-3 alone or in combination with 3nM VPS4 siRNA and collected after 24, 48 or 72 hours post-transfection

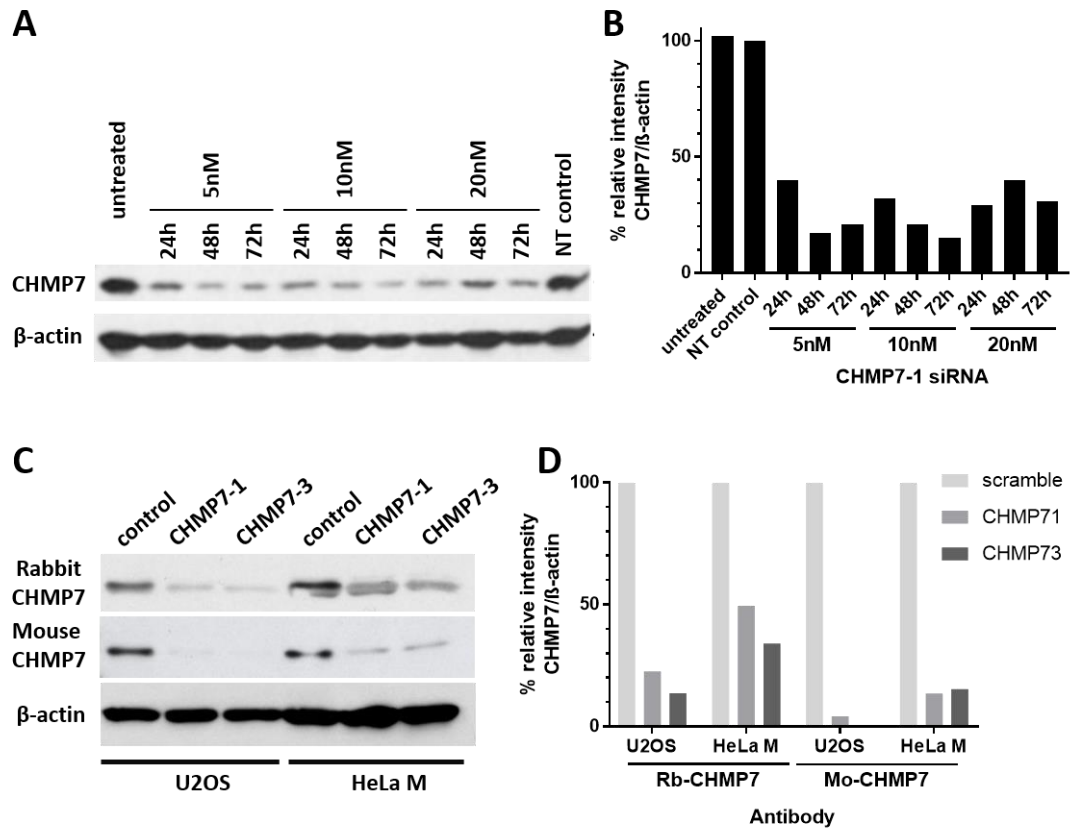


Figure 3.3. Confirmation and optimisation of CHMP7 and VPS4 depletion by siRNA using Western blots

a) Western blot showing knockdown of CHMP7 in HeLa cells by the CHMP7-1 siRNA sequence. HeLa cells were treated with either 5, 10 or 20nM siRNA for 24, 48 and 72 hours. The samples were blotted for CHMP7 using the rabbit-derived antibody, and β -actin antibody as a loading control. **b)** Quantification of the intensity of CHMP7 bands compared to its corresponding β -actin band was calculated using the Gel Analyzer feature of ImageJ, and plotted relative to the NT control lane. **c)** Western blot showing knockdown of CHMP7 in U2OS and HeLa M cells by the two key CHMP7 siRNA sequences used in this study. U2OS cells were treated with 10nM siRNA, and HeLa M cells with 20nM for siRNA, both for 48 hours. The same samples were blotted using both the rabbit and mouse-derived anti-CHMP7 antibodies. The rabbit antibody detects two very closely spaced bands, the uppermost (larger) of which is affected by the CHMP7 siRNA. **d)** Quantification of CHMP7 knockdown. The intensity of the CHMP7 band compared to the β -actin band from the Western blot was quantified using the Gel Analyzer feature of ImageJ, and plotted relative to the NT control lane.

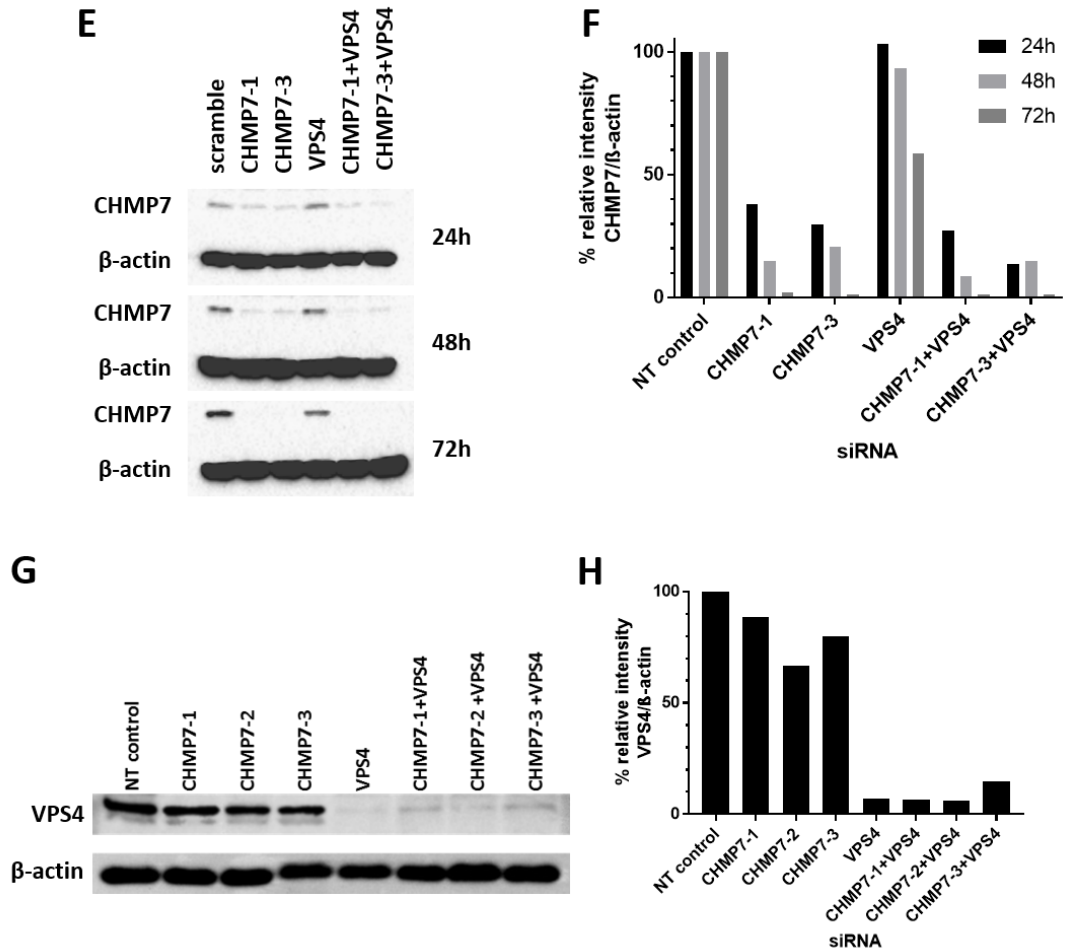


Figure 3.3 (continued)

e) Western blot showing knockdown of CHMP7 and VPS4 individually and in combination in HeLa cells at 24, 48 and 72 hours post-transfection. The samples were blotted with the mouse-derived anti-CHMP7 antibody. **f)** Quantification of the Western blot in (e). The intensity of the CHMP7 band compared to the β -actin band from the Western blot was quantified using the Gel Analyzer feature of ImageJ, and plotted relative to the NT control lane. **g)** Western blot showing the levels of VPS4 (rabbit-derived anti-VPS4A antibody) present in samples depleted of CHMP7 and VPS4 individually and in combination in HeLa cells at 48 hours post-transfection. **h)** Quantification of the Western blot in (g). The intensity of the VPS4 band compared to the β -actin band from the Western blot was quantified using the Gel Analyzer feature of ImageJ, and plotted relative to the NT control lane.

(Figure 3.3e and Figure 3.3f). Using the mouse antibody here shows effective CHMP7 knockdown using both sequences at 48 and 72 hours post-transfection, both alone and in combination with CHMP7. However, 72 hours following VPS4 knockdown, the level of CHMP7 reduced significantly to 58% of the control condition. This may be related to the high levels of cell death 72 hours post VPS4 siRNA transfection, or a more direct mechanism.

Knockdown of VPS4 was carried out using a SMARTpool of siRNA sequences targeting both VPS4A and VPS4B isoforms. Knockdown is carried out at an siRNA concentration of 3nM, owing to the highly toxic nature of the depletion. Figures 3.3g and Figure 3.3h demonstrate the efficacy of the VPS4 knockdown alone and in combination with the CHMP7-targeting siRNA sequences at a concentration of 20nM. When compared to the NT-control, the knockdown was 93% complete in the VPS4-only knockdown, and between 86% and 94% in the combined CHMP7 and VPS4 knockdowns.

Based on the above experiments, a 48-hour knockdown at 20nM with both CHMP7 siRNA, and 3nM VPS4 siRNA was determined to be the optimal transfection conditions and used in all subsequent experiments (unless otherwise stated) as this gives a good compromise between cell death and effective knockdown.

3.2.2 CHMP7 depletion is toxic and causes reduced cell viability and proliferation

In order to characterise the importance of CHMP7 in the ability of cells to grow and function, an MTT assay was used to assess the normal functioning of cellular metabolism. MTT assays utilise the ability of the cells to metabolise yellow MTT into purple formazan to determine the levels of viable cells. CHMP7 and VPS4 knockdowns, both alone and in combination, were carried out on HeLa, HeLa M and U2OS cells, which were analysed by MTT assay at 2, 4 and 6 day time points. Figure 3.4 shows the results normalised to the NT-control condition.

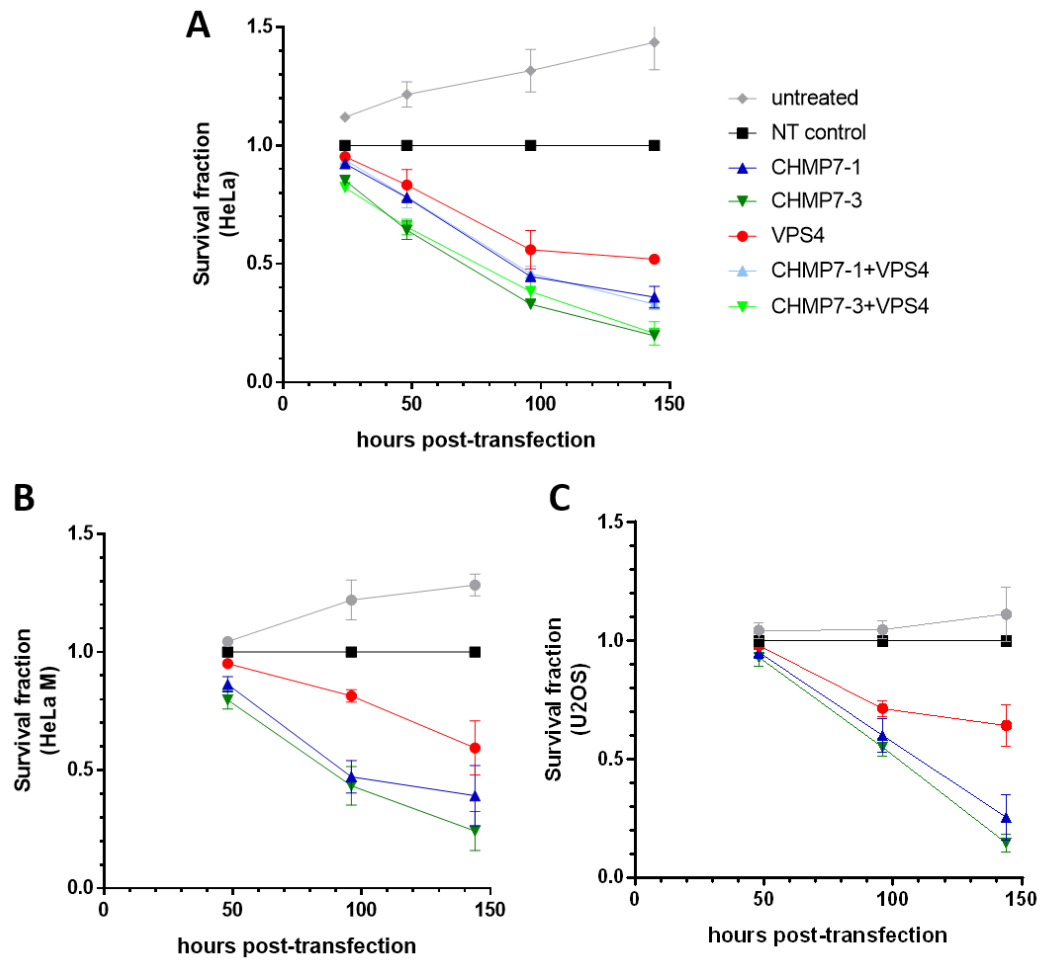


Figure 3.4. CHMP7 depletion results in decreased cell viability and proliferation rates in HeLa, HeLa M and U2OS cells

Results of MTT assay following knockdown of CHMP7 and VPS4 knockdown over the course of 6 days following transfection with 20 μ M of siRNA. Graphs are shown for **a)** HeLa, **b)** HeLa M and **c)** U2OS cell lines. Six replicates were performed for each timepoint, and averages and standard error are shown for three independent repeats.

The results demonstrate an effect on cell growth for both VPS4 and CHMP7 knockdowns, resulting in a significant decrease in proliferation in all cell lines. At 6 days post-transfection, rates of viability are at 15-36% of those observed in NT control treated cells, indicating either cell death or inhibition of growth. The double knockdowns (VPS4 and CHMP7) carried out in HeLa cells showed similar results to those of CHMP7 alone, showing that the addition of the VPS4 knockdown to the CHMP7 knockdown does not cause any additional deleterious effect on cell viability. The VPS4 knockdown alone shows a substantial decrease in cell viability, resulting in 52-64% of cells surviving compared to the control experiments. It should be remembered that transfection with VPS4 siRNA was carried out at a 3nM concentration, which is at the lowest end of recommended knockdown conditions, due to the severe toxicity of this knockdown.

3.2.3 Investigation of the toxicity of CHMP7 depletion

Loss of viability as measured by MTT assay can be caused by either active cell death, or by cell cycle arrest. In order to determine whether CHMP7 knockdown is directly cytotoxic, or causes inhibition of proliferation, cell cycle analysis using immunofluorescence, cell cycle profiling by FACS and quantification of apoptosis experiments were carried out. Profiling using FACS allows observation of changes in the broad phases of the cell cycle: G1, S and G2/M. FACS also collects information on apoptotic cells, in which DNA has been cleaved into fragments by apoptotic processes, in the subG1 category. Scoring using immunofluorescence allows finer observation and quantification of cells in different phases of mitosis or in the process of apoptosis.

3.2.4 CHMP7 depletion causes a reduction in mitotic cells, specifically those found in cytokinesis

In order to observe the progress of mitosis, HeLa cells were stained with DAPI and an antibody which specifically recognises phosphorylated Aurora kinases (pAuk). The Aurora

kinases are modified in a cell cycle-dependent manner and play a vital role in regulating mitosis, and as part of this function, localise specifically to different cellular structures as mitosis progresses. This antibody identifies the location of the centrosomes from the onset of prophase, and through anaphase. Phosphorylated Aurora kinase B accumulates at the cleavage plane as the furrow develops, and accumulates at the cytokinetic midbody as it forms. Mitotic cells were classified into interphase, prophase, metaphase, anaphase, telophase, or cytokinesis based on the subcellular distribution of pAuk following transfection (Figure 3.5a) with either NT-control, CHMP7-1, CHMP7-3 or VPS4 siRNA for 48 hours (Figure 3.5b). CHMP7 knockdown causes a significant reduction in the number of cells in mitosis, from 5.5% in NT-control cells, to 3.3 (CHMP7-1) and 4.1% (CHMP7-3). This difference appears to be mostly accounted for by a reduction in cytokinetic cells in CHMP7 knockdown cells when compared to control, with other phases of the cell cycle showing no significant difference between control and depleted cells.

3.2.5 CHMP7 depletion results in moderate accumulation of cells in G1 phase

FACS (fluorescence-assisted cell sorting) was used to further understand the difference in the cell cycle profile of CHMP7-depleted cells when compared with control, giving us insight into the fate of CHMP7-depleted cells. HeLa cells were transfected with either NT-control, CHMP7-1, CHMP7-3 or VPS4 siRNA, and both cell culture-suspended and adherent cells were collected at 24 and 48 hours post-transfection. The DNA-binding dye propidium iodide (PI) was used to stoichiometrically stain the genomic content of a cell and allow data to be gathered to indicate the cell cycle phase of each cell. Flow cytometric analysis of the cell cycle allows for quantification of thousands of cells from a sample condition; here, at least 10000 cells were analysed per sample.

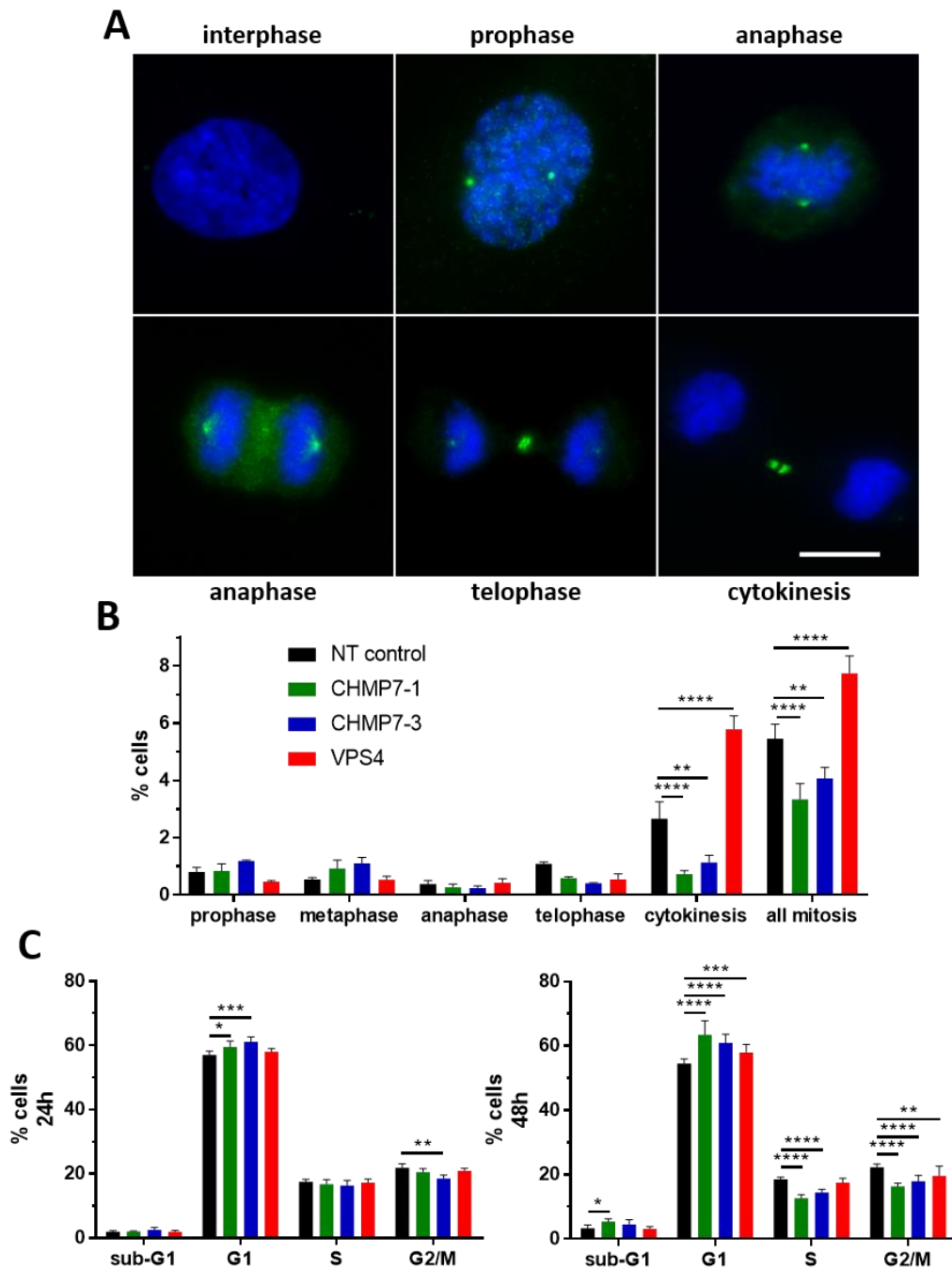


Figure 3.5. CHMP7 depletion causes a decrease in mitotic cells and some accumulation in G1

HeLa cells were stained to show phospho-Aurora kinases (pAuk) and counterstained with DAPI. **a)** pAuk staining was used to determine the stage of mitosis in the fixed cells. Scale bar represents 10 μ m. **b)** HeLa cells stained as above were scored, and the percentage of all cells observed in each phase of mitosis are shown. A minimum of 1000 cells were scored for each condition across three repeats, and standard error is shown. **c)** FACS analysis of HeLa cells depleted of either CHMP7 or VPS4 at 24 and 48 hours following siRNA transfection. Averages and standard error of three independent repeats are shown. Results were analysed using a two-way ANOVA with Dunnett's *post hoc* test compared to controls.

An effect can already be observed following transfection of CHMP7 siRNA after 24 hours, which agrees with the MTT assay observation that differences in cell viability were observed after only 24 hours in HeLa cells (Figure 3.5c). In NT-control populations, 57.0% cells are in G1. Depletion of CHMP7 causes a small significant increase in G1 cells, to 59.6% (CHMP7-1) and 61.2% (CHMP7-3). CHMP7-3-depleted population also show a significant decrease in the G2/M fraction of cells from 21.9% (NT-control) to 18.5% (CHMP7-3). This effect develops more strongly in the 48h post-transfection cells; from a NT-control average of 55.9% cells in G1, this increases to 58.3% (CHMP7-1) and 59.5% (CHMP7-3). Cells in S-phase and G2/M show significant reductions in their proportion in the CHMP7-depleted cell populations, and more subG1, or apoptotic cells, are detected. Taken together, the FACS analysis of CHMP7-depleted cells indicates a perturbation of the cell cycle, either due to a disruption or slowing of the cell cycle, or arrest in the G1 phase. If the FACS experiment were carried out on cells 6 days post-transfection, to correlate with the MTT assay, this profile may show a larger increase in this direction. However, due to the loss of cells in the knockdown conditions compared to control populations, too few cells could be collected at the 72h timepoint and beyond for analysis by FACS.

However, this small increase in apoptotic cells shown by FACS is not enough to account for the reduction of cell viability seen by MTT assay at 48 hours in HeLa cells (Figure 3.4a), implying that cell cycle arrest, resulting in lack of proliferation, may play a role in the deleterious effects of CHMP7 knockdown.

3.2.6 CHMP7 depletion results in increased apoptosis

Apoptosis is characterised by aggregation of chromatin and condensation of the nucleus, followed by nuclear fragmentation, phenotypes which can be determined by DAPI staining. Nuclei condense and become smaller and fluoresce more brightly due to the condensation of chromatin (Figure 3.6a). DAPI fluorescence was used to categorise those cells which were

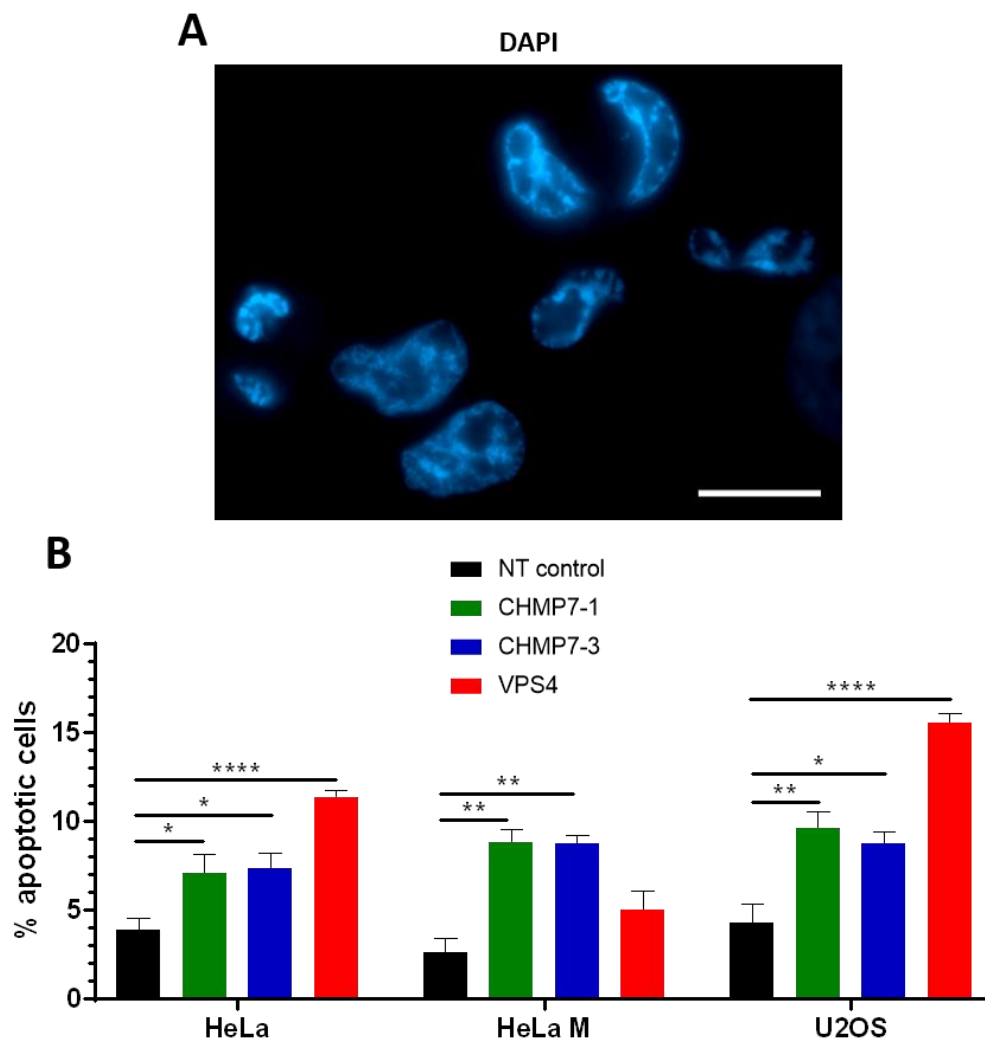


Figure 3.6. Depletion of CHMP7 results in an increase in apoptotic cells as observed by immunofluorescence

a) Examples of apoptotic HeLa cells stained with DAPI. Scale bar represents 10 μ m. **b)** Cells were transfected with either NT control, CHMP7 or VPS4 siRNA for 48h. HeLa, HeLa M and U2OS cells were scored based on the nuclear morphology (a minimum of 600 cells were scored per condition). Averages and standard error of three independent repeats are shown. Results were analysed using a one-way ANOVA with Dunnett's *post hoc* test compared to controls.

undergoing apoptosis, and scoring was carried out in HeLa, HeLa M and U2OS cells (Figure 3.6b) based on morphological changes to the nucleus. Cell cycle analysis by FACS carried out previously demonstrates a small increase in subG1 cells in CHMP7-depleted HeLa cells, which correspond to dead cells.

HeLa M cells transfected with either CHMP7 siRNA for 48 hours displayed a significant increase in apoptotic cells, from 2.6% (NT-control) to 8.8% (CHMP7-1) and 8.7% (CHMP7-3). U2OS cells also showed a significant increase, from an 4.3% in control cells, to 9.6% (CHMP7-1) and 8.7% (CHMP7-3). HeLa cells showed a slight but significant increase in apoptotic cells following the CHMP7 knockdowns, from 3.9% (NT-control) to 7.1% (CHMP7-1) and 7.3% (CHMP7-3). It should be considered that apoptotic cells shrink and condense, eventually losing their adherence to the glass substrate, becoming suspended in the culture medium prior to fixation. These cells are not scored using this method, but are accounted for in the subG1 fraction of the FACS profile.

3.2.7 CHMP7 depletion results in generation of multinucleated cells

Multinucleation is a sign of cytokinesis failure, whereby following chromatin replication and segregation into two daughter nuclei, the normal progression of cytokinesis is inhibited. This could occur as a failure to initiate furrow ingression, spindle-midzone defects, or activation of the NoCut pathway (Norden *et al.*, 2006) leading to furrow regression and resulting in a multinucleated cell.

HeLa, HeLa M and U2OS cells were co-stained with DAPI and an antibody against β -tubulin, in order to delineate individual cell boundaries. Cells in which more than one full-sized nucleus was observed was classified as multinucleated (Figure 3.7a). HeLa cells transfected with either CHMP7 siRNA for 48 hours displayed a significant increase in multinucleated cells (Figure 3.7b), from 1.9% to 8.5% (CHMP7-1) and 8.9% (CHMP7-3). HeLa M cells showed an increase from 0.9% to 18.5% (CHMP7-1) and 18.3% (CHMP7-3). U2OS cells

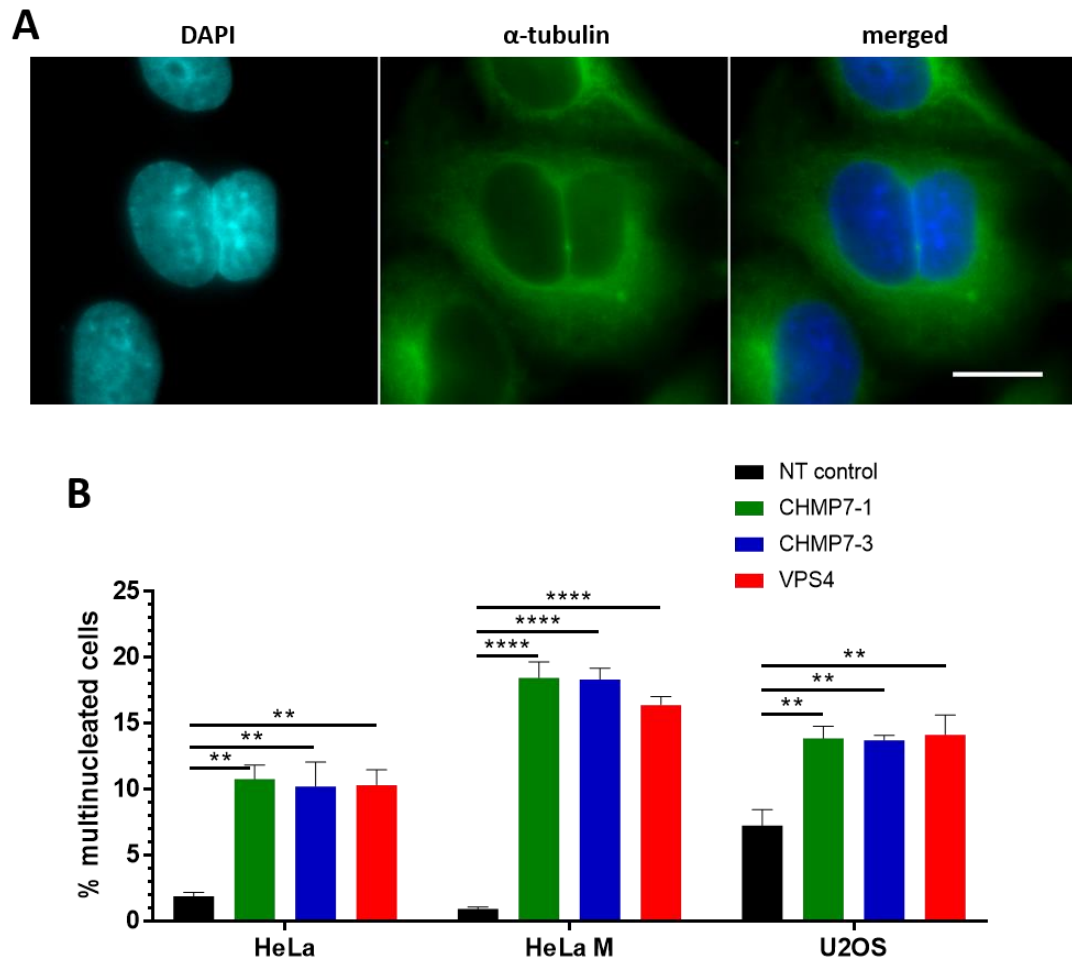


Figure 3.7. Depletion of CHMP7 results in an increase in multinucleated cells as observed by immunofluorescence

a) Example of a multinucleated HeLa cell stained to show DAPI and β -tubulin. Scale bar represents $10\mu\text{m}$. **b)** Cells were transfected with either NT control, CHMP7 or VPS4 siRNA for 48h. HeLa, HeLa M and U2OS cells were scored based on the presence of more than one full sized nucleus within the cell (a minimum of 500 cells were scored per condition). Averages and standard error of three independent repeats are shown. Results were analysed using a one-way ANOVA with Dunnett's *post hoc* test.

also showed a significant increase, from an higher baseline of 7.2% in control cells, to 13.9% (CHMP7-1) and 13.7% (CHMP7-3). VPS4 knockdown caused an increase in multinucleation in all cell lines, via a known mechanism whereby VPS4-depleted cells are unable to complete cytokinesis.

3.2.8 CHMP7 depletion causes abnormalities of nuclear shape

In order to determine the nature of the cellular changes which lead to the deleterious effect of CHMP7 knockdown, the effect of CHMP7 depletion on nuclear integrity was investigated. A healthy cell nucleus has a regular, smooth circular or oval shape, with changes in the shape indicative of various pathologies. Nuclear deformation can occur due to external mechanical stresses, including the extracellular environment as well as cytoskeletal pressures. The ability of the nucleus to retain its normal shape is determined by the stiffness or flexibility of the nuclear structure, determined by the nuclear membrane and lamina (Lammerding *et al.*, 2006).

The deformed nuclear category covers a variety of phenotypes in which the nucleus no longer has a consistent shape, and is either lobed or misshapen, indicating a nuclear envelope defect (Figure 3.8a). All tested cell lines – HeLa, HeLa M and U2OS show nuclear deformation in a higher proportion of cells following CHMP7 knockdown for 48h, compared to control (Figure 3.8b). In HeLa cells, 11.3% of NT-control cells show some degree of deformation, rising to 18.8% (CHMP7-1) and 13.9% (CHMP7-3) upon CHMP7-depletion. The CHMP7-3 siRNA knockdown does not give a statistically significant difference. HeLa M cells displayed a greater increase in deformed nuclei, rising from 11.9% to 25.5% (CHMP7-1) and 25.7% (CHMP7-3). U2OS cells also showed a significant increase, from 6.0% in control cells to 13.8% (CHMP7-1) and 11.9% (CHMP7-3). This indicates that loss of CHMP7 has an effect on the integrity of the nucleus.

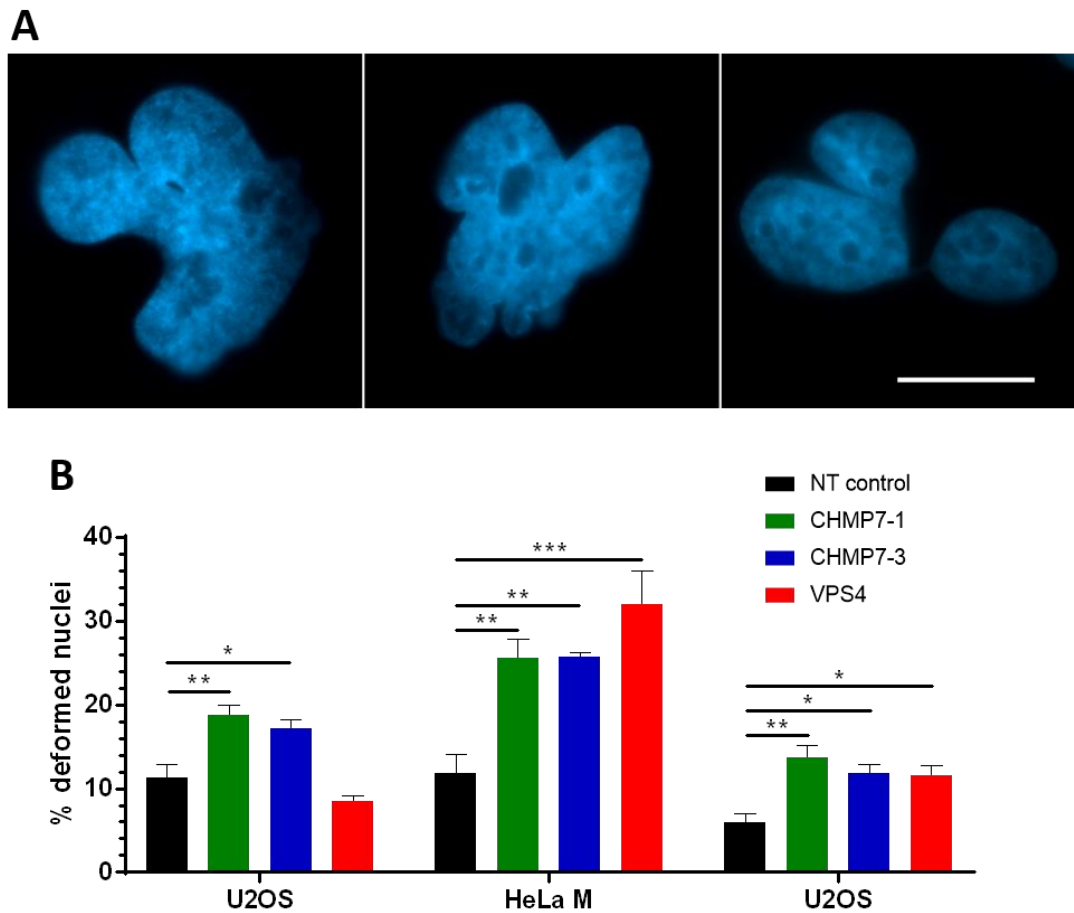


Figure 3.8. CHMP7 depletion causes abnormalities of nuclear morphology

a) Examples of HeLa cells with aberrant nuclear shape, stained with DAPI. Scale bar represents 10 μ m. **b)** Cells were transfected with either NT control, CHMP7 or VPS4 siRNA for 48h. HeLa, HeLa M and U2OS cells were scored based on the nuclear morphology (a minimum of 500 cells were scored per condition). Averages and standard error of three independent repeats are shown. Results were analysed using a one-way ANOVA with Dunnett's *post hoc* test.

3.2.9 CHMP7 depletion causes specific defects of nuclear envelope structure, which do not appear in VPS4-depleted cells

The disruption of normal nuclear morphology may be caused by extranuclear or extracellular pressures, however the flexibility of the nuclear structure is determined by its lamin composition. Nuclear deformation and fragmentation are common characteristics of laminopathy conditions (Schreiber and Kennedy, 2013). Therefore, the nuclear lamina of HeLa and HeLa M cells was visualised using Lamin B and Lamin A/C-targeting antibodies.

Staining for the nuclear lamina reveals that even apparently regularly-shaped nuclei display abnormal nuclear envelope composition. The HeLa cell observed in the upper panel of Figure 3.9a appears to have a relatively normal nuclear morphology when observed using DAPI staining. However, revealing the distribution of Lamin B shows a region of the nucleus which is incompletely enclosed in nuclear lamina. There are wide holes and regions of reduced Lamin B staining at the edge of the nuclear structure. The phenotype resembles those seen in some laminopathy conditions, referred to as a “moth-eaten” (Theodoropoulos *et al.*, 1999) or “honeycomb” (Tamiello *et al.*, 2013) phenotype, characterised by large holes and reduced intensity of Lamin B staining at areas of the nuclear envelope.

This honeycomb phenotype was scored, with nuclei with at least one patch of disorganised lamin scored as positive for the honeycomb defect (Figure 3.9b). In HeLa cells, this was observed in 0.8% transfected (NT) control cells, which increased significantly to 17.3% (CHMP7-1) and 13.6% (CHMP7-3) of cells upon CHMP7 depletion. Interestingly however, occurrence of this defect was not significantly increased following VPS4 knockdown (1.9% cells).

Another abnormal phenotype was observed, that of chromatin herniation, in which disorganisation of the nuclear lamina can cause weak regions of nuclear membrane where chromatin extrusion can occur through holes in the lamina (Hatch and Hetzer, 2014).

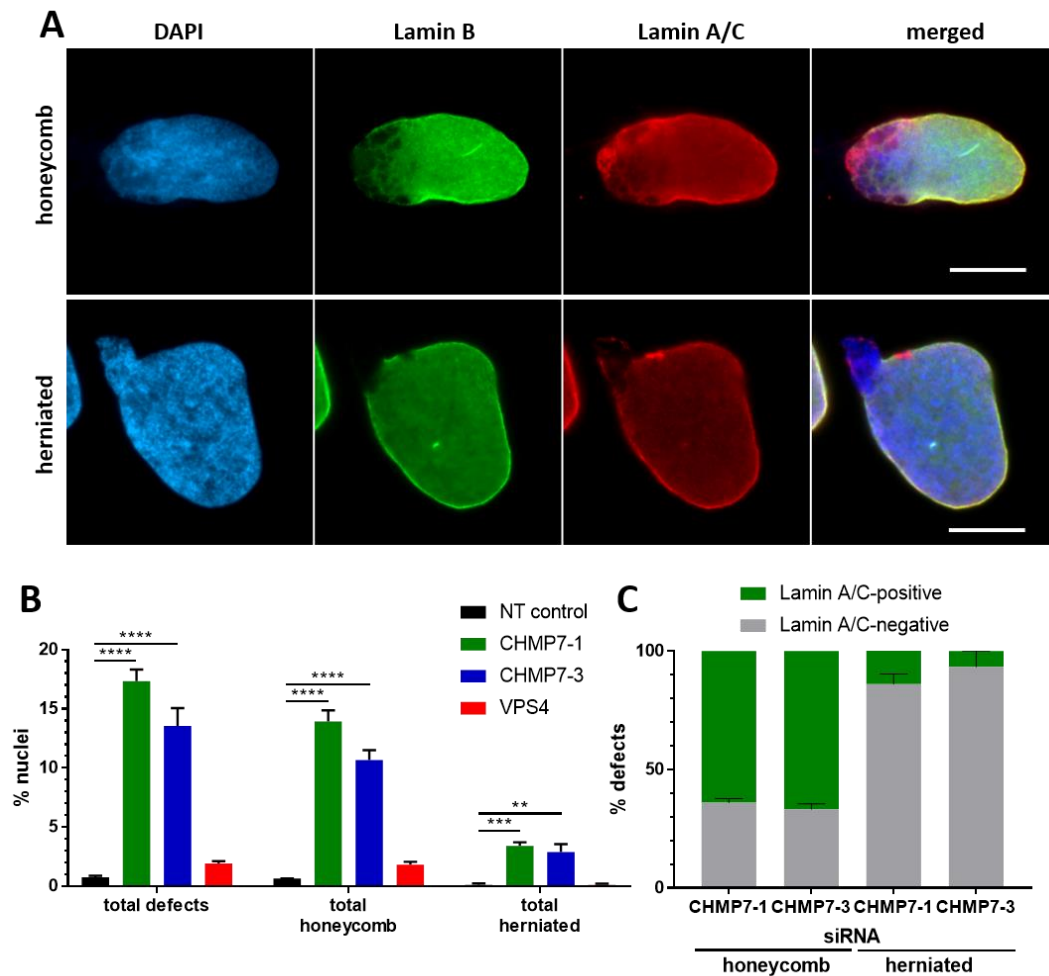


Figure 3.9. CHMP7 depletion causes nuclear lamina defects

a) Image of the honeycomb and herniated nuclear phenotype, immunostained with goat anti-Lamin A/C and rabbit anti-Lamin B antibodies, and counterstained with DAPI. Scale bars represent 10 μ m. **b)** HeLa cells stained as above were scored using Lamin B staining for the presence of these abnormalities. A minimum of 300 cells were scored for each condition. Averages and standard error of three independent repeats are shown. **c)** The percentage of defects in each condition which were Lamin A/C-positive were scored. A minimum of 30 honeycomb and 20 herniated defects were scored. Averages and standard error of three independent repeats are shown. Results were analysed using a one-way ANOVA with Dunnett's *post hoc* test.

Herniation and lamina gaps are related to nuclear rupturing, a phenomenon observed to occur transiently in human cancer cells in interphase (Vargas *et al.*, 2012), commonly in laminopathies (De Vos *et al.*, 2011) characterised by loss of nucleocytoplasmic compartmentalisation. Overexpression of Lamin B has been shown to prevent the formation of chromatin herniations and nuclear rupture (Hatch *et al.*, 2013), highlighting the importance of nuclear lamina integrity in the formation of these abnormalities.

A small proportion of HeLa cells show herniation of chromatin upon CHMP7 knockdown, 3.4% (CHMP7-1) and 2.9% (CHMP7-3) of cells compared to NT-control cells (0.1%), a statistically significant increase (Figure 3.9b). This phenotype shows no increase upon knockdown of VPS4, with only 0.1% of these cells showing herniation of the nucleus, again showing the specificity of this phenotype to CHMP7 knockdown.

Interestingly, the nuclear envelope defects observed here are found at an increased frequency in CHMP7-depleted cells, but not in VPS4-depleted cells, in which the function of ESCRT-III is impaired. This may indicate a unique role for the CHMP7 protein in maintenance of nuclear envelope integrity.

3.2.10 CHMP7-depleted cells display loss of nuclear envelope organisation

Lamin A/C proteins are key to maintenance of nuclear stiffness and integrity, with a particular role in maintaining the mechanical rigidity required to regulate nuclear shape (Lammerding *et al.*, 2006). The loss of Lamin B staining is characteristic of these nuclear abnormalities; Lamin A/C staining is not always correlated with Lamin B staining. Figure 3.9c shows the results of scoring of Lamin B-defined defects for presence or absence of Lamin A/C staining. At honeycomb Lamin B lamina defects, 36.0% and 33.3% of aberrations (in CHMP7-1 and CHMP7-3-depleted cells, respectively) also lacked Lamin A/C. However, at herniation events, 86.1% (CHMP7-1 knockdown) and 93.2% (CHMP7-3 knockdown) of defects lacked Lamin A/C. From this data, it appears that the absence of both Lamin A/C and Lamin B from a region of

the nuclear envelope indicates a greater likelihood of chromatin herniation at the nuclear envelope in a herniation event.

In addition, the presence of nuclear pore complexes at the site of nuclear lamina disorganisation defects, were observed and scored (Figure 3.10b). NPC localisation, as determined by anti-mab414 antibody staining, correlated closely with Lamin B localisation in CHMP7-depleted cells (Figure 3.10a). An average of 85.8% of honeycomb defects across both CHMP7 knockdowns also demonstrated loss of nuclear pore complex localisation in the region of the defect, which increased to 96.3% at herniation events.

Together, the loss of Lamin A/C and nuclear pore complexes demonstrates a substantial loss of nuclear envelope integrity and organisation at these defects found in CHMP7-depleted cells.

3.2.11 HeLa M cells display a unique nuclear fragmentation phenotype upon CHMP7 depletion

A distinctive phenotype can be found in HeLa M cells depleted of CHMP7, and very rarely observed in HeLa and U2OS cells, in which the nuclei show severe signs of degeneration, with nuclear margins ill-defined and faded, incorporating numerous bleb-like structures and invaginations (Figure 3.11b). Fragments of DNA also appear separated from the main nucleus, both discretely and connected by thin stalks, and the smooth edge of the nucleus is lost.

This 'fragmentation' phenotype is only observed significantly in HeLa M cells depleted of CHMP7 (Figure 3.11a), with 12.2% (CHMP7-1) and 11.6% (CHMP7-3) of cells showing this abnormality, compared to 0.2% NT-control cells. This fragmentation is not replicated in the other cell lines or caused by the VPS4 knockdown, making it unique to the loss of CHMP7.

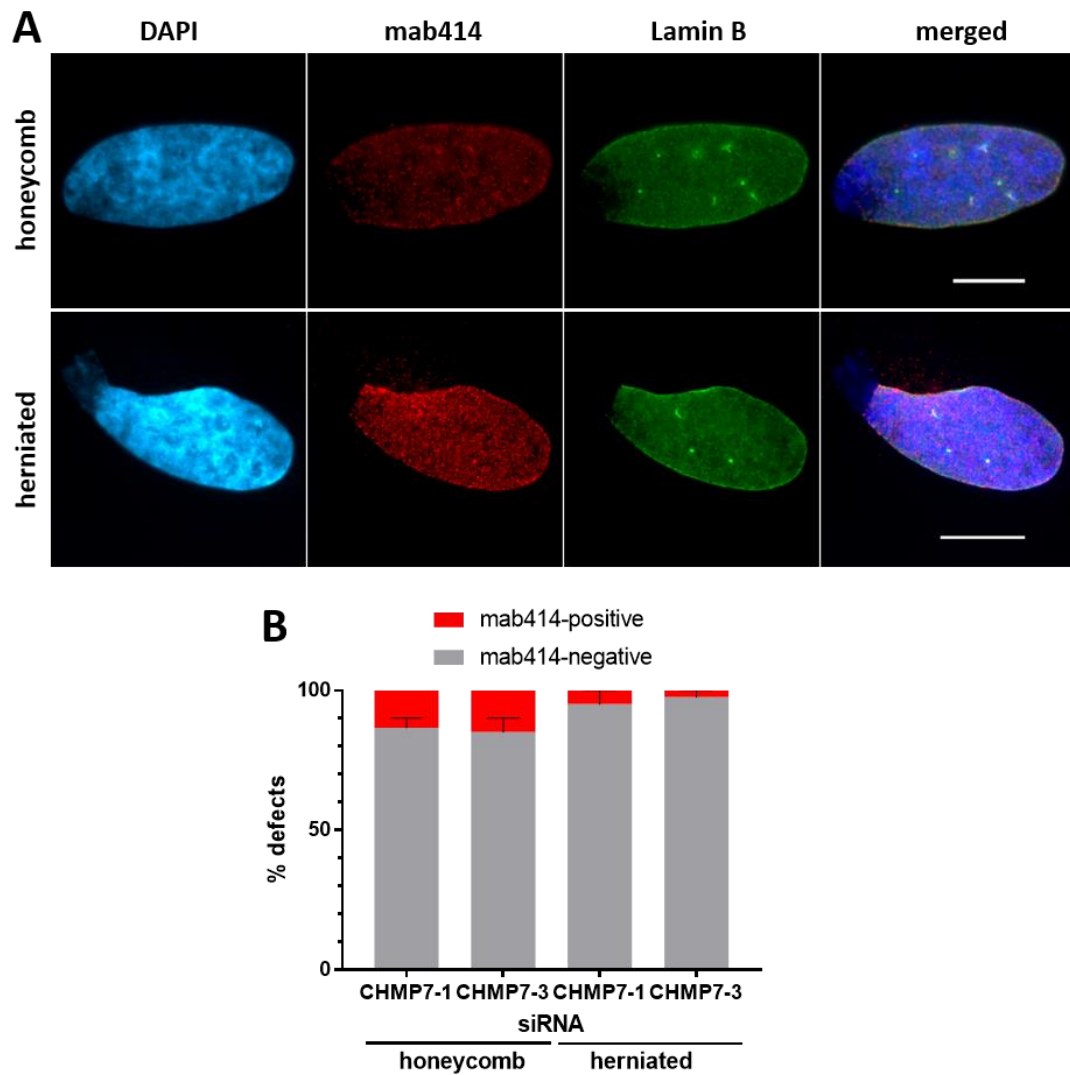


Figure 3.10. The relationship of nuclear pore complexes to nuclear envelope abnormalities in HeLa cells

a) Image of the honeycomb and herniated nuclear phenotypes, stained to show Lamin B and NPCs (mab414), and counterstained with DAPI. Scale bars represent 10 μ m. **b)** The percentage of defects in each condition which were mab414-positive were scored. A minimum of 30 honeycomb and 20 herniated defects were scored. Averages and standard error of two independent repeats are shown.

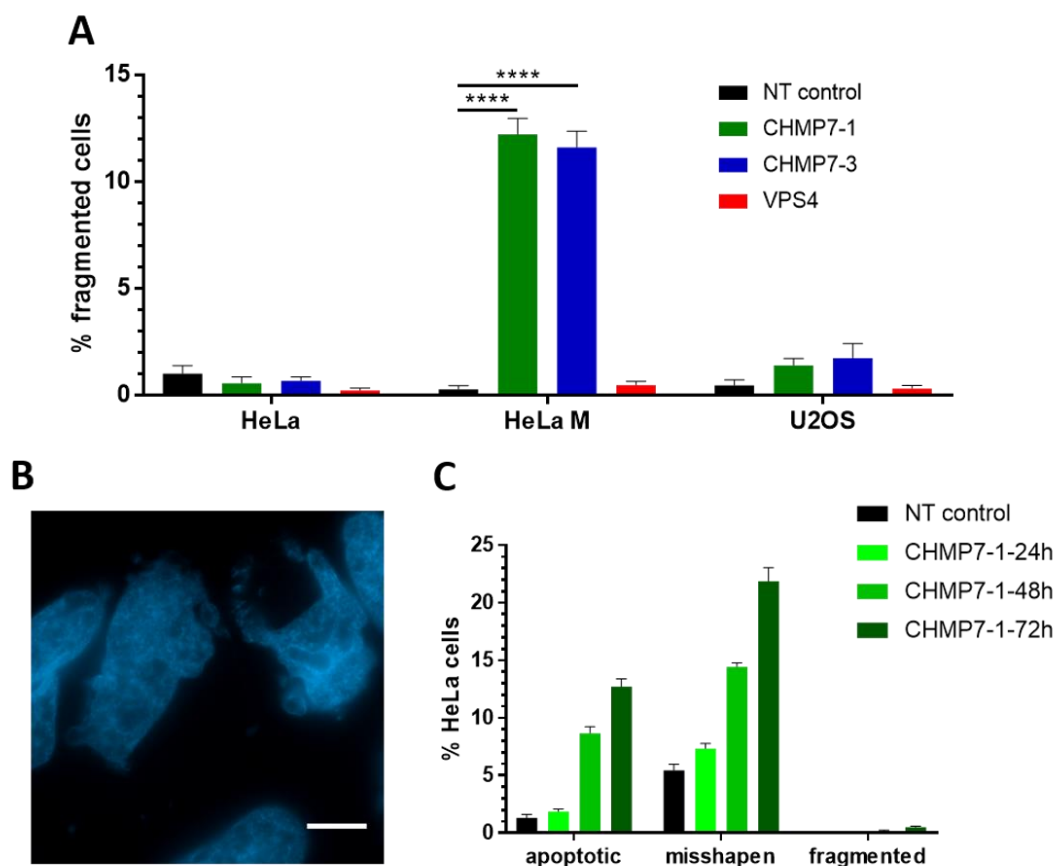


Figure 3.11. CHMP7-depleted HeLa M cells display a dramatic loss of nuclear envelope integrity and organisation not observed in other cell lines

a) Cells were transfected with either NT control, CHMP7 or VPS4 siRNA for 48h. HeLa, HeLa M and U2OS cells were scored based on the nuclear morphology (a minimum of 500 cells were scored per condition). Averages and standard error of three independent repeats are shown. Results were analysed using a one-way ANOVA with Dunnett's *post hoc* test. **b)** Example of fragmented HeLa M cells stained with DAPI. Scale bar represents 10 μ m. **c)** HeLa cells were transfected with either 100nM NT control or CHMP7-1 siRNA, and 600 cells were scored for each condition. Averages and standard error of three independent repeats are shown.

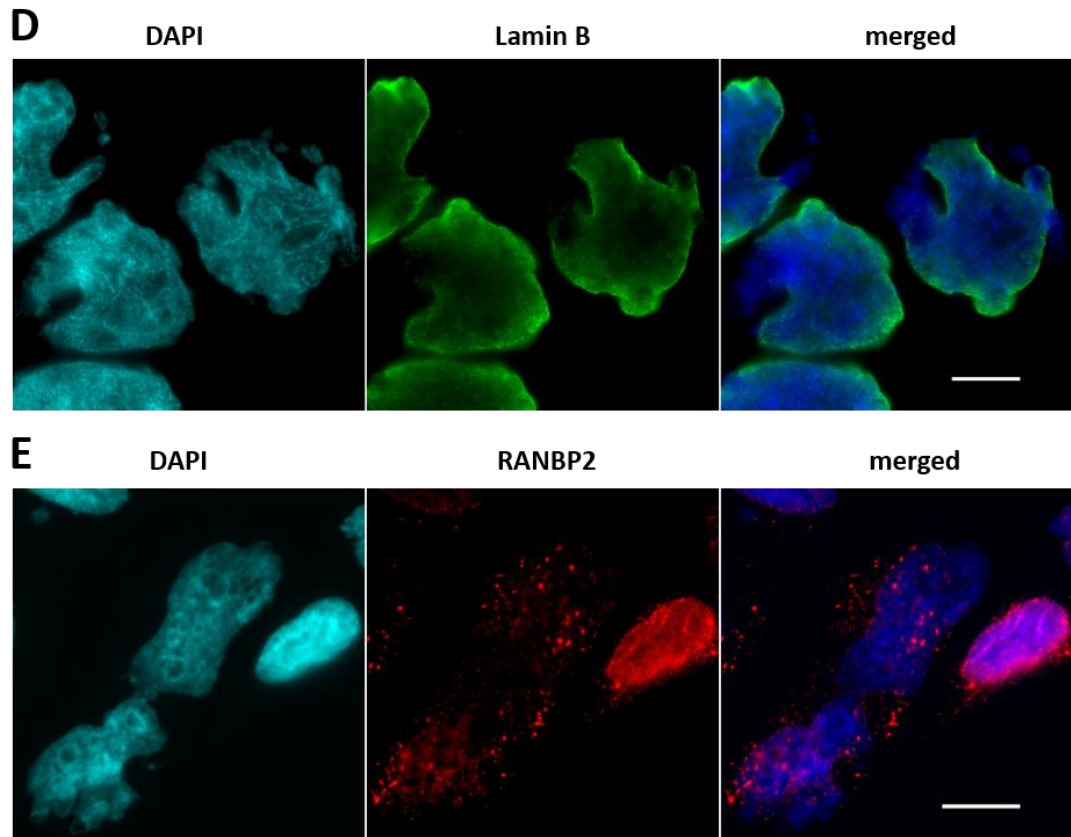


Figure 3.11. (continued)

d) HeLa M cells transfected with 20nM CHMP7-1 siRNA for 48 hours and stained to show Lamin B and DAPI. **e)** HeLa M cells treated as in (d), stained with anti-RANBP2 antibody to show nuclear pore complexes and counterstained with DAPI. Scale bars represent 10 μm.

In order to determine if the fragmented phenotype can be induced in HeLa cells, they were transfected with a high level of siRNA (100nM CHMP7-1 siRNA) and monitored at 24, 48 and 72 hours post-transfection (Figure 3.11c). While higher rates of apoptotic and misshapen nuclei were observed, the fragmented phenotype was not observed to occur in these cells. This may be due to the nature of HeLa cells - due to cell and nucleus size and composition, differing mechanical forces acting upon the nuclei or a propensity for cells to die or detach from the glass slide prior to reaching the fragmented state.

3.2.12 Large lamina ruptures, protruding chromatin and mislocalised nuclear pore complexes are observed in CHMP7-depleted HeLa M nuclei

As shown in Figure 3.11, the effect of the CHMP7 knockdown is particularly dramatic in some HeLa M cells. In order to determine the state of the nuclear envelope in these cells, HeLa M cells were immunostained with an anti-Lamin B antibody (Figure 3.11d). The nuclei which are defined as displaying the fragmented phenotype show broken regions of nuclear lamina, through which chromatin is protruding. Upon scoring it was found that all of the nuclei defined as fragmented, of which 100 were observed, showed at least one region in which a chromatin protrusion was not entirely enclosed in the nuclear lamina. It therefore seems that a broken nuclear lamina is a feature of this phenotype.

In order to monitor the organisation of the nuclear envelope, the state of nuclear pore complexes was examined through observing the immunofluorescence signal using an anti-RANBP2 antibody (Figure 3.11e). RANBP2, also known as nucleoporin 358 (Nup358) is a peripheral cytoplasmic nuclear pore complex protein with SUMO E3 ligase activity (Pichler *et al.*, 2002) implicated in a number of functions including chromosome segregation, onset of anaphase and anchoring centrosomes to the nuclear envelope (Dawlaty *et al.*, 2008; Ibarra and Hetzer, 2015). Nuclei which are classified as fragmented show severely aberrant localisation of RANBP2, in which proper localisation at the nuclear envelope is reduced, and

bright accumulations of RANBP2 are observed in the cytoplasm. Upon scoring it was found that all of the nuclei defined as fragmented, of which 100 were observed, showed either severe or mild aberrance of RANBP2, featuring cytoplasmic accumulations of the protein.

This phenotype was also observed using an anti-mab414 antibody, and antibody which recognises the FXFG repeated sequence found in numerous nucleoporins, therefore acting as a general nuclear pore complex stain.

3.2.13 CHMP7 knockdown causes mislocalisation and accumulation of cytoplasmic NPC proteins

As shown above, abnormality in the distribution of NPCs was observed in the fragmented HeLa M cells, following CHMP7 knockdown. Upon observation of HeLa and U2OS cells stained with the mab414 antibody, a similar phenotype was observed in some cells, despite the absence of the fragmentation nuclear phenotype. Therefore, localisation of nuclear pore complexes was subsequently explored in each of the available cell lines, for which three categories of NPC distribution were used.

Examples of the normal, mildly aberrant, and severely aberrant phenotypes observed in HeLa cells are shown in Figure 3.12a. HeLa, HeLa M and U2OS cells were scored for a mildly or severely aberrant, or normal phenotype following transfection of either NT-control, CHMP7-1, CHMP7-3 or VPS4 siRNA for 48 hours. HeLa and HeLa M cells showed a significant increase in the number of cells showing both mild and severe aberrance of nuclear pore complex distribution upon knockdown of CHMP7 and VPS4 (Figure 3.12b and Figure 3.12c). After the CHMP7 knockdown, an average of 27.9% of HeLa cells showed a highly aberrant phenotype, similar to the 24.7% seen in HeLa M populations. VPS4 knockdown caused this in 23.7% of HeLa and 19.8% HeLa M cells, suggesting this phenotype is related to the function of the ESCRT-III. A similar proportion of cells were classified as mildly aberrant across both cell lines,

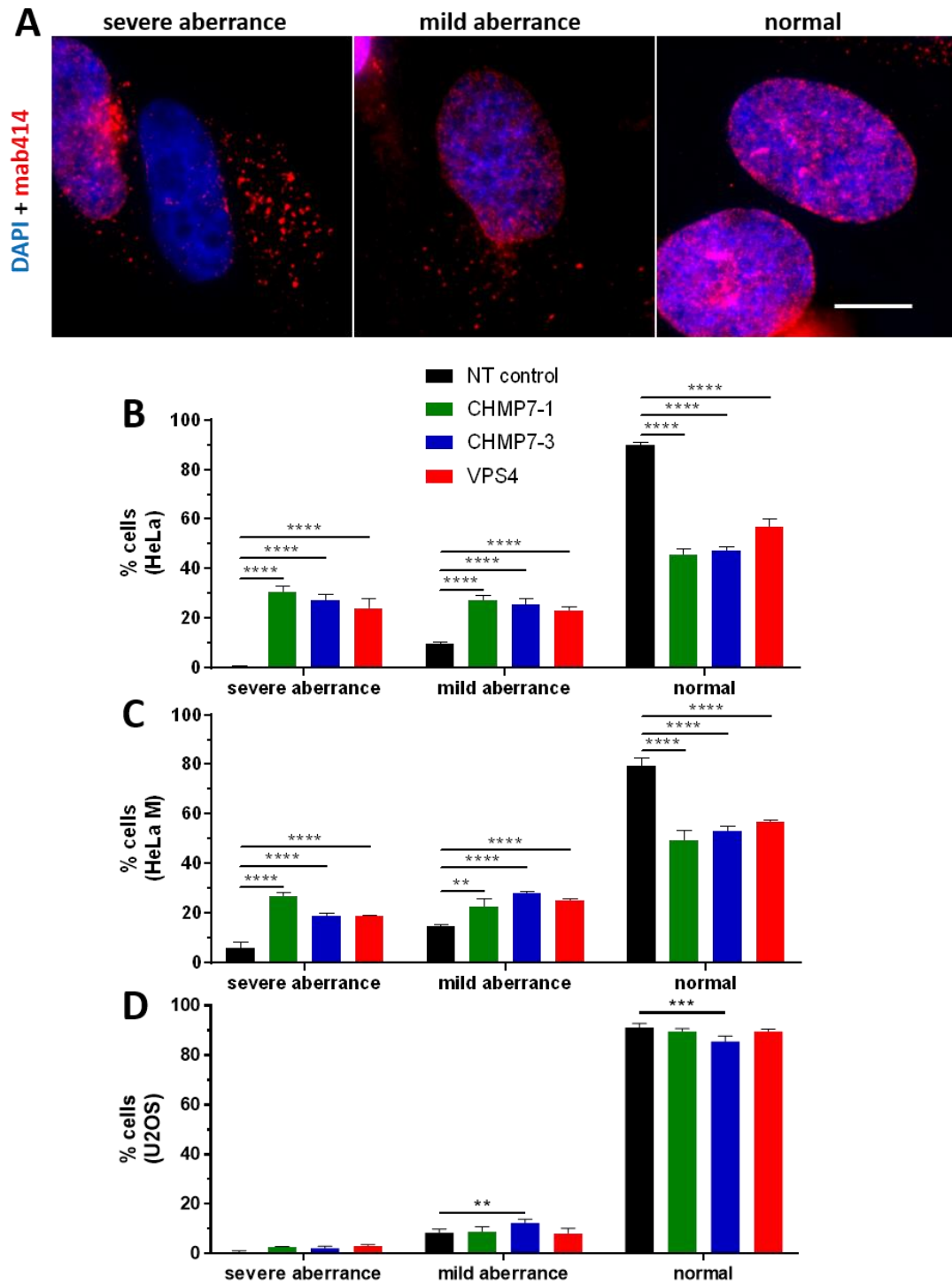


Figure 3.12. Nuclear pore complex proteins are found in cytoplasmic accumulations following CHMP7 knockdowns

a) Representative images of the mab414 phenotypes. Scale bar represents 10 μ m. **b)** HeLa, **c)** HeLa M and **d)** U2OS cells were scored for these phenotypes following transfection for 48 hours with the indicated siRNA. The percentage of cells displaying each phenotype are shown for at least 200 cells per condition. Averages and standard error of three independent repeats are shown. Results were analysed using a one-way ANOVA with Dunnett's *post hoc* test.

causing a significant reduction in the percentage of cells classified as having a normal NPC distribution. Interestingly however, U2OS cells did not display a significant increase in severely aberrant cells (Figure 3.12d). The CHMP7-3 siRNA depletion caused a small significant increase in mildly aberrant cells, and a corresponding decrease in normal U2OS cells.

3.2.14 CHMP7 knockdown causes an increase in DNA damage

Since nuclear integrity appears to be compromised in CHMP7 or VPS4-depleted cells, it was hypothesised that this may have an effect on the integrity of the DNA in these cells. Therefore, HeLa cells depleted of either CHMP7 or VPS4 were stained to show γ H2AX (Figure 3.13c), a common marker of DNA damage, which indicates the phosphorylation of the H2AX variant histone component of chromatin. Foci of γ H2AX form around the site of a DNA double-strand breaks, and forms the basis for identification of a DNA lesion and a platform for recruitment of DNA repair proteins. DNA damage foci marked by γ H2AX can be resolved through DNA repair, however persistent unrepaired damage results in large foci as the damage signalling becomes amplified (Polo and Jackson, 2011).

HeLa cells were scored for the number of γ H2AX foci found per nucleus in control and knockdown cells. Control cells showed a baseline average of 7.3 foci per nucleus. CHMP7 and VPS4 knockdowns demonstrated a significant increase in the number of foci, to 37.9 (CHMP7-1), 33.6 (CHMP7-3) and 27.2 (VPS4; Figure 3.13a). These knockdowns also caused an increase in γ H2AX foci size; the average size in control cells was found to be $0.57 \pm 0.03 \mu\text{m}$, increasing to $2.00 \pm 0.11 \mu\text{m}$ and $2.20 \pm 0.09 \mu\text{m}$ in the CHMP7 knockdowns, and $1.74 \pm 0.11 \mu\text{m}$ in the VPS4 depletion (Figure 3.13b). Together, these data demonstrate the increased occurrence and persistence of DNA damage in CHMP7/VPS4-depleted cells, a sign of loss of genomic integrity.

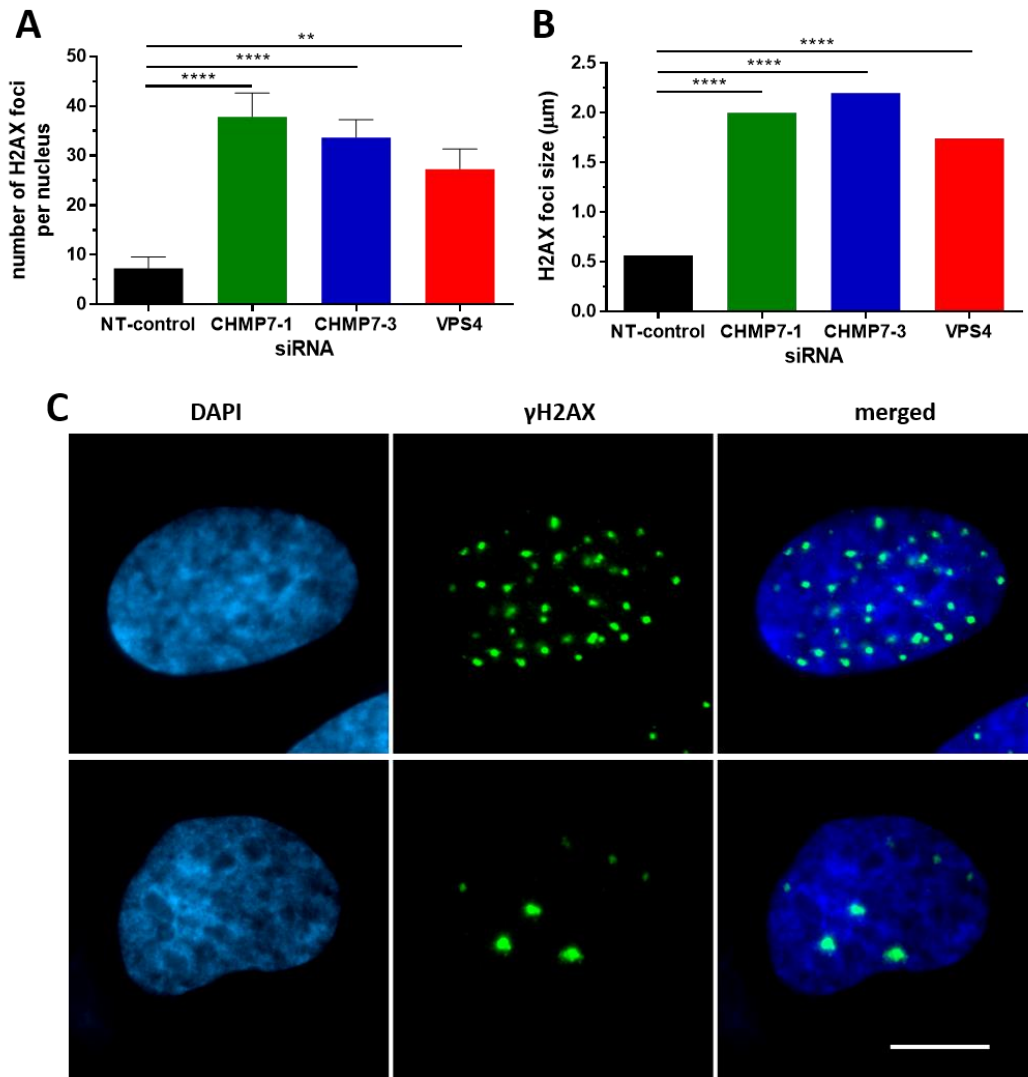


Figure 3.13. The effect of CHMP7 knockdown on DNA damage as marked by γ H2AX foci

a) HeLa cells were scored for the number of γ H2AX foci in the nucleus. A minimum of 30 cells were scored. Averages and standard error of three independent repeats are shown. **b)** γ H2AX foci in each condition were visualised and the area of the foci were measured in ImageJ (NT-control – 218 foci; CHMP7-1 – 1587 foci; CHMP7-3 – 1076 foci; VPS4 – 1076 foci) Results were analysed using a one-way ANOVA with Dunnett's *post hoc* test. **c)** Image of γ H2AX foci staining in HeLa cells. Scale bar represents 10 μ m.

3.2.15 CHMP7 depletion compromises centrosomal cohesion and positioning in interphase HeLa, but not U2OS, cells

In order to fully characterise the causes of the CHMP7-depleted loss in viability, key cellular structures were visualised in knockdown cells. It has been shown that CHMP proteins and VPS4 are required for integrity of the centrosomal machinery (Morita *et al.*, 2010), however CHMP7 was omitted from these observations of centrosomal defects. Centrosomes were visualised using anti-pericentrin antibody, which targets a component of the filamentous centrosome matrix. Pericentrin visualises centrosomes as two spots close together, or appearing, depending on orientation or focal plane, as one dot (Figure 3.14g). Centrosomes are normally tethered close to the nuclear periphery throughout interphase (Figure 3.1), and the normal cycle of centrosome duplication and separation is shown in Figure 3.2.

A change in centrosomal positioning was observed following CHMP7 depletion, and phenotypes for scoring purposes were defined as separated and unseparated. Unseparated represents a normal interphase centrosomal phenotype, in which the pericentrin is visualised as two closely spaced (<2 μ m) dots. Prematurely separated centrosomes are defined as two pericentrin structures are separated by a distance of more than 2 μ m in an interphase cell, an established scoring criterion (Meraldi and Nigg, 2001; Panic *et al.*, 2015).

HeLa and U2OS cells in which two centrosome dots could be observed were scored for the distance between the two structures as shown in Figure 3.14g. HeLa M cells were not scored due to a high level of multiple or fragmented pericentrin structures observed in untreated cells, complicating the scoring of aberrant phenotypes. The proportion of HeLa cells with separated centrosomes rises from an average of 5.5% in NT-control cells to 27.0% and 23.1% in CHMP7-1 and CHMP7-3-depleted cells, respectively (Figure 3.14a). The average inter-centrosome distance increases from $0.70\pm 0.08\mu\text{m}$ (NT-control) to $1.40\pm 0.16\mu\text{m}$ (CHMP7-1) and $1.57\pm 0.17\mu\text{m}$ (CHMP7-3; Figure 3.14e). VPS4 depletion also influences premature

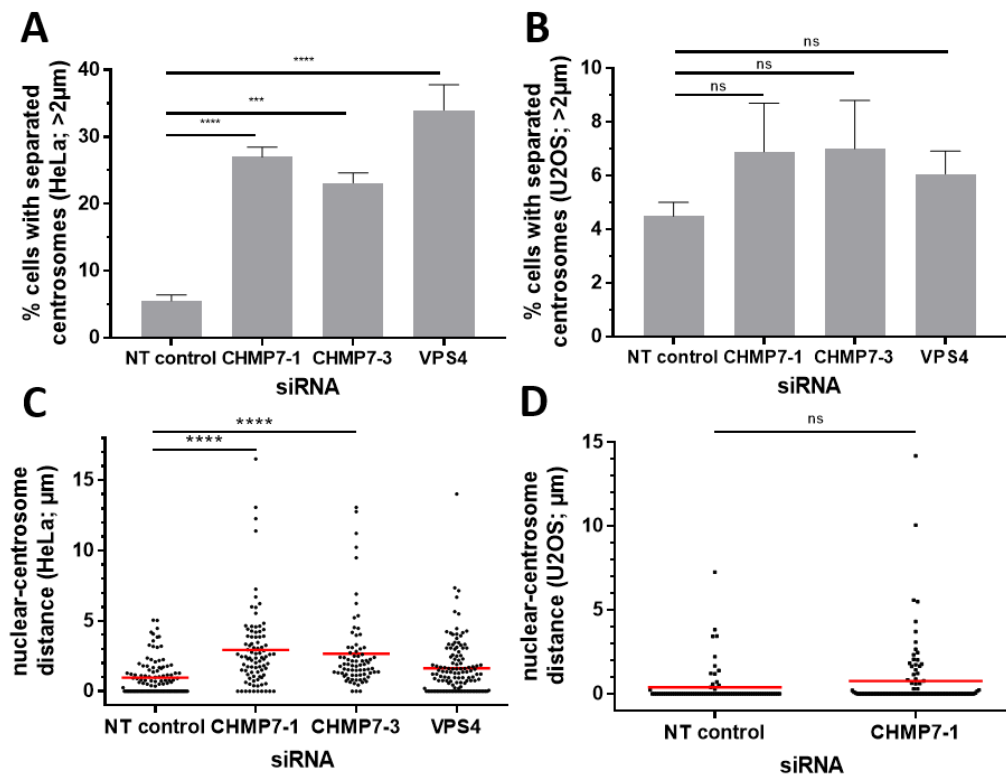


Figure 3.14. Changes in centrosome positioning and separation in interphase cells following CHMP7 knockdown

HeLa or U2OS cells transfected with either NT control, CHMP7-1 or CHMP7-3 siRNA for 48 hours were stained with rabbit-derived pericentrin antibody to observe centrosomes. **a)** HeLa and **b)** U2OS cells were scored for the premature separation of centrosomes (defined as interphase cells in which the two centrosomes are more than 2 μ m apart). A minimum of 300 cells were scored per treatment. Averages and standard error of three independent repeats are shown. Results were analysed using a one-way ANOVA with Dunnett's *post hoc* test. **c)** The distance between the closest edge of the nucleus and centrosomes were measured in ImageJ for HeLa cells depleted of: NT control – 111 cells, CHMP7-1 – 90 cells, CHMP7-3 – 76 cells and VPS4 127 cells. Results were analysed using a one-way ANOVA with Dunnett's *post hoc* test. **d)** This was also scored in U2OS NT control – 73 cells and CHMP7-1 knockdown – 100 cells. Averages and individual measurements are shown. Results were analysed using an unpaired, two-tailed *t*-test.

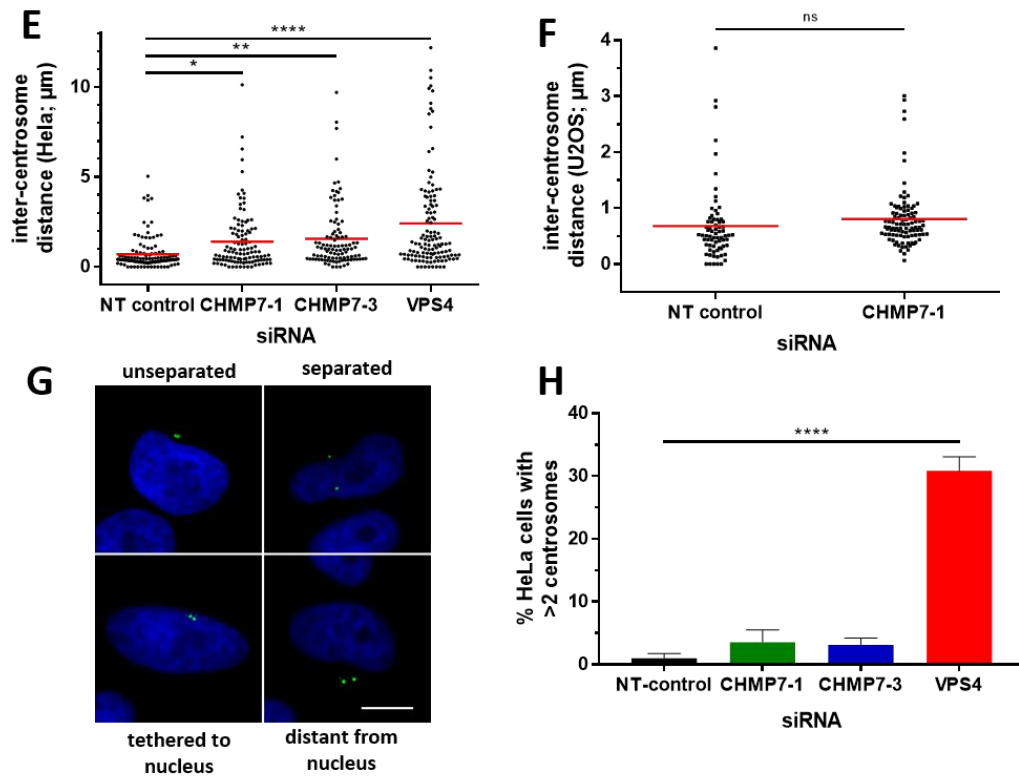


Figure 3.14. (continued)

e) The inter-centrosome distance was measured in ImageJ for HeLa cells depleted of: NT control – 120 cells, CHMP7-1 – 112 cells, CHMP7-3 – 103 cells and VPS4 – 124 cells. Results were analysed using a one-way ANOVA with Dunnett's *post hoc* test. **f)** This was also scored in U2OS NT control - 72 cells and CHMP7-1 knockdown – 99 cells. Averages and individual measurements are shown. Results were analysed using an unpaired, two-tailed *t*-test. **g)** Examples of each phenotype as displayed by HeLa cells stained with anti-pericentrin antibody (green) and DAPI (blue). Scale bar represents 10 μm . **h)** The percentage of HeLa cells in which supernumerary (>2) centrosomes were observed in a minimum of 200 cells per condition. Averages and standard error of three independent repeats are shown. Results were analysed using a one-way ANOVA with Dunnett's *post hoc* test.

centrosome separation, with 33.8% of cells with two centrosomes displaying the separated phenotype, with an average inter-centrosome distance of $2.41 \pm 0.25 \mu\text{m}$. In contrast to this striking effect, the same conditions in U2OS cells produced no significant changes in the proportion of interphase cells with separated centrosomes in CHMP7 or VPS4 knockdown conditions (Figure 3.14b) or the inter-centrosome distances, following CHMP7 knockdown (Figure 3.14f).

Another aspect of centrosomal aberrance observed is the loss of close association between the nucleus and the centrosome structure. Cells were scored for the distance between a centrosome and the closest point on the nuclear envelope. In NT-control HeLa cells, the average nuclear-centrosome distance was found to be $0.97 \pm 0.12 \mu\text{m}$, rising to $2.93 \pm 0.30 \mu\text{m}$ upon CHMP7-1-depletion, $2.74 \pm 0.31 \mu\text{m}$ (CHMP7-3) and $1.60 \pm 0.17 \mu\text{m}$ (VPS4; Figure 3.14c). NT-control U2OS cells show a shorter average distance ($0.39 \pm 0.13 \mu\text{m}$) with an increase to $0.76 \pm 0.36 \mu\text{m}$ upon CHMP7-1 depletion (Figure 3.14d), however based on the data collected, this is not a significant difference. The proposal that increased centrosome separation is due to a higher proportion of cells being in the late stages of G2 phase can be discounted based on the previously obtained FACS data, which showed a decrease in the G2/M population of HeLa cells following CHMP7 knockdown at 48 hours (Section 3.2.5).

Depletion of other ESCRT-III proteins has been shown to have an effect on centrosome number, resulting in either supernumerary centrosomes (upon depletion of CHMPs 1A, 2B, 4B, 4C, and both VPS4 isoforms) or single centrosomes (CHMP2B and CHMP5). However, a comparable defect was not observed here looking at CHMP7 depletion. Following VPS4 knockdown, 30.8% of HeLa cells had at least three distinct centrosome structures (Figure 3.14h). However, there was no significant change compared to NT-control when CHMP7-1 and CHMP7-3 siRNA were transfected into cells.

3.2.16 CHMP7-depleted cells demonstrate loss of nuclear compartmentalisation

PML (promyelocytic leukaemia) nuclear bodies are nuclear-matrix associated protein aggregates formed from the PML protein, to which a variety of nuclear proteins are recruited (further discussed in Section 4.1.5) Upon observation of PML bodies in CHMP7-depleted cells, it was observed that in some cells, PML bodies were mislocalised to the cytoplasm (Figure 3.15a). Cytoplasmic PML bodies have previously been observed, but only in the case of truncation mutations of the PML protein; under normal conditions PML-NBs are confined to the nuclear compartment (Bellodi *et al.*, 2006). Incorrect localisation of PML bodies is caused by rupture of the nuclear envelope, leading to loss of compartmentalisation (De Vos *et al.*, 2011). Nuclear envelope tears can be repaired, and soluble proteins can be translocated through the nuclear barrier into their correct compartment to restore proper localisation. However, organelles such as vesicles, mitochondria and PML bodies can become trapped in the inappropriate cellular compartment (Houben *et al.*, 2013).

HeLa and U2OS cells were stained for PML and DAPI, and the number of cells in which PML bodies were found in the cytoplasm were scored. In NT-control HeLa cells this was observed in 2.4% of cells, increasing significantly to 13.7% (CHMP7-1), 10.7% (CHMP7-3) and 12.2% (VPS4) in knockdown populations (Figure 3.15b). A similar result was seen in U2OS cells with the phenotype scored in NT-control cells at 4.3% (Figure 3.15c), again increasing significantly following knockdowns to 15.8% (CHMP7-1), 12.8% (CHMP7-3) and 11.6% (VPS4). While PML localisation is an indirect measure of nuclear rupture, it clearly demonstrates a defect of nuclear envelope integrity and nucleocytoplasmic compartmentalisation. This dysfunction may be due to current or previous nuclear rupture events, or due to improper reincorporation of PML bodies into the nucleus following a previous mitosis.

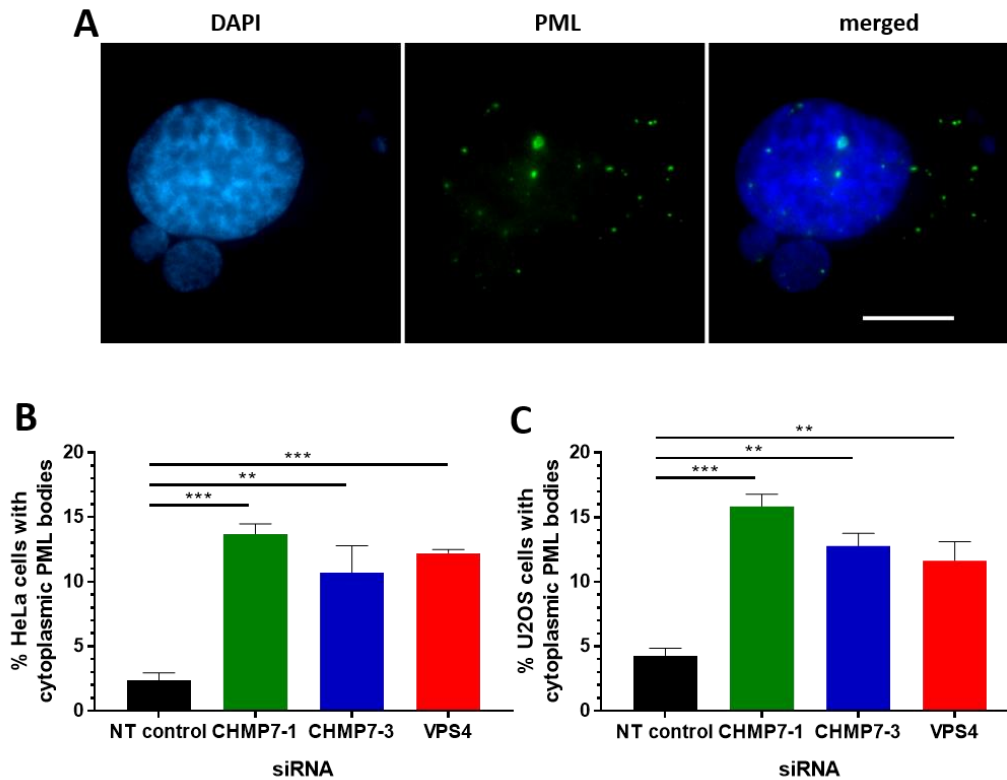


Figure 3.15. The percentage of cells in which PML is mislocalised into the cytoplasm in HeLa and U2OS cell lines

a) A HeLa cell in which PML bodies have mislocalised to the cytoplasmic compartment. Scale bar represents 10 μ m. **b)** The proportion of HeLa and **c)** U2OS cells which show this abnormality were scored across NT control, CHMP7 and VPS4 siRNA transfection. A minimum of 550 cells were scored per condition. Averages and standard error of three independent repeats are shown. Results were analysed using a one-way ANOVA with Dunnett's *post hoc* test.

3.3 Discussion

This chapter explores the significance and effects of the depletion of CHMP7 on three different cancer cell lines, giving us evidence of its role and importance in maintenance of normal cellular function.

Upon observing the effect of the CHMP7 knockdown, it was observed that cell viability was affected, with an MTT assay showing that cell survival was reduced to between 15 and 36% across all tested cell lines (HeLa, HeLa M and U2OS when compared to transfected NT-control after 6 days of transfection). Profiling the cell cycle revealed a reduction in the number of mitotic cells in population of HeLa cells scored by immunofluorescence using DAPI staining, and significantly fewer cytokinetic cells were observed following CHMP7 knockdown. Cell cycle profiling using FACS showed that CHMP7 depletion causes a modest but significant accumulation of HeLa cells in G1, with a concomitant decrease in S-phase and G2/M phase cells. Analysis of apoptotic cells as visualised using DAPI staining and imaging showed that all tested cell lines display a significant increase in fixed cells in the process of apoptosis following CHMP7 knockdown, indicating increased levels of cell death. Additionally, they show an increase in multinucleated cells, a sign of aberrant mitosis or cytokinesis failure. The centrosomal machinery was shown to be disturbed in HeLa but not U2OS cells, characterised by loss of centrosomal cohesion prematurely in interphase.

Analysis of nuclear morphology using DAPI staining showed that CHMP7 knockdown causes a significant increase in cells with deformed nuclei, in which the shape is irregular or lobed, however the nucleus retains a defined, smooth nuclear boundary. The phenotype was observed across all cell lines. As a distinct phenotype in the form of a fragmented nuclear morphology was also seen in HeLa M cells, in which there is significant deterioration of nuclear integrity, with edges of the nucleus being poorly defined, and fragments of DNA being separated from the primary nucleus. All cell lines were shown to have increased

abnormality of nuclear envelope organisation upon CHMP7 knockdown, incorporating lamina holes or large pores, and mislocalisation of nuclear pore complexes into cytoplasmic aggregates. On a related measure, HeLa and U2OS cell lines showed evidence of loss of nucleocytoplasmic compartmentalisation, through mislocalisation of PML nuclear bodies to the cytoplasm. This was accompanied by an increase in size and number of DNA damage-induced γ H2AX foci.

Together these data indicate a significant role for the CHMP7 protein in maintenance of mitotic and genomic integrity, and a variety of aberrations which occur upon its loss from various cancer cell lines (Figure 3.17). It should be noted that a number of these aberrant phenotypes were observed uniquely following CHMP7 depletion, as opposed to the VPS4 knockdown-mediated impairment of ESCRT-III function. Defects specifically linked to CHMP7 depletion included the nuclear lamina disorganisation, including nuclear herniation in all cell lines, and nuclear fragmentation in HeLa M cells.

The use of different cell lines has allowed observation of the variance of phenotype observed following CHMP7 depletion – for example, the loss of CHMP7 was sufficient to cause increased interphase centrosome separation in HeLa cells, but not in U2OS cells. Also, HeLa M cells demonstrate a unique phenotype not seen in HeLa or U2OS cells – multiple, large nuclear envelope ruptures leading to chromatin fragmentation. However, certain characteristics appear to be shared between cell lines, being a serious loss of nuclear integrity leading to nuclear envelope rupture, escaped and fragmented chromatin.

3.3.1 Discussion of the mitotic role of CHMP7

It is clear that the cell cycle undergoes disruption following depletion of CHMP7. Cell cycle analysis by FACS, which shows some accumulation of cells in G1 phase, indicates that cells are progressing through S-phase and mitosis, however are unable to progress through G1 phase into S-phase. This slowing or arrest of the cell cycle offers an explanation for the

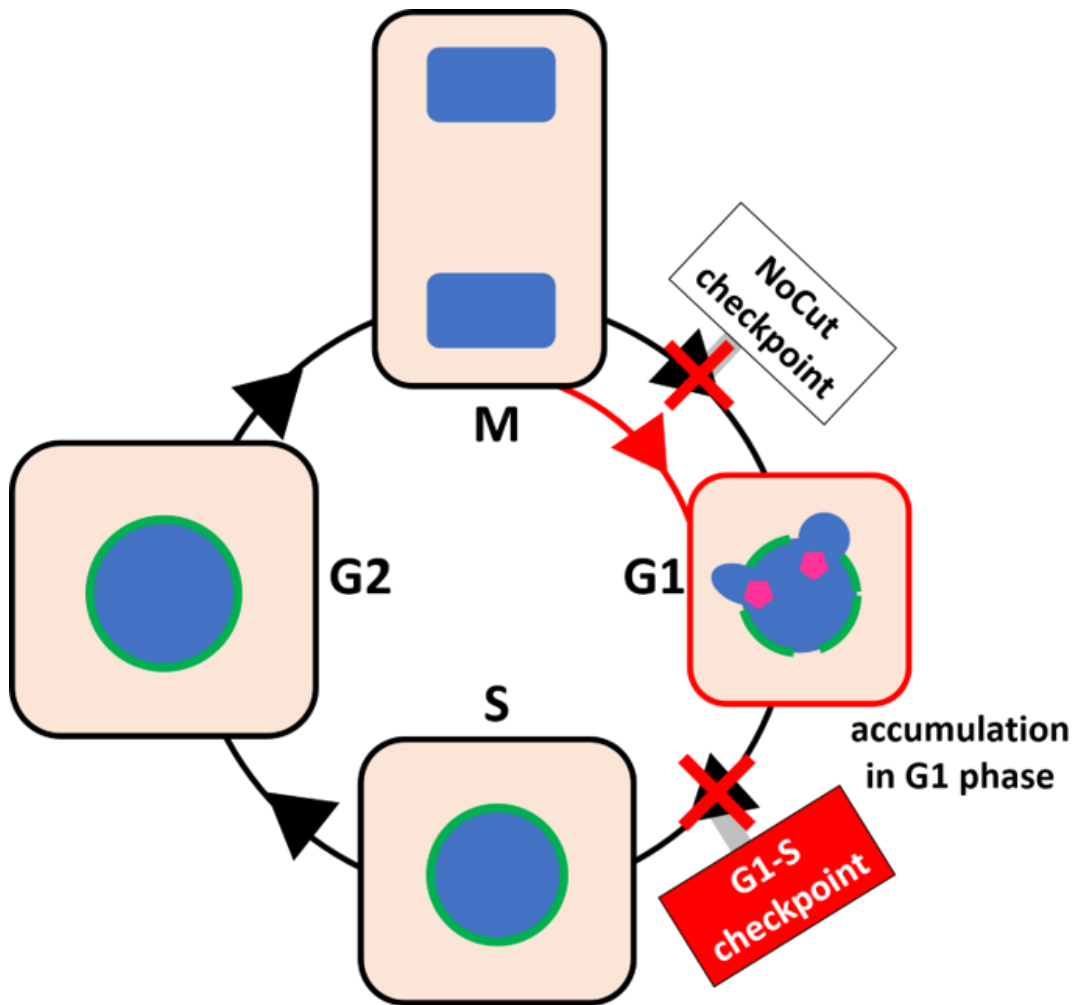


Figure 3.16. A model of the cell cycle progression of CHMP7-depleted cells

CHMP7-depleted cells display aberrant progression through mitosis, leading to either cytokinesis failure and multinucleation, or an accelerated cytokinesis. Increased speed of cytokinesis and mitotic exit is associated with the deregulation or bypass of the NoCut abscission checkpoint, and consequent damage to nuclear and genomic integrity. It is hypothesised that these aberrant daughter cells are subsequently unable to satisfy the G1-S nuclear integrity checkpoint, resulting in G1 arrest of these impaired cells.

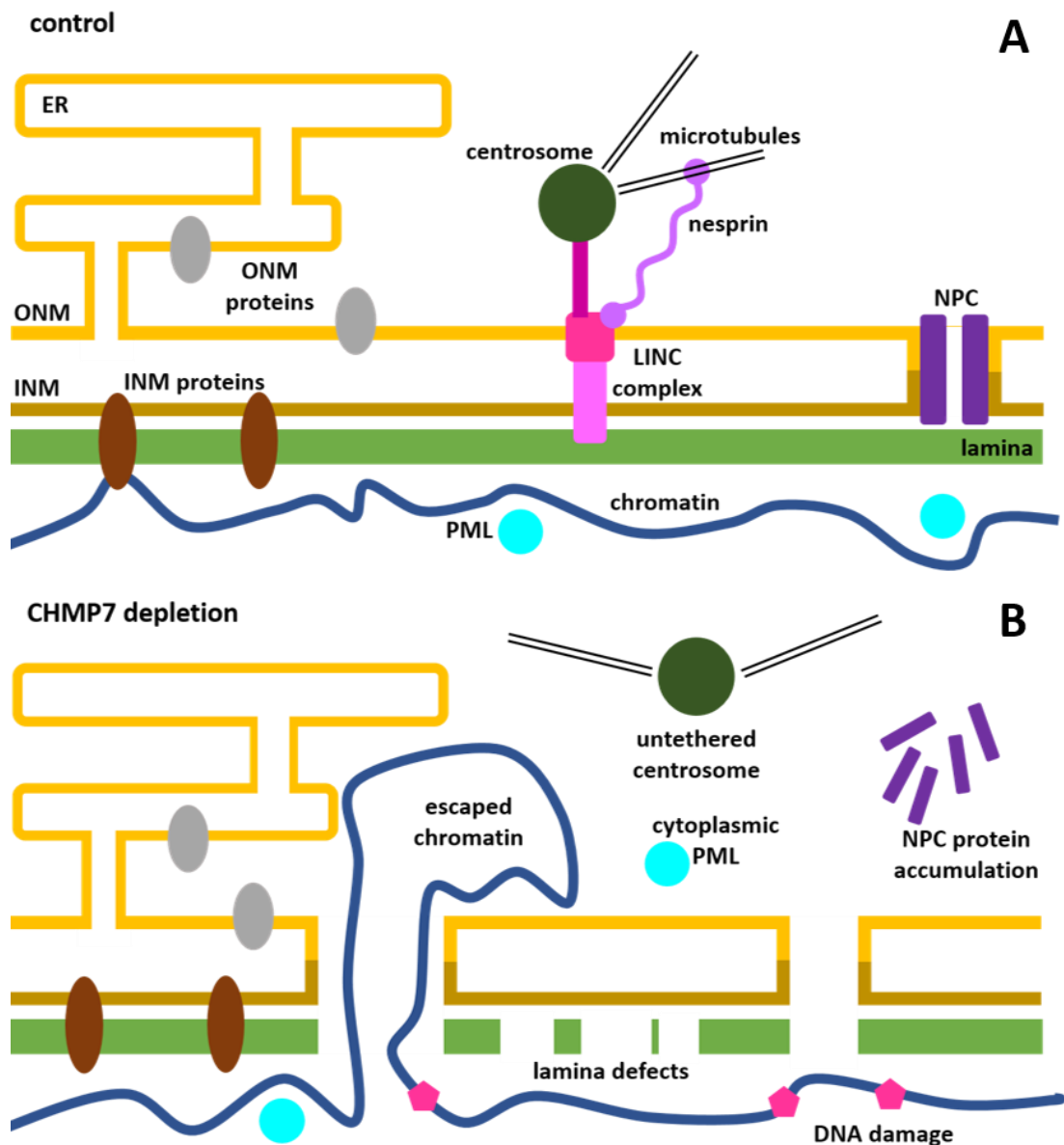


Figure 3.17. A model of the defects caused by depletion of CHMP7

A diagram showing a **a)** normal nuclear envelope and **b)** a model of defects caused by CHMP7 knockdown. In the depleted cell, the continuity of the nuclear envelope is compromised, potentially leading to herniation of chromatin and loss of PML nuclear bodies into the cytoplasm. The nuclear lamina is disorganised, leading to gaps and discontinuities in the lamin network, which is observed as holes or honeycomb phenotype in CHMP7-depleted cells. Nuclear pore complex proteins are not properly incorporated into the nuclear envelope, instead being found in cytoplasmic accumulations of unknown structure. Exposure of chromatin to mechanical stress or cytoplasmic components may lead to the observed increase in DNA damage as marked by H2AX histone phosphorylation. Centrosomes appear further from the nucleus in CHMP7-depleted cells, which may be due to a loss of tethering components or microtubule organisation around the nuclear envelope.

reduced proliferation rates of CHMP7-depleted cells. The G1 delay implies an inability to satisfy the cell integrity checkpoints required to enter the replication phase (Figure 3.16). Findings described in this chapter show many possible causes of this arrest, including compromised nuclear compartmentalisation, centrosome aberration, and increased DNA damage (Figure 3.17). Centrosome loss or separation has been shown to cause G1 arrest through a p53-dependent pathway (Mikule *et al.*, 2007). A high level of unresolved DNA damage foci, such as those seen in CHMP7-depleted cells, also activates a p53-mediated delay in progression into S-phase, to avoid formation of double strand breaks or replication stress (Dasika *et al.*, 1999). While a subset of cancers display a p53-null genotype, HeLa and U2OS cell lines are known to contain a wild-type form of the tumour suppressor p53 (Jia *et al.*, 1997).

Another key aspect of the CHMP7-depletion phenotype is the reduction in cytokinetic cells compared to control when mitotic cells were scored. This suggests either faster mitotic resolution and abscission than occurs in control cells, or a failure to enter or maintain the cytokinesis stage, resulting in aberrant or failed mitosis and tetraploid G1 cells (Figure 3.18). Deregulated resolution of cytokinesis, characterised by increased speed through the NoCut abscission checkpoint, is associated with increased DNA damage, due to the failure to ensure complete and correct DNA segregation prior to abscission (Ganem and Pellman, 2012; Figure 3.16). Indeed, CHMP7 depletion is associated with increased DNA damage.

The hypothesis that CHMP7 depletion is linked to aborted mitosis, leading to a multinucleated daughter cell is also plausible given the increase in multinucleated cells following the knockdown. VPS4 is known to cause multinucleation due to its crucial role in the final part of abscission, whereby the ESCRT-III complex cannot complete scission without the driving force of VPS4 (Thoresen *et al.*, 2014). However, CHMP7 is not known to have a role in the abscission step of cytokinesis, and loss of CHMP7 appears to result in increased

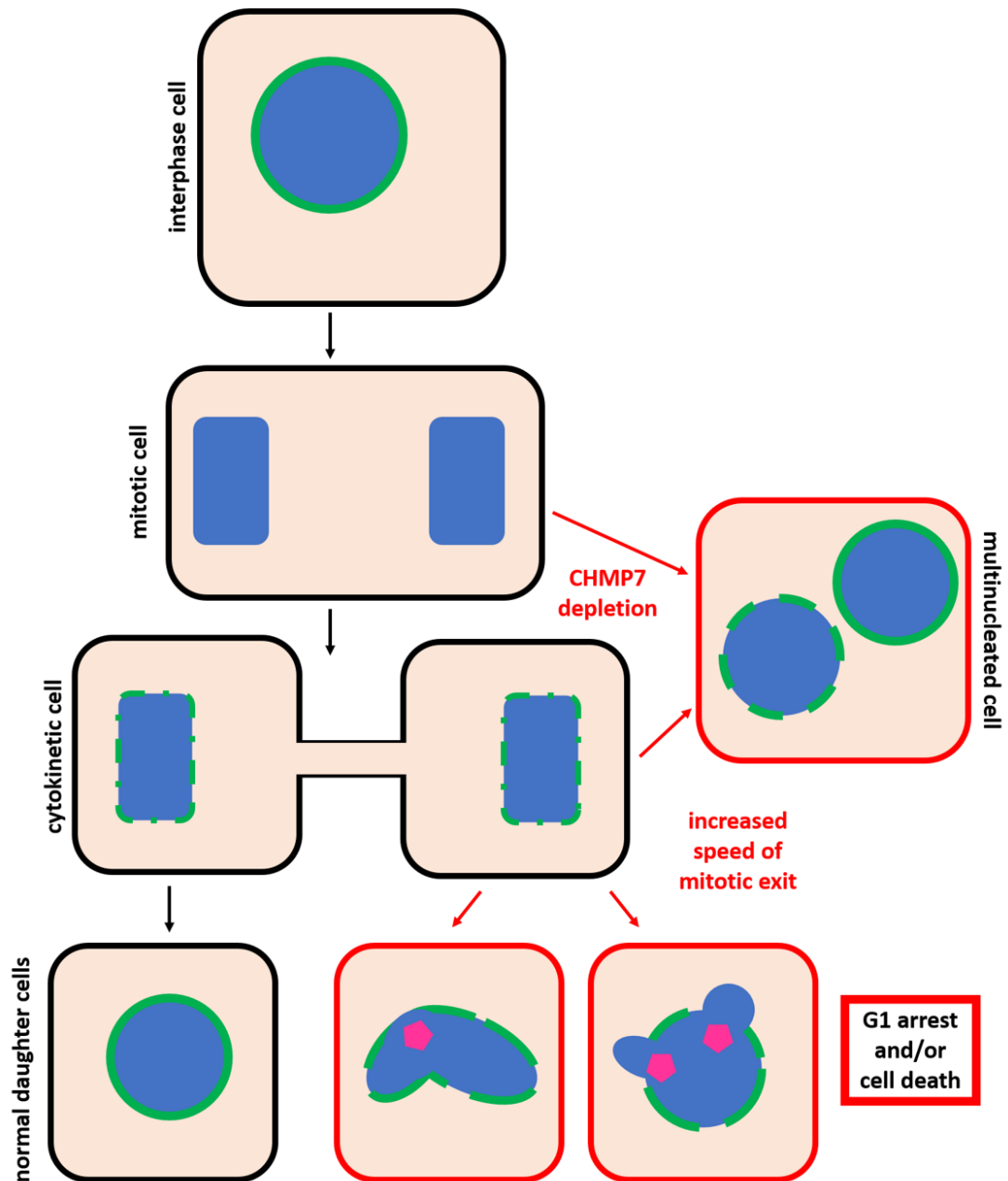


Figure 3.18. A model to show development of nuclear defects in CHMP7-depleted cells

CHMP7-depleted cells display aberrant progress through mitosis, including either increased speed of mitotic exit or failure to enter and complete the cytokinetic step of cell division. Aborted cytokinesis results in formation of multinucleated cells, which are observed in CHMP7 knockdown conditions. Progress through cytokinesis at an accelerated rate may result in daughter cells displaying nuclear and mitotic defects, leading to cell dysfunction, arrest and eventually death.

speed of cytokinetic exit, as opposed to the increase in the number of cytokinetic cells observed upon VPS4 knockdown. This observation appears similar to that seen upon depletion of one other ESCRT-III subunit, CHMP4C, in which abscission time was significantly reduced (Carlton *et al.*, 2012), due to its crucial role in the NoCut checkpoint.

The third key cell cycle-related observation upon CHMP7 knockdown was the aberrations in centrosome cohesion and positioning in interphase, which may have resulted from or in some of the mitotic problems observed in CHMP7-depleted cells. Interestingly, HeLa cells showed a significant increase in cells with centrosome separation and distance from the nucleus in interphase, whereas U2OS cells did not show the same aberration. The lack of problems with centrosomes in U2OS cells may be explicable using the findings of (Panic *et al.*, 2015), who demonstrated that the link between centrosomes in HeLa cells is more robust than that seen in U2OS cells. Depletion of a centrosomal linker protein C-Nap1 caused separation of centrosomes in HeLa cells, but not in U2OS. Microtubule dynamics acted to keep U2OS centrosomes close together, with depolymerisation of microtubules by nocodazole treatment required to cause separation of centrosomes in U2OS cells, and to a lesser but still significant extent in control cells. Microtubule organisation protein (CDK5RAP2) depletion was shown to cause separation of centrosomes in both HeLa and U2OS cells, though the penetrance of this phenotype was greater in HeLa cells (Graser *et al.*, 2007). Therefore, it seems more likely that the effect of CHMP7 knockdown is related to centrosome cohesion, as opposed to through cytoskeletal (microtubule) disruption. Additionally, the nuclear envelope disorganisation observed upon CHMP7 knockdown, which is further discussed below, may result in a failure of proper tethering of centrosomes to the nuclear envelope, which is mediated through the LINC complex which links the cytoskeleton to the nuclear lamina (Figure 3.17). This would result in an indirect effect on centrosome positioning. Since CHMP7-depleted U2OS showed little aberration of nuclear pore complex

localisation, it may be the case that the linker between the nuclear envelope and centrosomes also remains intact.

Preliminary scoring of one live cell imaging experiment, observing mitosis in CHMP7-3-depleted HeLa cells, shows an increase in the number of mitotic cells demonstrating multipolar mitoses appearing to derive from fragmenting spindle poles (Dr N Flores-Rodriguez, University of Queensland, AU), resulting in cytokinetic failure (generating a multinucleated cell) or multinucleated daughter cells. If this finding is substantiated, it may demonstrate another consequence of the aberrant centrosomal phenotype observed in some cells lacking CHMP7. While little can be deduced at this early stage, live cell imaging is likely to yield further insights into the problems encountered by CHMP7-depleted cells in mitosis.

3.3.2 The effect of CHMP7 knockdown on nuclear envelope organisation and integrity

Knockdown of CHMP7 results in loss of nuclear envelope organisation, resulting in chromatin herniations and loss of compartmentalisation, indicating occurrences of nuclear rupturing (Figure 3.17). There also appears to be an associated effect on genomic integrity, as shown by the presence of DNA damage markers.

In this chapter, it has been shown that CHMP7 depleted cells show increased rates of cytoplasmic-localised PML bodies. It is not possible to tell if the nuclear envelope is ruptured in these cells, or whether it had been previously ruptured and repaired, however these results show that the integrity of the nuclear envelope has been compromised in these cells. Houben *et al.* (2013) investigated the link between nuclear aberrations (including nuclear envelope honeycombs, blebs and herniations) and cytoplasmic PML bodies, however, a definite correlation was not found. Not all cells which rupture show mislocalisation of PML bodies, hypothesised to be due to small rupture size, short duration of loss of

compartmentalisation, or tight association of PML bodies with the nuclear matrix or chromatin, resulting in anchoring to the nucleus. In addition, degradation of cytoplasmic PML bodies has been observed (Houben *et al.*, 2013). Therefore, the rates of nuclear rupture are likely to be higher than the rates of cells with cytoplasmic PML bodies, and a more direct method of measuring nuclear envelope rupture would be a useful tool to determine the exact proportion of ruptured cells. However, this was outside the scope of this study.

It was previously assumed that holes in the nuclear envelope were only made as part of regulated processes such as apoptosis, mitosis, and the nuclear budding to export large mRNPs, or when manipulated by viral infections. However, transient nuclear ruptures which occur randomly in interphase and result in compromised nuclear integrity have now been described in both laminopathic cells (De Vos *et al.*, 2011), and normal HeLa and U2OS cells (Vargas *et al.*, 2012). The term NERDI (nuclear envelope rupturing during interphase) refers to these transient events, in which nuclear integrity is compromised, resulting in loss of compartmentalisation. These ruptures are repaired, with associated restoration of nuclear and cytoplasmic compartmentalisation, allowing normal continuation of the cell cycle and cell division. However, mislocalisation of large structures such as mitochondria and PML bodies is not reversible following nuclear envelope repair. Depletion of Lamin B in U2OS cells causes an increased incidence of interphase nuclear ruptures, mimicking the structural abnormalities which occur in laminopathies. Ruptures in interphase originate from localised nuclear envelope deformations or herniations, which occur at regions of nuclear lamina weakness, absence or disorganisation in wild-type HeLa and U2OS cells (Vargas *et al.*, 2012).

Several aspects of nuclear disorganisation as seen upon CHMP7 depletion appear similar to a laminopathy phenotype, including the honeycomb pattern or holes in the nuclear lamina. Frequent aberrations of the nuclear lamina upon CHMP7 depletion as documented in this chapter may indicate an increased likelihood of nuclear membrane fragility and rupture,

leading to loss of PML bodies from the nuclear compartment. Loss of compartmentalisation through nuclear rupture is a strong driver of genomic instability leading to and perpetuating cancer development (Lim *et al.*, 2016), and thus seems likely to be the cause of the increased rates of DNA damage observed in HeLa cells in this study.

It is also possible that PML protein structures, which remain aggregated but lose chromatin association during mitosis (Chen *et al.*, 2008), fail to be reincorporated back into the nucleus following an aberrant exit from mitosis in the CHMP7 knockdown. Interestingly, direction of PML to the nucleus at the end of mitosis is closely related to that of nucleoporins, with formation of CyPNs (cytoplasmic assemblies of PML and nucleoporins) described in human cells (Jul-Larsen *et al.*, 2009). These compartments form prior to the end of mitosis, and are transported via a microtubule network to the nuclear periphery, where they associate with nuclear membrane. The failure of both PML and nuclear pore complexes to be properly localised in some CHMP7-depleted cells may be related. Further work could be carried out to determine whether PML localises with the nuclear pore protein aggregations which are observed in CHMP7 depleted cells in order to address this question.

Additionally, mis-segregation of chromosomes can lead to problems in lamina formation at the end of mitosis, through formation of chromosome “bridges” in mitosis, as unseparated chromosomes pulled to the spindle poles remaining connected by a thin stretch of DNA, around which lamina forms incompletely, leading to nuclear ruptures (Maciejowski *et al.*, 2015). It has been speculated that other mitotic events, such as lagging or late-segregating chromosomes causing disruption or delay of nuclear envelope and lamina rebuilding in late mitosis may result in areas of weakened nuclear integrity (Lim *et al.*, 2016). Therefore, there may be a connection between the effects of the CHMP7 knockdown on accurate mitosis and the resulting nuclear envelope and lamin defects.

3.3.3 A role for CHMP7 in nuclear pore complex organisation

CHMP7 depletion was shown in this chapter to cause aberration of nuclear pore complex insertion into the nuclear envelope, instead demonstrating aggregation of NPC proteins in the cytoplasm. The phenotype was also observed at comparable levels in VPS4-depleted cells, indicating that loss of ESCRT-III function also produces the same or equivalent effect as CHMP7 knockdown.

Nuclear pore complexes (NPCs) are incorporated into the nuclear envelope upon nuclear envelope reassembly following mitosis, but are also inserted into the nuclear envelope during interphase. The method of nuclear pore complex insertion into the intact interphase nuclear envelope is currently unknown, however, it has been hypothesised that it would require membrane remodelling around the site of the insertion including fusion of the inner and outer nuclear membranes, in order to create a hole for NPC assembly. An alternative theory has been posited based on work carried out in *Drosophila* (Hampoelz *et al.*, 2016), based on the insertion of multiple pre-assembled nuclear pore complexes through the integration of a sheet of NPC-studded ER membrane into the outer nuclear membrane, contributing to both nuclear expansion and increased NPC numbers as the cell cycle progresses. However, this model would also involve membrane cutting and sealing, in order to integrate stretches of new membrane into the nuclear envelope. It is tempting to hypothesise a role for ESCRT-III in a membrane scission/sealing capacity related to the insertion of NPCs into the nuclear envelope, and an essential role for CHMP7 in this process, based on the defects observed upon their depletion.

Recently, a link between the yeast form of CHMP7 (Chm7) has been shown to play a role in surveillance and quality control of nuclear pore complexes inserted in the yeast nuclear membrane (Webster *et al.*, 2016). In this study, it is shown that Chm7 is responsible for sealing the nuclear envelope around defective NPCs, preventing inappropriate transport

through the defective channel, thus maintaining nuclear compartmentalisation and therefore, cell viability. Nuclear pore complex accumulation was observed in VPS4-depleted yeast cells in a structure named a "SINC" (storage of improperly assembled nuclear pore complexes) compartment. It is possible that the accumulations of NPCs observed in this chapter represent a form of SINC compartment, and that a similar role is performed by human CHMP7 and ESCRT-III.

The results shown here may represent the first evidence of a role for CHMP7, possibly in conjunction with the ESCRT-III complex, in nuclear pore complex quality control and insertion in human cells, based on the defects commonly observed in cells depleted of CHMP7.

Chapter Four

The role of CHMP7 and the ESCRT-III complex at the nuclear envelope

Contents

	Page
4.1 Introduction	113
4.1.1 Chapter Summary	113
4.1.2 Initiation of nuclear envelope reformation in anaphase	113
4.1.3 Recruitment and sealing of a nuclear envelope from ER membrane	114
4.1.4 Organisation of the nuclear envelope: the nuclear lamina and pore complexes	117
4.1.5 PML nuclear bodies	118
4.2 Results	120
4.2.1 Immunofluorescence microscopy for study of CHMP7	120
4.2.2 Subcellular distribution of CHMP7 throughout mitosis	120
4.2.3 CHMP7 accumulates in foci on nuclei in VPS4-depleted cells	123
4.2.4 CHMP7 is required for the accumulation of nuclear-associated ESCRT-III complex	125
4.2.5 CHMP7 and VPS4 knockdown affect PML body number and size	127
4.2.6 Co-occurrence of PML bodies with CHMP7 foci in VPS4 knockdown cells is foci size-dependent	129
4.2.7 DNA damage and repair protein markers associate with CHMP7 nuclear foci	131
4.2.8 CHMP7 does not form foci in response to UV-induced DNA damage	133
4.2.9 LAP2 is enriched at CHMP7 interphase nuclear foci, indicating a role for CHMP7 at the nuclear membrane	135
4.2.10 CHMP7 foci occur at holes in the nuclear lamina	135
4.2.11 CHMP7/ESCRT-III foci correspond to the interphase nuclear envelope	138
4.2.12 CHMP7 localises to chromatin in the late stages of mitosis	138
4.2.13 Characterisation of CHMP7 localisation to chromatin in mitosis	142
4.2.14 The ESCRT-III complex localises with CHMP7 in late mitosis	142
4.2.15 CHMP7 is essential for the recruitment of the ESCRT-III complex in late mitosis	146
4.2.16 Investigating the relationship between centromeres and CHMP7	146
4.2.17 ESCRT-III assembles with nuclear membrane in mitosis	147
4.2.18 CHMP7 appears with membranes structures on the edge of the reforming nuclear envelope	151
4.2.19 CHMP7 colocalises with INM protein LAP2 at the reforming nuclear envelope	153
4.2.20 Investigating direct interactions between CHMP7/CHMP4B and LAP2	156
4.2.21 CHMP7 localises to chromatin prior to nuclear lamina formation and adjacent to Lamin B	156
4.2.22 CHMP7 is not necessary for the recruitment of nuclear envelope components	159
4.2.23 Overexpression of HA-tagged CHMP7 constructs	159

4.2.24	Overexpression of HA-CHMP7-FL and HA-CHMP7-NT results in NE deformation and misshapen nuclei	164
4.2.25	Endogenous CHMP7 in untreated interphase cells localises to the nuclear envelope	165
4.3	Discussion	167
4.3.1	A model for CHMP7/ESCRT-III function at the nuclear envelope	168
4.3.2	A model for formation of interphase nuclear CHMP7/ESCRT-III foci in VPS4-depleted cells	170
4.3.3	Perturbation of ESCRT-III activity results in DNA damage and repair pathway signalling	172
4.3.4	CHMP7 associates with nuclear structures through its N-terminal half	174
4.3.5	A potential role for CHMP7/ESCRT-III in repairing interphase nuclear envelope ruptures	175

List of Figures

Figure	Title	Page
4.1	Formation of the nuclear envelope from ER membrane during mitosis	114
4.2	ER membrane recruitment and nuclear envelope sealing in telophase	115
4.3	Subcellular localisation of CHMP7 throughout the cell cycle	120
4.4	VPS4 knockdown causes nuclear accumulation of CHMP7 into foci	123
4.5	CHMP7 nuclear foci in VPS4-depleted cells also contain CHMP4B and CHMP1B	125
4.6	CHMP7 and VPS4 knockdown affect PML body number, size, and shape	127
4.7	Large CHMP7 nuclear foci associate with or are encircled by PML protein	129
4.8	CHMP7 nuclear foci associate with various DNA damage and repair proteins	131
4.9	CHMP7 does not form nuclear foci upon induction of DNA damage with UVC radiation	133
4.10	Large CHMP7 foci show strong LAP2 colocalisation	135
4.11	Large CHMP7 foci correspond with gaps in the nuclear lamina	136
4.12	CHMP7 foci localise at the periphery of the nucleus	138
4.13	CHMP7 displays a novel, chromatin-associated pattern of accumulation into puncta in VPS4-depleted cells	139
4.14	Features of CHMP7 localisation in mitosis	142
4.15	CHMP4B and CHMP1B colocalise with CHMP7 at late anaphase/early telophase	143
4.16	CHMP7 occasionally shows localisation near centromeres in telophase cells	147
4.17	Optimisation of ER membrane staining	149
4.18	CHMP7 localises to telophase chromatin with ER membranes	151
4.19	CHMP7 colocalises with LAP2 at the reforming nuclear envelope	153
4.20	CHMP7 localises adjacent to Lamin B at the reforming nuclear envelope	156
4.21	CHMP7 knockdown does not affect recruitment of LAP2, Lamin B or NPCs to the nascent nuclei	159
4.22	Overexpressed full length and N-terminal CHMP7 in HeLa cells	161
4.23	Endogenous CHMP7 and CHMP4B are found on the nuclear rim following detergent pre-extraction	165
4.24	A nuclear role for the ESCRT-III complex	168
4.25	A model for nuclear envelope sealing in CHMP7 and VPS4-depleted cells	170
4.26	Perturbation of ESCRT-III activity results in DNA damage	172

4.1 - Introduction

4.1.1 - Chapter Summary

The previous chapter elucidated the importance of CHMP7 for normal cellular function, and how loss of this protein causes a number of aberrant phenotypes. In this chapter, data are presented to support a function for the CHMP7 protein and the ESCRT-III complex at the nuclear envelope. These results aim to investigate the mechanisms of nuclear deformation, nuclear envelope disorganisation, and loss of nuclear and genomic integrity determined in the previous chapter following CHMP7 depletion.

The Human Protein Atlas, which collates data from proteomic studies, describes CHMP7 as primarily nuclear, with some cytoplasmic localisation (Uhlen *et al.*, 2015). Further work by Cleasby (PhD thesis, 2013) on CHMP7 shows large nuclear accumulations, however these observations have been carried out on the exaggerated phenotype generated by VPS4 depletion, and the drastic localisation of CHMP7 to the nucleus which this induces. While interphase localisation of CHMP7 has been investigated, the distribution of CHMP7 throughout the cell cycle has not been documented.

Here, immunofluorescence studies and Western blots are used to observe the localisation of endogenous CHMP7 and ESCRT-III throughout the cell cycle. In addition, CHMP7 full-length and uncharacterised N-terminal half protein constructs were used to observe overexpression phenotypes. CHMP7 is found to localise to the nuclear envelope in interphase, and ESCRT-III accumulates into large foci in late mitosis on the reforming nuclear envelope. However, ESCRT-III foci were never found to form in the absence of CHMP7. Tagged, overexpressed N-terminal CHMP7 showed localisation to the nuclear envelope and perinuclear endoplasmic reticulum.

The previously observed CHMP7 nuclear foci, which accumulate upon depletion of VPS4 (Cleasby, PhD thesis, 2013), are dissected in order to understand their relationship with

nuclear structures. These structures were found to be composed of ESCRT-III proteins, occurring at holes in the nuclear lamina but showing colocalisation with inner nuclear membrane proteins and occurring adjacent to regions of DNA damage and PML protein. Together, this chapter demonstrates a key role for CHMP7 in the recruitment of ESCRT-III to the nuclear membrane in mitosis.

4.1.2 Initiation of nuclear envelope reformation in anaphase

Metazoan cells use open mitosis, which requires disassembly of the nuclear envelope to allow spindle microtubules to interact with chromosomes. The mitotic spindle aligns chromosomes to regulate chromatid separation to either end of a dividing cell. Vertebrate cells undergo a complete disassembly of the nuclear envelope structure, including dispersal of nuclear proteins throughout the cell, integration of nuclear membrane and transmembrane proteins into the endoplasmic reticulum, and dismantling of the nuclear lamina and pore complexes. Reassembly of the nuclear envelope around the segregated chromatin is a complex process consisting of tightly-regulated stages, resulting in restored separation between the nuclear and cytoplasmic compartments of cells.

A new nuclear double-membrane is recruited from the ER, coordinated with severing interaction between microtubules and chromatin, chromosome decondensation, NPC reassembly and insertion, and lamina formation, leading to a complete, sealed nuclear envelope structure. Nuclear envelope reformation begins in the late anaphase stage of mitosis, following chromatid segregation, and is concluded in telophase. Reassembly of NE components is initiated by reversion of mitotic kinase phosphorylation events which led to nuclear envelope breakdown, in particular the inactivation of master mitotic regulator Cdk1.

4.1.3 Recruitment and sealing of a nuclear envelope from ER membrane

Nuclear envelope sealing at the end of mitosis is a crucial step in the cell cycle, allowing creation of the nuclear compartment and ensuring proper cell function and viability. The

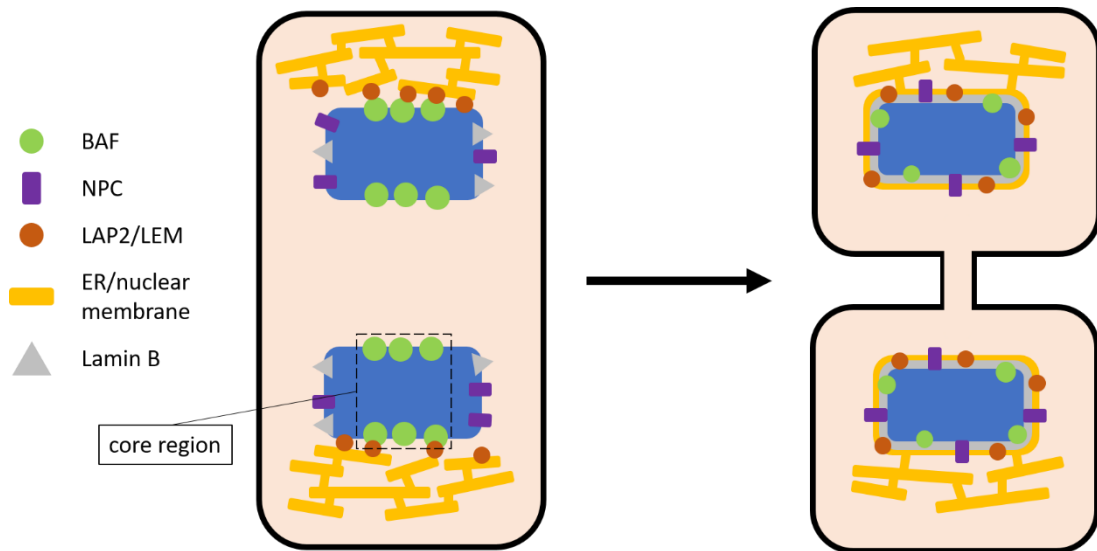


Figure 4.1. Formation of the nuclear envelope from ER membrane during mitosis

Following the segregation of chromosomes into two distinct daughter nuclei, proteins including BAF, LBR, Lamin B and nucleoporins associate with chromatin, creating core and peripheral subdomains in the reforming nucleus. ER membrane is recruited to the surface of chromatin through the LEM family INM proteins (such as LAP2) proteins which are inserted into ER membranes and bind to BAF and chromatin. Following ER membrane spreading, nuclear lamina and nuclear pore complexes fully form, and nuclear envelope components distribute evenly across the surface of the nucleus.

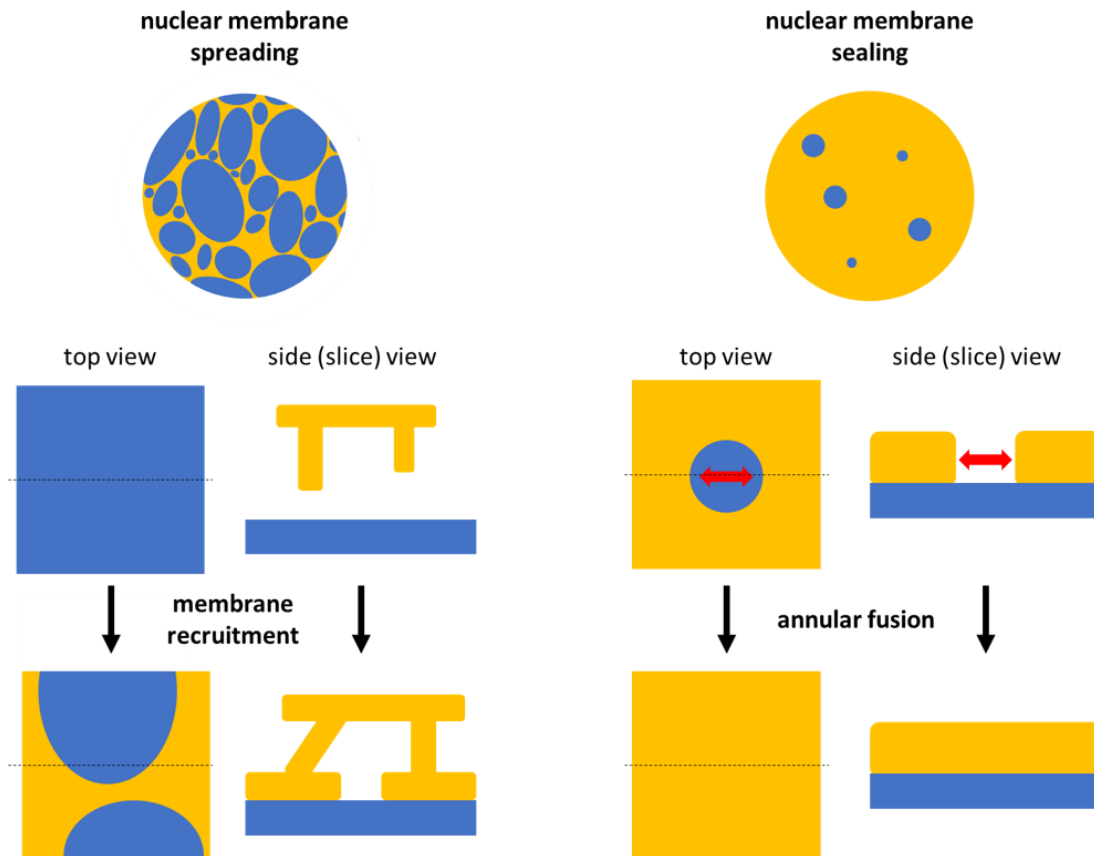


Figure 4.2. ER membrane recruitment and nuclear envelope sealing in telophase

ER membrane is recruited to chromatin, and flattens, spreads and expands across the surface of the nascent nucleus. Sheets of ER membrane are thought to fuse on the nuclear surface, however the final sealing step of NE reformation requires resolution of small circular holes in the membrane. Annular fusion describes the required process, whereby the edges of the circular hole are brought together, concurrently with a fusion step which allows for sealing of the hole.

nuclear membranes are derived from mitotic ER structures, which are recruited to the surface of chromatin, flatten, and expand over the surface (Figure 4.1; Figure 4.2). ER remodelling requires proteins such as Reticulons and the DP1/REEP family (Shemesh *et al.*, 2014), and in *in vitro Xenopus* systems, NSF and SNAREs were found to be required for formation of sealed “nuclei” from ER membranes and chromatin (Wang *et al.*, 2013), although this requires further investigation *in vivo*.

While the model for membrane spreading across chromatin is still debated, it is known that association of ER membrane to chromatin is driven by several INM proteins localised to the ER membrane following nuclear envelope breakdown, including LBR (Lamin B receptor), POM121 and the LEM domain family of proteins (LAP2, Emerin and MAN1; Figure 4.1), which interact with various chromatin-associated proteins or DNA (Anderson *et al.*, 2009). These INM proteins form a redundant, reliable system, whereby loss of any one is insufficient to prevent NE reformation from occurring (Anderson *et al.*, 2009). This anchoring of membrane to chromatin aids membrane sheet spreading across the chromatin surface.

The final closure of gaps or holes in a double-membraned structure requires a specific fusion event, that of annular (circular) fusion (Figure 4.2). Annular fusion requires both constriction of the hole, reducing its diameter and bringing the membranes close enough for fusion to occur, as well as the fusion activity itself. A mechanism mediated by a p97/Ufd1/Npl4 complex has been suggested (Burke and Ellenberg, 2002), as well as the insertion of nuclear pore complexes into these holes, thereby removing the need for an annular fusion event (Güttinger *et al.*, 2009).

4.1.4 Organisation of the nuclear envelope: the nuclear lamina and pore complexes

Nuclear pore complexes begin to assemble on chromatin before the recruitment of ER membrane, however the mode of incorporation of NPCs into the nuclear envelope in mitosis

is as yet uncertain, though two models exist. The first is an insertion model, whereby the NPC is inserted into an intact nuclear membrane, through creation of a hole which is sealed around an inserted NPC (Fichtman *et al.*, 2010). The second is an enclosure model, whereby ER membrane sheets spreading across the surface of chromatin spreads around a chromatin-associated NPC, enveloping the structure without a need for a hole to be generated by inner and outer nuclear membrane fusion (Anderson and Hetzer, 2007). Association of some lamin protein with the nuclear membrane is observed during its formation, however, the majority of lamina assembly occurs following restoration of compartmentalisation, with Lamin B protein imported into the nucleus through nuclear pore complexes (Güttinger *et al.*, 2009).

4.1.5 PML nuclear bodies

In this chapter, the relationship between CHMP7 and PML bodies is examined. PML nuclear bodies are complex and dynamic subnuclear protein structures found in most mammalian cells, which are nucleated and organised by the PML (promyelocytic leukaemia) tumour suppressor protein (Salomoni and Pandolfi, 2002). Association between PML bodies and nuclear CHMPs in VPS4-depleted HeLa M cells have been proposed and observed by Cleasby (PhD thesis, 2013).

PML bodies form in the nuclear matrix, making extensive contacts with chromatin, which may be important for both stability and function. PML foci occur at a frequency of approximately 1-30 per cell, and measure 0.1-1.0 μ m in diameter, with composition, morphology and distribution dependent on cell-cycle phase, cell type, cell stress or DNA damage (Dellaire and Bazett-Jones, 2004). PML bodies are known to be highly dynamic structures which disassemble and fragment in response to DNA damage and cellular stresses including viral infection, heat shock and oxidative stress, dispersing protein factors to numerous sites. Splicing of the human PML gene results in 6 different nuclear isoforms of

the proteins which differ at the C-terminus (Brand *et al.*, 2010), which may explain why PML bodies are implicated in a wide range of functions.

A mature PML nuclear body is spherical, with a PML polymer casing, and recruits a wide variety of proteins to its core. The presence of nucleic acids within the structure is uncertain, with Boisvert *et al.* (2000) demonstrating that no nucleic acids are present. However, Luciani *et al.* (2006) studied unusually large PML nuclear bodies, showing in these cases that proteins were assembled in rings around a core of DNA. These structures are thought to act as a store for proteins, while also enacting partner protein sequestration, modification, activation, or degradation.

PML is phosphorylated by ATM and CHK2 following DNA damage (Yang *et al.*, 2002), and some proteins localise to PML bodies only upon DNA damage, including ATM, γ H2AX and BRCA1 (Bernardi and Pandolfi, 2007). PML bodies are implicated in the DNA damage response, localising with persistent DNA damage foci in humans cells (Münch *et al.*, 2014). In addition, PML has a tumour suppressor role, with PML mutations and deficiencies resulting in susceptibility to tumour formation (Salomoni and Pandolfi, 2002). Luciani *et al.* (2006) propose a further interesting function for PML nuclear bodies in chromatin remodelling, specifically in G2 phase, aiding with the condensation of late-replicating DNA into heterochromatin.

4.2 - Results

4.2.1 Immunofluorescence microscopy for study of CHMP7

Using immunofluorescence allows the distribution of endogenous CHMP7 and other proteins to be observed through specific antibody-based targeting and visualisation by fluorescent microscopy. In addition, the effects of various conditions, such as knockdown or overexpression of other proteins and introduction of stresses such as DNA damage, on CHMP7 localisation and abundance can be observed. Using multiple antibodies, as specified in Section 2.1.1, the relationship of CHMP7 to other proteins can be elucidated. The use of three CHMP7 specific antibodies derived from different host animals will allow for a range of counterstaining antibodies to be used alongside them, and allows for double validation of any observations.

4.2.2 Subcellular distribution of CHMP7 throughout mitosis

Firstly, it is important to observe the native localisation status of CHMP7 throughout the cell cycle. To observe the subcellular distribution of CHMP7, HeLa cells were used, stained with the mouse-derived anti-CHMP7 antibody. Representative images of CHMP7 localisation in interphase and each mitotic phase are shown in Figure 4.3a.

In interphase HeLa cells, CHMP7 is primarily nuclear, although it is also found significantly in the cytoplasm. Throughout prophase and prometaphase, CHMP7 is still observed to be significantly nuclear, localising in the region of DNA. As the cell progresses into metaphase and anaphase, CHMP7 becomes more excluded from the area of chromatin, remaining diffuse throughout the cell. Telophase cells display a previously unseen pattern of CHMP7 localisation, in which CHMP7 accumulates into intense puncta. These bright structures appear transiently, and are therefore infrequently captured in a population of fixed cells, and correspond to the periphery of the nascent daughter nuclei. This observation is characterised more fully from Section 4.2.12 onwards.

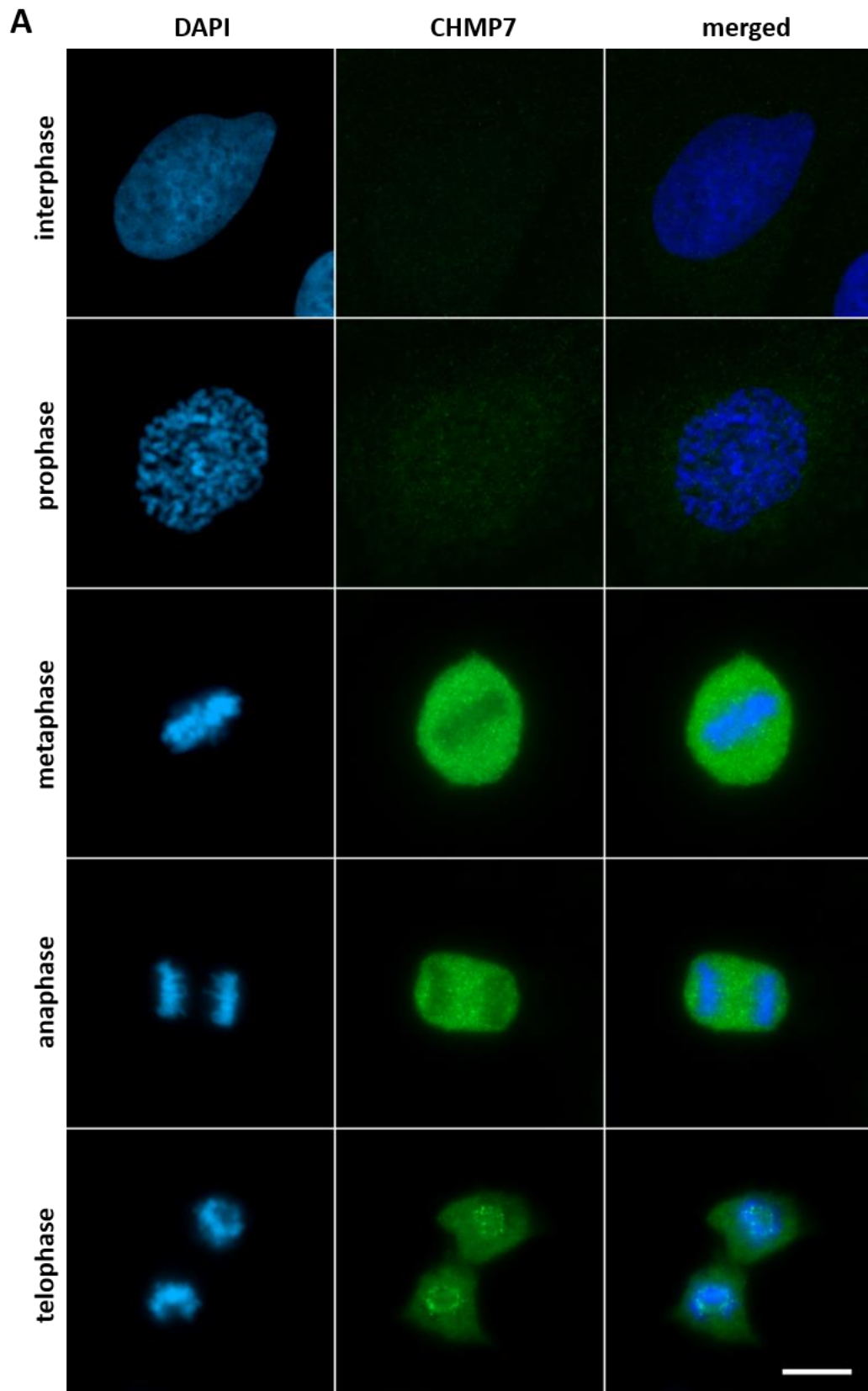


Figure 4.3. Subcellular localisation of CHMP7 throughout the cell cycle.

a) Untreated HeLa cells were stained with DAPI and mouse anti-CHMP7 antibody. Scale bar represents 10 μ m.

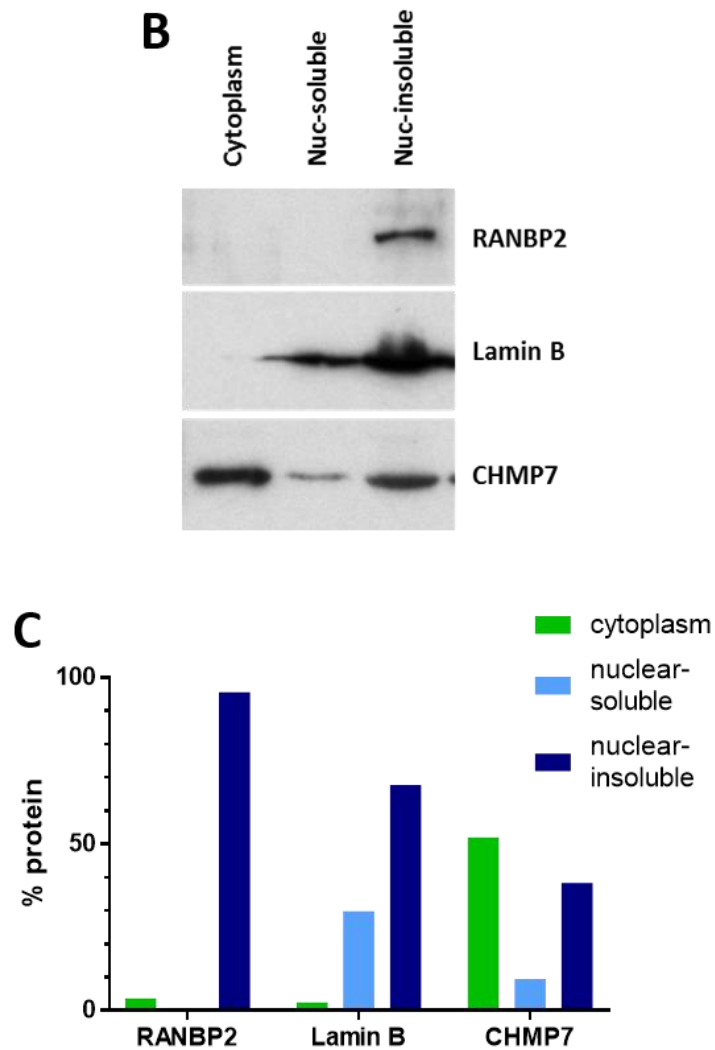


Figure 4.3. (continued)

b) Western blot of untreated HeLa cell lysates separated into three fractions - 1: cytoplasm, membranes, and cell debris, 2: the soluble content of cell nuclei and 3: the insoluble content of cell nuclei. **c)** Quantification of the intensity of Western blot bands in (b), showing the percentage of protein in each fraction. Intensity was calculated using the Gel Analyzer feature of ImageJ.

Based on the interphase localisation of CHMP7 in the region of the nucleus, we were interested to investigate to which portion of the nucleus this occurs.

Therefore, subcellular fractionation of HeLa cells was carried out to separate a pellet of whole, untreated HeLa cells into three fractions – cytoplasmic, soluble nuclear and insoluble nuclear contents (Figure 4.3b). Quantification of the proportion of CHMP7 which was found in each fraction shows that approximately half of the protein in this pellet was found in the cytoplasmic fraction (which includes cell membrane and cell debris), with the remainder found in the soluble nuclear (9.5%) and insoluble nuclear (38.4%) portions (Figure 4.3c).

4.2.3 CHMP7 accumulates in foci on nuclei in VPS4-depleted cells

VPS4 is necessary for the reshaping and recycling of the ESCRT-III complex, through its ability to remove CHMP subunits from the complex, providing the driving force for constriction of the associated membrane and eventual scission. Therefore, depletion of VPS4 causes impairment of several ESCRT-III-related processes, such as accumulation of endosomal CHMPs on abnormally large early endosomes, due to the failure of multivesicular body formation. In addition, the final abscission step of cytokinesis is prevented from completion, resulting in cytokinesis failure. However, work in HeLa M cells (Cleasby, PhD thesis, 2013) has shown CHMP7 is not observed to accumulate at either endosomes or at the midbody, instead displaying a predominant nuclear foci pattern of localisation.

This observation of CHMP7 foci in HeLa M cells depleted of VPS4 was repeated here (Figure 4.4a), with 97.7% HeLa M cells transfected with 3nM VPS4 siRNA for 48 hours showing at least one nuclear foci per cell, with an average of 13.9 foci per cell. HeLa and U2OS cells were also scored for the presence of CHMP7 foci after VPS4 depletion, with 82.0% HeLa cells and 93% U2OS cells displaying at least one CHMP7 nuclear foci, with an average of 4.8 and 6.2 foci per cell, respectively (Figure 4.4b). Significantly more foci are observed per nucleus in HeLa M cells compared to HeLa and U2OS cells. The increased size of the HeLa M nuclei in

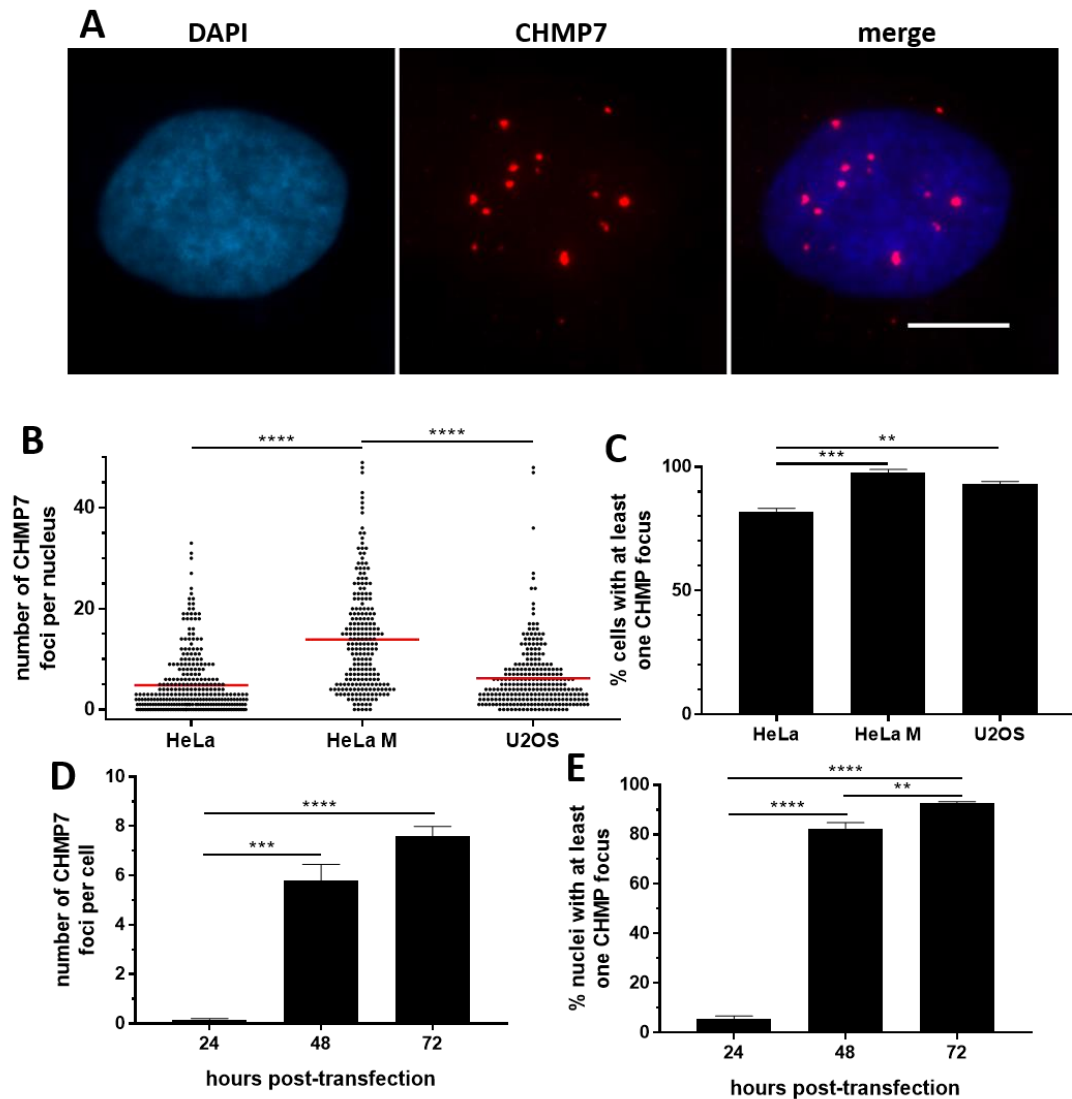


Figure 4.4. VPS4 knockdown causes nuclear accumulation of CHMP7 into foci

a) Image of CHMP7 foci in a HeLa cell depleted of VPS4. Scale bar represents 10 μ m. **b)** The number of CHMP7 foci found per nucleus in HeLa (n=305), HeLa M (n=222) and U2OS (n=257) cells. Averages and individual measurements are shown. **c)** The percentage of cells with at least one CHMP7 focus were scored in a minimum of 500 cells. Averages and standard error of three independent repeats are shown. **d)** The percentage of CHMP7 foci in HeLa cells following knockdown at 24, 48 and 72 hours post transfection. **e)** The percentage of HeLa cells containing at least one accumulation of CHMP7 (focus) following knockdown at 24, 48 and 72 hours post transfection. A minimum of 200 cells were scored per condition. Averages and standard error of three independent repeats are shown. Results were analysed using a one-way ANOVA with Tukey's *post hoc* test compared to control.

comparison to the other cell lines may account for this disparity. It is clear that nuclear formation of CHMP7 foci is shared across cell lines under these conditions.

The formation of CHMP7 foci in HeLa cells was measured over time (Figure 4.4c and 4.4d), with cells scored at 24, 48 and 72 hours for the number of foci per cell, as well as the number of cells with at least one CHMP7 focus. Few foci were observed after 24 hours, with an average of 0.2 foci per cell, and 5.6% of cells displaying at least one CHMP7 focus. This increased substantially after 48 hours, with 82.5% of cells displaying foci, and an average of 5.7 foci. There is another, smaller increase between 48 and 72 hours, with a larger proportion of cells affected (92.7%) and a higher average foci count (7.6 per cell). This shows that cells with CHMP7 nuclear foci are accumulating with successive cell divisions and persisting over time.

4.2.4 CHMP7 is required for the accumulation of nuclear-associated ESCRT-III complex

In order to determine the nature of these CHMP7 structures in HeLa cells, the presence of other members of the ESCRT-III complex were visualised using immunofluorescence, and scored based on their colocalisation with CHMP7 foci. As can be observed in the HeLa cells in Figure 4.5a, CHMP4B can be observed localising to structures adjacent to the nucleus, presumed to be endosomal accumulation of ESCRT-III due to the VPS4 depletion, whereas CHMP7 is observed only in the nuclear foci. CHMP4B was observed to be present in 96.7% of CHMP7 foci after 48 hours of VPS4 depletion, and CHMP1B was observed in 59.2% of CHMP7 foci (Figure 4.5b). No CHMP4B or CHMP1B foci were observed in the absence of CHMP7. This data demonstrates that the nuclear localisation of CHMP4B and CHMP1B is conditional on the presence of CHMP7.

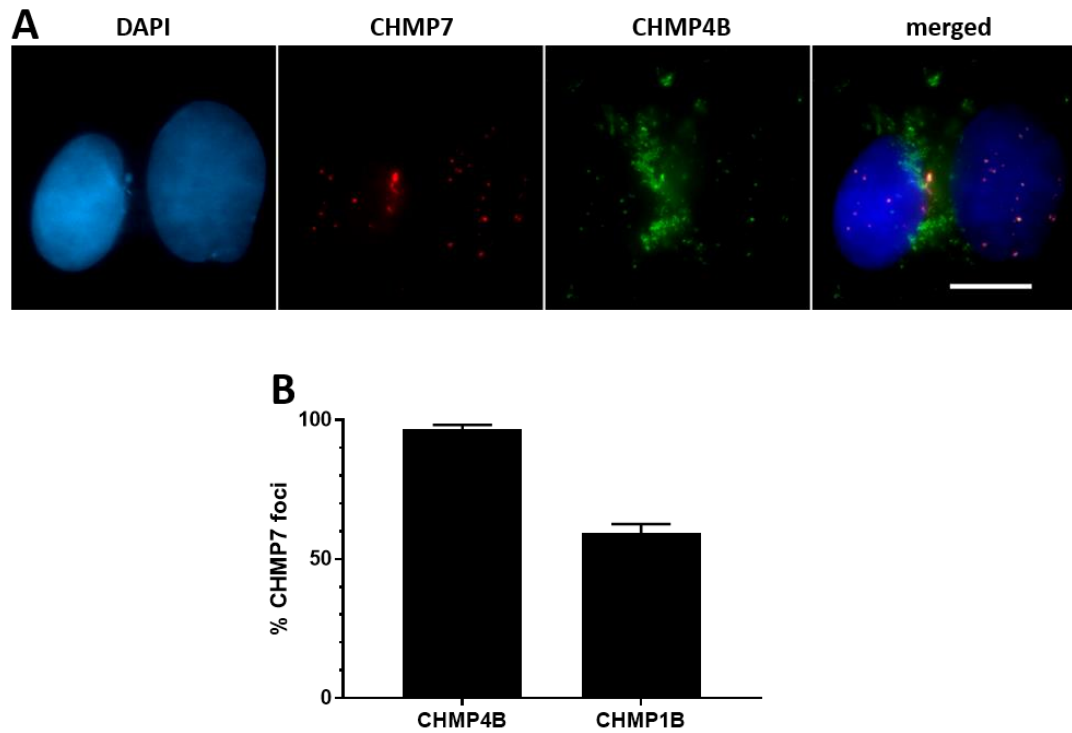


Figure 4.5. CHMP7 nuclear foci in VPS4-depleted cells also contain CHMP4B and CHMP1B

a) HeLa cells were co-stained with anti-CHMP7 and anti-CHMP4B antibody. Scale bar represents 10 μ m. **b)** CHMP7 foci in VPS4-depleted HeLa cells were scored for presence of CHMP4B or CHMP1B. A minimum of 300 nuclei were scored. Averages and standard error of three independent repeats are shown.

4.2.5 CHMP7 and VPS4 knockdown affect PML body number and size

Previous work by our group (Cleasby, PhD thesis, 2013) showed that there may be an association between PML bodies and CHMP7 nuclear foci in HeLa M cells. Therefore, the effect of CHMP7 or VPS4 depletion on PML bodies was investigated in transfected HeLa (and U2OS) cells stained with an anti-PML antibody. The number of PML bodies found in each nucleus was scored across the NT-control, CHMP7-1, CHMP7-3 and VPS4 knockdowns (Figure 4.6a). In control cells, an average of 12.8 PML bodies were present per nucleus, with all cells containing PML bodies. Following CHMP7 depletion, there is a significant increase in the number of discrete PML bodies seen, to 19.6 (CHMP7-1) and 19.0 (CHMP7-3) per cell. VPS4 knockdown shows the opposite effect with 8.8 bodies per cell, a slight but significant decrease.

PML bodies were imaged in three dimensions using a Deltavision deconvolution microscope, and the diameter of PML structures were measured in ImageJ (Figure 4.6c). The average diameter of a PML-NB in control cells was $0.59 \pm 0.02 \mu\text{m}$, and a small decrease in average size was observed in CHMP7-1 ($0.52 \pm 0.01 \mu\text{m}$) and CHMP7-3 ($0.52 \pm 0.1 \mu\text{m}$) knockdowns, a change which is barely significant at $p \leq 0.05$ (Figure 4.6b). The diameter of some PML-NBs in the VPS4-depleted cells appears by eye to be much larger than in control cells, and indeed, a few PML structures were measured at a diameter of up to $4.64 \mu\text{m}$. Giant PML bodies (defined as $2\text{-}4 \mu\text{m}$) have been observed previously in lymphocytes of patients with ICF (immunodeficiency, centromeric instability and facial dysmorphism) syndrome (Luciani *et al.*, 2006), however, the difference in composition and function compared to the normal PML-NB is not known. Therefore, on average there is an increase to a diameter of $0.61 \pm 0.02 \mu\text{m}$, which does not reach the threshold for statistical significance compared to the NT-control condition.

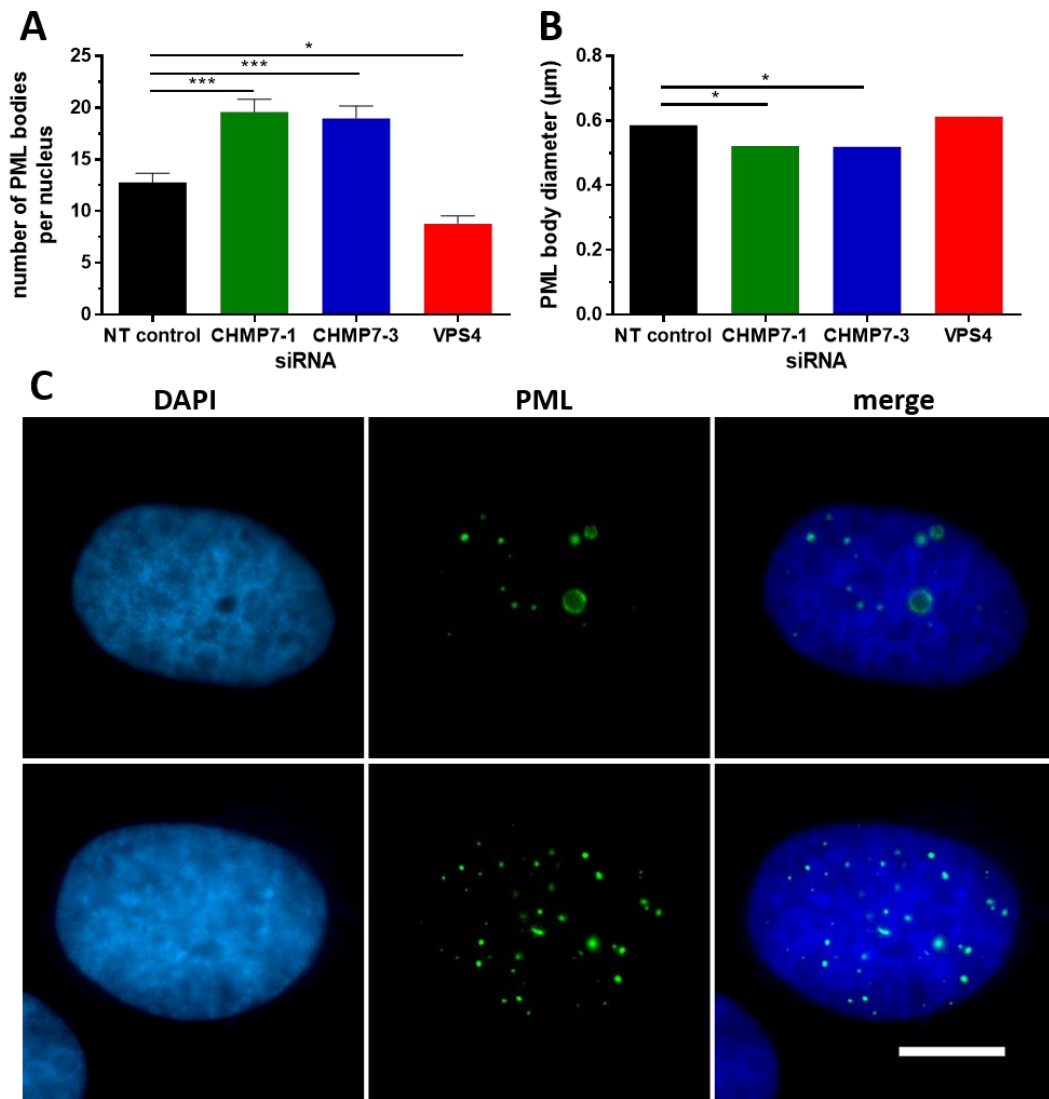


Figure 4.6. CHMP7 and VPS4 knockdown affect PML body number, size, and shape

a) The number of PML bodies found in each nucleus following depletion of CHMP7 or VPS4. A minimum of 50 cells were scored per condition. Averages and standard error of three independent repeats are shown. **b)** PML bodies in each condition were visualised using a Deltavision deconvolution microscope and sizes were measured in ImageJ (NT-control – 524 foci; CHMP7-1 – 627 foci; CHMP7-3 – 702 foci; VPS4 – 414 foci). **c)** An example of the larger and smaller PML body sizes in HeLa cells. Scale bar represents 10µm. Results were analysed using a one-way ANOVA with Tukey's *post hoc* test compared to control.

4.2.6 Co-occurrence of PML bodies with CHMP7 foci in VPS4 knockdown cells is foci size-dependent

CHMP7 foci were scored for association with PML in HeLa cells depleted of VPS4 protein, with the result that 46.0% of CHMP7 foci show some form of localisation with PML. There appeared to be variation in the relationship of CHMP7 and PML staining, as the two proteins do not precisely colocalise with each other. CHMP7 foci were classified as being independent from PML, associated with PML (whereby PML and CHMP7 structures are touching, adjacent to each other) or encircled by PML, a phenotype in which the PML in at least one plane of vision forms a complete circle around the CHMP7 focus (Figure 4.7a). The diameter of CHMP7 foci were measured in HeLa cell nuclei using ImageJ (Figure 4.7b). CHMP7 foci which were not associated with PML had an average diameter of $0.61 \pm 0.04 \mu\text{m}$, which is significantly different to those with a PML association ($0.85 \pm 0.5 \mu\text{m}$), and those encircled by PML ($1.23 \pm 0.08 \mu\text{m}$). Therefore, PML appears to preferentially localise with larger CHMP7 foci, and encircles primarily the largest foci.

Deltavision deconvolution microscopy was used to image the PML/CHMP7 structure in three dimensions, and the z-slices of a representative structure shows that while PML staining appears to encircle the CHMP7 foci, it does not appear to entirely enclose it (Figure 4.7c). These PML structures appear similar to “torus” or “doughnut” PML shapes which have been reported (Bernardi and Pandolfi, 2007; Butler *et al.*, 2009) and can be seen in the upper panel of Figure 4.6c, however it is uncertain whether these are unique PML structures, or large forms of normal PML bodies. In addition, there is work to be done to determine if the torus PML structures previously seen are the same phenomenon as those observed surrounding CHMP7, or if they are a unique occurrence.

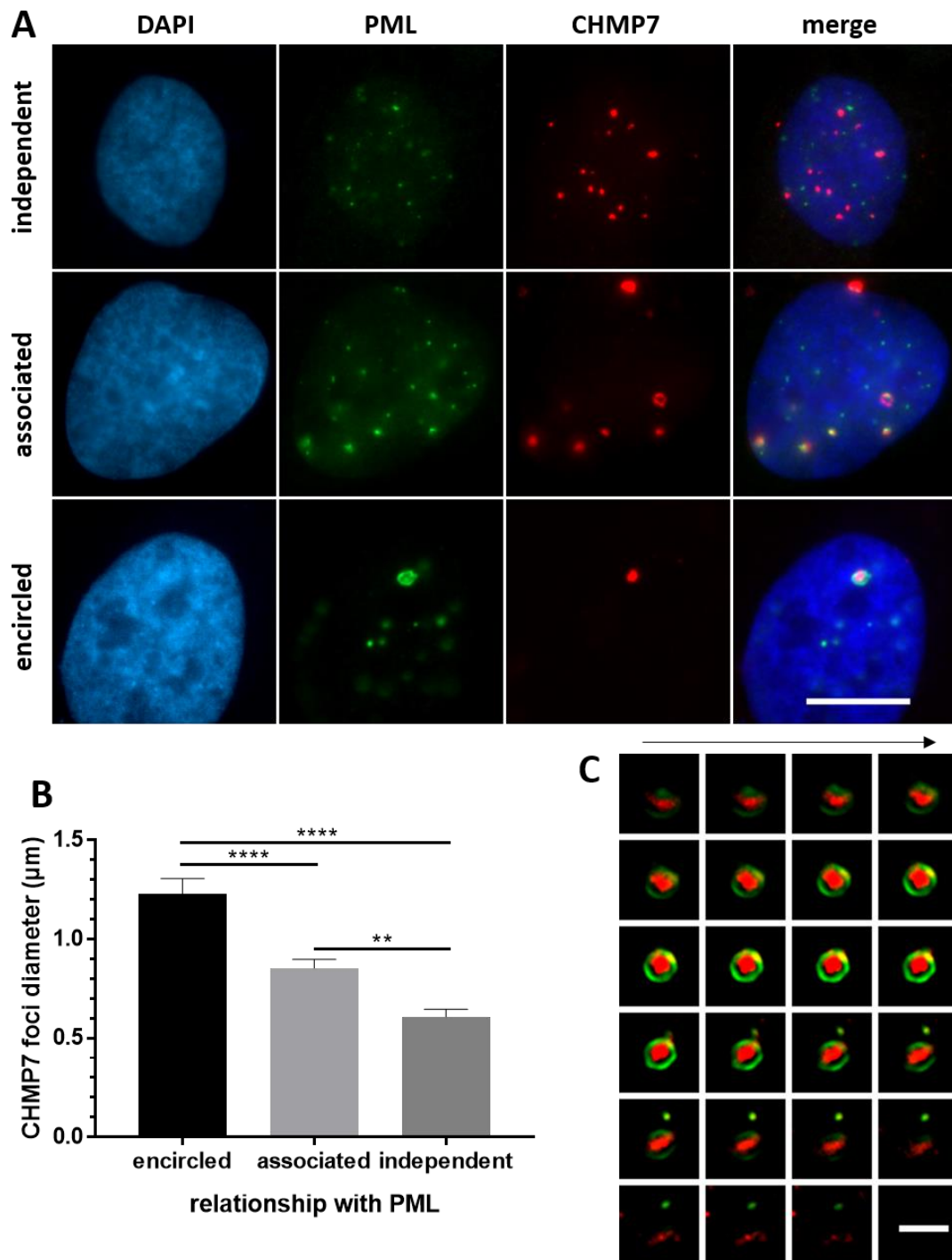


Figure 4.7. Large CHMP7 nuclear foci associate with or are encircled by PML protein

a) CHMP7 foci have been observed to be entirely independent of PML protein, adjacent or associated with PML accumulations, or entirely encircled within a PML structure. Scale bar represents 10µm. **b)** The relationship of PML to CHMP7 appears to be dependent on the size of the CHMP7 foci. CHMP7 foci in VPS4-depleted HeLa cells immunostained to show CHMP7 and PML were classified according to their relationship to PML staining, and the diameter of the CHMP7 foci (encircled – 50 foci; associated – 68 foci; independent – 61 foci) were visualised using a Deltavision deconvolution microscope and measured in ImageJ. Averages and standard error are shown. Results were analysed using a one-way ANOVA with Tukey's *post hoc* test. **c)** Z-stack images of a CHMP7 foci encircled by PML protein. Spacing between slices is 0.1µm. Scale bar represents 2µm.

4.2.7 DNA damage and repair protein markers associate with CHMP7

nuclear foci

The presence of CHMP7 foci in the nucleus was hypothesised to relate to sites of DNA damage and repair, and the relationship with the DNA damage sensor PML supports this idea, as PML is recruited to sites of DNA damage. The relationship between markers of the DNA damage response (DDR) and CHMP7 foci in interphase was explored using various protein markers.

The histone variant H2AX is phosphorylated in the region of damage in response to double-strand DNA breaks (Rogakou *et al.*, 1998), and therefore is used as a marker of the formation and resolution of such DNA damage events. H2AX phosphorylation is propagated along the DNA around the break, forming a γ H2AX focus, which acts as the centre of recruitment for DNA damage repair proteins. A rabbit-derived anti- γ H2AX antibody which recognises H2AX phosphorylated at serine-39, was used to co-stain HeLa cells depleted of VPS4 alongside CHMP7. CHMP7 foci were scored for association with γ H2AX foci, which denote regions of DNA damage. It was found that an average of 71.3% of CHMP7 foci in HeLa cells show association with γ H2AX (Figure 4.8c).

Scoring was carried out to determine the size of CHMP7 foci with which γ H2AX was colocalising, with diameter measured for γ H2AX-positive and γ H2AX-negative foci (Figure 4.8b). The average size of γ H2AX-negative foci was $0.37 \pm 0.01 \mu\text{m}$, which is significantly smaller than the average of $0.75 \pm 0.04 \mu\text{m}$ measured for γ H2AX-positive foci. Concordant with the results found for PML body localisation, DNA damage was found around the larger CHMP7 foci.

RPA (replication protein A) is a single-stranded DNA (ssDNA) binding protein which is phosphorylated and ubiquitylated in response to DNA damage. RPA accumulates on ssDNA at damaged regions, and plays a role in recruitment of downstream repair proteins. The

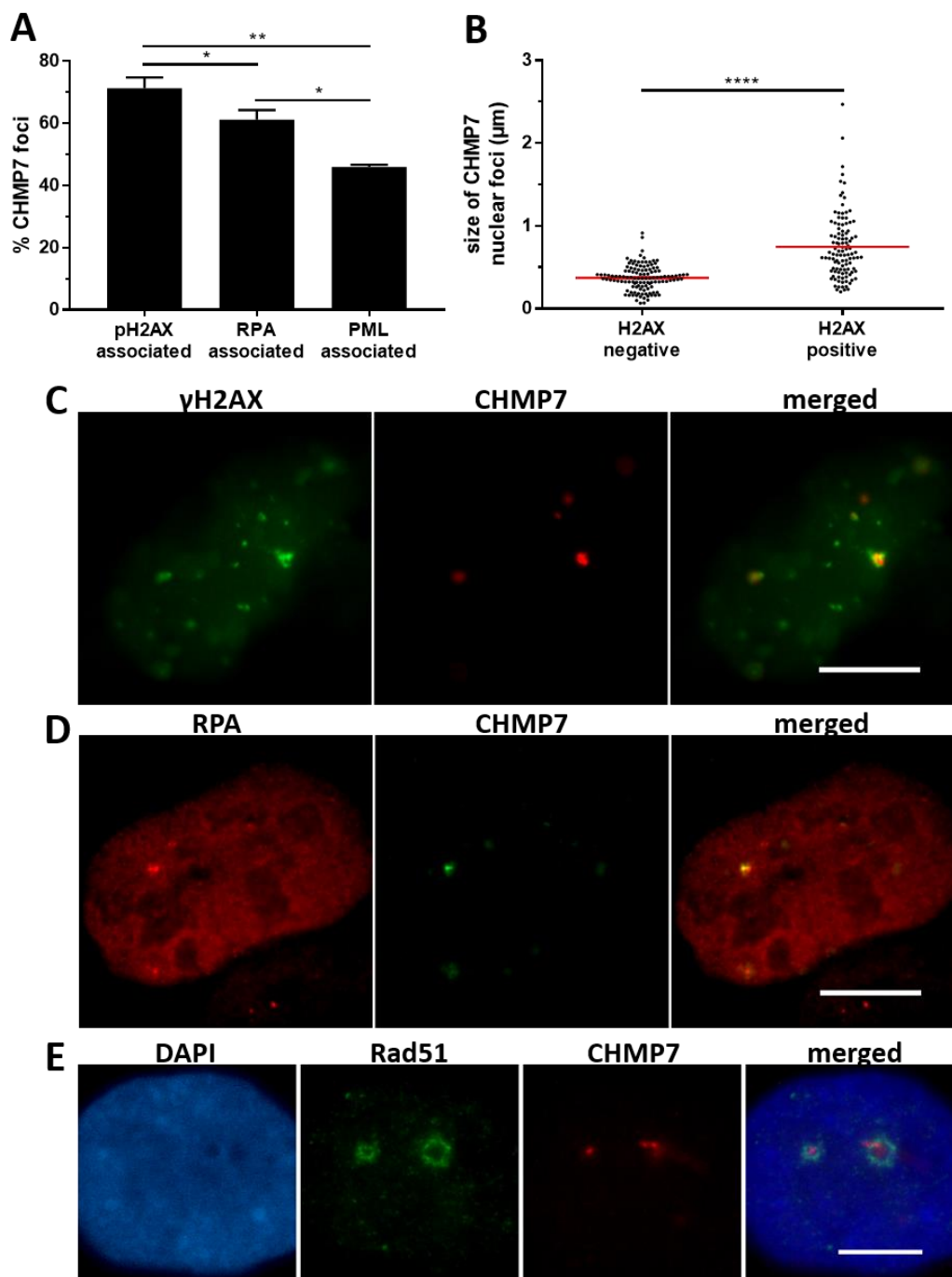


Figure 4.8. CHMP7 nuclear foci associate with various DNA damage and repair proteins

a) HeLa cells transfected with 3nM VPS4-targeting siRNA for 48 hours were fixed and co-stained to show both CHMP7 and either PML, RPA or γ H2AX. CHMP7 foci were scored for association with each of the proteins. A minimum of 300 foci were scored for each condition. Averages and standard error of three independent repeats are shown. Results were analysed using a one-way ANOVA with Tukey's *post hoc* test. **b)** CHMP7 foci were classified according to their relationship to γ H2AX staining (γ H2AX-negative – 122 foci; γ H2AX-positive – 109 foci), and the diameter of the CHMP7 foci were measured in ImageJ. Results were analysed using an unpaired, two-tailed *t*-test. **c)** Colocalisation between γ H2AX and CHMP7. DAPI channel is omitted for clarity. **d)** Colocalisation between RPA and CHMP7. DAPI channel is omitted for clarity. **e)** Rad51 rings around CHMP7 foci. All scale bars represent 10 μ m.

RPA34 antibody available for this experiment recognises the phosphorylated as well as unphosphorylated forms of RPA, therefore giving nuclear background staining to the RPA foci, which appear as bright spots. CHMP7 foci were scored for colocalisation with RPA foci in HeLa cells depleted of VPS4 protein, with the result that 61.2% of CHMP7 foci show association with RPA (Figure 4.8d). The homologous recombination protein Rad51 is also observed forming the unusual circular distribution around CHMP7 foci (Figure 4.8e).

The presence of both the marker of DNA damage, γ H2AX, and the downstream repair proteins shows an active response to DNA damage. These results show that many CHMP7/ESCRT-III foci are associated with DNA damage foci. This could be explained by recruitment of ESCRT-III to sites of DNA, or the formation of a DNA damage response around the aberrant ESCRT-III accumulations.

4.2.8 CHMP7 does not form foci in response to UV-induced DNA damage

We set out to investigate the hypothesis that CHMP7 may play an active role in the DNA damage response, due to its nuclear localisation, uncharacterised chromatin-related functions, and the colocalisation of DNA damage repair proteins such as BRCA1 to CHMP7 foci in VPS4-depleted cells (Cleasby, PhD thesis, 2013). In order to determine whether CHMP7 is responsive or related to DNA damage and the associated signalling response, DNA damage was induced using UVC irradiation.

UVC (short wavelength) UV radiation is well absorbed by DNA, causing DNA damage (pyrimidine dimers and 6-4 photoproducts), and unlike UVA and UVB radiation, do not cause other cellular stresses such as oxidative stress and protein denaturation. These DNA lesions lead to DSBs upon replication of DNA and collapse of replication forks (Federico *et al.*, 2016).

HeLa M cells were exposed to 10mJ/cm² UVC radiation and fixed with 3% PFA at timepoints following irradiation. Cells were observed at 0h, 1h, 4h, 8h, 16h, 24h, 48h and 72h post-

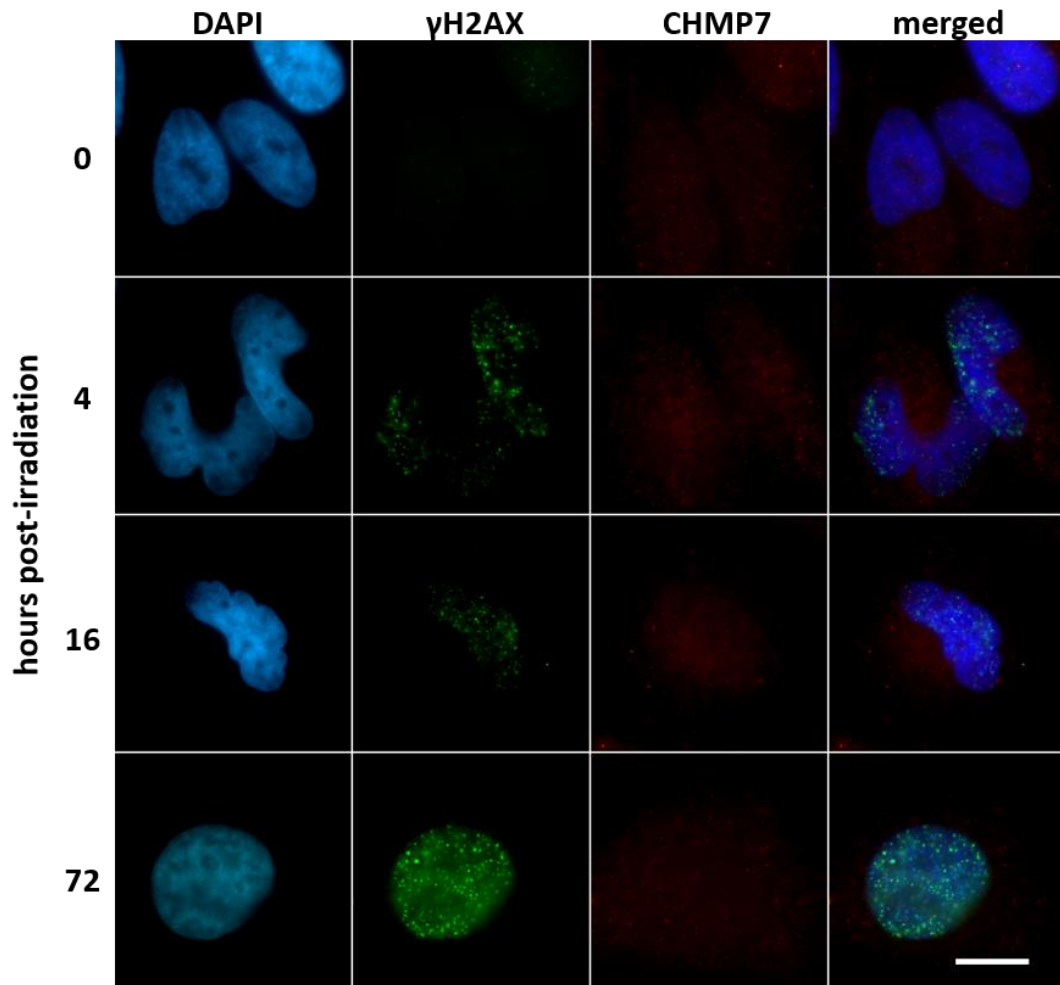


Figure 4.9. CHMP7 does not form nuclear foci upon induction of DNA damage with UVC radiation

HeLa cells exposed to $10\text{mJ}/\text{cm}^2$ UVC radiation were fixed at various timepoints following irradiation, and immunostained to show CHMP7 and γH2AX , and counterstained with DAPI. Scale bar represents $10\mu\text{m}$.

irradiation, following staining for CHMP7 alongside a marker of DNA damage, γ H2AX (Figure 4.9). No noticeable change in the distribution of CHMP7 to the nucleus or into foci was observed across thousands of observed cells at each timepoint, indicating that CHMP7 is not recruited to sites of DNA damage, and therefore may not be important in such a process.

4.2.9 LAP2 is enriched at CHMP7 interphase nuclear foci, indicating a role for CHMP7 at the nuclear membrane

In order to determine the relationship between CHMP7 and nuclear proteins, CHMP7 was visualised alongside LAP2, a member of the LEM inner nuclear membrane family of proteins. LAP2 (lamin associated polypeptide 2) associates with inner nuclear membrane and the lamina, binding to lamins, acting to associate the lamina to the inner nuclear membrane. The key isoforms are LAP2 α , a nucleoplasmic protein which interacts with A-type lamins, and LAP2 β , an integral inner nuclear membrane protein which binds Lamin B and plays a vital role in nuclear envelope and lamina formation. The antibody targeting LAP2 used here is polyclonal, and binds to both isoforms of the protein.

In HeLa cells, the majority of CHMP7 foci (73.0%) showed direct colocalisation with the inner nuclear membrane protein LAP2 in VPS4-depleted HeLa cells. While LAP2 is distributed across the entire nuclear envelope, the protein shows bright patches of LAP2 staining which colocalises with CHMP7 foci (Figure 4.10c). Those CHMP7 foci which show colocalisation with LAP2 are on average of a larger size ($0.98 \pm 0.03 \mu\text{m}$) than those which correspond with normal uniform LAP2 nuclear lamina staining ($0.55 \pm 0.03 \mu\text{m}$; Figure 4.10b).

4.2.10 CHMP7 foci occur at holes in the nuclear lamina

Upon observing Lamin B staining in VPS4-depleted cells, it is particularly obvious with large CHMP7 foci that Lamin B staining is absent in those regions which correspond to CHMP7 (Figure 4.11a). VPS4-depleted HeLa cells were scored, determining that Lamin B is excluded from $66.1 \pm 1.8\%$ of CHMP7 foci (Figure 4.10a). The diameter of CHMP7 foci was measured,

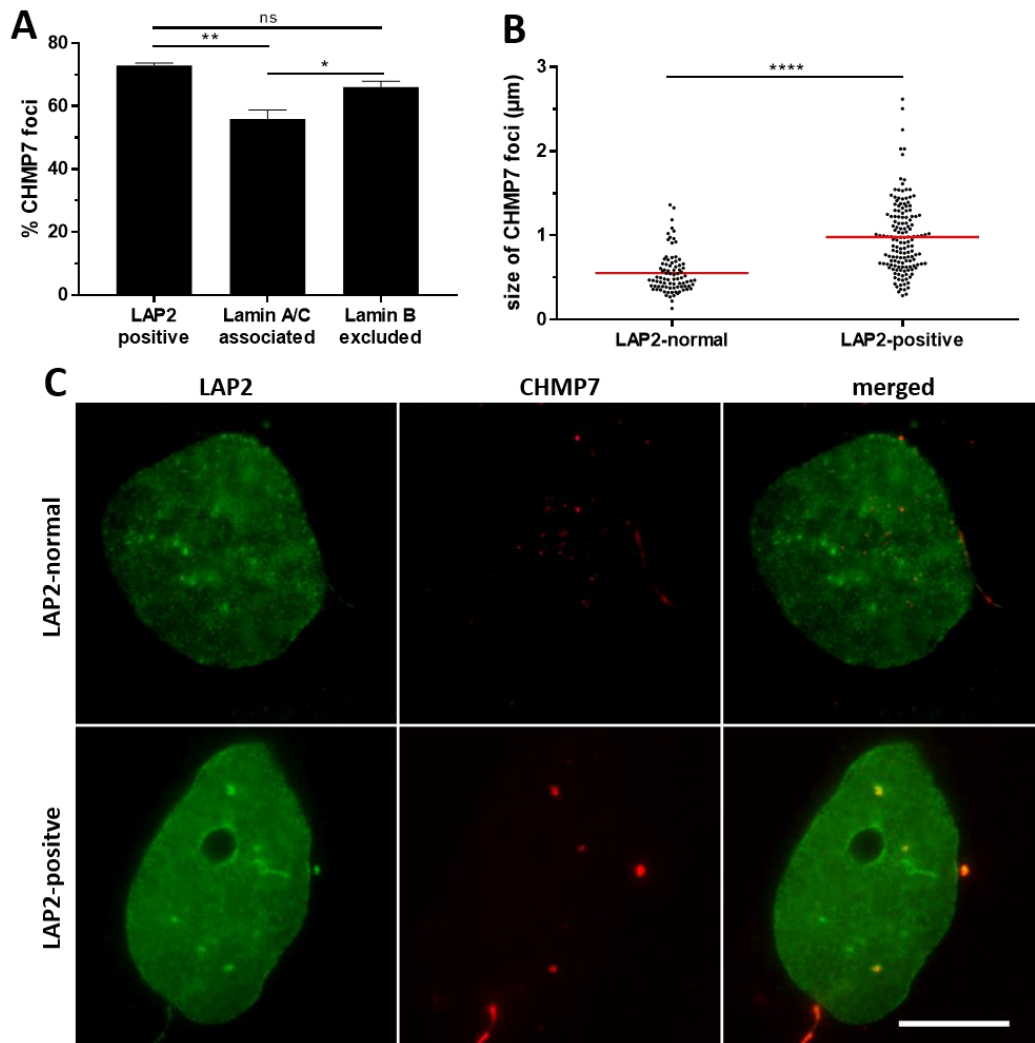


Figure 4.10. Large CHMP7 foci show strong LAP2 colocalisation

a) HeLa cells transfected with 3nM VPS4-targeting siRNA for 48 hours were fixed and co-stained to show both CHMP7 and either LAP2, Lamin A/C or Lamin B. CHMP7 foci were scored for association with each of the proteins. A minimum of 400 foci were scored for each condition. Averages and standard error of three independent repeats are shown. Results were analysed using a one-way ANOVA with Tukey's *post hoc* test. **b)** CHMP7 foci were classified according to their relationship to LAP2 staining (LAP2-normal – 148 foci; LAP2-positive – 125 foci), and the diameter of the CHMP7 foci were measured in ImageJ. Averages and individual measurements are shown. Results were analysed using an unpaired, two-tailed *t*-test. **c)** Images of CHMP7 foci showing colocalisation with LAP2 foci (LAP2-positive) or lack of colocalisation (LAP2-normal). Scale bar represents 10µm.

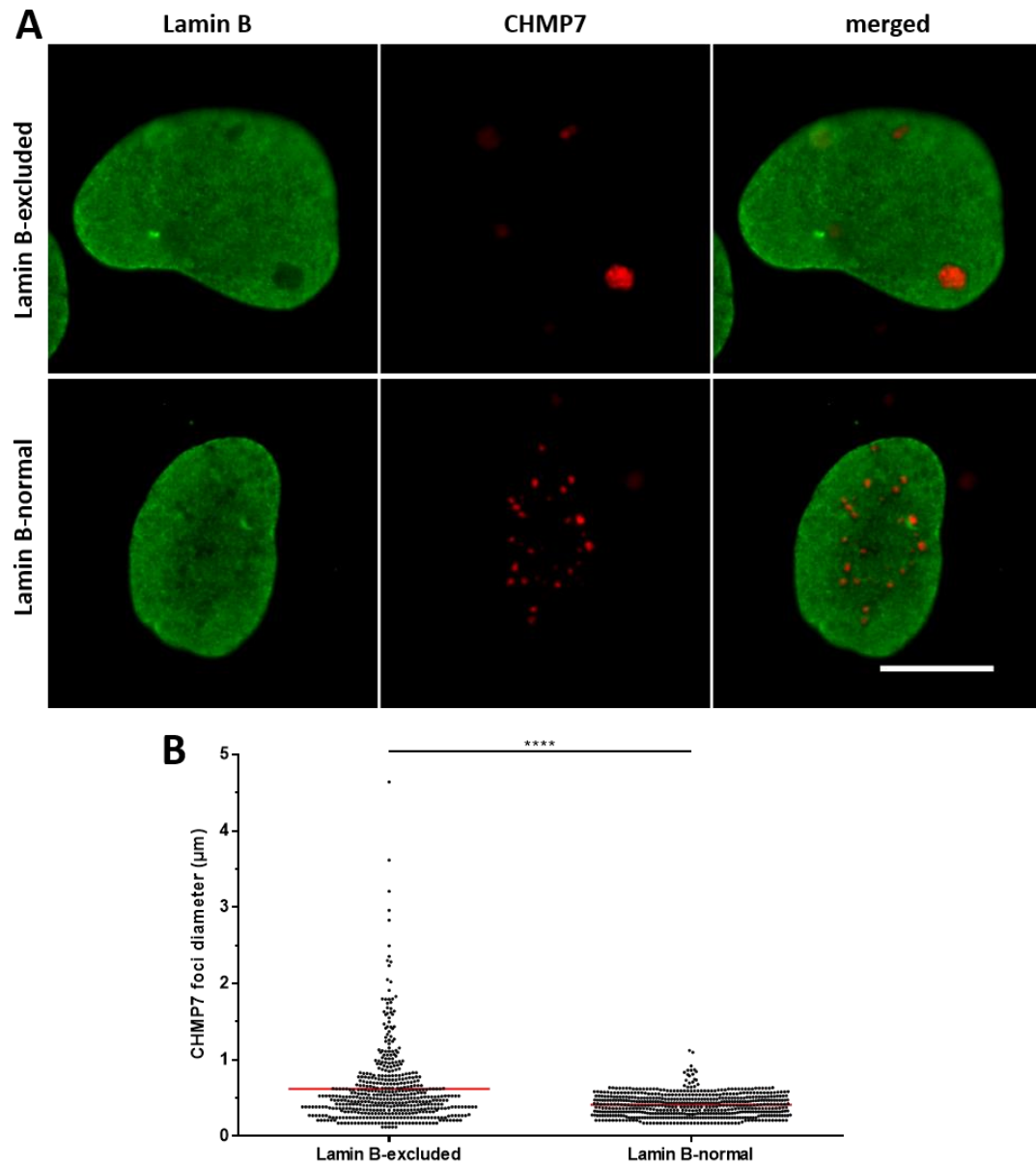


Figure 4.11. Large CHMP7 foci correspond with gaps in the nuclear lamina

HeLa cells transfected with 3nM VPS4-targeting siRNA for 48 hours were fixed and co-stained to show both CHMP7 and Lamin B. **a)** Images of CHMP7 foci showing exclusion of Lamin B from the areas of CHMP7 nuclear foci. Scale bar represents $10\mu\text{m}$. **b)** CHMP7 foci were classified according to their relationship to Lamin B staining, and the diameter of the CHMP7 foci (Lamin B-normal – 588 foci; Lamin B-excluded – 501 foci) were measured in ImageJ. Averages are shown. Results were analysed using an unpaired, two-tailed *t*-test.

and classified as either Lamin B-normal or Lamin B-excluded. No instances of Lamin B enrichment were observed at CHMP7 foci. Scoring of over 500 foci per category shows that Lamin B-excluded foci have an average size ($0.62\pm 0.02\mu\text{m}$) which is significantly larger than those which appear to show no Lamin B absence, Lamin-B normal ($0.41\pm 0.01\mu\text{m}$; Figure 4.11b). This further supports the hypothesis that CHMP7 is located at the nuclear envelope, and shows the localisation of the ESCRT-III complex to the nuclear envelope at gaps in the nuclear lamina.

4.2.11 CHMP7/ESCRT-III foci correspond to the interphase nuclear envelope

Observing CHMP7 foci on the edge of the nucleus as viewed down the microscope gives us a different perspective on the CHMP7 structure and their relationship to various other proteins (Figure 4.12). Proteins such as LAP2 and Lamin A/C appear to colocalise with the CHMP7 foci. The markers which do not colocalise with CHMP7, but localise adjacent to the foci, include PML and Rad51, as well as γH2AX . The spatial relationship here shows that CHMP7 is found on the outer edge of the nuclei, with the DNA damage markers extending further into the nucleus.

4.2.12 CHMP7 localises to chromatin in the late stages of mitosis

Following initial observations of CHMP7 localisation in mitosis, as seen in Figure 4.3, an interesting observation was made of bright CHMP7 accumulations close to the nuclear material in mitotic cells, following the segregation of chromatids into nascent daughter nuclei (Figure 4.13a). In order to confirm this observation, all available antibodies were used to visualise CHMP7. This phenotype was consistently observed in telophase cells with all three CHMP7 antibodies in HeLa cells (rabbit, mouse, and sheep) and additionally has been observed in all cell lines used in this study – HeLa, HeLa M and U2OS. Figure 4.13a shows a

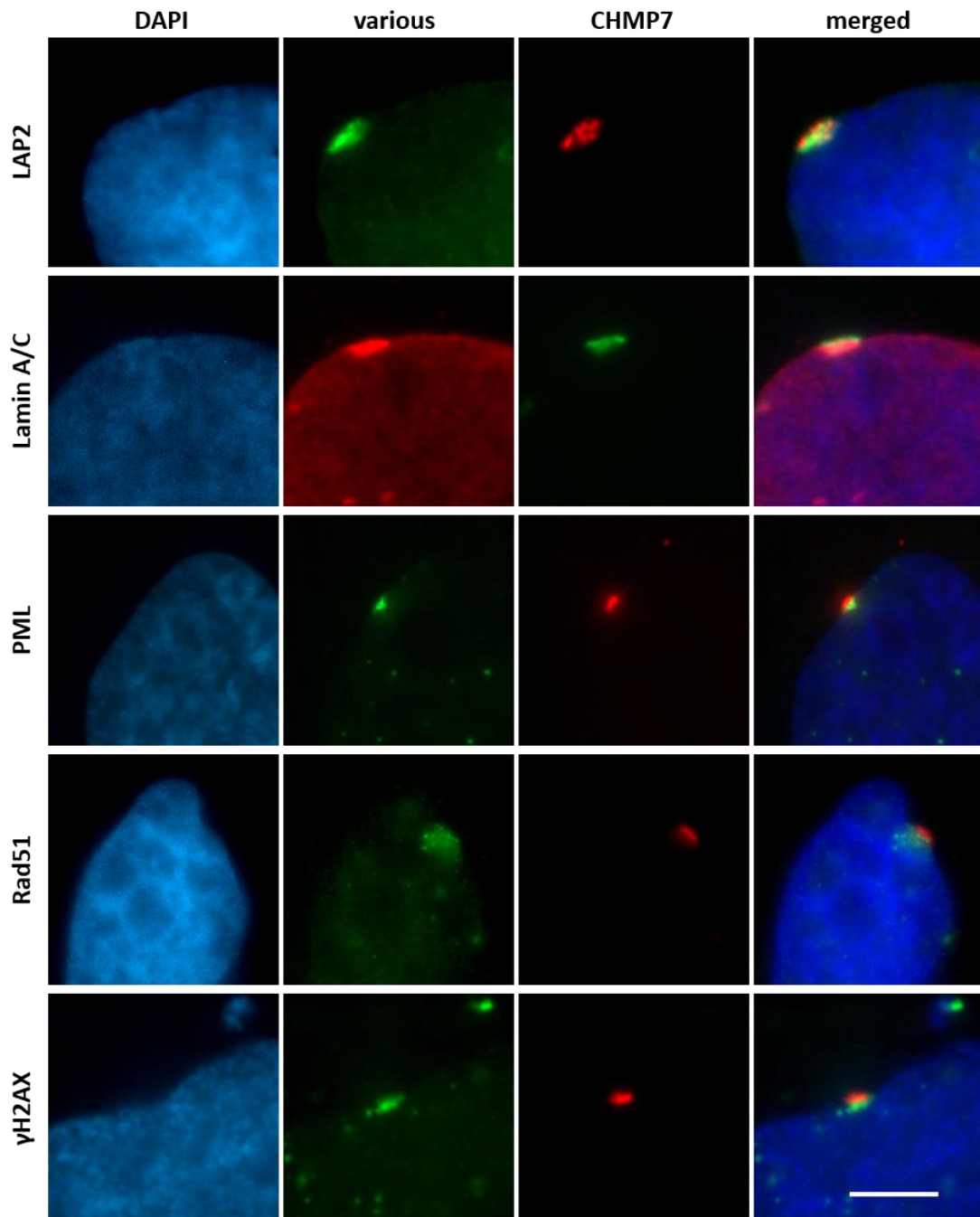


Figure 4.12. CHMP7 foci localise at the periphery of the nucleus

HeLa cells were co-stained with both anti-CHMP7 and anti-various other markers as labelled above. Foci positioned at the edge of the nucleus were imaged, and representative images of each pair of antibodies are shown. Scale bar represents 5 μ m.

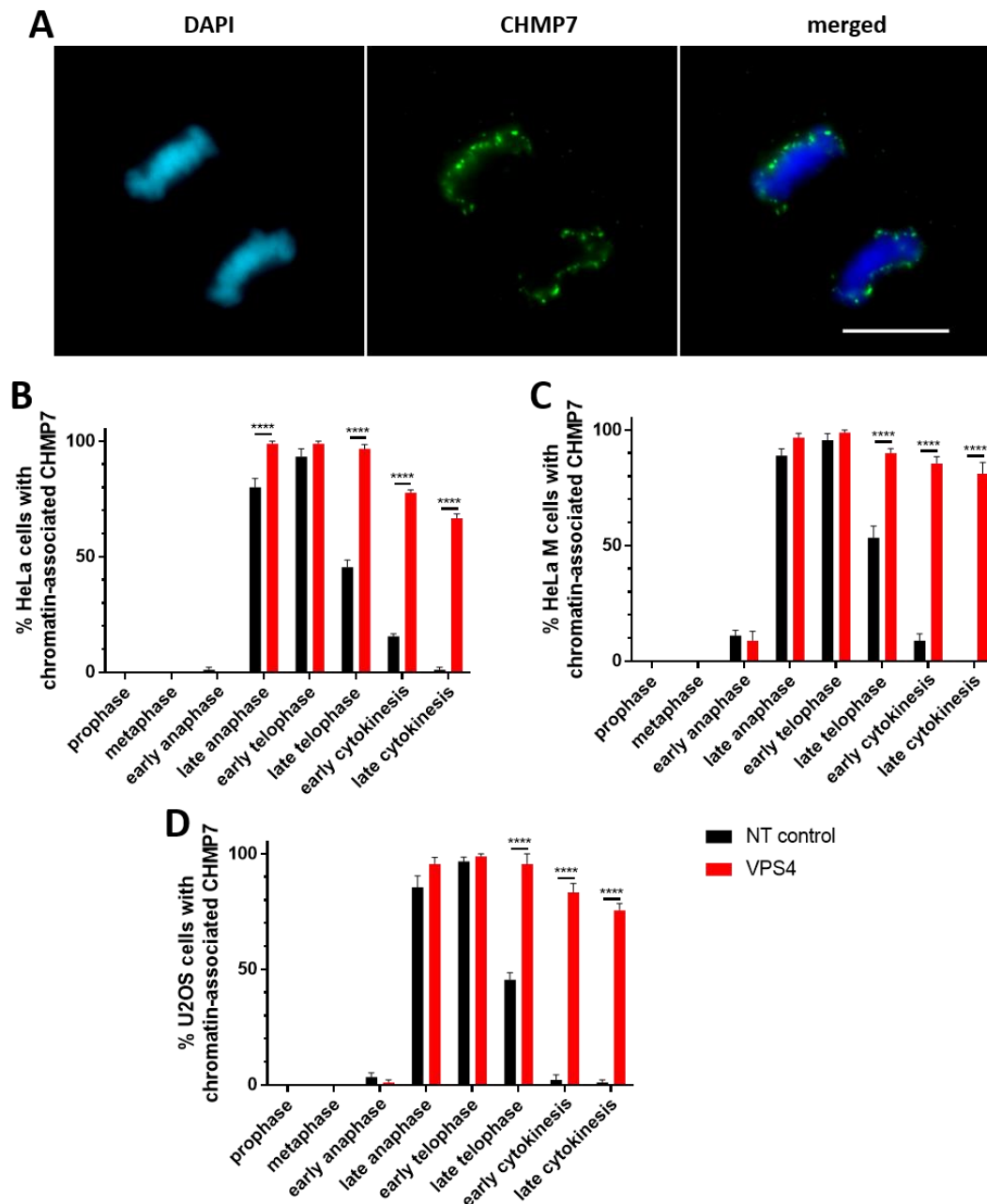


Figure 4.13. CHMP7 displays a novel, chromatin-associated pattern of accumulation into puncta in VPS4-depleted cells

a) An untreated U2OS cell, stained with DAPI and rabbit anti-CHMP7 antibody, displaying a punctate CHMP7 phenotype adjacent to chromatin in mitosis. Scale bar represents 10 μ m. **b)** HeLa, **c)** HeLa M and **d)** U2OS cells were scored for chromatin-associated CHMP7 in cells treated with either NT control or VPS4 siRNA for 48 hours. Thirty cells were scored per phase. Averages and standard error of three independent repeats are shown. Results were analysed using a two-way ANOVA with Sidak's *post hoc* test.

late anaphase U2OS cell stained with rabbit anti-CHMP7 antibody, displaying bright, chromatin-associated foci.

It appears that this bright, chromatin-associated phenotype is only observed in a specific, short period of mitosis, making its frequency low in a population of fixed cells. Quantification of the frequency with which this is seen was carried out in both siRNA control and VPS4 knockdown conditions. HeLa, HeLa M and U2OS cells were transfected with siRNA for 48 hours, before being fixed and stained with DAPI, mouse anti-CHMP7 and rabbit anti-phosphorylated Aurora kinase (pAuk). The pAuk antibody detects Aurora A, B and C mitotic kinases when phosphorylated at key threonine residues in a cell cycle-dependent manner. Mitotic cells were classified into prophase, metaphase, early or late anaphase, early or late telophase, and early or late cytokinesis based on the subcellular distribution of pAuk in the same manner as in Figure 3.5.

CHMP7 was never observed associating with chromatin in prophase or metaphase in any tested cell line (Figure 4.13b, 4.13c and 4.13d). In some cases, CHMP7 associated with chromatin in early anaphase, particularly in HeLa M cells (1.1, 11.1% and 3.3% in HeLa, HeLa M and U2OS cells respectively). The majority of late anaphase and early telophase cells, an average of 84.8% and 95.2% respectively across all three cell lines in control cells, displayed the phenotype. CHMP7 appears to dissociate from the chromatin as mitosis progresses, with 48.1% of late telophase and 8.9% of early cytokinesis cells maintaining some CHMP7 localisation. By the time the cells have reached the late cytokinesis stage, only 0.7% of cells show any signs of CHMP7 accumulation.

Depletion of VPS4 affects the dissociation of CHMP7 from chromatin, appearing to prevent its removal. As in the control cells, no prophase or metaphase cells, and few (3.3%) early anaphase cells display the phenotype. Almost all late anaphase and early telophase cells (97.0% and 98.9%, respectively) have chromatin-associated CHMP7. In late telophase and

early cytokinesis this percentage falls slightly to 94.1% and 82.2% respectively, persisting at significantly higher levels than in control cells. Even in late cytokinesis, 74.4% cells still maintain some chromatin-associated CHMP7 foci.

4.2.13 Characterisation of CHMP7 localisation to chromatin in mitosis

From observation of fixed cells, it can be observed that CHMP7 initially localises to the outer edge (furthest from the site of the cleavage furrow) of the chromatin mass, as demonstrated by the anaphase cell in Figure 4.14a. However, by telophase CHMP7 appears to extend around the sides of the chromatin, before surrounding the structure (Figure 4.14b) including localisation on lagging arms of chromosomes (Figure 4.14c)

In some cases, the foci appear to be concentrated around the core region (as indicated in Figure 4.1) of telophase chromatin (Figure 4.14d). The core chromatin is the central region at which Lamin A/C, LAP2 β and emerin become enriched in telophase in contrast to the peripheral non-core region, at which Lamin B, LBR and nucleoporins begin to accumulate, prior to the uniform distribution of proteins across the completed nuclear envelope (Haraguchi *et al.*, 2008; Figure 4.1). Another interesting observation, which will be further explored in Chapter 5, is the presence of a CHMP7 filament or bridge between the two nuclei, as seen in Figure 4.14e.

4.2.14 The ESCRT-III complex localises with CHMP7 in late mitosis

With the aim of determining the composition and function of these chromatin-associated CHMP7 puncta, and the relationship of the ESCRT-III complex with CHMP7, the presence or absence of other CHMP proteins was observed. CHMP7 was visualised using immunofluorescence alongside either CHMP4B or CHMP1B, using the rabbit anti-CHMP4B and anti-CHMP1B antibodies alongside the mouse-CHMP7 antibody. Figure 4.15a shows the localisation of CHMP7 and CHMP4B throughout the cell cycle. Figure 4.15b shows the colocalisation of CHMP7 with CHMP4B, with most of the large foci of CHMP7 corresponding

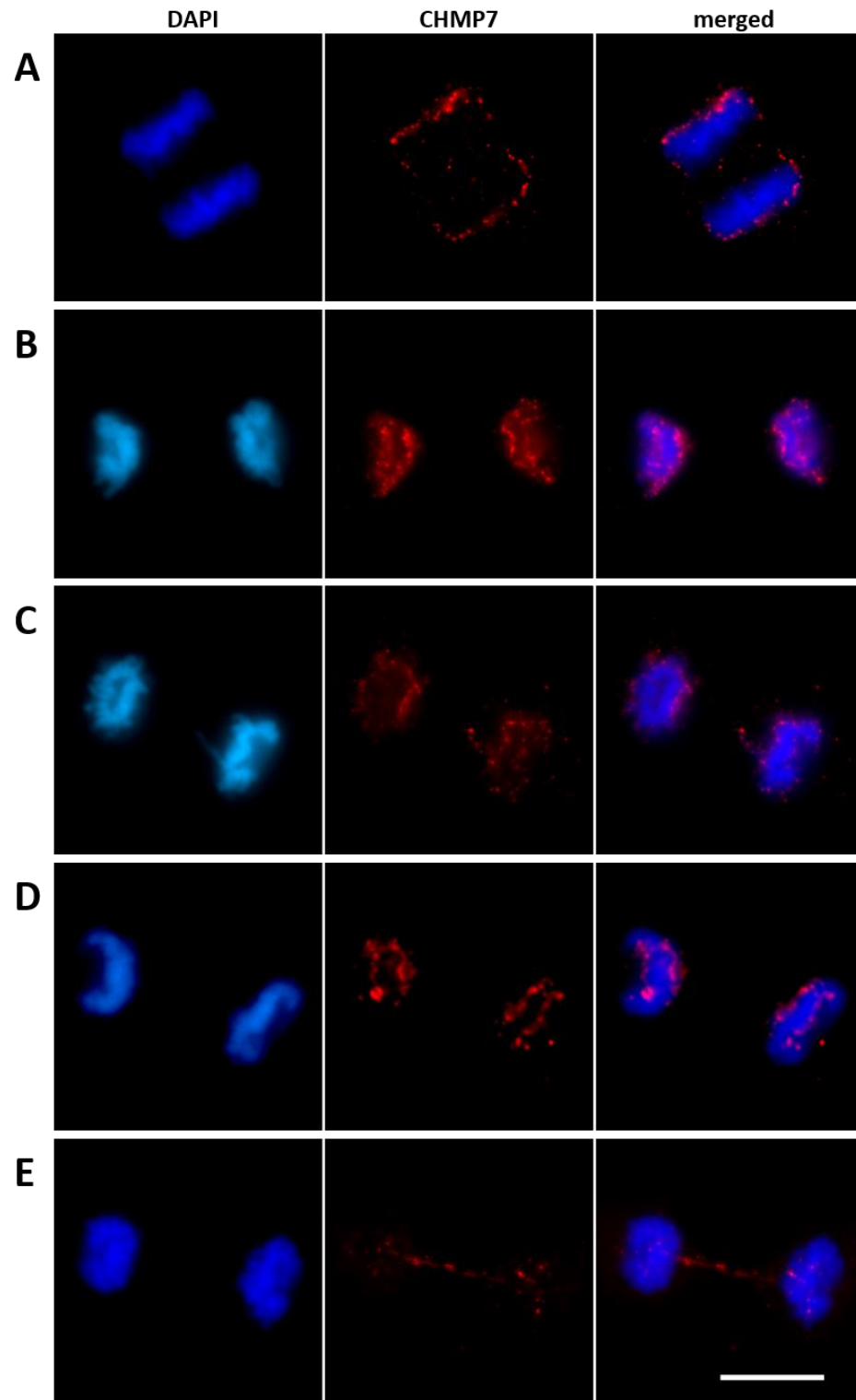


Figure 4.14. Features of CHMP7 localisation in mitosis

Untreated HeLa cells were stained with DAPI and mouse anti-CHMP7 antibody. Scale bar represents 10 μ m. **a)** CHMP7 accumulates first at the outer edge of chromatin in anaphase cells. **b)** By telophase, CHMP7 localisation has spread around the rim of the nascent nuclei. **c)** CHMP7 puncta are found on lagging chromatid arms. **d)** In some cells, CHMP7 displays strong staining around the core region of telophase chromatin. **e)** In some telophase cells, CHMP7 bridges or filaments are observed connecting the two nuclei.

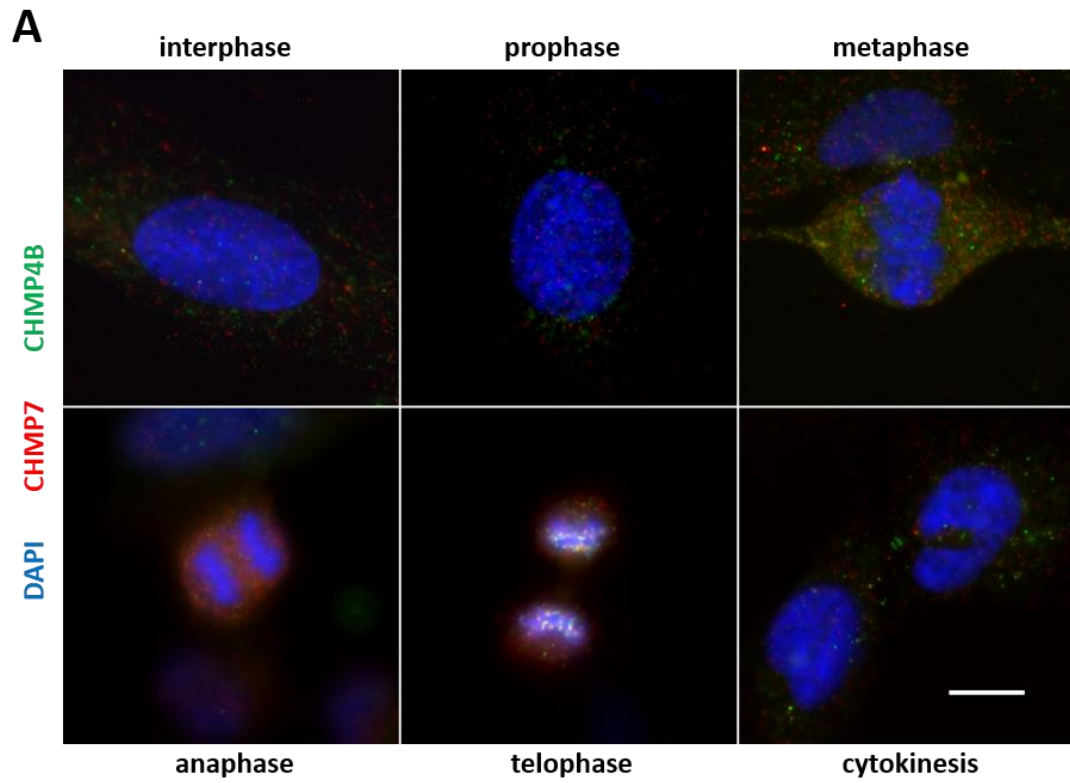


Figure 4.15. CHMP4B and CHMP1B colocalise with CHMP7 at late anaphase/early telophase cells

a) Distribution of CHMP7 (red fluorescence) and CHMP4B (green fluorescence) throughout the cell cycle in untreated HeLa cells.

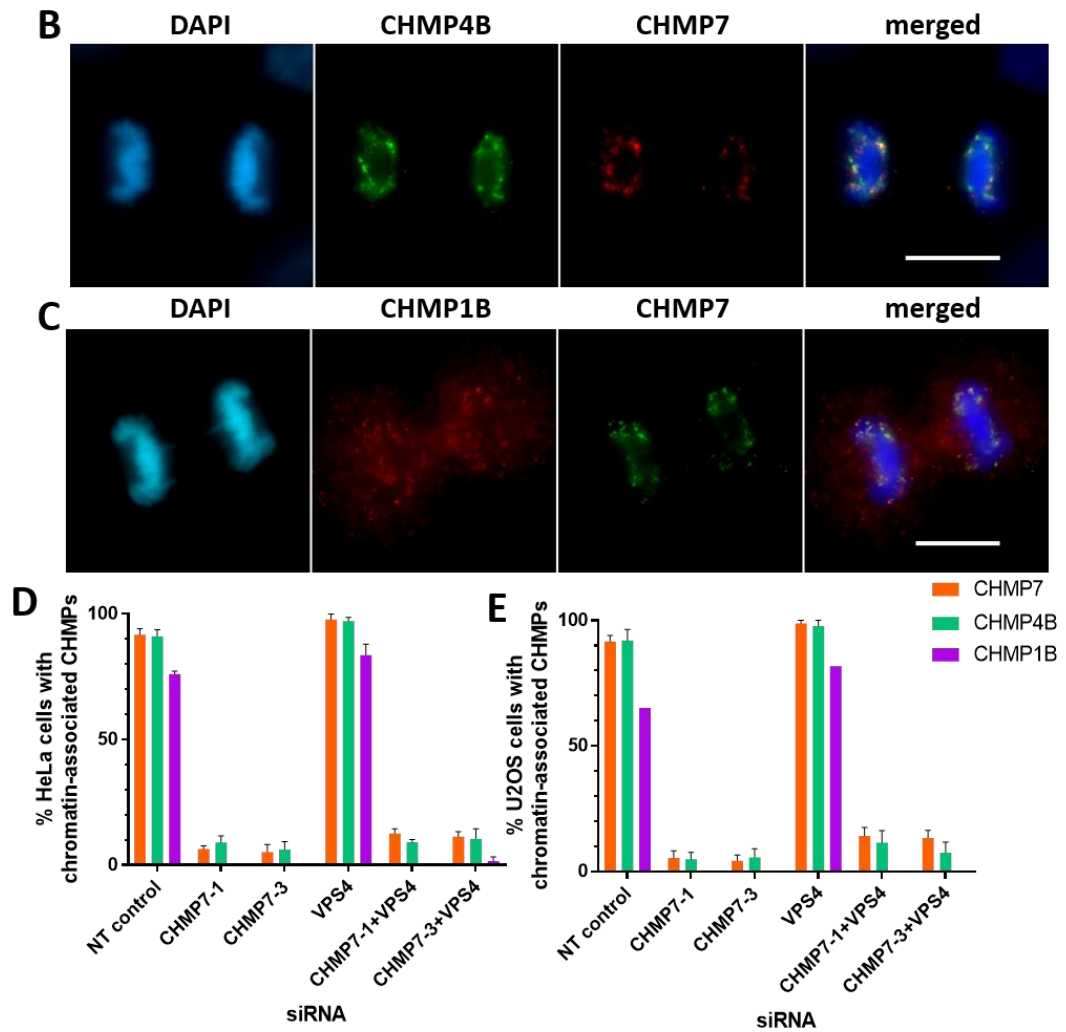


Figure 4.15. (continued)

b) Colocalisation of CHMP4B and CHMP7. **c)** Colocalisation of CHMP1B and CHMP7. **d)** HeLa and **e)** U2OS cells were scored for chromatin-associated CHMP7, CHMP4B and CHMP1B in late anaphase/early telophase cells treated with in cells transfected with siRNA for 48 hours. Between 20 and 30 cells were scored per condition. Averages and standard error of three independent repeats are shown for CHMP7 and CHMP4B; averages and standard error of two independent repeats for CHMP1B (HeLa), and results of one experiment are shown for CHMP1B (U2OS).

to a similar accumulation of CHMP4B. CHMP1B is also found at localising around chromatin, though the staining appears weaker than that of CHMP7 or CHMP4B (Figure 4.15c). Taken together with the failure of the structure to be disassembled in the absence of VPS4, this indicates the presence of the ESCRT-III complex.

4.2.15 CHMP7 is essential for the recruitment of the ESCRT-III complex in late mitosis

In order to determine an order of recruitment for CHMP proteins in mitosis, early telophase/late anaphase HeLa and U2OS cells were scored for chromatin associated CHMP7, CHMP4B or CHMP1B. CHMP7 knockdown was carried out using CHMP7-1 and CHMP7-3 siRNA, individually and in combination with VPS4 siRNA. CHMP7 knockdown abrogates both CHMP4B and CHMP1B localisation to chromatin in both HeLa and U2OS cells (Figure 4.15d, 4.15e), demonstrating a necessity for CHMP7 presence for the formation. VPS4-depleted cells display no significant differences between the occurrence of CHMP4B and CHMP1B compared to the control, though in the case of CHMP1B this may be due to lack of repeated data. When VPS4 is depleted alongside CHMP7, the results do not significantly differ from those of the CHMP7-only knockdowns, indicating that the loss of CHMP7 is the essential factor here for the recruitment of ESCRT-III to chromatin

4.2.16 Investigating the relationship between centromeres and CHMP7

Since CHMP7 appears to form multiple bright foci, often in a polarised fashion on the region of chromatin most distant from the cleavage furrow, it was hypothesised that these may correspond to centromeres. Therefore, the relationship between CHMP7 and kinetochore-spindle attachment points was investigated using an anti-CREST antibody combination with the anti-CHMP7 antibody.

The majority of telophase-stage HeLa cells showed centromeres found within the DAPI-stained region of the cell, which showed no association to CHMP7 foci which localised around

the rim of chromatin, and not within it (Figure 4.16b, upper panel). However, in some cells, where CHMP7 staining was observed to be more spread across the DAPI-stained region, CHMP7 foci are found adjacent to, and sometimes colocalising with, centromeres (Figure 4.16b, lower panel). Upon scoring of these phenotypes, it was found across three independent repeats that an average of $88.9 \pm 2.94\%$ of these telophase cells showed the first, non-associated phenotype, with the remaining 11.1% showing some association between CHMP7 foci and centromeres. Potential reasons for the two phenotypes may include that they are distinct stages of progression through mitosis, indicating a transient accumulation close to centromeres, or positioning of the cell with respect to the plane of the camera.

Localisation of CHMP7 adjacent to centromeres at any other phase of the cell was not observed in any of the tested cell lines (Figure 4.16a)

4.2.17 ESCRT-III assembles with nuclear membrane in mitosis

The key role of the ESCRT-III complex is remodelling of cellular membranes, and the assembly of ESCRT-III is reliant on membranes for its recruitment and assembly. Therefore, visualisation of membrane structures was attempted in order to determine the relationship between CHMP7 and perinuclear membranes.

In order to visualise the ER membrane, a transient transfection of GFP-Sec61 α -expressing plasmid was used. Sec61a is one of three subunits (the others being β and γ) of the heterotrimeric Sec61 complex, an endoplasmic reticulum pore protein with a role in protein translocation in and out of the ER lumen. GFP-Sec61 α showed clear visualisation of ER membranes in the HeLa and HeLa M cell populations used (Figure 4.17a). However, despite optimisation of transfection reagents and conditions, it was found that the transfection rate of the GFP-Sec61 α -containing plasmid was not high enough to allow for enough late anaphase/early telophase stage cells to be observed, and few mitotic cells of any stage were observed with successful overexpression. Attempts to generate a stable HeLa cell line

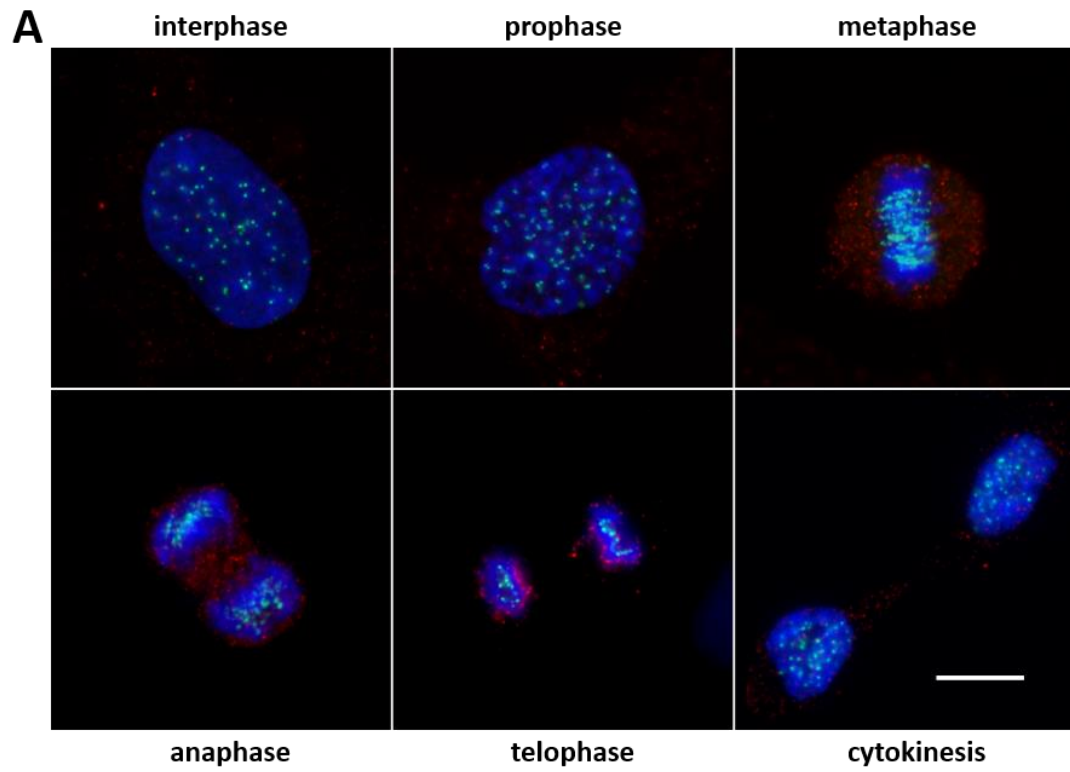


Figure 4.16. CHMP7 occasionally shows localisation near centromeres in telophase cells

a) Distribution of CHMP7 (red fluorescence) and CREST (green fluorescence) throughout the cell cycle in untreated HeLa cells. Scale bar represents 10 μ m.

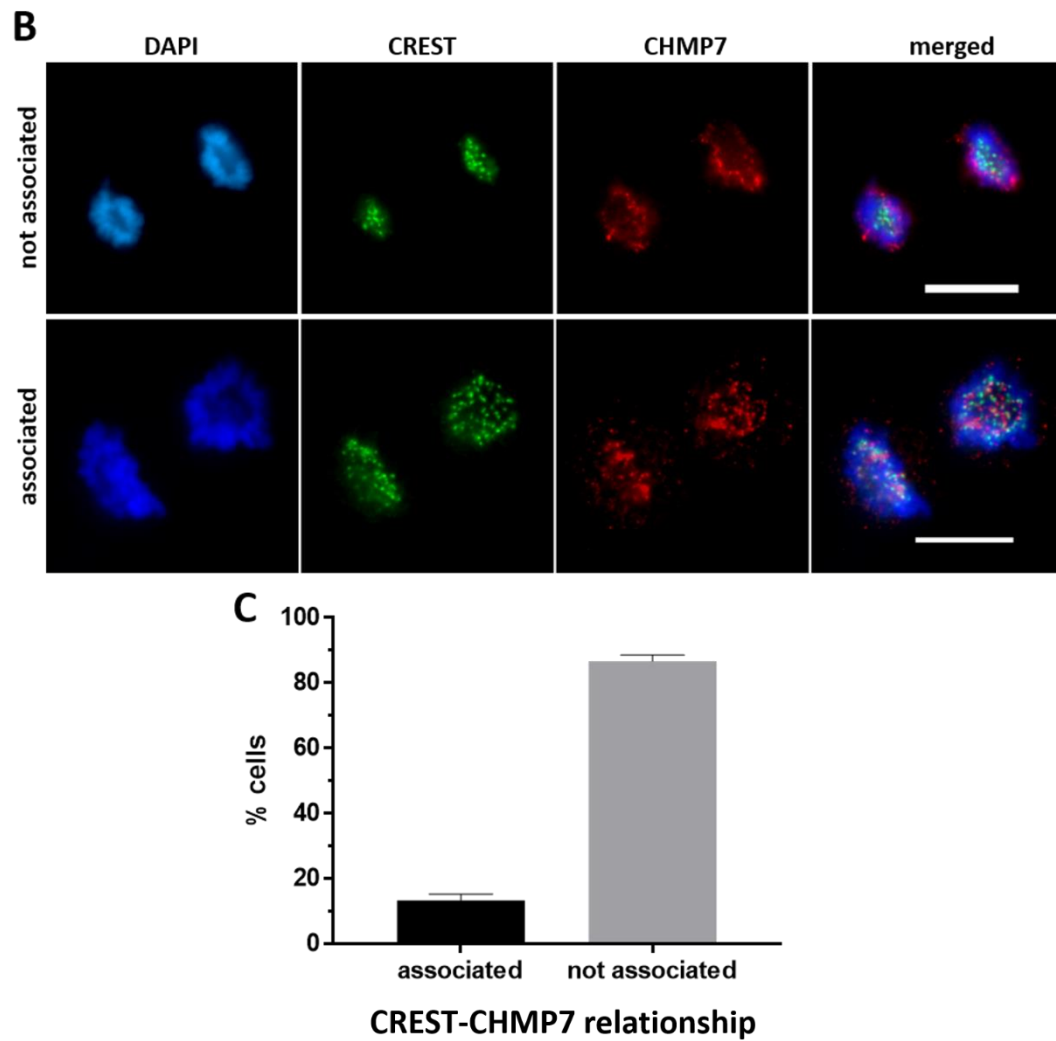


Figure 4.16. (continued)

b) The percentage of telophase cells in which CREST-labelled centromeres localise near to CHMP7 foci (associated) and show no close localisation (not associated) in untreated HeLa cells. Scale bars represent 10 μ m. **c)** Thirty telophase cells were scored per condition. Averages and standard error of three independent repeats are shown.

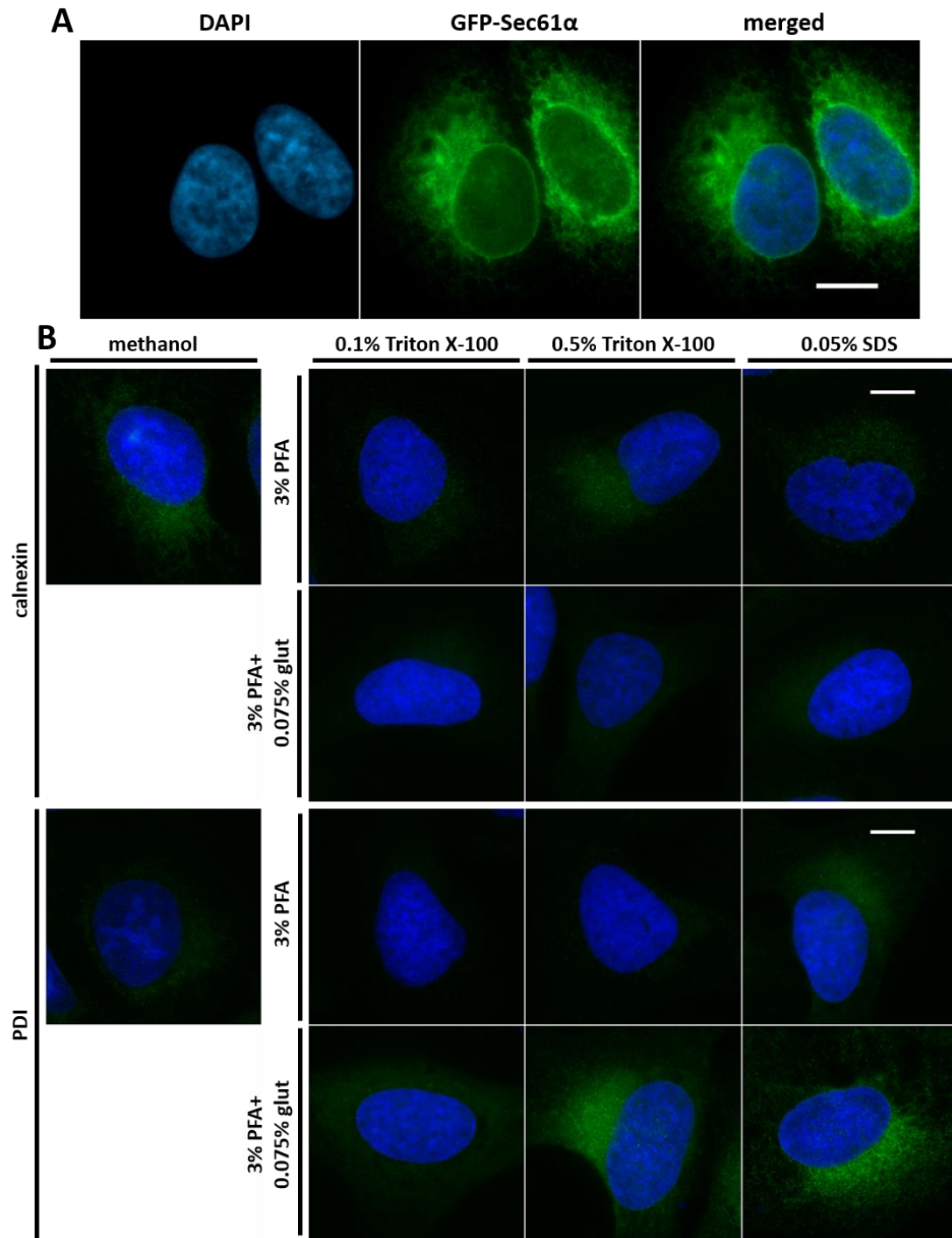


Figure 4.17. Optimisation of ER membrane staining

a) HeLa cells transfected with a GFP-Sec61 α -expressing plasmid for 24 hours and stained with DAPI. **b)** Optimisation of fixation and permeabilisation conditions for PDI and calnexin antibody staining. Scale bars represent 10 μ m.

containing the GFP-Sec61 α -expressing plasmid was unsuccessful, and unable to be repeated due to time constraints.

It was therefore decided to use an antibody-based method of ER membrane detection. Suitable, available antibodies were determined which targeted the calnexin and PDI proteins. Calnexin is a 67kDa integral endoplasmic reticulum protein which functions as a molecular chaperone aiding in correct protein folding in the ER. PDI, or protein disulphide-isomerase, is a 57kDa soluble enzyme found in the lumen of the endoplasmic reticulum, which catalyses folding of newly synthesised polypeptides by rearranging disulphide bond conformations.

Several different fixation and permeabilisation methods were tested in order to optimise the staining of the endoplasmic reticulum (Figure 4.17b). The only condition tried which resulted in a successful staining was that involving fixation using PFA containing 0.075% glutaraldehyde, and harsh permeabilisation using 0.05% SDS in PBS.

4.2.18 CHMP7 appears with membranes structures on the edge of the reforming nuclear envelope

With this new method, it was possible to observe mitotic cells stained for CHMP7 and PDI. Observation of the relationship of the two proteins appears to show that CHMP7 and PDI are recruited at the same point during mitosis (Figure 4.18a), with CHMP7 foci present at the point where an incomplete membrane can be seen around portions of the chromatin material (Figure 4.18b). The observation of membranes in mitosis is complicated by the density of PDI in the rounded cell around the nascent nuclei, however distinct patches of membrane can be observed spreading over the chromatin.

This corresponds with the point in nuclear envelope reformation at which ER membrane is being recruited in patches and joined together to form a sheet which becomes the sealed nuclear double-membrane structure. It was not possible to distinguish the order of

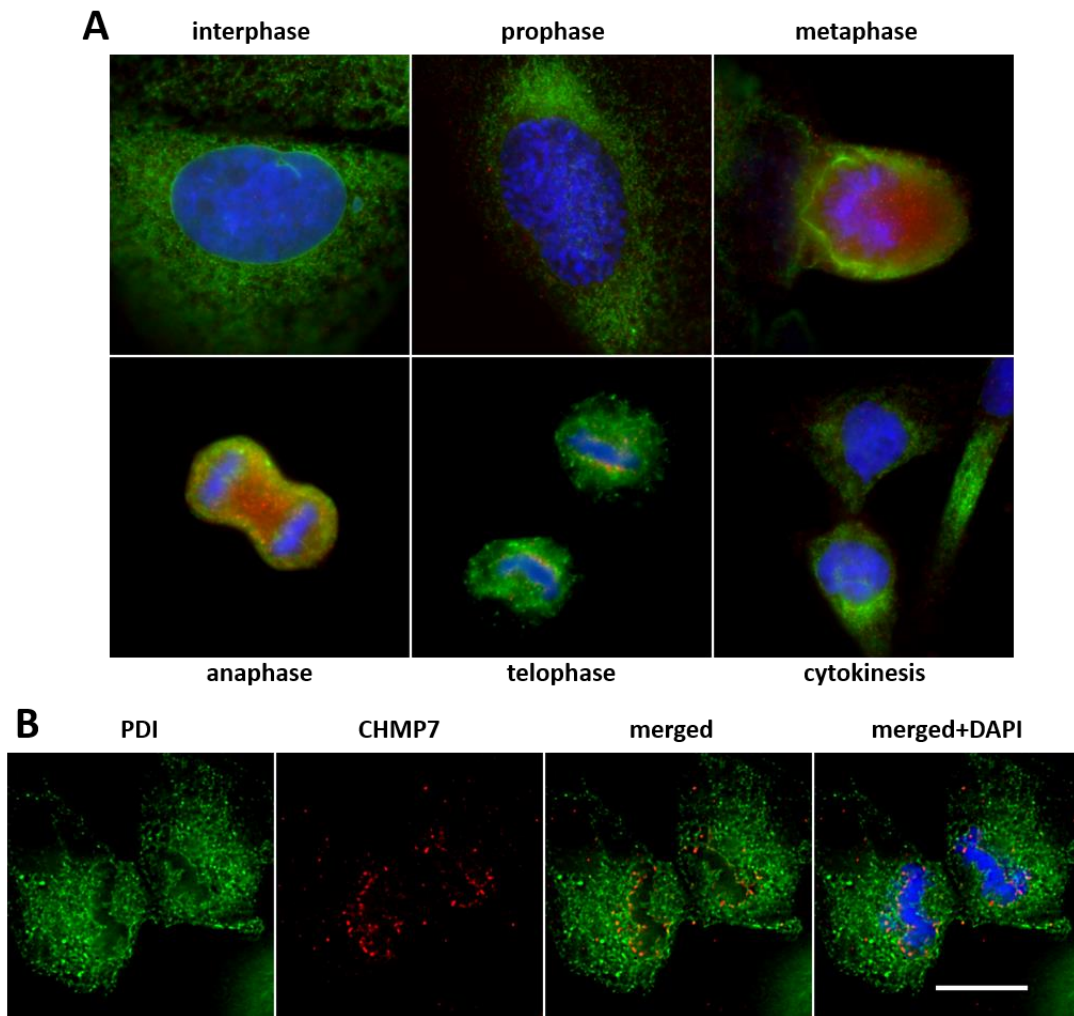


Figure 4.18. CHMP7 localises to telophase chromatin with ER membranes

a) Distribution of CHMP7 (red fluorescence) and PDI (green fluorescence) throughout the cell cycle in untreated HeLa cells. **b)** Deconvolved image taken on Deltavision microscope showing juxtaposition of CHMP7 and PDI staining in telophase HeLa cell. Full z-stack can be found in Appendix 2a. Scale bars represent 10 μ m.

recruitment for membrane and CHMP7 to the nuclear material, suggesting they arrive at the reforming nuclei at a similar timepoint. PDI-staining membrane segments associated with chromatin were found when CHMP7 foci were present, and CHMP7 foci were always associated with sections of membrane.

The two proteins were imaged in three dimensions using the Deltavision microscope (Appendix 2a) showing that some regions of the nuclear material are coated in membrane, with other regions as yet lacking this organised structure. While CHMP7 foci appear around the nuclear material, it seems most concentrated where PDI membrane is also present, and at the outer periphery (most distant side from the midbody) where the membrane is forming.

4.2.19 CHMP7 colocalises with INM protein LAP2 at the reforming nuclear envelope

Through analysis of the fixed images the relationship between LAP2 and CHMP7 proteins can be observed throughout the cell cycle (Figure 4.19a). A more detailed analysis of CHMP7 and LAP2 in the late mitotic phases can be found in Figure 4.19e. LAP2 formation around the chromatin can be observed from mid-to-late anaphase, at which time CHMP7 is not accumulating around the chromatin. As anaphase progresses into telophase, LAP2 becomes more enriched around the nascent nuclei, and CHMP7 colocalises with LAP2. As the LAP2 relocates more completely from the cytoplasm to the new nuclear membrane, remaining CHMP7 foci colocalise with the brightest patches of LAP2 staining. Once the daughter nuclei have formed, and LAP2 has been distributed across the surface of the chromatin, CHMP7 foci are no longer associated with the nucleus.

A telophase cell depleted of VPS4 was imaged in three dimensions with the Deltavision deconvolution microscope, from which it can be seen that CHMP7 and LAP2 frequently colocalise (Figure 4.19b and Appendix 2b). The LAP2 envelope itself is mostly formed but still

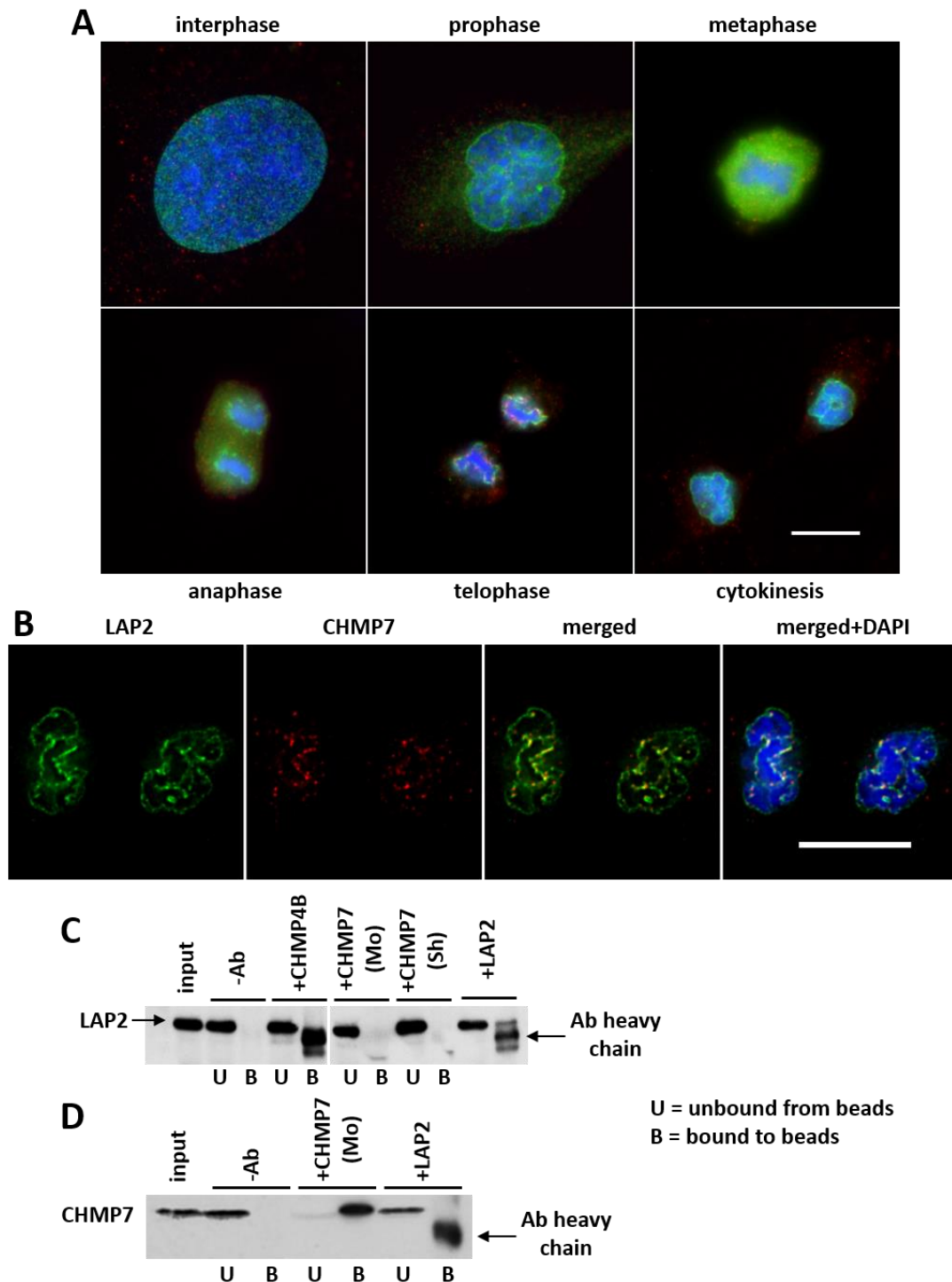


Figure 4.19. CHMP7 colocalises with LAP2 at the reforming nuclear envelope

a) Distribution of CHMP7 (red fluorescence) and LAP2 (green fluorescence) throughout the cell cycle in an untreated HeLa cell. **b)** Deconvolved image taken on DeltaVision microscope showing colocalisation of CHMP7 and LAP2 staining in telophase HeLa cell. Full z-stack can be found in Appendix 2b. Scale bars represent 10 μ m. **c)** Immunoprecipitation of untreated HeLa cell lysates for CHMP4B and CHMP7 (mouse and sheep-derived antibodies). Western blotting was carried out using LAP2 antibody. **d)** Immunoprecipitation of untreated HeLa cell lysates for CHMP7 (mouse-derived antibody) and LAP2. Western blotting was carried out using the rabbit CHMP7 antibody.

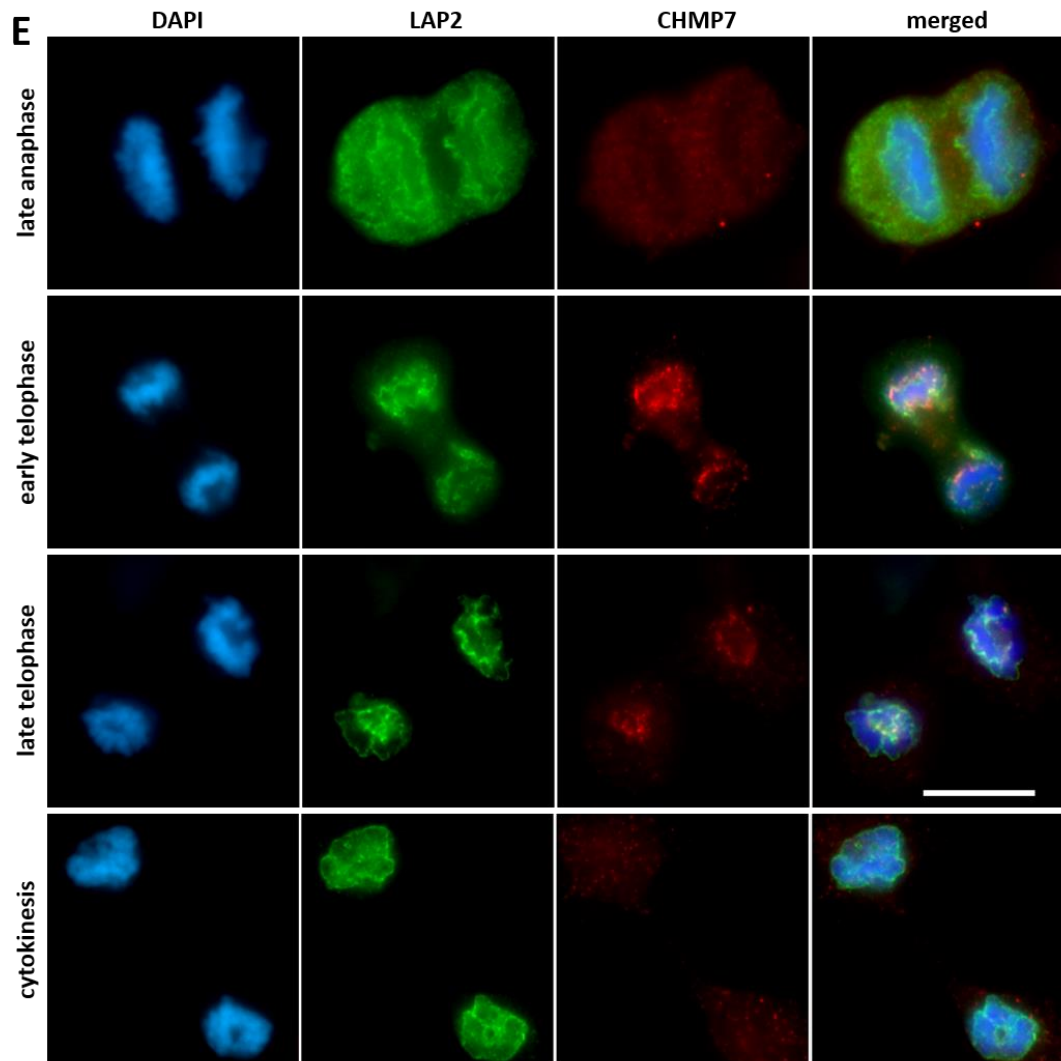


Figure 4.19 (continued)

e) The relationship of LAP2 and CHMP7 throughout the late stages of mitosis in untreated HeLa cells. Scale bar represents 10 μ m.

displays some gaps in staining. CHMP7 foci are rarely found independently of LAP2, either localising with or adjacent to the protein

4.2.20 Investigating direct interactions between CHMP7/CHMP4B and LAP2

Due to the observed colocalisation between LAP2 and CHMP7/CHMP4B, coimmunoprecipitation of the proteins was attempted in order to observe possible direct interactions (Figure 4.19c and 4.19d). The Western blots of the immunoprecipitation experiment display input and no-antibody control lanes, with both immunoprecipitated material (bound to the agarose beads: B) and protein remaining in the supernatant (not bound to the beads: U) samples analysed. Immunoprecipitation was carried out using both the mouse and sheep-derived anti CHMP7 antibodies, which target different regions of the protein, as well as anti-CHMP4B and anti-LAP2 antibodies. Western blotting was carried out using the rabbit anti-CHMP7 and LAP2 antibodies. Testing the interactions in both directions demonstrated no coimmunoprecipitation between CHMP7, CHMP4B and LAP2 in this experiment, although the transient nature of the interactions may hinder sufficient detection of co-precipitation.

4.2.21 CHMP7 localises to chromatin prior to nuclear lamina formation and adjacent to Lamin B

The nuclear lamina reforms with the nuclear envelope at the end of mitosis. Import of Lamin B protein continues to occur following the reestablishment of nuclear compartmentalisation, reinforcing the shape of the nucleus as the cell progresses out of mitosis (Schellhaus *et al.*, 2016). Through analysis of the fixed images the recruitment of CHMP7 and Lamin B with respect to each other can be observed (Figure 4.20c). In anaphase, both Lamin B and CHMP7 are distributed throughout the cytoplasm. As telophase begins, CHMP7 is recruited to chromatin, and is found around the reforming nucleus. Lamin B is subsequently recruited to

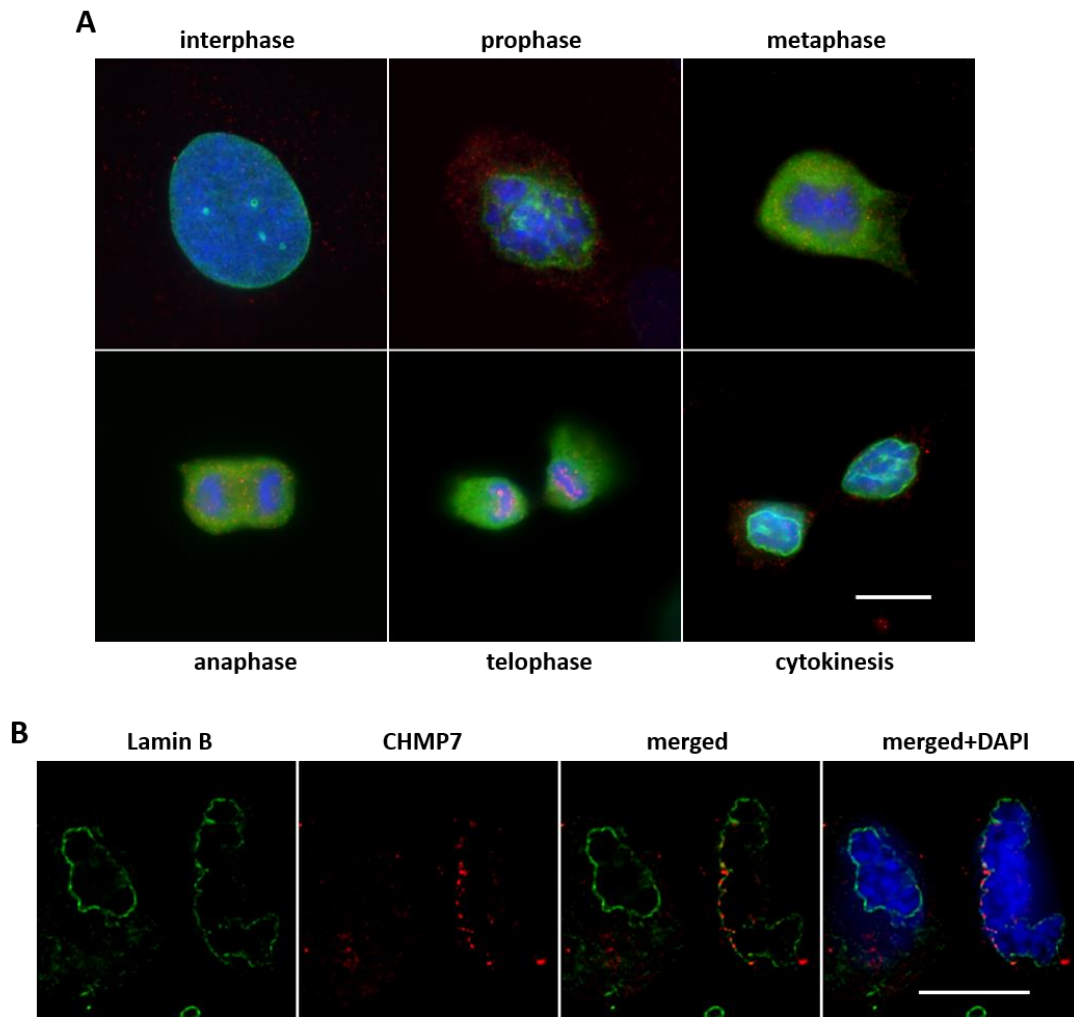


Figure 4.20. CHMP7 localises adjacent to Lamin B at the reforming nuclear envelope

a) Distribution of CHMP7 (red fluorescence) and Lamin B (green fluorescence) throughout the cell cycle in untreated HeLa cells. **b)** Deconvolved image taken on Deltavision microscope showing CHMP7 at the nuclear envelope adjacent to but not colocalising with Lamin B in telophase HeLa cell. Full z-stack can be found in Appendix 2c. Scale bars represent 10 μ m.

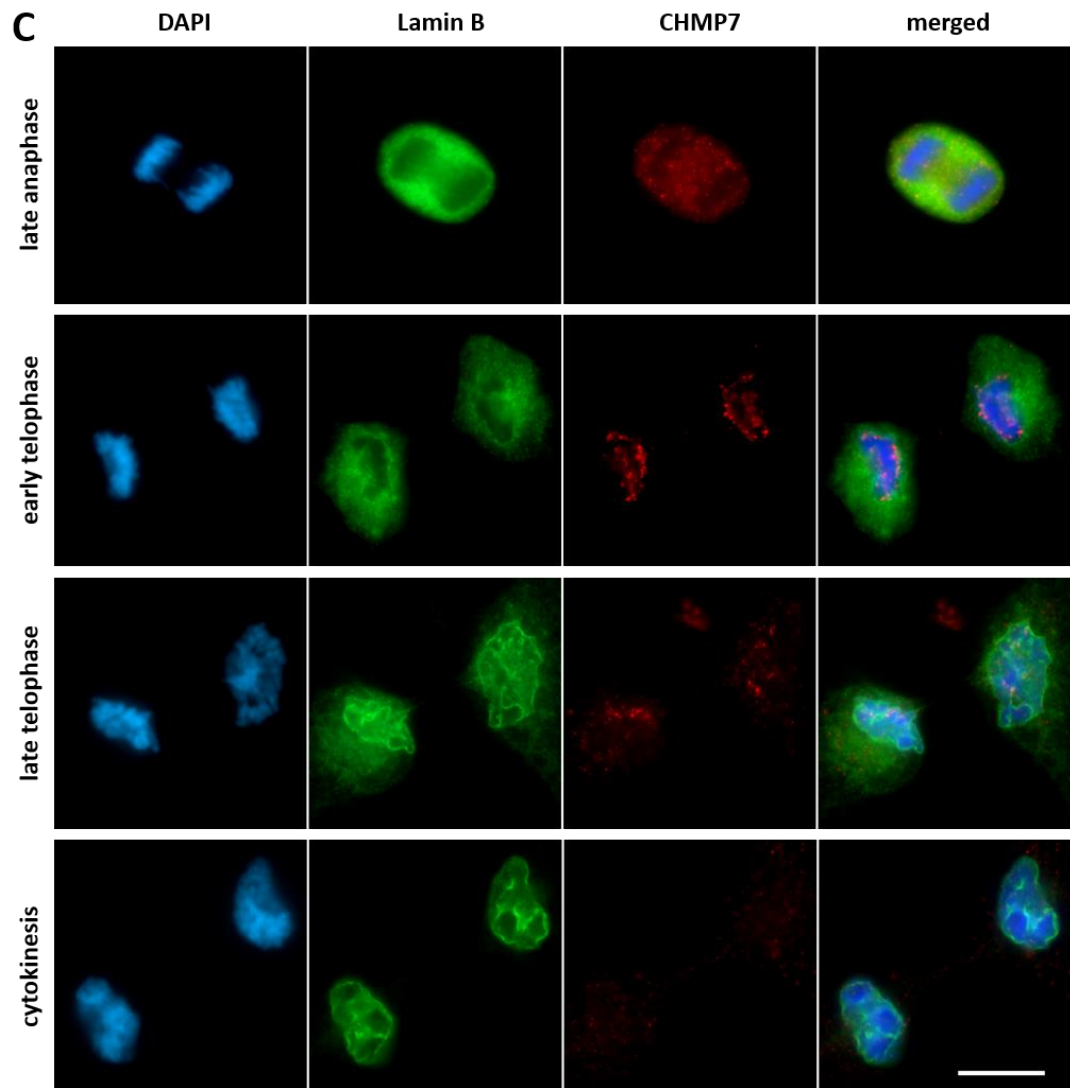


Figure 4.20. (continued)

c) The relationship of Lamin B and CHMP7 throughout the late stages of mitosis in untreated HeLa cells. Scale bar represents 10 μ m.

the nuclear envelope, and the remaining CHMP7 foci do not appear to colocalise directly with Lamin B. By the point of cytokinesis, a complete lamina is seen around the nuclei, and CHMP7 foci are no longer seen at the nuclear surface.

A telophase cell depleted of VPS4 was imaged in three dimensions with the Deltavision deconvolution microscope, from which it can be seen that CHMP7 and Lamin B do not appear to colocalise, though they are found adjacent to each other on the rim of chromatin (Figure 4.20b, Appendix 2c).

In contrast to the INM protein LAP2, which arrives at chromatin before CHMP7 (Figure 4.19e), Lamin B protein, and therefore the nuclear lamina meshwork, forms subsequently to CHMP7 association with the nuclear envelope.

4.2.22 CHMP7 is not necessary for the recruitment of nuclear envelope components

In this chapter, it has been shown that loss of CHMP7 prevents the ESCRT-III complex being recruited to the nuclear envelope, and causes subsequent problems with nuclear envelope integrity such as those observed in Chapter 3. The effect of the loss of CHMP7 on the key components of the reforming nuclear envelope was observed by looking at the nuclear membrane protein LAP2, the nuclear lamina protein Lamin B, and the marker of nuclear pore complexes mab414. HeLa, HeLa M and U2OS telophase cells were observed following the knockdown of CHMP7-1 and CHMP7-3. In each cell line, LAP2, Lamin B and mab414 staining was seen in all observed telophase cells (Figure 4.21a and 4.21b), showing that CHMP7 and ESCRT-III recruitment is not required for their localisation to the reforming nuclear envelope.

4.2.23 Overexpression of HA-tagged CHMP7 constructs

The data presented in this chapter shows that VPS4 depletion causes an aberrant accumulation of CHMP7 and ESCRT-III proteins at the nuclear envelope. In order to confirm whether nuclear foci could also be induced by other conditions causing CHMP7 accumulation

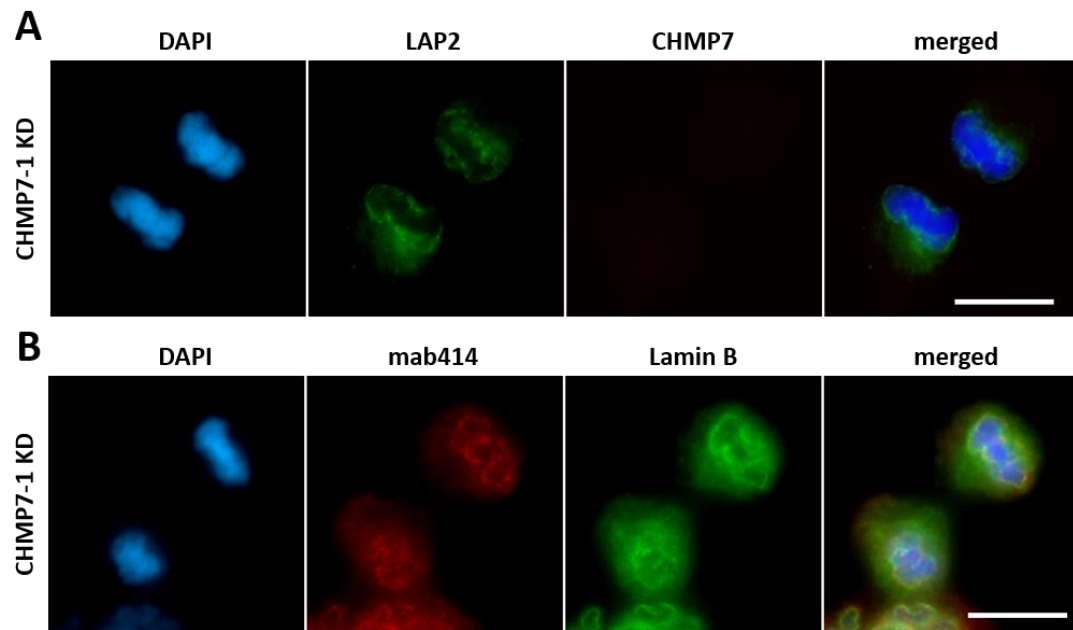


Figure 4.21. CHMP7 knockdown does not affect recruitment of LAP2, Lamin B or NPCs to the nascent nuclei

HeLa cells were transfected for with either CHMP7-1 or CHMP7-3 siRNA for 48 hour prior to staining. **a)** A representative image of a CHMP7-1-knockdown telophase HeLa cell stained to show LAP2 and CHMP7. **b)** A representative image of a CHMP7-1-knockdown telophase HeLa cell stained to show Lamin B and NPCs (mab414 antibody). Scale bars represent 10 μ m.

in VPS4-normal cells, CHMP7 was overexpressed in HeLa and HeLa M cells. Full-length CHMP7 (amino acids 1-453) was cloned into a plasmid vector, adding a HA-tag sequence to the N-terminal end of the protein. As previously determined (Section 1.4.6), the N-terminal half of the CHMP7 protein has an unverified structure and function, though is predicted to have a double winged-helix structure which most closely resembles part of ESCRT-II family member VPS25. Therefore, amino acids 1-226 of CHMP7, which encompasses the N-terminal half and truncates the protein prior to the canonical CHMP domain, were cloned into a plasmid vector with an added N-terminal HA tag. The HA tag was used as a small addition to the protein which can be detected using anti-HA antibody for immunofluorescence and western blot.

Western blots showing the success of expression of both constructs in HeLa cells can be seen in Figure 4.22a. The additional expression of CHMP7 protein can be seen above endogenous CHMP7 when the rabbit anti-CHMP7 antibody is used. The rabbit-derived antibody targets the C-terminal portion of CHMP7, therefore, HA-CHMP7-NT is not visualised using this antibody in the Western blot in Figure 4.22a and the immunofluorescence in Figure 4.22e. Overexpression caused approximately 14% of observed fixed cells to be in the process of apoptosis (Figure 4.22b), compared to 2.8% in the empty plasmid vector control. Given the high levels of exogenous additional protein, it is expected that transfected cells will be stressed and that expressed protein can interfere with normal cellular function.

Instead of the anticipated nuclear-associated CHMP7 staining, much of the protein visualised using both the anti-HA and anti-CHMP7 antibodies corresponds to very bright cytoplasmic accumulations (Figure 4.22d). These large aggregations of protein are found most strongly in the perinuclear region and at the rim of the nucleus.

Overexpression of the N-terminal half of CHMP7 (CHMP7-NT) did not cause the large accumulations of the protein within the cell. This can be explained by the loss of the CHMP

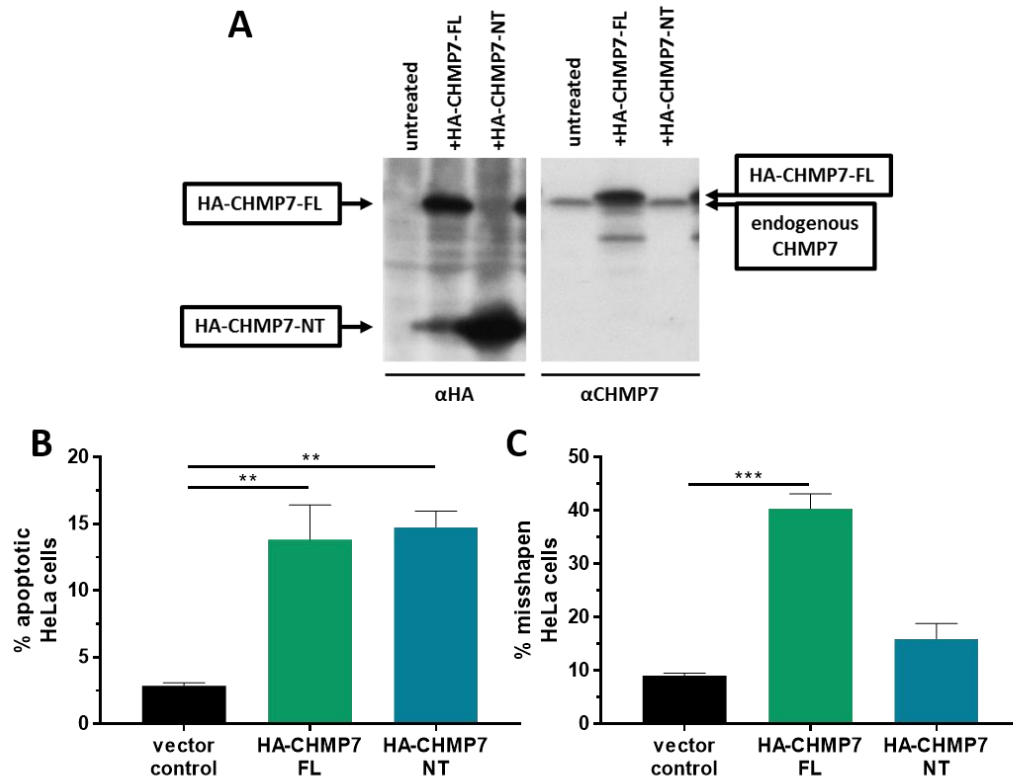


Figure 4.22. Overexpressed full length and N-terminal CHMP7 in HeLa cells

a) Western blot showing the transfection of HA-CHMP7-FL (full-length protein) and HA-CHMP7-NT (residues 1-226) into HeLa cells. **b)** HeLa cells were transfected with 0.2 μ g/ml empty vector control (pcDNA3.1+), HA-CHMP7-FL or HA-CHMP7-NT for 24 hours, fixed and stained with anti-HA and rabbit anti-CHMP7 antibody and counterstained with DAPI. A minimum of 420 cells per condition were scored for **b)** apoptosis and **c)** deformed (misshapen) nuclear morphology. Averages and standard error of two independent repeats are shown. Results were analysed using a one-way ANOVA with Dunnett's *post hoc* test compared to control.

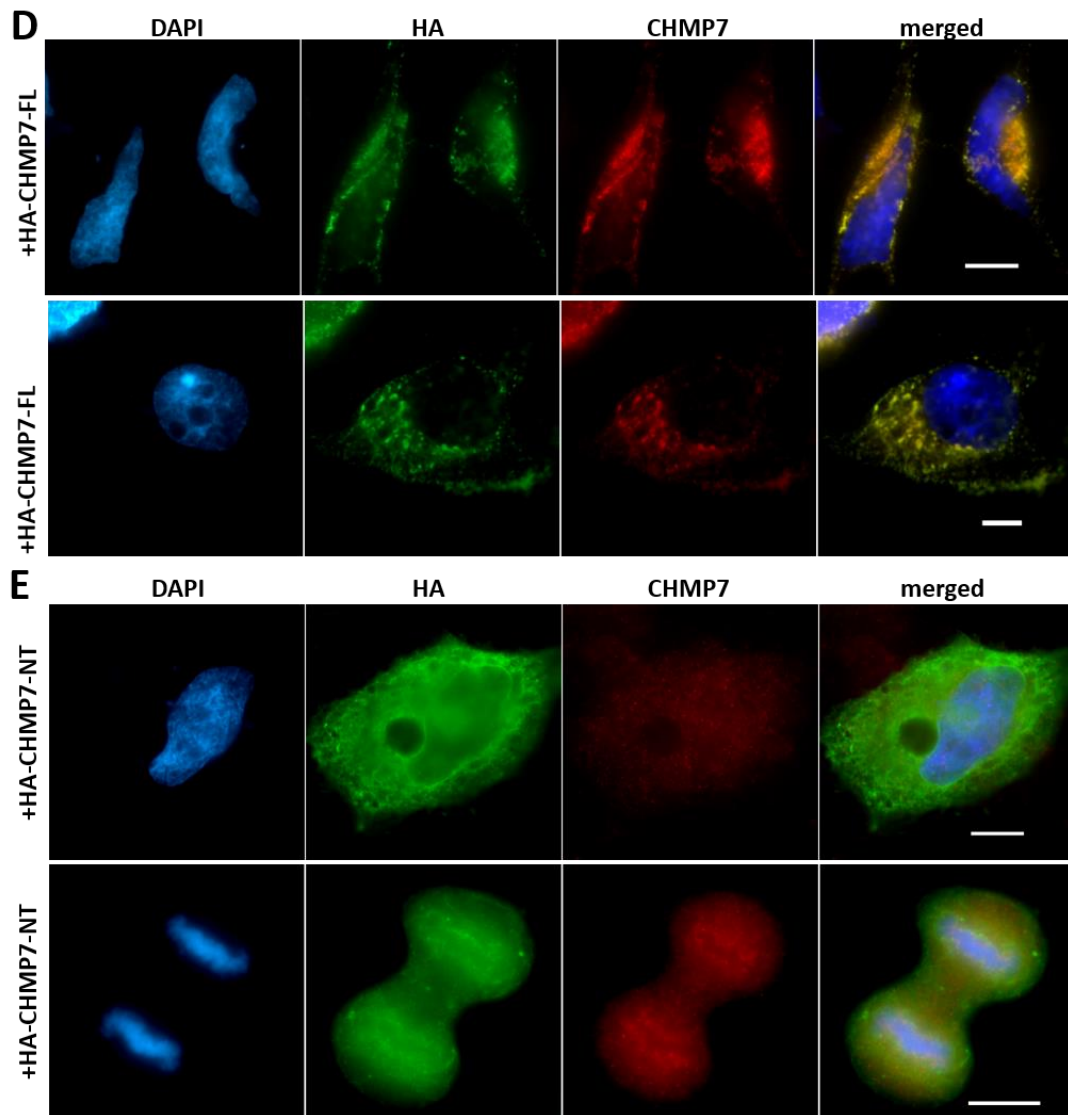


Figure 4.22. (continued)

d) HeLa cells transfected with a HA-CHMP7-FL-expressing plasmid. **e)** HeLa cells transfected with a HA-CHMP7-NT-expressing plasmid. All scale bars represent 10 μ m.

module which is responsible for CHMP-CHMP interactions and formation of CHMP polymers. The HA-CHMP7-NT protein can be clearly seen at the at the rim of the nucleus or nuclear envelope, and was also distributed throughout the cytoplasm in a pattern similar to that observed by ER membrane detection (Figure 4.17). In mitotic cells (lower panel, Figure 4.22e), HA-CHMP7-NT was observed at the rim of chromatin in telophase, appearing to surround the whole of the nuclear material, whereas endogenous CHMP7 accumulations were primarily seen at the chromatin core region.

HA-CHMP7-NT transfection combined with the PDI staining process used previously (Figure 4.17) was attempted several times, however many cells were lost following the SDS extraction procedure, with the remaining cells showing unclear CHMP7 staining. The necessary high quality of staining required to visualise both PDI and CHMP7-NT was not achieved in this study.

4.2.24 Overexpression of HA-CHMP7-FL and HA-CHMP7-NT results in NE deformation and misshapen nuclei

Deformation of nuclear morphology, such as that seen in the upper panel of Figure 4.22d was evident in the transfected cells. Due to the fact that not all cells had been successfully transfected, those which displayed anti-HA antibody staining were scored. It should be taken into account that cells showed variable levels of exogenous protein expression. An average of 40.4% HA-CHMP7-FL and 16.0% HA-CHMP7-NT cells displayed loss of regular nuclear shape, compared to the empty vector control, in which 9.0% of cells were abnormal. There is a significant increase in misshapen nuclei following the transfection of the tagged, full length protein. The nuclear deformation may be due to the significant amount of CHMP7 accumulation which is occurring within the cell. This could suggest that CHMP7 interacts with the nuclear envelope, or with the endoplasmic reticulum, the composition of which affects nuclear morphology through its connection to the nuclear membrane (Walters *et al.*, 2012).

4.2.25 Endogenous CHMP7 in untreated interphase cells localises to the nuclear envelope

In order to determine whether CHMP7 is associated with the nuclear envelope under normal conditions, an *in situ* detergent pre-extraction prior to fixation and immunofluorescent staining was carried out on untreated HeLa and HeLa M cells. Pre-extraction permeabilises the cell and removes soluble protein, allowing for clearer staining of proteins associated with membrane structures and the nucleus. CHMP7 was visualised following this process, and found to localise in small foci or patches across the nuclear surface in a HeLa cell (Figure 4.23a) and a HeLa M cell (Figure 4.23b). Figure 4.23a shows a slice through the middle of the nucleus, with CHMP7 localised around the edge of the nucleus, and a slice at the top of the nucleus, where CHMP7 is spread across the surface.

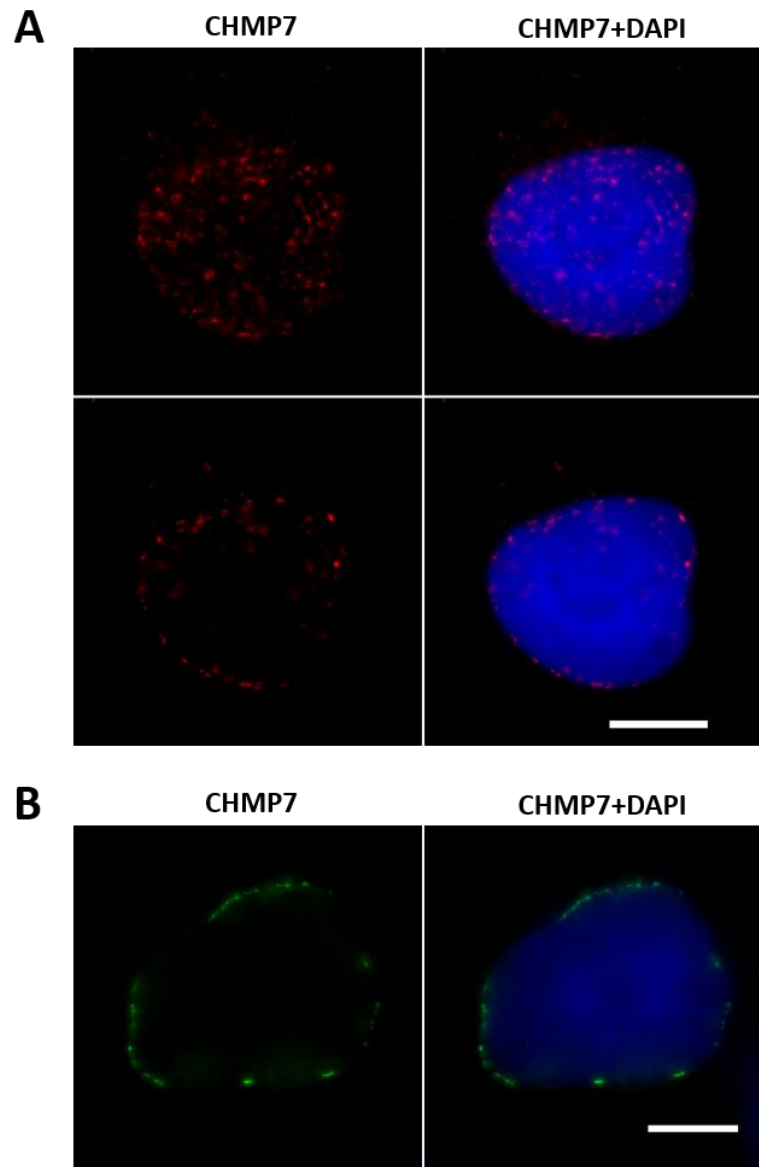


Figure 4.23. Endogenous CHMP7 is found on the nuclear rim following detergent pre-extraction

Untreated cells were subjected to pre-extraction for 2 minutes prior to fixation, and stained to show DAPI and CHMP7. **a)** Two focal planes of the same HeLa nucleus are shown, the upper panel showing the top surface of the nucleus, and the lower panel shown a slice through the centre of the nucleus. **b)** A slice through a HeLa M cell nucleus. Scale bars represent 10 μ m.

4.3 Discussion

In this chapter, the relationship of CHMP7 with the nuclear envelope has been established and investigated through a number of routes. Initial clues for the nuclear role of CHMP7 came from the presence of large CHMP nuclear accumulations following the depletion of VPS4. These accumulations were found to contain key components of the ESCRT-III complex, which become unable to disassemble in the absence of VPS4, allowing observation of these structures to be carried out. CHMP7 has been shown to be essential for the formation of the nuclear ESCRT-III structures, establishing a clear order of recruitment. Nuclear CHMP7 structures occur at gaps in the nuclear lamina and appear to cause induction of DNA damage at larger, persistent foci, to which DNA damage repair proteins and PML bodies are recruited. The relationship with the nuclear lamina, as well as CHMP7 colocalisation with nuclear envelope proteins LAP2 and Lamin A/C and observation of nuclei in three dimensions indicate development of these structures at the nuclear envelope. This would be consistent with the known roles of ESCRT-III, which all involve formation at a cell membrane.

While investigation was being carried out on nuclear localisation of CHMP7, a novel arrangement of endogenous, chromatin-associated CHMP7 staining was observed in both control and VPS4-depleted mitotic cells. This gives us a clear insight into a role of CHMP7 and ESCRT-III in untreated cells in all observed cell lines, HeLa, HeLa M and U2OS. This indicates localisation of ESCRT-III in a CHMP7-dependent manner to the nuclear envelope at the time of its reformation. Based on observations of CHMP7 localisation relative to staining of membrane structures (PDI), the nuclear lamina (Lamin B) and the INM protein LAP2, it can be determined that CHMP7 recruitment to the NE occurs after LAP2 association to chromatin, but prior to significant nuclear lamina formation.

4.3.1 A model for CHMP7/ESCRT-III function at the nuclear envelope

Based on the data collected thus far, we hypothesise a role for CHMP7 and ESCRT-III at nuclear membranes, given the effects on nuclear envelope organisation and integrity (Chapter 3), the location of CHMP7 in both mitosis and interphase shown in this chapter, and the known functions of the ESCRT-III complex. CHMP7 depletion leads to loss of compartmentalisation and genomic damage, indicating that the nuclear envelope is not correctly sealed. Additionally, CHMP7-depleted cells display improperly formed and organised nuclear envelope structures, including the nuclear lamina and nuclear pore complexes. ESCRT-III complexes work at membrane neck structures with a shared topology. Upon first inspection, the topology of annular fusion differs from those of all known sites of ESCRT-III action as shown in Figure 4.24. However, ESCRT-III has demonstrated a flexibility of function, with cytokinesis, viral budding, multivesicular body biogenesis and plasma membrane repair having different overall membrane architecture, but sharing the basic curved, circular membrane neck shape (Figure 4.24). Therefore, a role for ESCRT-III in annular fusion, as recruited specifically to the nuclear membrane by CHMP7, would be consistent with the known mechanism of action for ESCRT-III. It would also satisfy the criteria for annular fusion, which requires a drawing together of the membrane neck in combination with simultaneous membrane fusion and scission as described in Section 4.1.3.

ESCRT-III-mediated processes require an upstream protein adaptor to recruit CHMP4B and nucleate ESCRT-III filament formation. These include CEP55, HD-PTP, ALIX and ESCRT-0/ESCRT-I proteins, which have all been shown not to localise to the nuclear envelope by Vietri *et al.* (2015). Therefore, the link between the nuclear membrane and the ESCRT-III complex has not yet been established. CHMP7 has been shown to interact directly with CHMP4B through their shared CHMP domains (Horii *et al.*, 2006), and therefore could undertake a role as a site of CHMP4B/ESCRT-III filament nucleation on the curved surface of the nuclear membrane. This role would place it as an adaptor between nuclear membranes

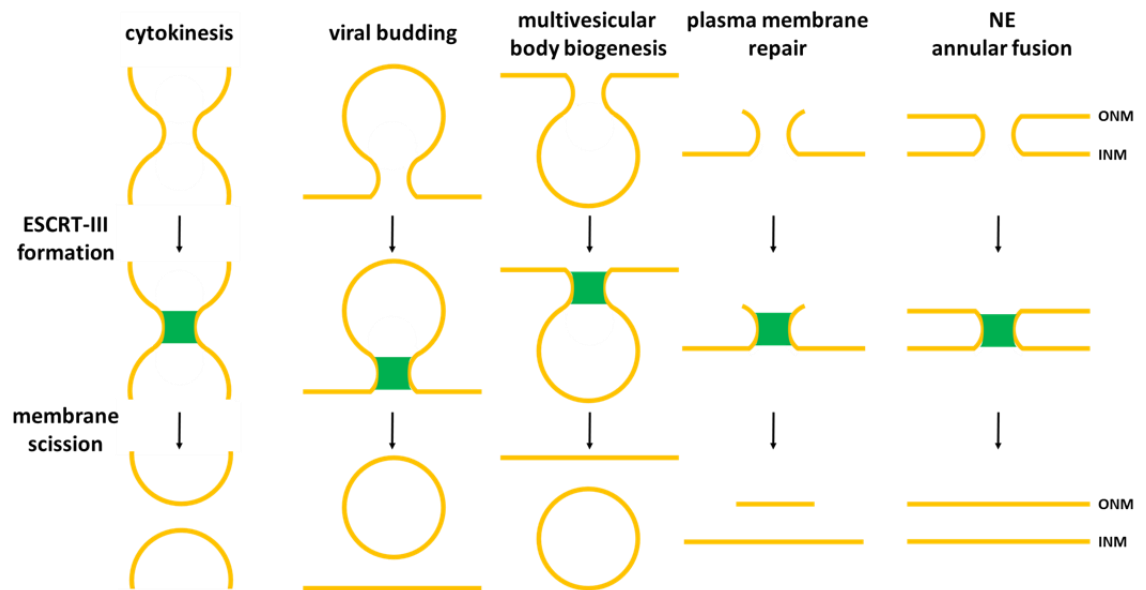


Figure 4.24. A nuclear role for the ESCRT-III complex

Diagrams illustrating the topology of known membrane structures to which ESCRT-III localises and carries out scission, and a model of the equivalent nuclear membrane structure. It is proposed that ESCRT-III localises to small holes in the nuclear envelope (NE) and cuts and fuses the nuclear membranes to create continuous, separated inner and outer nuclear membranes (INM and ONM).

in particular and the ESCRT-III complex, explaining the specificity of nuclear function exhibited by the CHMP7 protein.

CHMP7 and the ESCRT-III complexes are observed at gaps in the nuclear lamina in late anaphase/telophase cells, and very strikingly in VPS4-depleted cells, where large lamin holes are filled by CHMP protein accumulations. Presence at nuclear envelope holes strongly indicates a role in nuclear membrane remodelling and/or fusion at these sites. The persistence of these CHMP7/ESCRT-III structures is due to the inability of cells to complete membrane fusion/fission in the absence of VPS4, which provides the driving force for ESCRT-III-mediated scission. The presence of large lamina holes, chromatin herniation and loss of compartmentalisation in CHMP7-depleted cells demonstrated in this study implies a reduced ability of cells to seal the nuclear envelope in the absence of CHMP7, due to the failure to recruit ESCRT-III (Figure 4.25).

4.3.2 A model for formation of interphase nuclear CHMP7/ESCRT-III foci in VPS4-depleted cells

It seems likely that the CHMP7/ESCRT-III foci observed upon VPS4 depletion, and the specific persistence of similar foci into the final stages of mitosis following VPS4 depletion are likely to be linked. Therefore, a model whereby CHMP7/ESCRT-III recruited to the nuclear envelope in mitosis persists through mitotic exit or failure into interphase cells, is suggested in Figure 4.25. The presence of ESCRT-III at the nuclear envelope in mitosis, which cannot be disassembled due to the absence of VPS4, will therefore lead to the persistence of ESCRT-III complexes beyond the bounds of mitosis, explaining the presence of nuclear-associated interphase foci found only in VPS4-depleted cells.

Additionally, it was determined in Chapter 3 that VPS4 depletion did not lead to the nuclear lamina defects and chromatin herniation observed following the CHMP7 depletion. Based on the model shown in Figure 4.25, this could be explained by the fact that nuclear holes are

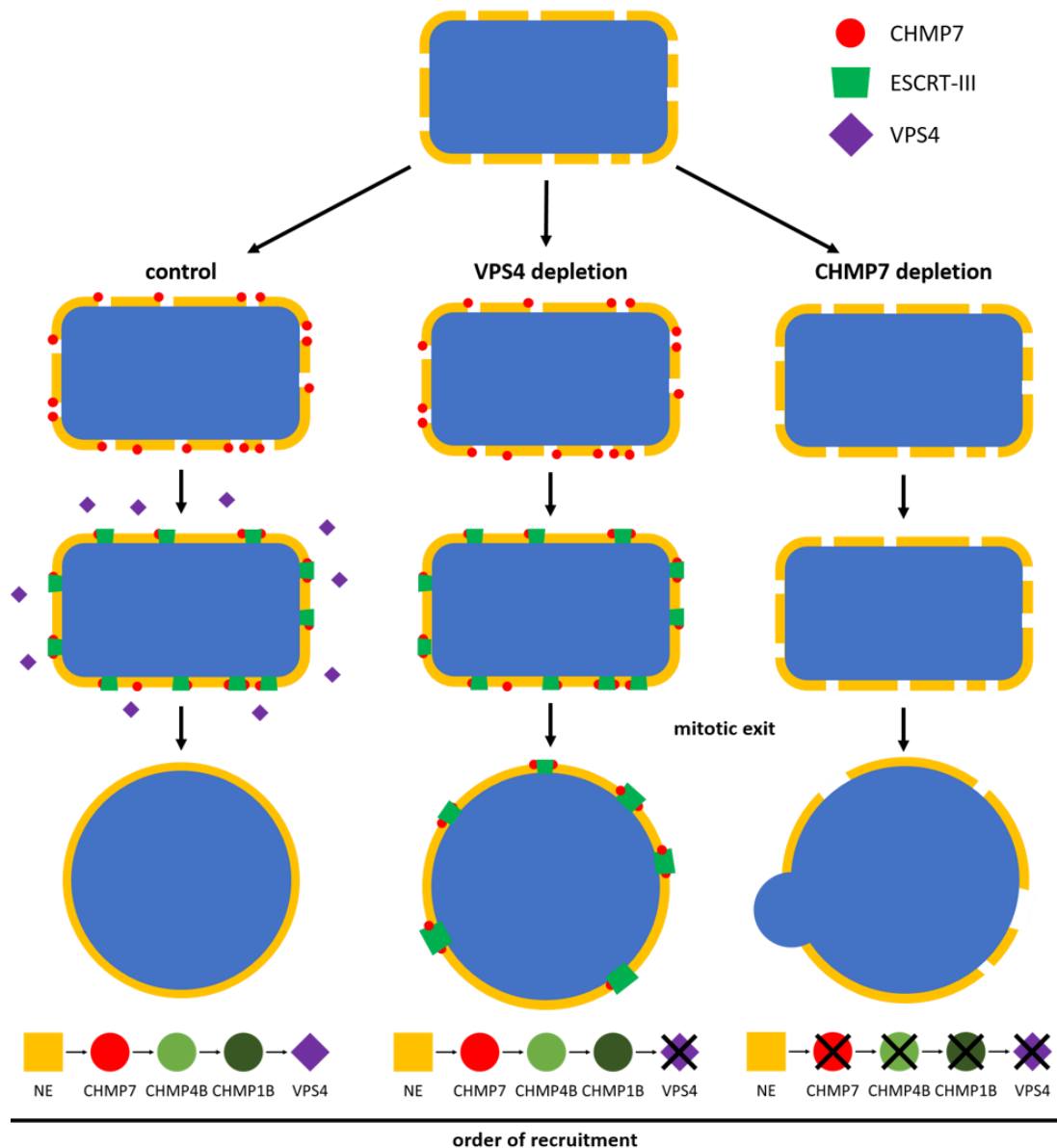


Figure 4.25. A model for nuclear envelope sealing in CHMP7 and VPS4-depleted cells

Following membrane recruitment and spreading over the nuclear material, holes remain which require annular fusion to be closed and the nuclear envelope sealed. In control cells, CHMP7 is recruited to the nuclear membrane, and nucleate, possibly through CHMP7-CHMP4B direct interaction, the formation of an ESCRT-III spiralling complex. VPS4 drives the completion of the ESCRT-III membrane scission and fusion, resulting in recycling of the ESCRT-III complex and a sealed nuclear envelope. Following VPS4 depletion, ESCRT-III complexes are formed on the nuclear envelope, but fail to be recycled and persist on the nuclear envelope into interphase, resulting in the CHMP7 nuclear foci originally observed, but maintaining overall integrity of the nuclear envelope. In CHMP7 depleted cells, ESCRT-III is never recruited to the nuclear envelope, causing holes to remain unsealed through mitosis and into interphase. This may explain the loss of compartmentalisation and nuclear and genomic integrity observed in CHMP7-depleted cells.

'plugged' to prevent chromatin escape and maintained at a small size by the ESCRT-III complex, which draws together the membrane neck despite being unable to complete scission. In CHMP7-depleted cells, ESCRT-III does not interact with the nuclear membrane, resulting in further deterioration of nuclear envelope integrity as holes are neither repaired nor supported by the presence of the ESCRT-III complex.

4.3.3 Perturbation of ESCRT-III activity results in DNA damage and repair pathway signalling

Genomic instability is a term used to describe an increased rate of genomic mutations within a cell, which can arise from imprecise DNA replication, improper segregation of chromosomes during mitosis, ineffective DNA damage repair and misregulated cell cycle progression. High levels of genomic instability result in increased risk of cancer development or cell death. Depletion of ESCRT-III-related proteins CHMP7 and VPS4 has here been shown to result in compromised nuclear integrity and increased rates of DNA damage (Figure 4.26). In the case of VPS4-depletion, persistent DNA damage has been shown to be associated in a localised manner with ESCRT-III nuclear foci.

The persistence of CHMP foci into interphase in VPS4-depleted cells appears to lead to an increase in size as CHMPs accumulate, with larger, more obstructive foci resulting in damage to DNA and a subsequent damage signalling response (Figure 4.26c). The high proportion of CHMP foci associated with PML bodies indicates this persistence, as PML bodies are known to non-randomly associate with sustained DNA damage foci, though they are not essential for repair of these foci (Boichuk *et al.*, 2011). It is not known whether PML bodies are present due to their role in the DNA damage response, or in a chromatin remodelling capacity, as PML bodies have been shown to play a role in aiding chromatin condensation (Luciani *et al.*, 2006).

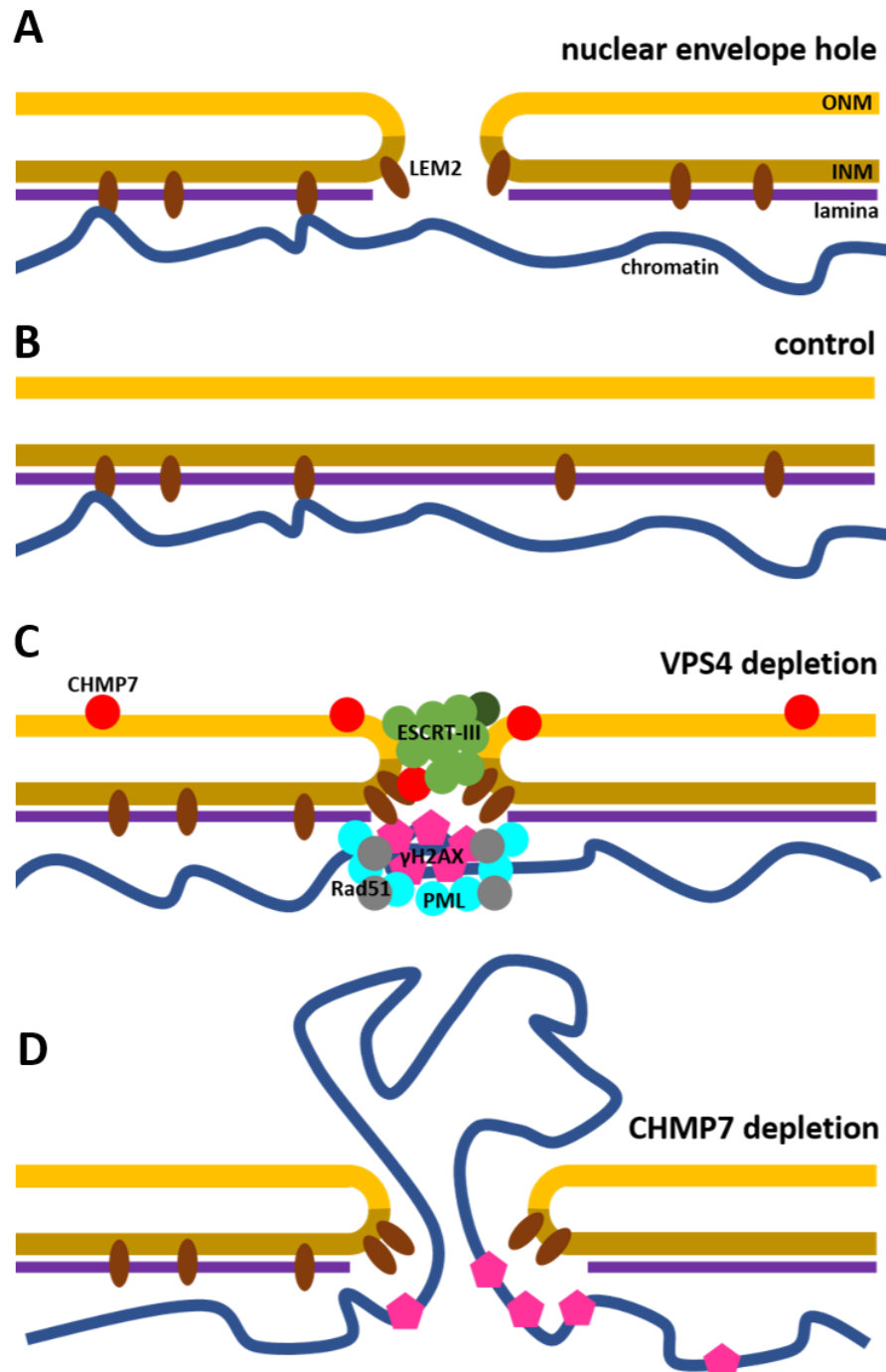


Figure 4.26. Perturbation of ESCRT-III activity results in DNA damage

a) A diagram showing a perforated nuclear envelope, as found in mitotic cells undergoing nuclear envelope reformation, or transient nuclear rupture. **b)** A diagram of a properly sealed nuclear envelope following proposed ESCRT-III sealing activity. **c)** A diagram of a nuclear envelope hole "plugged" by an ESCRT-III complex in a VPS4-depleted condition. CHMP7 results in recruitment of CHMP4B and ESCRT-III complex formation in the membrane neck. Localised DNA damage causes phosphorylation of histone H2AX and recruitment of repair protein Rad51, and PML nuclear body protein, and a gap in the nuclear lamina in the vicinity of the hole. **d)** A diagram of a nuclear hole in a CHMP7-depleted cell, lacking ESCRT-III recruitment. This results in a persistent nuclear envelope hole, including a broken nuclear lamina. Chromatin may be able to escape from the nucleus through the hole, resulting in herniation. Exposure of chromatin to the cytoplasmic environment may result in DNA damage and phosphorylated H2AX.

The specific cause of the DNA damage in the region of CHMP foci is not known, however, it can be concluded that the CHMPs do not localise to pre-existing sites of DNA damage, as CHMPs are not found at UV-induced DNA damage foci (Figure 4.9). Therefore, it suggests that dysfunctional accumulation of ESCRT-III creates a condition conducive to the formation of DNA lesions. This could be due to imperfect compartmentalisation at the site of accumulation, leading to localised exposure to genotoxic agents from the cytoplasm. Alternatively, perturbation of the nuclear envelope could lead to mechanical stress on chromatin proximate to the ESCRT-III structure as the nuclear envelope is remodelled and disturbed by the continued accumulation of CHMP proteins.

CHMP7 knockdown has shown increased rates of nuclear rupture and deformation. Nuclear envelope rupture is known to be a key contributor to genomic instability and tumour progression in cancerous cells (Lim *et al.*, 2016), due to the exposure of DNA to the cytoplasmic environment resulting in mutagenesis. Aberrations of nuclear morphology is also a hallmark of cancerous cells, demonstrating problems with nuclear envelope organisation and affecting gene transcription and expression. The combination of both nuclear envelope rupture and mechanical nuclear deformation can result in chromatin fragmentation or extrusion from the nucleus, such as that seen in HeLa M cells depleted of CHMP7.

4.3.4 CHMP7 associates with nuclear structures through its N-terminal half

Overexpression of HA-tagged CHMP7 protein leads to aggregation of CHMP7 in the perinuclear area in interphase cells, indicating that it normally localises in this area. Interestingly, the N-terminal half of CHMP7 alone shows localisation to chromatin in mitosis (Figure 4.22e), indicating that the key region for recruitment to the reforming nuclear envelope is found in the N-terminal region of the protein. This may explain the key and specific role of CHMP7 in nuclear function with ESCRT-III, as no other ESCRT-III proteins

contain the N-terminal domains found in CHMP7. It may be possible that CHMP7 is already associated with ER membranes prior to their recruitment to chromatin, or that it is recruited from a pool of CHMP7 protein found in the ER lumen or perinuclear area at the appropriate time.

4.3.5 A potential role for CHMP7/ESCRT-III in repairing interphase nuclear envelope ruptures

As has been previously described fully in section 3.3.2, transient nuclear rupture at areas of disorganised or absent nuclear lamina is a common occurrence in cancer cells. These ruptures are commonly repaired successfully, with associated restoration of nuclear and cytoplasmic compartmentalisation, allowing normal continuation of the cell cycle and cell division.

If the role of ESCRT-III at the nuclear envelope in nuclear envelope reformation after mitosis is substantiated, it is tempting to speculate an additional, similar role at nuclear envelope ruptures occurring outside mitosis. Interphase nuclear CHMP foci found in the VPS4 knockdown condition are found at lamina holes, which could represent likely sites of nuclear envelope rupture. This could also explain the presence of CHMP7 at the interphase nuclear envelope seen in control cells in Figure 4.23.

It is not possible to see without live cell imaging whether the CHMP foci observed in VPS4-depleted cells originate in mitosis or from interphase ruptures, however all cell lines observed here show fewer cells exiting mitosis with CHMP7 foci compared to the percentage of interphase cells which have nuclear foci. In U2OS cells, 93.0% of interphase VPS4-depleted cells display CHMP7 foci (Figure 4.4b), however, only 75.6% of cells exiting mitosis display these foci (Figure 4.13d). This disparity may represent *de novo* rupture events occurring during interphase, to which ESCRT-III accumulates and becomes unable to dissociate. This pattern is also observed in HeLa cells (82.0% in interphase; 66.7% upon mitotic exit) and HeLa

M cells (97.7% in interphase; 75.6% upon mitotic exit). However, based on the data obtained here, the origin of the nuclear envelope holes to which ESCRT-III localises cannot be determined. However, live cell imaging could be used to determine the point of nuclear rupture and ESCRT-III recruitment.

Chapter Five

CHMP7 and ESCRT-III associate with the nuclear envelope of micronuclei and chromosome bridges: structures characteristic of genomic instability

Contents

	Page
5.1 Introduction	181
5.1.1 Chapter Summary	181
5.1.2 The origin and fate of micronuclei	181
5.1.3 Generation and resolution of chromosome bridges	184
5.2 Results	189
5.2.1 CHMP7 localises to micronuclei in untreated cells	189
5.2.2 ESCRT-III subunits localise to micronuclei only when CHMP7 is present	189
5.2.3 CHMP7 localises more frequently to smaller micronuclei containing chromosome fragments	192
5.2.4 CHMP7 localises to micronuclei lacking a continuous nuclear lamina	194
5.2.5 CHMP7 localises to micronuclei lacking nuclear pore complexes	195
5.2.6 CHMP7-positive micronuclei show loss of compartmentalisation	198
5.2.7 Invasion of ER membrane into CHMP7-positive micronuclei	198
5.2.8 CHMP7 depletion causes increased micronuclei generation	202
5.2.9 CHMP7 knockdown generates more micronuclei containing chromosome fragments	204
5.2.10 ESCRT-III impairment generates more lamina and NPC-defective micronuclei	204
5.2.11 ESCRT-III impairment results in more disrupted and collapsed micronuclei	206
5.2.12 A link between CHMP7 and DNA damage in micronuclei	207
5.2.13 CHMP7 forms bridge structures in untreated HeLa, HeLa M and U2OS cells	210
5.2.14 ESCRT-III components localise at bridge structures when CHMP7 is present	210
5.2.15 CHMP bridges associate with nuclear material	213
5.2.16 CHMP7 does not localise to BLM ultrafine anaphase bridges	216
5.2.17 Development of CHMP7 bridges in mitosis	216
5.2.18 CHMP7 bridges occur in multinucleated, cytokinetic, and separated cells	218
5.2.19 Nuclear membrane assembles on CHMP7 internuclear bridges	221
5.2.20 Other nuclear envelope components are not present at CHMP7 bridges	223
5.2.21 The prevalence of bridges in ESCRT-III knockdown cells	225
5.3 Discussion	228
5.3.1 CHMP7 relationship with micronuclei	228
5.3.2 CHMP7 recruitment to micronuclei	229
5.3.3 A role for CHMP7 and ESCRT-III in micronuclear integrity	230
5.3.4 A role for CHMP7/ESCRT-III in micronuclear collapse	232
5.3.5 A role for CHMP7/ESCRT-III in autophagic degradation of micronuclei	233

5.3.6	The relationship between CHMP7 and chromosome bridges	234
5.3.7	Formation of CHMP7 bridges	235
5.3.8	A proposed role for CHMP7 bridges in the NoCut pathway	235
5.3.9	A potential role for CHMP7/ESCRT-III in chromosome bridge resolution	238

List of Figures

Figure	Title	Page
5.1	Generation and fate of micronuclei	183
5.2	Generation and resolution of chromosome bridges	185
5.3	CHMP7 localises to micronuclei in various cell lines in control and VPS4-depleted cells	190
5.4	ESCRT-III localises to micronuclei in the presence of CHMP7	191
5.5	CHMP7 localises more frequently to smaller micronuclei containing chromosome fragments	193
5.6	CHMP7 preferentially localises to micronuclei lacking an intact nuclear lamina	196
5.7	CHMP7 preferentially localises to micronuclei lacking nuclear pore complexes	197
5.8	CHMP7-positive micronuclei retain LAP2 staining, but show loss of soluble nuclear protein	199
5.9	CHMP7-positive micronuclei show ER membrane invasion into chromatin	201
5.10	Impairment of ESCRT-III function increases multinucleation of HeLa cells	203
5.11	Impairment of ESCRT-III function decreases micronuclear integrity and increases loss of compartmentalisation	205
5.12	Scoring of HeLa cells for CHMP7 and γ H2AX micronuclear foci	208
5.13	CHMP7 forms filamentous structures in various cell lines in control and VPS4-depleted cells	211
5.14	ESCRT-III components localise at bridge structures when CHMP7 is present	212
5.15	CHMP7 bridges connect nuclear structures	214
5.16	CHMP7 bridges do not correspond to anaphase BLM bridges, but appear later in mitosis	217
5.17	Occurrence of CHMP7 bridges at different cell stages	219
5.18	Nuclear envelope assembly around CHMP7 internuclear bridges	222
5.19	Lamin B and mab414 are absent from CHMP7 nuclear bridges	224
5.20	The effect of ESCRT-III impairment on the prevalence of internuclear bridges	226
5.21	Model for the relationship between CHMP7/ESCRT-III and micronuclei	231
5.22	Model for the relationship between CHMP7/ESCRT-III and chromosome bridges	236

5.1 - Introduction

5.1.1 - Chapter Summary

Given the relationship between the nuclear ESCRT-III complex and ruptures in the nuclear envelope shown in Chapter 4, we set out to explore if presence on broken nuclear structures was a general characteristic of the CHMP7-nucleated ESCRT-III complex. The data presented in this chapter show that structures generated through genomic instability - micronuclei and chromosome bridges - are also closely associated with the nuclear ESCRT-III complex.

Cleasby (PhD thesis, 2013) has previously observed that the percentage of HeLa M cells containing micronuclei increased from a baseline of approximately 5% for this cell line, to 25% following VPS4 knockdown for 72 hours. Depletion of VPS4 in HeLa M cells results in genetic instability (Morita *et al.*, 2010) causing a significant increase in the number of micronuclei found in cells. Interestingly, CHMP7 localises to 70% micronuclei originated during mitosis and cytokinesis impairment caused by depletion of VPS4 for 72 hours (Cleasby, PhD thesis, 2013).

This chapter uses immunofluorescence to observe the presence of ESCRT-III on cancer cell micronuclei, and determines the specific characteristics of CHMP7-positive micronuclei through co-staining experiments with nuclear envelope and nucleoplasmic proteins. Inter-nuclear CHMP7 bridges, which appear to form as mitosis progresses and connect nuclear material even upon nuclear segregation into daughter cells, are also characterised. This chapter hypothesises a role for CHMP7 and the ESCRT-III complex and the nuclear envelope of these structures which occur when DNA is improperly segregated.

5.1.2 The origin and fate of micronuclei

Micronuclei are a common marker for genomic instability and genotoxic events, as they indicate aberrance of chromosome segregation and indicate loss, gain or breakage of genetic material (Fenech *et al.*, 2011). Micronuclei are derived primarily in mitosis from whole

chromosomes or acentric chromosome or chromatid fragments, due to their failure to attach properly to the mitotic spindle, leaving them displaced from the reforming daughter nuclei. There are two key origin events which produce micronuclei: aneugenic events, which involve improper segregation of a whole chromosome or chromatid, and clastogenic events, which involve chromosome or chromatid breakage, forming acentric chromatin fragments (Figure 5.1a). Aneugenic events can occur due to spindle or kinetochore defects, resulting in lack of spindle attachment or merotelic attachment. Clastogenic, or breakage, events, can occur due to a misrepaired or unrepaired double-strand break in DNA, or through mechanical breakage of a chromosome bridge structure. Micronuclei have also been observed forming in interphase – through budding or blebbing of the nuclear membrane at breaks in the nuclear lamina (Utani *et al.*, 2011).

Despite their isolation from the primary daughter nuclei, these chromosome fragments or whole chromosomes are enclosed by nuclear membrane, with nearly 100% of micronuclei showing compartmentalisation upon mitotic exit in HeLa and U2OS cells (Hatch *et al.*, 2013). Micronuclei can form functional nuclear units, with a nuclear lamina, nuclear pore complexes and competent DNA replication and repair mechanisms. However, those micronuclei which do not develop a complete, functioning nuclear envelope, including a lamina and nuclear pore complexes, are incapable of being transcribed, replicated, or participating in mitosis. It has been proposed that micronuclei which lack a competent lamina are formed from nuclear budding and chromosome bridge breakage events (Utani *et al.*, 2010).

The fate of micronuclei is not clearly understood; however, it is known that micronuclei, particularly whole chromosomes, can be re-incorporated back into the primary nucleus. Otherwise, the chromatin contained in micronuclei can be lost, potentially through extrusion from the cell into the extracellular environment (Shimizu *et al.*, 2000) or degradation within the cell cytoplasm (Terradas *et al.*, 2010; Figure 5.1b).

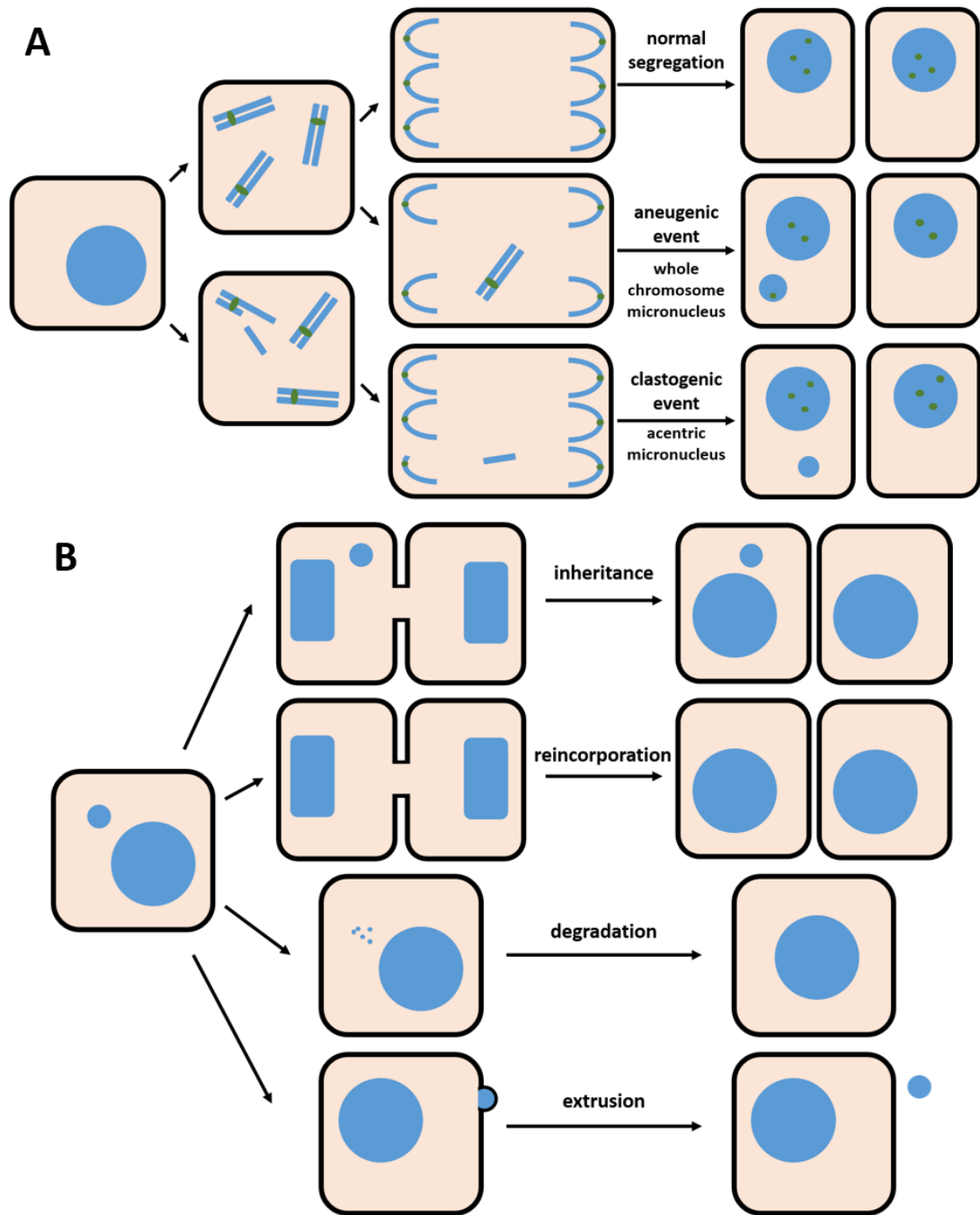


Figure 5.1. Generation and fate of micronuclei

a) Diagram showing formation of whole chromosome and acentric micronuclei, compared to normal chromosome segregation. **b)** Possible fates of micronuclei, showing micronuclear elimination by extrusion or degradation, proper segregation in a subsequent mitosis or inheritance by a daughter cell.

Chromothripsis refers to a genomic rearrangement event in which specific chromosomes or chromosome regions undergo potentially thousands of breakage and fusion events, resulting in extensive rearrangement of genetic material confined to a particular chromosome or region. This phenomenon is associated with development of cancer due to the swift accumulation of mutations, generation of oncogenic fusions or loss of tumour suppressors, all of which are known to drive cancer development (Forment *et al.*, 2012). Zhang *et al.* (2015) showed that isolation of chromosomes into micronuclei, combined with micronuclear rupture provide the ideal conditions for chromothripsis to occur. Chromosomes are isolated and lack the normal mechanisms of genome protection and repair, and can be subsequently reincorporated into the primary nucleus in a later mitosis, introducing many new mutations or rearrangements into the genome.

5.1.3 Generation and resolution of chromosome bridges

Defects in chromosome segregation in mitosis can result in lagging chromosomes and chromosome bridges. Such defects are estimated to occur in approximately 1% of somatic cell divisions (Cimini *et al.*, 2003), and can interfere with completion of cytokinesis due to the presence of chromatin in the division plane. In order to maintain genomic stability and correct segregation of DNA between the two daughter cells, and avoid breakage of the chromosome through abscission, the NoCut checkpoint exists which stalls the progression of abscission until chromatin is removed from the cleavage plane (Mendoza *et al.*, 2009; Section 1.3.5). Lagging chromosomes have been shown not to activate the NoCut checkpoint (Janssen *et al.*, 2011). This checkpoint has been shown to require the ESCRT-III protein CHMP4C (Carlton *et al.*, 2012).

Chromosome bridges can arise through several mechanisms. Dicentric chromosomes form from the end-to-end fusion of two chromosomes, resulting in a structure which has two centromeres and therefore cannot separate properly in anaphase (Figure 5.2a). Incomplete

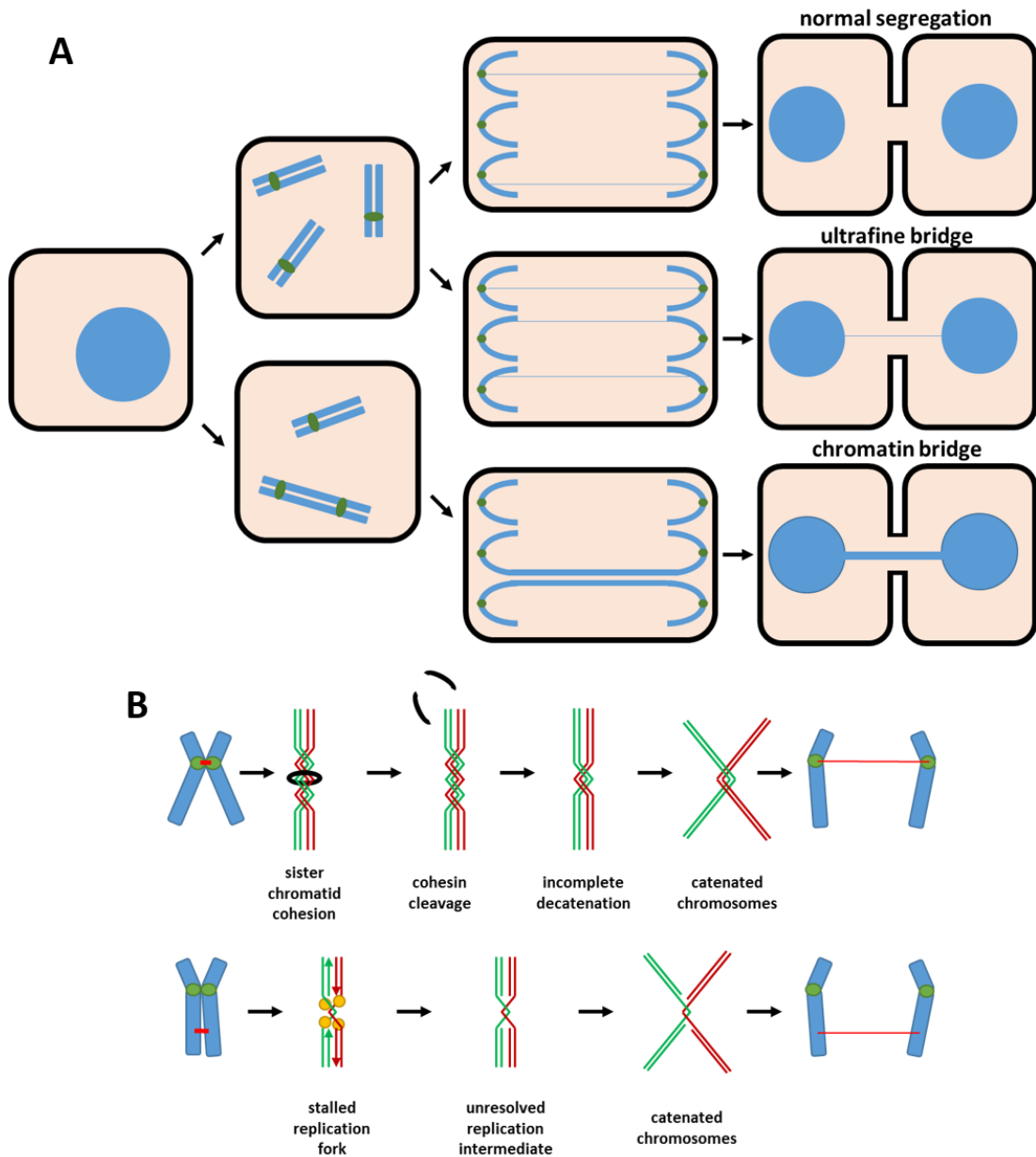


Figure 5.2. Generation and resolution of chromosome bridges

a) Diagram showing sources of chromosome bridge formation, including chromosome fusion events and inter-chromatid bridges derived from catenation. **b)** Representation of chromatid catenation events due to sister chromatid centromeric attachment or unresolved replication intermediates.

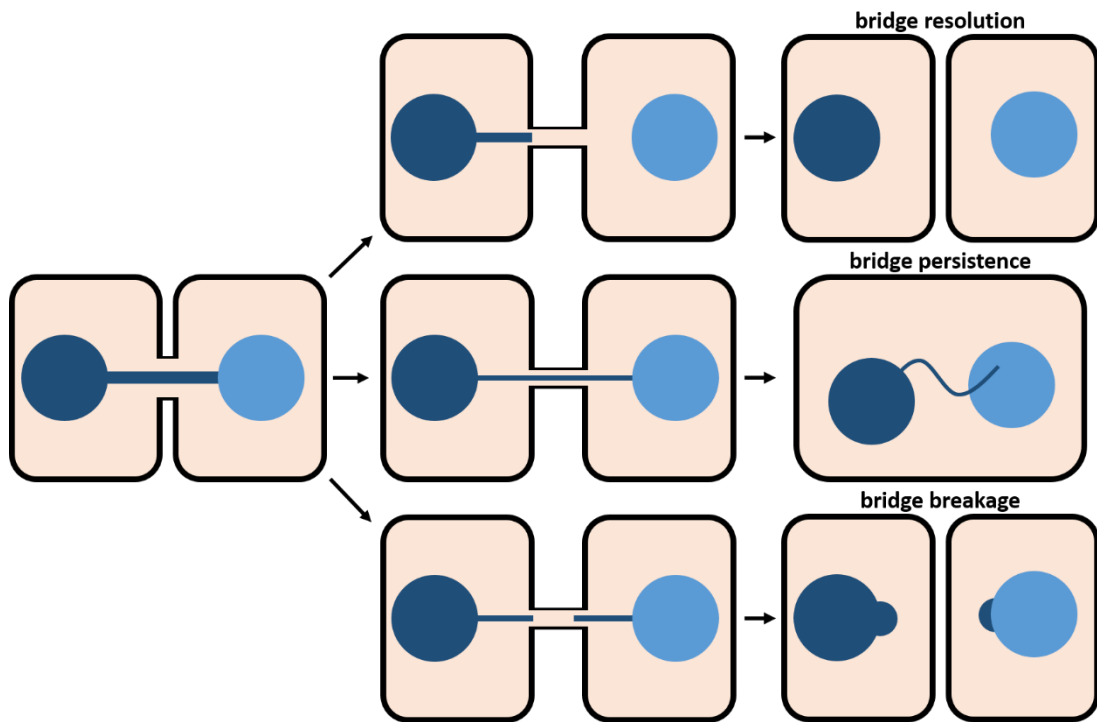


Figure 5.2. (continued)

c) Diagram showing possible outcomes for chromosome bridge resolution, demonstrating bridge breakage causing improper segregation of chromatin, bridge persistence and cytokinesis failure, and the hypothesised “correct” resolution of bridges resulting in proper chromosome segregation.

DNA replication, or unresolved replication intermediates, result in inter-chromatid bridges which can persist throughout mitosis (Chan *et al.*, 2009). Bridging between centromeres is a common phenomenon, caused by incomplete decatenation of centromeric DNA which contributes to sister chromatid cohesion prior to anaphase (Rouzeau *et al.*, 2012; Figure 5.2b).

Chromosome bridges caused by 'tangling' of DNA, as opposed to chromosome fusion, form ultrafine DNA bridges in anaphase, which are defined by their inability to be stained by DAPI or other intercalating DNA dyes. These bridges frequently stain for the BLM and PICH helicases, which work with topoisomerase to untangle the DNA in order to resolve and properly segregate the nuclear material (Biebricher *et al.*, 2013). BLM and PICH also function to prevent the condensation of DNA through preventing incorporation of histones into the bridges, maintaining the DNA in an open flexible state to prevent breakage and promote resolution (Ke *et al.*, 2011) However, unresolved chromosome bridges persist through mitosis up to the point of cytokinesis, where they can activate the NoCut checkpoint and form a stable intercellular bridge structure. Interestingly, in yeast cells, bridges derived from replication stress, failed decatenation or condensation results in Aurora-B mediated cytokinesis delay, however dicentric chromosome-related bridges resulted in no delay (Amaral *et al.*, 2016).

Persistent chromosome bridges can be resolved in a number of ways (Figure 5.2c) Firstly, the bridge can theoretically be resolved successfully, resulting in the reincorporation of bridge DNA into the appropriate daughter nucleus, although the mechanism for persistent chromosome bridge resolution is not known. The bridges can be snapped under mechanical tension. Secondly, despite abscission delay lasting many hours, the chromosome bridge causes aborted cytokinesis and regression of the cleavage furrow, forming a multinucleated cell (Shi and King, 2005). Thirdly, the chromosome bridge can be broken, or snaps as a

consequence of mechanical tension, in order to clear the cleavage plane to allow abscission to continue as normal. However, genomic integrity is compromised by improper segregation and the formation of broken chromosome ends which follows bridge breakage. This can initiate a breakage-fusion-bridge cycle, whereby broken chromosomes inappropriately re-fuse and break again in subsequent mitoses, causing large deleterious chromosome rearrangements and gene amplifications (Fenech *et al.*, 2011). Broken chromosome bridges can produce chromosome fragments which may subsequently form micronuclei.

5.2 - Results

5.2.1 CHMP7 localises to micronuclei in untreated cells

CHMP7 has previously been observed to localise to micronuclei in VPS4-depleted cells (Cleasby, PhD thesis, 2013). CHMP7 nuclear foci, characterised in Chapter 4 of this thesis, are only visible upon VPS4 knockdown, therefore the next step was to determine whether CHMP7 micronuclear staining is also found in control cells.

Micronuclei in HeLa, HeLa M and U2OS cell populations were scored for the presence or absence of CHMP7 in NT-control and VPS4 knockdown conditions. The pattern of CHMP7 localisation varies from the presence of one or multiple discrete foci, to a bright pan-micronuclear staining (Figure 5.3a). CHMP7 was observed at a similar rate on control micronuclei across cell lines, with 26.5% HeLa, 28.0% HeLa M and 25.7% U2OS micronuclei CHMP7-positive. In VPS4-depleted cells, this rose to 59.7% and 59.1% in HeLa and U2OS cells, and 66.2% in HeLa M cells (Figure 5.3b). This demonstrates that the presence of CHMP7 at micronuclei is a common phenomenon in these cancer cell lines, though its occurrence is increased by the depletion of VPS4.

5.2.2 ESCRT-III subunits localise to micronuclei only when CHMP7 is present

Since the depletion of VPS4 resulted in increased accumulation of CHMP7 at micronuclei, it was hypothesised that the ESCRT-III complex may be present in micronuclei. In order to determine whether other members of the ESCRT-III complex are present in micronuclei with CHMP7, HeLa cells stained for CHMP7 were counterstained for either endogenous CHMP4B or CHMP1B (Figure 5.4a and Figure 5.4b). CHMP4B and CHMP1B were observed to colocalise with CHMP7 at micronuclei in control cells, with 24.2% and 15.5% of micronuclei showing staining of the respective CHMPs, compared to 26.7% which were positive for CHMP7 (Figure 5.4c). Upon VPS4 depletion, the presence of CHMP4B and CHMP1B in micronuclei also

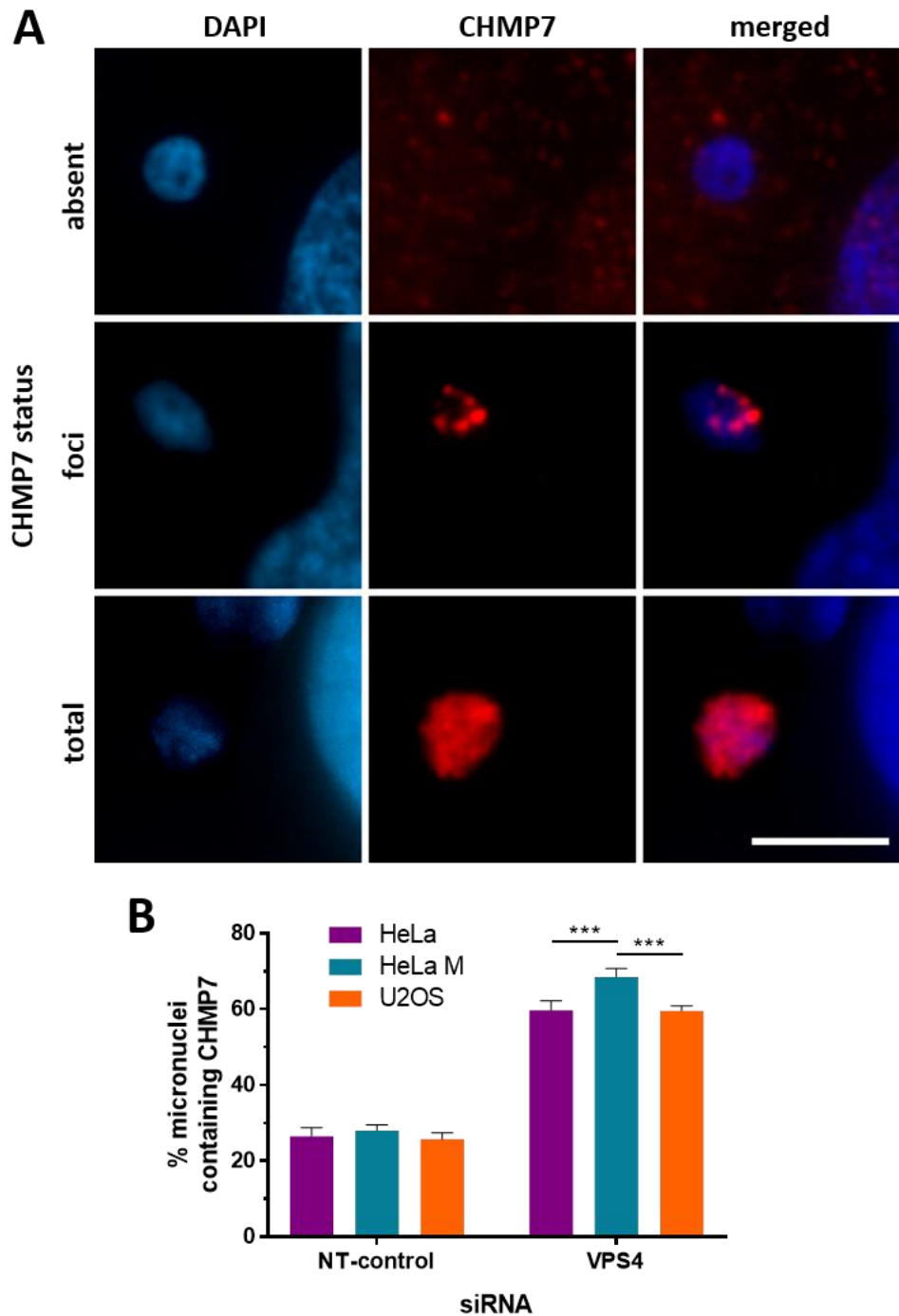


Figure 5.3. CHMP7 localises to micronuclei in various cell lines in control and VPS4-depleted cells

a) Untreated HeLa cells were stained using a standard immunofluorescence protocol, using a mouse-anti-CHMP7 antibody. Micronuclei in which CHMP7 is entirely absent, present in the form of multiple foci or localise across the whole micronucleus are shown. Scale bar represents 5 μ m. **b)** Three different human cell lines were transfected with scramble or VPS4-directed siRNA for 48h, and stained with mouse-derived anti-CHMP7 antibody. Micronuclei were scored for presence or absence of CHMP7. A minimum of 400 micronuclei were scored per condition. Averages and standard error of three independent repeats are shown. Results were analysed using a two-way ANOVA with Tukey's *post hoc* test.

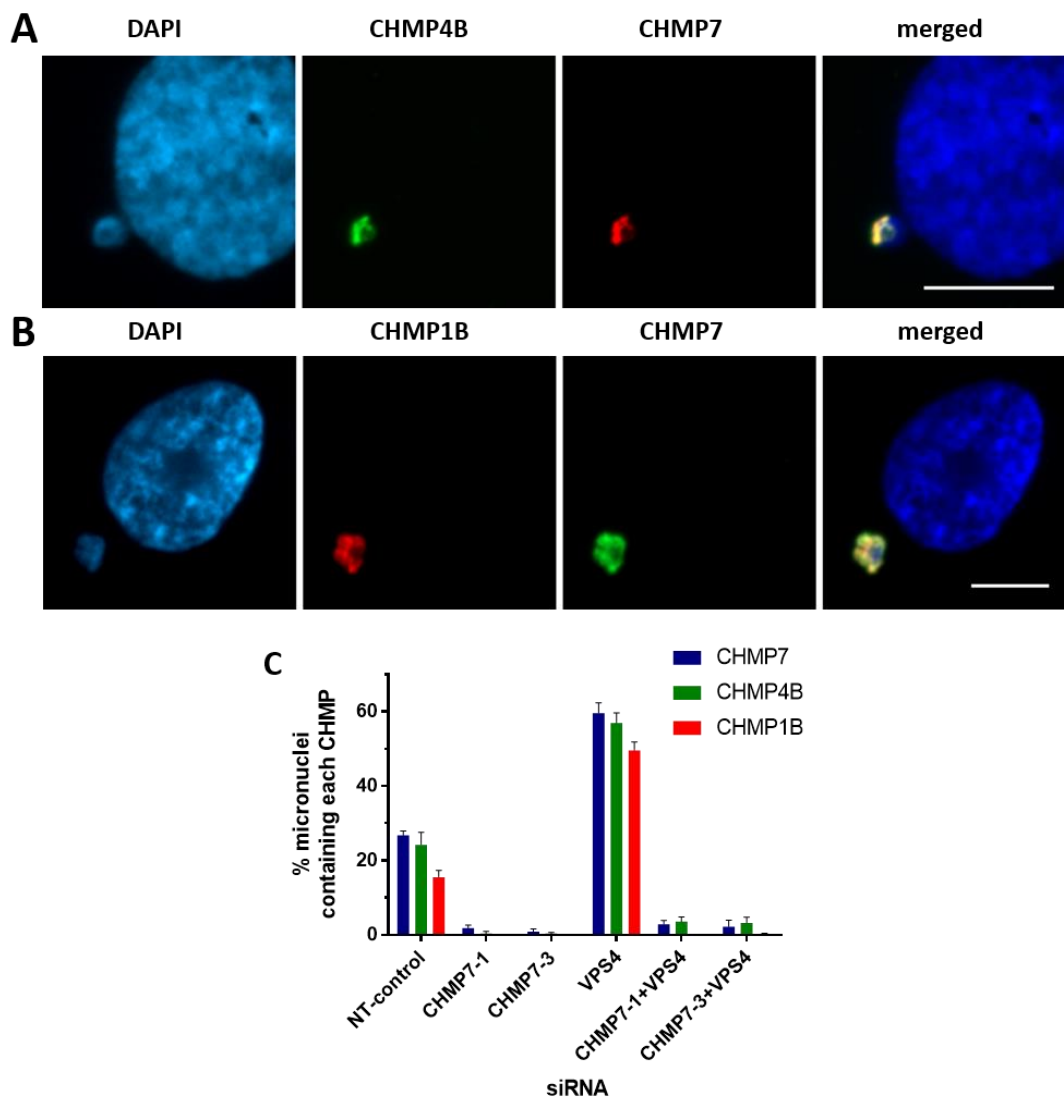


Figure 5.4. ESCRT-III localises to micronuclei in the presence of CHMP7

a) Untreated HeLa cells were stained to show CHMP7 and CHMP4B, and a micronucleus showing localisation of both proteins is shown. **b)** Untreated HeLa cells were stained to show CHMP7 and CHMP1B, and a micronucleus showing localisation of both proteins is shown. Scale bars represent 10 μ m. **c)** HeLa cells were transfected with siRNA for 48 hours and stained using an immunofluorescence protocol for either CHMP7, CHMP4B, or CHMP1B alongside DAPI staining. Quantification of the percentage of micronuclei displaying CHMP staining was performed for each treatment (minimum 200 micronuclei per condition). Averages and standard error of three independent repeats are shown. Results were analysed using a two-way ANOVA with Dunnett's *post hoc* test, with all knockdowns for each of CHMP7, CHMP4B and CHMP1B significantly different to the NT-control at $p < 0.0001$.

increased in line with the increase in CHMP7 staining. Depletion of CHMP7, both alone and in combination with VPS4, resulted in the loss of CHMP4B and CHMP1B accumulation at micronuclei.

This effect of reduced ESCRT-III localisation to micronuclei in CHMP7-depleted cells reflects the pattern observed for the same ESCRT-III subunits at nuclei foci in primary nuclei thus suggesting that the order of recruitment of ESCRT-III was maintained in the micronuclei structures, and that these accumulations represented a functional ESCRT-III complex. Furthermore, these data demonstrate that CHMP7 is necessary to recruit CHMP4B and CHMP1B to micronuclei, mirroring the previous finding that CHMP7 is necessary for localisation of other members of the ESCRT-III complex to localise to the foci in the primary nucleus.

5.2.3 CHMP7 localises more frequently to smaller micronuclei containing chromosome fragments

Micronuclei can arise through either aneugenic or a clastogenic events – arising from either a whole chromosome mis-segregation, or from a fragment resulting from chromosome breakage (Norppa and Falck, 2003). To determine the class of micronuclei to which CHMP7 is localising, micronuclei were classified as containing whole or partial chromosomes using a centromeric stain, the human anti-CREST antibody. CREST-positive micronuclei contain at least one centromere, and therefore are likely to represent whole mis-segregated chromosomes, in comparison to acentric fragment-based micronuclei, which appear CREST-negative (Norppa and Falck, 2003; Figure 5.5a)

Investigating the relationship between CHMP7 and each type of micronucleus was carried out by co-staining NT-control and VPS4 knockdown HeLa cells to show both CHMP7 and CREST. The proportion of CHMP7-positive micronuclei which contain whole chromosomes is

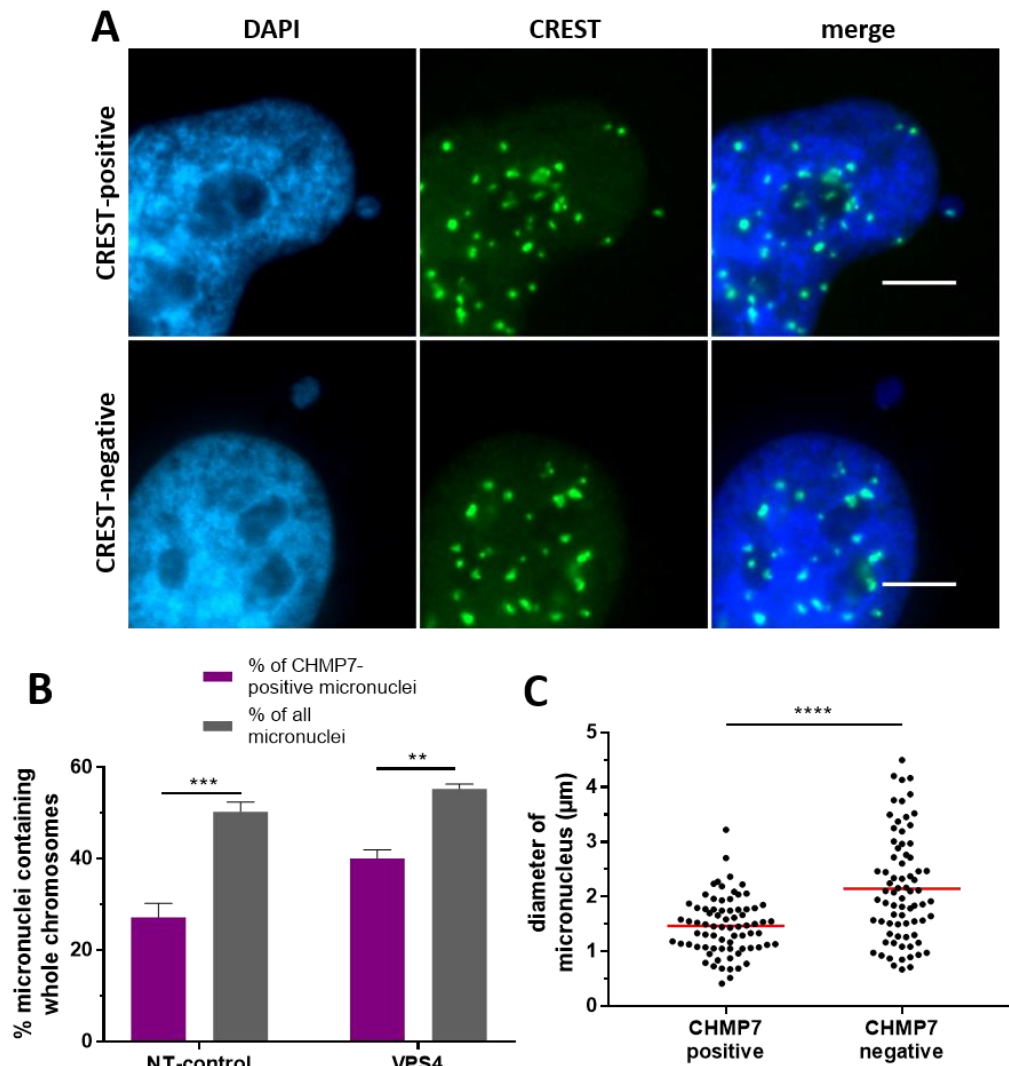


Figure 5.5. CHMP7 localises more frequently to smaller micronuclei containing chromosome fragments

HeLa cells were transfected with siRNA for 48 hours and stained to show CREST, CHMP7 and DAPI. **a)** Examples of CREST-positive (whole chromosome) and CREST-negative (chromosome fragment) micronuclei in control HeLa cells. Scale bars represent 3μm. Scale bars represent 5μm. **b)** HeLa cells transfected with either scramble control or VPS4 siRNA for 48h hours were to show CREST, CHMP7 and DAPI. Micronuclei were scored on the microscope for presence or absence of at least one definite CREST foci which resembles those found in the primary nucleus and CHMP7 (minimum 200 micronuclei per treatment). The percentage of whole chromosome (CREST-positive) micronuclei are shown for each category. Averages and standard error of three independent repeats are shown. Results were analysed using a two-way ANOVA with Sidak's *post hoc* test. **c)** Untreated HeLa cells were stained using the immunofluorescence protocol with mouse-derived CHMP7 antibody and DAPI. Images were taken, and the diameter of micronuclei measured in ImageJ (75 CHMP7-positive and 75 CHMP7-negative micronuclei were measured). Averages and individual measurements are shown. Results were analysed using an unpaired, two-tailed *t*-test.

compared to the proportion of all micronuclei in which this is the case in Figure 5.5b. In all micronuclei in control cells, 50.3% of micronuclei consisted of whole chromosomes, however this is reduced to 27.2% when only CHMP7-positive micronuclei are scored. This shows that the majority of CHMP7-positive micronuclei (72.8%) are acentric fragments of chromosomes. In the VPS4 knockdown, slightly more micronuclei are whole chromosomes (55.3%) and 40.1% of CHMP7-positive micronuclei were CREST-positive, possibly reflecting the increased number of micronuclei which are CHMP7-positive following VPS4 depletion (Figure 5.3b).

The diameter of CHMP7 positive and negative micronuclei was measured in order to estimate the DNA content of the structures. CHMP7-positive micronuclei average $0.41 \pm 0.06 \mu\text{m}$ in diameter, which makes them significantly smaller than CHMP7-negative micronuclei, which have an average diameter of $0.67 \pm 0.11 \mu\text{m}$ (Figure 5.5c). While this is a good indicator of the DNA content of micronuclei, it may be confounded by the levels of chromatin compaction in the micronuclei, suggesting that chromatin condensation is increased in CHMP7-positive micronuclei. Nonetheless, taken together with the scoring of CREST staining these data further support the occurrence of CHMP7 and ESCRT-III at acentric micronuclei

5.2.4 CHMP7 localises to micronuclei lacking a continuous nuclear lamina

A key component of the structural integrity of micronuclei is the lamina, as in the primary nucleus. It has been shown (Hatch *et al.*, 2013) that micronuclei vary in their stability based on the lamin content of the micronuclear envelope. Micronuclei commonly lack a nuclear lamina due to their origin or inability to transport lamin proteins into the structure, with lamina-negative micronuclei rendered incompetent for functions such as DNA replication (Utani *et al.*, 2011).

Micronuclei were categorised based on the status of the nuclear lamina as indicated by Lamin B staining (Figure 5.6b). Micronuclei were classified as those in which lamina is entirely

absent, those in which is present but there are gaps or discontinuities, and those which display a continuous lamina. CHMP7-positive micronuclei in HeLa cells treated with either NT-control or VPS4 siRNA were scored for Lamin B. In control cells, few (5.9%) CHMP7-positive micronuclei have an apparently intact lamina (Figure 5.6c), with the majority of CHMP7-positive micronuclei displaying a broken or absent lamina, with 46.3% of control and 47.0% VPS4 knockdown CHMP7-containing micronuclei lacking Lamin B entirely. Interestingly, CHMP7 and Lamin B, when present in the same micronucleus, do not appear to colocalise, with CHMP7 staining present in gaps or areas of weaker Lamin B staining (Figure 5.6d). These data again reflect an association of CHMP7 with nuclear envelope with compromised integrity of the nuclear lamina, as is observed in both mitotic and interphase primary nuclei (Chapter 4).

5.2.5 CHMP7 localises to micronuclei lacking nuclear pore complexes

Micronuclei often contain a lower density of nuclear pore complexes compared to the nuclear envelope of the primary nucleus, leading to defects in nuclear import and subsequent functions reliant on imported proteins (Crasta *et al.*, 2012). In order to see if CHMP7-positive micronuclei also lack a normal complement of nuclear pore complex structures, micronuclei were classified based on the status of the density of nuclear pore complexes as measured by the appearance of the anti-mab414 antibody staining. One class of micronuclei entirely lack nuclear pore complexes (absent), another refers to those with a reduced density of NPCs compared to the primary nucleus (reduced) and the third to micronuclei displaying a density comparable to the primary nucleus (normal; Figure 5.7b). Micronuclei in HeLa cells treated with either NT-control or VPS4 siRNA were scored for presence or absence of CHMP7. In control cells, CHMP7 was observed in 63.2% of NPC-absent micronuclei, 46.0% of NPC-reduced micronuclei, and was almost entirely absent from NPC-normal micronuclei (1.9%; Figure 5.7c). This demonstrates a strong preference for

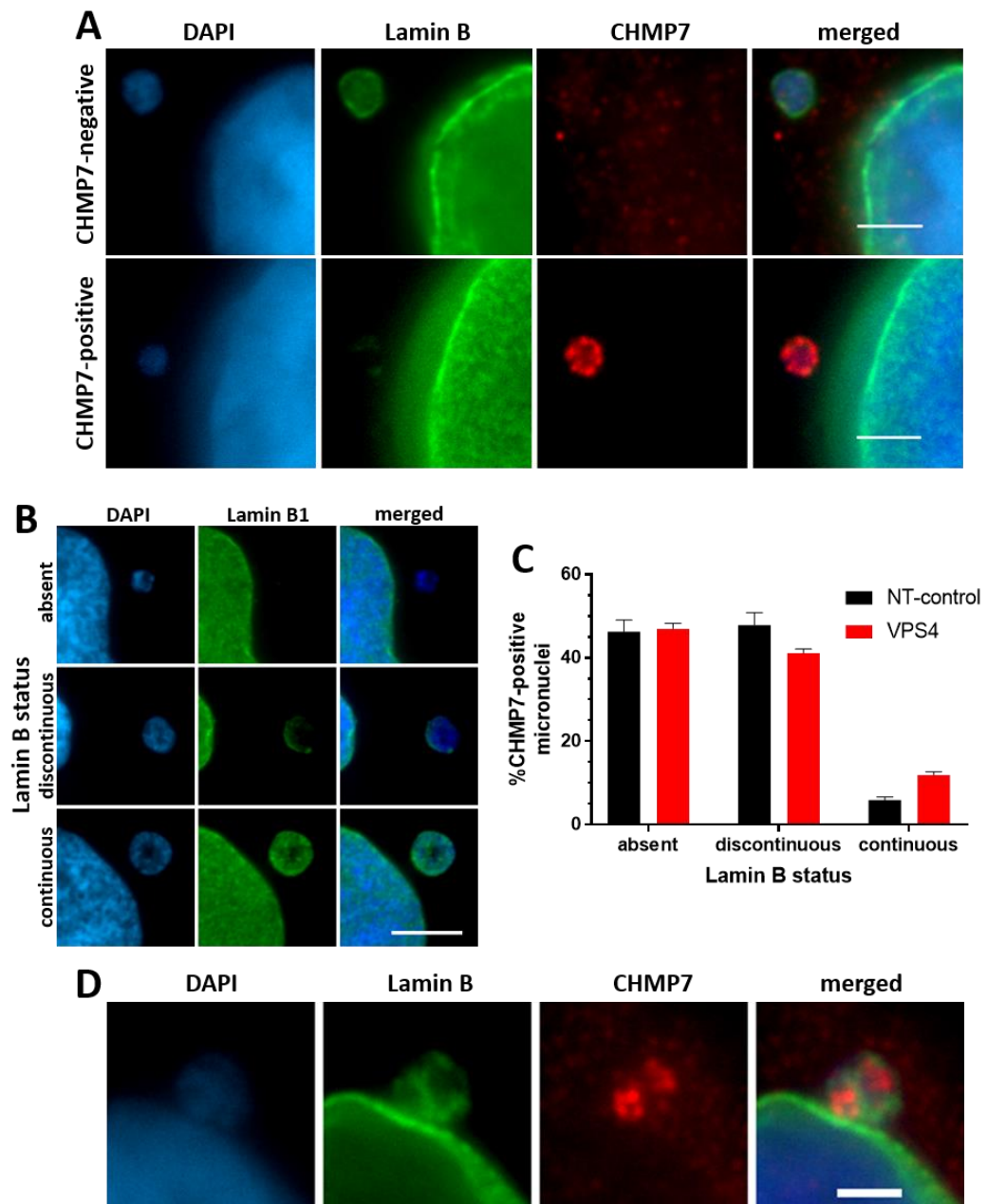


Figure 5.6. CHMP7 preferentially localises to micronuclei lacking an intact nuclear lamina

HeLa cells were transfected with siRNA for 48 hours and stained to show Lamin B, CHMP7 and DAPI. **a)** Examples of CHMP7-positive and negative micronuclei with Lamin B staining in control HeLa cells. Scale bars represent 3 μ m. **b)** Examples of micronuclei in which the nuclear lamina is intact (continuous), broken (discontinuous) or entirely absent. Scale bar represents 5 μ m. **c)** HeLa cells were transfected with siRNA for 48 hours and stained to show Lamin B, CHMP7 and DAPI. Micronuclei were scored on the microscope for presence or absence of Lamin B and CHMP7 staining within the same micronucleus (minimum 200 micronuclei scored per treatment). The percentage of CHMP7-positive micronuclei in each category are shown. Averages and standard error of three independent repeats are shown. **d)** A micronucleus in a cell treated with NT-control siRNA for 48 hours stained for Lamin B and CHMP7. CHMP7 localises strongly to those regions of the micronucleus with decreased Lamin B presence. Scale bar represents 3 μ m.

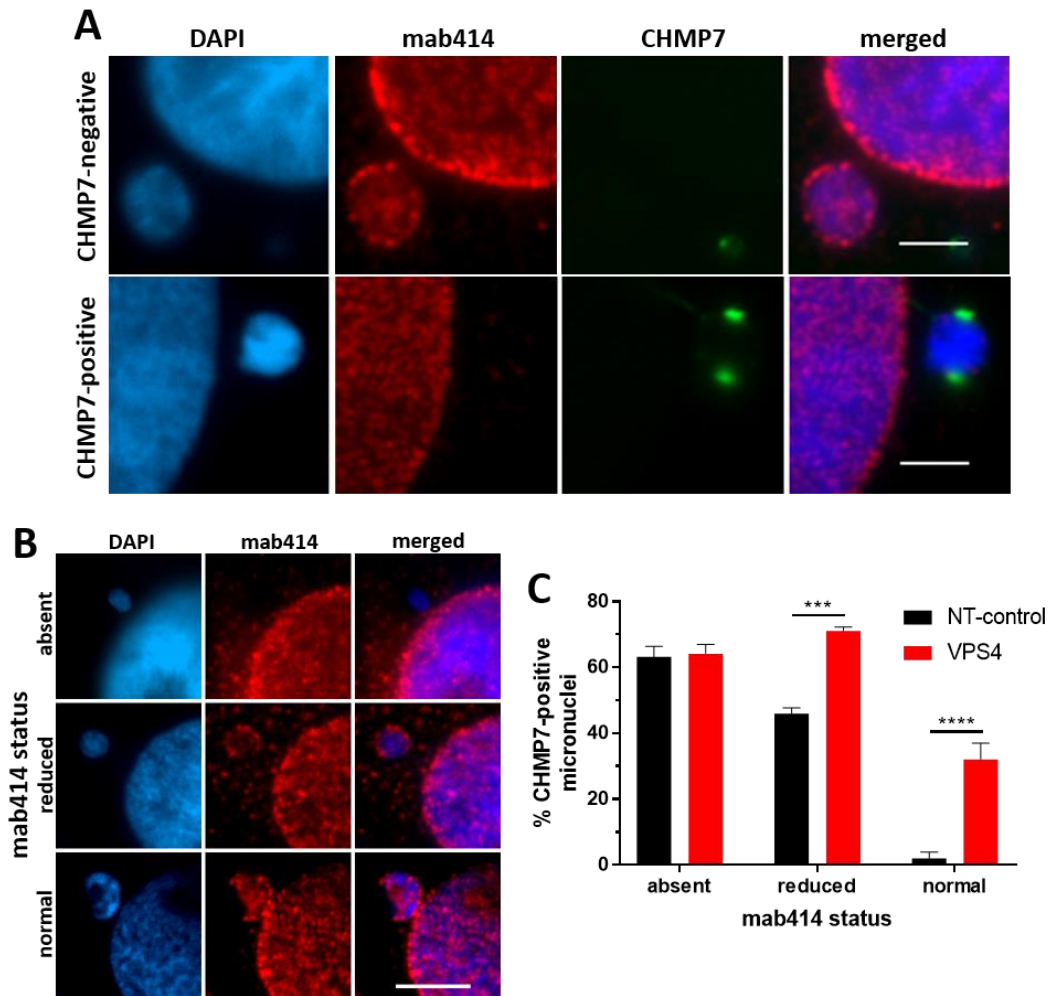


Figure 5.7. CHMP7 preferentially localises to micronuclei lacking nuclear pore complexes

HeLa cells were transfected with siRNA for 48 hours and stained to show mab414, CHMP7 and DAPI. **a)** Examples of CHMP7-positive and negative micronuclei with mab414 staining in control HeLa cells. Scale bars represent 3 μ m. **b)** Examples of micronuclei in which the NPCs are present at normal levels, at reduced levels or are entirely absent. Scale bar represents 5 μ m. **c)** HeLa cells were transfected with siRNA for 48 hours and stained to show mab414, CHMP7 and DAPI. Micronuclei were scored on the microscope for presence or absence of mab414 and CHMP7 staining within the same micronucleus (minimum 200 cells per treatment). The percentage of CHMP7-positive micronuclei in each category are shown. Averages and standard error of three independent repeats are shown. Results were analysed using a two-way ANOVA with Sidak's *post hoc* test.

CHMP7 accumulation at NPC-defective micronuclei, which is in agreement with the presence of ESCRT-III to nuclear envelope structures lacking in structural organisation and integrity.

5.2.6 CHMP7-positive micronuclei show loss of compartmentalisation

In order to see whether the integrity of the nuclear membrane was compromised along with the defects in NE composition, soluble nuclear protein PARP1 was used. Hatch *et al.* (2013) determine that loss of endogenous nuclear proteins is a reliable indicator of micronuclear disruption. Poly(ADP-ribose) polymerase-1 (PARP1) is an abundant soluble nuclear protein (Murai *et al.*, 2012), an enzyme which plays a key role in the repair of double and single-stranded breaks in DNA. In intact, functional micronuclei, PARP1 is present and therefore will be used as a representative soluble protein to characterise the loss of micronuclear compartmentalisation (Figure 5.8b).

Micronuclei in HeLa cells treated with either NT-control or VPS4 siRNA were scored for presence or absence of both PARP1 and CHMP7 within the same micronucleus (Figure 5.8d). In control cells, no PARP1-positive (intact) micronuclei, showed association with CHMP7, however a small number (2.7%) of intact micronuclei in VPS4 knockdown cells were positive for CHMP7. Of the PARP1-negative micronuclei population, 58.0% displayed association with CHMP7, with this rising to 75.3% in VPS4-depleted cells. This shows that all CHMP7-positive micronuclei in control cells have lost compartmentalisation, and that a high proportion of disrupted micronuclei display CHMP7 localisation.

5.2.7 Invasion of ER membrane into CHMP7-positive micronuclei

Hatch *et al.* (2013) describe a process by which micronuclei can undergo irreversible “collapse”, involving loss of compartmentalisation and invasion of ER membrane tubules into the micronuclear chromatin. Micronuclear envelope collapse is associated with subsequent DNA damage and genomic instability, and is induced by nuclear lamina defects and weakness. In order to see if CHMP7-positive micronuclei are collapsed and display invasion

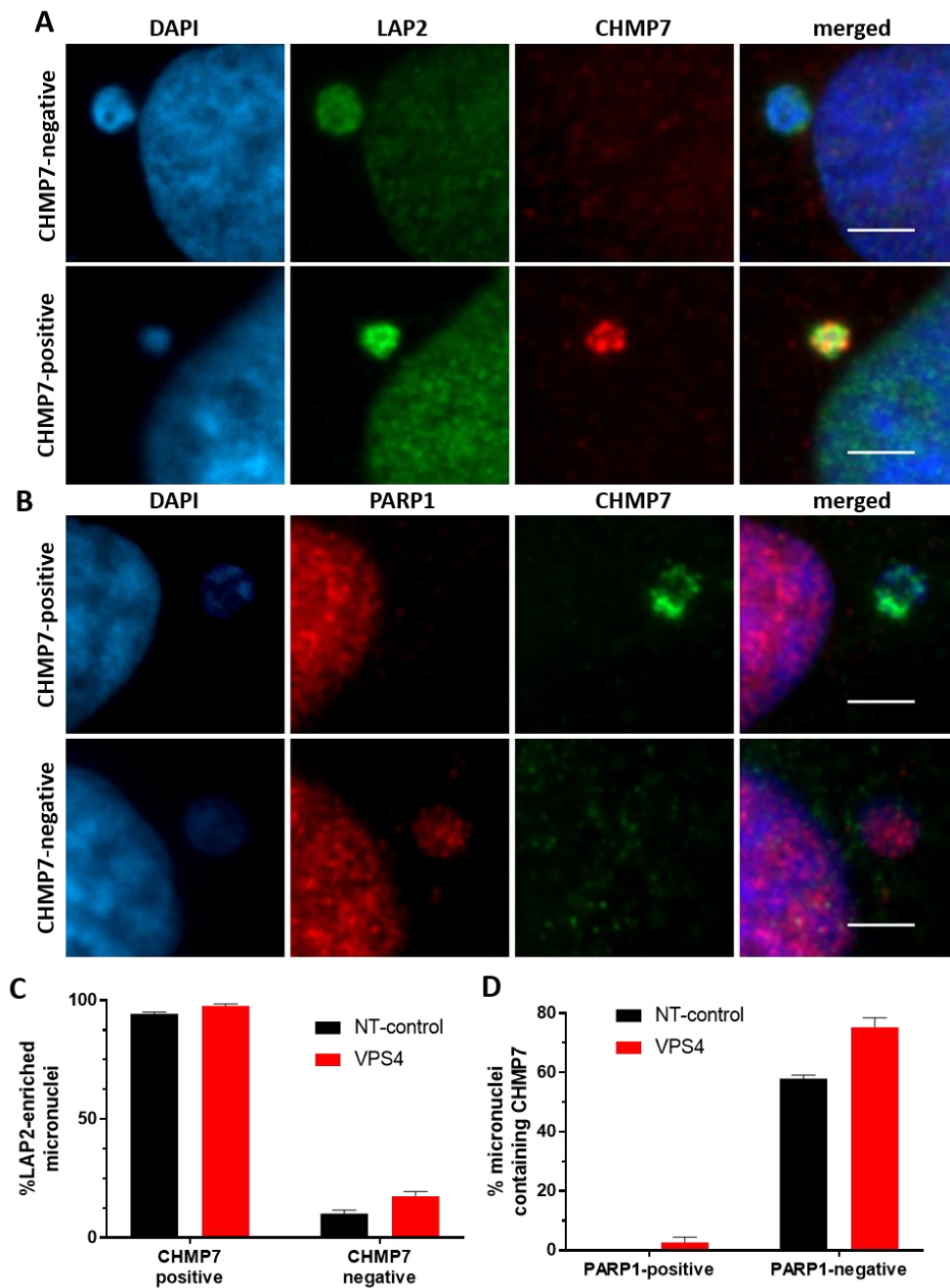


Figure 5.8. CHMP7-positive micronuclei retain LAP2 staining, but show loss of soluble nuclear protein

a) Examples of CHMP7-positive and negative micronuclei with LAP2 staining in untreated HeLa cells. Scale bars represent 3 μ m. **b)** Examples of CHMP7-positive and negative micronuclei with PARP1 staining in untreated HeLa cells. Scale bars represent 3 μ m. **c)** HeLa cells were transfected with siRNA for 48 hours and stained to show LAP2, CHMP7 and DAPI. CHMP7-positive and CHMP7-negative micronuclei (300 micronuclei were scored in each category) were scored for the presence of LAP2 enrichment on the structure. The percentage of LAP2-enriched micronuclei in each category are shown. **d)** HeLa cells were transfected with siRNA for 48 hours and stained to show PARP1, CHMP7 and DAPI. Micronuclei were scored on the microscope for presence or absence of PARP1 and CHMP7 staining within the same micronucleus (minimum 200 cells per treatment). The percentage of CHMP7-positive micronuclei in each category are shown. Averages and standard error of three independent repeats are shown.

of ER tubules, HeLa cells were stained with anti-PDI antibody to co-visualise the ER with CHMP7 and DAPI. Micronuclei showed two distinct phenotypes (Figure 5.9a), in which micronuclei displayed a normal membrane border similar to that around the primary nucleus (intact), or in which PDI staining was enriched on the micronuclear chromatin (invaded or collapsed micronuclei). These two populations of cells were scored for presence of CHMP7 in NT-control and VPS4-depleted cells (Figure 5.9b and Figure 5.9c) The majority (69.6% and 90.6% in control and VPS4-depleted cells respectively) of collapsed micronuclei show accumulation of CHMP7 on the chromatin. Very few (0.9%) of intact control micronuclei show association with CHMP7, however this rises to 15.0% in VPS4-depleted cells. Figure 5.9d shows a deconvolved image taken on the Deltavision microscope, which shows clearly the relationship between ER membranes and CHMP7 within a micronucleus. CHMP7 and PDI do not appear to directly colocalise, but the staining for ER membrane within the micronuclear structure is enriched compared to ER in the rest of the cell. These data show that a high proportion of CHMP7-positive micronuclei have a disrupted nuclear envelope, and are infiltrated with ER membrane.

The INM protein LAP2 was also observed in its role as a nuclear membrane protein (Figure 5.8a). All micronuclei display some LAP2 localisation, corresponding to the nuclear membrane. However, the intensity of LAP2 when compared to the primary nucleus was increased in CHMP7-positive micronuclei in both control and VSP4-depleted cells, with 94.3% (control) and 97.7% (VPS4 knockdown) of micronuclei showing enriched LAP2 staining that is more intense than that seen on the primary nucleus (Figure 5.8c). This may be related to the invasion of membrane into micronuclei, or to the potential compaction of the micronuclei which occurs upon their nuclear envelope collapse.

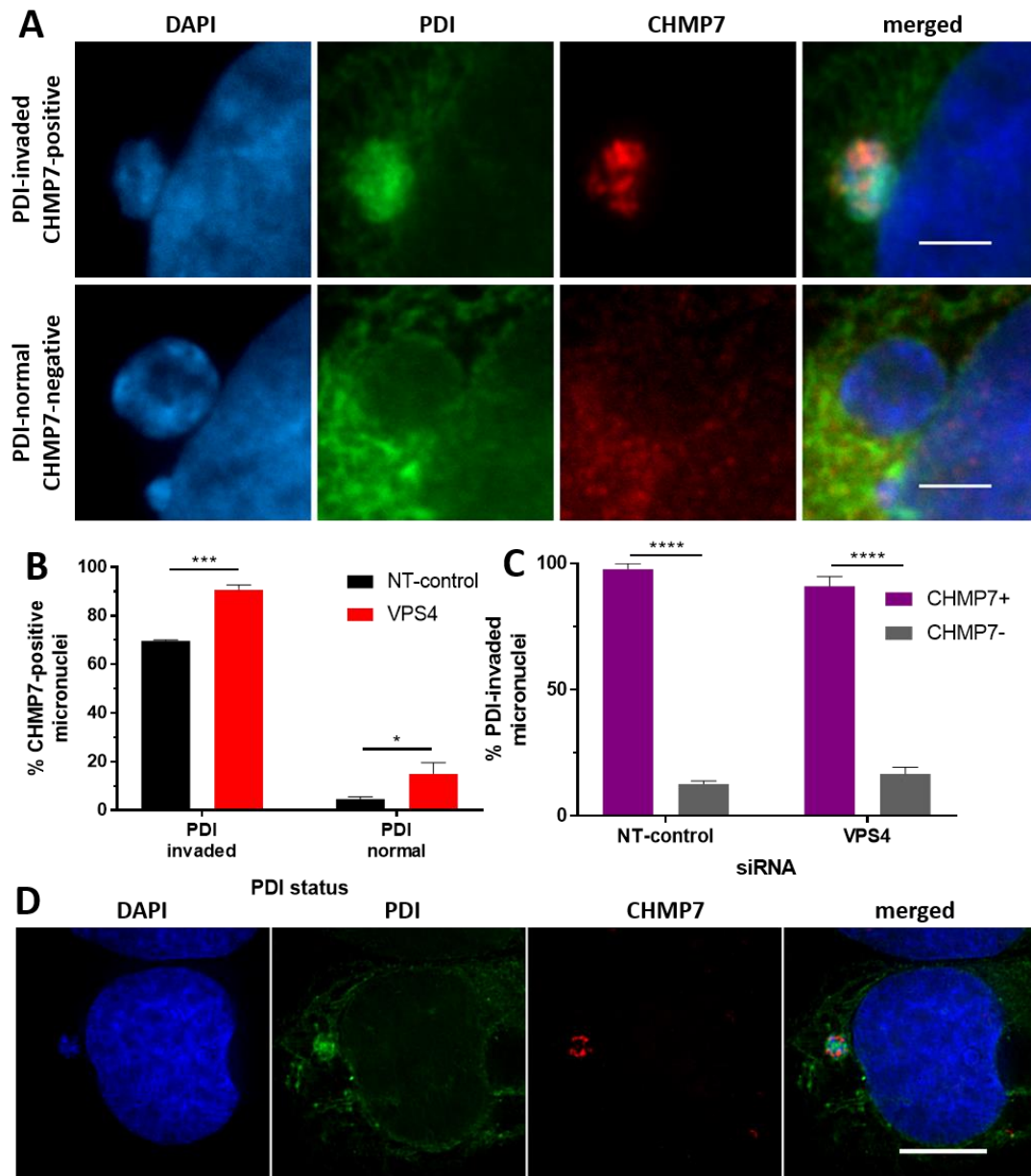


Figure 5.9. CHMP7-positive micronuclei show ER membrane invasion into chromatin

HeLa cells were transfected with siRNA for 48 hours and stained to show PDI, CHMP7 and DAPI. **a)** Examples of CHMP7-positive and negative micronuclei with PDI staining in control HeLa cells. Scale bars represent 3 μ m. PDI-negative cells have endoplasmic reticulum excluded from the micronuclear interior. PDI-positive cells have ER staining inside the micronuclear boundary, indicating micronuclei collapse. **b)** Micronuclei were scored on the microscope for presence or absence of PDI invasion and CHMP7 staining within the same micronucleus (minimum 200 micronuclei per treatment). The percentage of CHMP7-positive micronuclei in each category are shown. Averages and standard error of three independent repeats are shown. Results were analysed using a two-way ANOVA with Sidak's *post hoc* test. **c)** A control U2OS cell imaged and deconvolved using the Deltavision microscope. Scale bar represents 10 μ m.

5.2.8 CHMP7 depletion causes increased micronuclei generation

In order to further investigate the relationship between ESCRT-III proteins and micronuclei, the number of micronucleated cells produced upon knockdown of CHMP7 and VPS4 were examined. HeLa cells were stained with DAPI and an α -tubulin-targeting antibody to determine cell boundaries. The number of cells containing at least one micronucleus were scored across CHMP7 and VPS4 individual and double knockdown conditions (Figure 5.10a).

Under control conditions, 11.7% of cells contained at least one micronuclei. All of the observed CHMP7 and VPS4 knockdowns resulted in a highly significant increase in the percentage of cells which were micronucleated, between 25.8% and 30.4%, with no significant differences between the various knockdowns.

In addition, the number of micronuclei per micronucleated cell was scored (Figure 5.10b). The number of micronuclei generated by a cell gives an indication of the severity of genomic instability within the cell. In micronucleated NT-control cells, an average of 1.31 micronuclei were found. A small significant increase was observed in cells transfected with CHMP7-3 (1.57 micronuclei), CHMP7-1+VPS4 (1.57 micronuclei) and CHMP7-3+VPS4 (1.56 micronuclei) siRNA, demonstrating a consistent increase in micronuclei in all CHMP7 depletion conditions.

In order to observe the formation of micronuclei over time, the number of micronucleated cells were scored at 24, 48 and 72 hours post-transfection of siRNA (Figure 5.10c). In both CHMP7 and VPS4 knockdowns, the number of micronucleated cells rose significantly above control at all time points, with the greatest increase in micronuclei occurring between 24 and 48 hours post-transfection.

Taken together, these data show that the knockdowns of CHMP7 and VPS4 – regulators of the ESCRT-III machinery, cause increased micronucleation in HeLa cells.

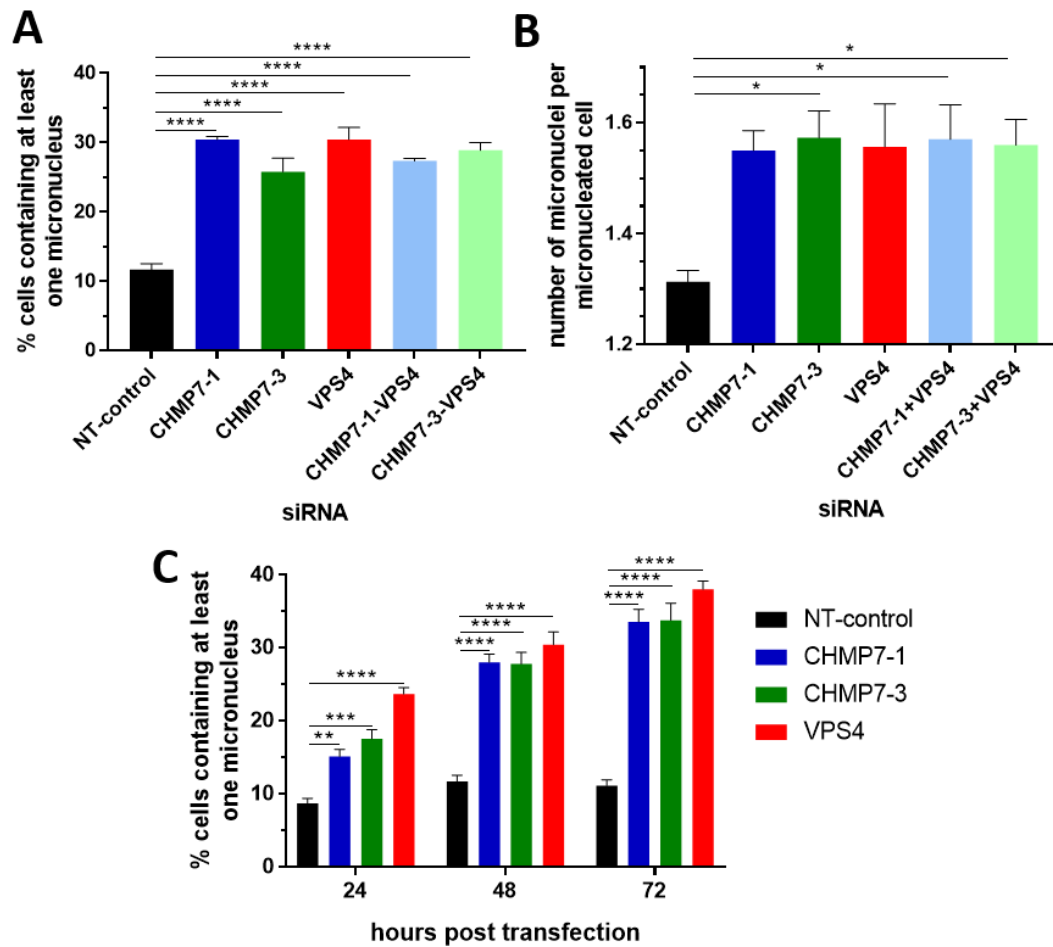


Figure 5.10. Impairment of ESCRT-III function increases micronucleation of HeLa cells

a) HeLa cells were transfected with siRNA for 48h, followed by DAPI staining. The percentage of cells with at least one micronuclei were quantified for each treatment (minimum 250 cells per sample). Also, **(b)** the average number of micronuclei observed per micronucleated cell were quantified (minimum 150 cells per sample). Results were analysed using a one-way ANOVA with Dunnett's *post hoc* test. **c)** HeLa cells were transfected with siRNA for either 24, 48 or 72h, and stained with DAPI. Quantification of the number of micronucleated cells was carried out across each of the treatments (minimum 200 cells were scored for each sample). Averages and standard error of three independent repeats are shown. Results were analysed using a two-way ANOVA with Dunnett's *post hoc* test.

5.2.9 CHMP7 knockdown generates more micronuclei containing chromosome fragments

In order to determine the nature of CHMP7-positive micronuclei HeLa cell micronuclei were scored on the microscope for presence or absence of at least one CREST-defined centromere, in order to identify whole or acentric chromosome structures (Figure 5.11a). In scramble control conditions, 50.3% of micronuclei are centromere-positive, indicating a whole chromosome content. The single CHMP7 knockdowns both show a small significant difference, with 43.1% and 42.0% of micronuclei positive for centromeres in CHMP7-1 and CHMP7-3 knockdowns respectively. Depletion of VPS4 in combination with either CHMP7 siRNA sequence showed a slight but insignificant decrease in whole chromosome-containing micronuclei compared to the control. Conversely, the VPS4 knockdown showed an increase to 55.3%, however this was not statistically significant compared to the control.

While this is not a strongly significant result, it demonstrates that slightly fewer micronuclei in CHMP7 knockdown cells are whole, mis-segregated chromosomes. This suggests they are derived more often from clastogenic events, such as those caused by the breakage of chromosome bridges or unrepaired double-stranded DNA breaks.

5.2.10 ESCRT-III impairment generates more lamina and NPC-defective micronuclei

In order to determine if the knockdown of CHMP7 and VPS4 has an effect on the composition of micronuclei, which may indicate the kind of micronuclei which are being generated as a result of these knockdowns, the nuclear lamina and NPC content were examined.

The nuclear lamina was assessed and scored using the criteria established in Figure 5.6b in cells stained to show Lamin B content of micronuclei. Micronuclei in CHMP7-depleted cells show a significant decrease in the micronuclei displaying continuous Lamin B staining, which indicates an intact nuclear lamina, and a corresponding significant increase in micronuclei

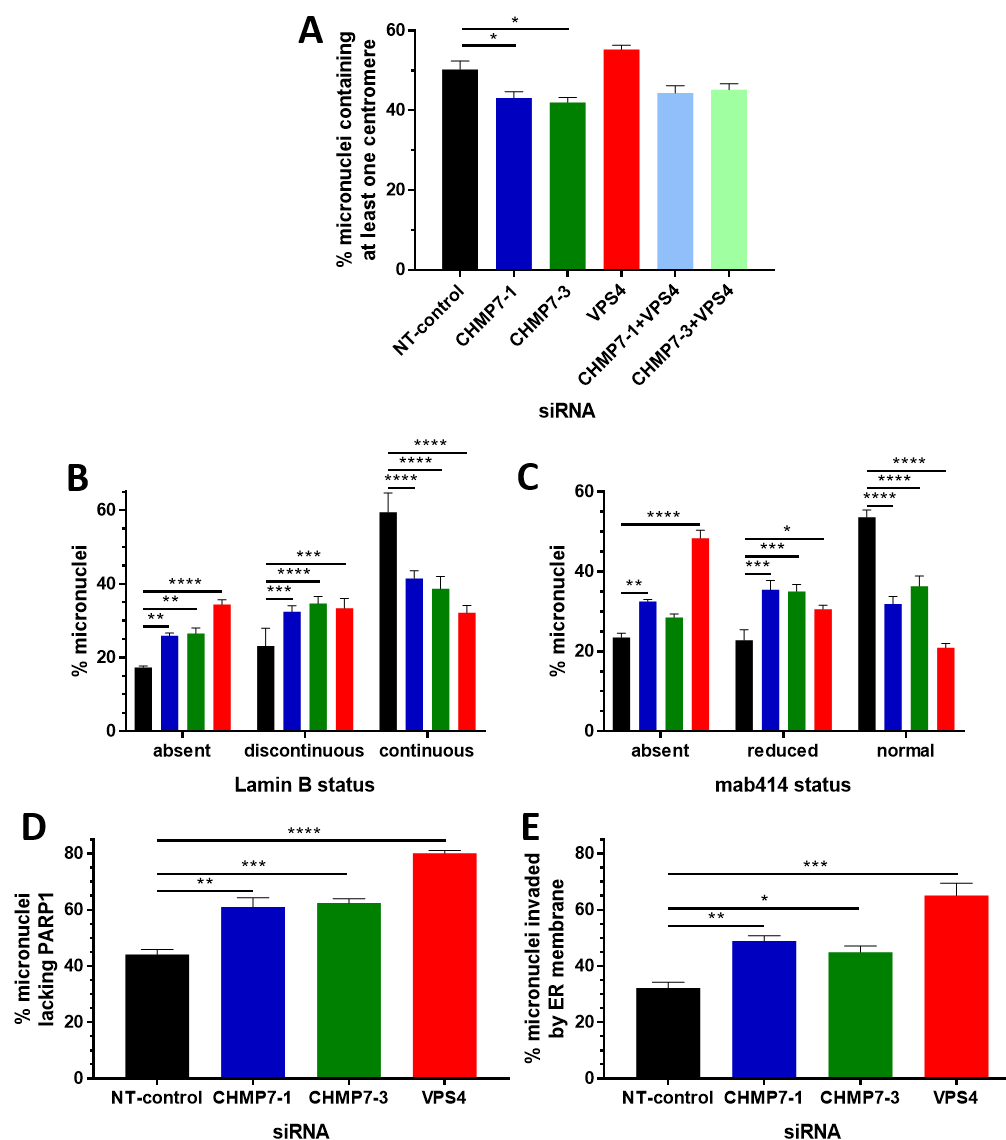


Figure 5.11. Impairment of ESCRT-III function decreases micronuclear integrity and increases loss of compartmentalisation

a) HeLa cells were transfected with siRNA for 48 hours and stained to show CREST and DAPI. Micronuclei were scored on the microscope for presence or absence of at least one CREST-positive centromere (minimum 200 micronuclei per treatment) and the percentage of whole chromosome micronuclei is shown. **b)** HeLa cells were transfected with siRNA for 48 hours and stained to show Lamin B and DAPI. Micronuclei were scored for the presence of Lamin B at the micronuclear envelope (minimum 100 micronuclei per treatment). The percentage of micronuclei in each Lamin B category (as defined in Figure 5.6b) are shown. **c)** HeLa cells were transfected with siRNA for 48 hours and stained to show mab414 and DAPI. Micronuclei were scored for the presence of mab414 at the micronuclear envelope (minimum 100 micronuclei per treatment). The percentage of micronuclei in each mab414 category (as defined in Figure 5.7b) are shown. **d)** Micronuclei in HeLa cells transfected for 48h with siRNA and stained for PARP1 and DAPI were scored for presence of PARP1 (minimum 100 micronuclei per treatment). **e)** Micronuclei in HeLa cells transfected for 48h with siRNA and stained for PDI and DAPI were scored for presence of PDI within micronuclear chromatin (minimum 100 micronuclei per treatment). Averages and standard error of three independent repeats are shown. Results in (a, d, and e) were analysed using a one-way ANOVA with Dunnett's *post hoc* test. Results in (b and c) were analysed using a two-way ANOVA with Dunnett's *post hoc* test.

with a discontinuous or wholly absent lamina (Figure 5.11b). The effect was also pronounced in VPS4-depleted cells, indicating that impairment of ESCRT-III function results in micronuclei with a disorganised nuclear envelope structure.

Nuclear pore complexes were visualised using mab414 antibody staining, and micronuclei were scored as per Figure 5.7b for NPC density. Observation of NPCs as determined by mab414 staining, there was a significant decrease in micronuclei containing a normal level of nuclear pore complexes following both CHMP7 and VPS4 knockdowns (Figure 5.11c). There was a corresponding increase in micronuclei with a reduced complement of NPCs in both knockdowns. VPS4 knockdown showed a significant increase in micronuclei with no NPCs, however the effect was less drastic in the CHMP7 knockdown, with the CHMP7-1 siRNA depletion showing a small significant increase, and the CHMP7-3 siRNA showing no significant difference.

Taken together, this demonstrates an increase in micronuclei with an incomplete nuclear envelope composition following the ESCRT-III knockdowns, which is especially pronounced in the VPS4 knockdown. This change may be due to an increased number of these defective micronuclei being produced, or due to the loss of ESCRT-III function at micronuclei. The latter hypothesis is intriguing since it suggests a specific role for ESCRT-III to maintain nuclear envelope integrity at micronuclei. Properly organised and functional micronuclei can be re-incorporated into the primary nucleus in the next cell cycle, therefore ESCRT-III occurrence specifically on broken MN may represent a novel mechanism for ESCRT-III in maintaining genomic stability.

5.2.11 ESCRT-III impairment results in more disrupted and collapsed micronuclei

In order to determine whether CHMP7 or VPS4 knockdowns have an effect on the integrity of micronuclear compartmentalisation, the presence of the soluble PARP1 in micronuclei was

scored across cells treated with either CHMP7 or VPS4 siRNA for 48 hours (Figure 5.11d). The depletion of either VPS4 or CHMP7 resulted in a significant decrease in PARP1-containing, properly compartmentalised micronuclei, from 55.8% in control cells to 38.9% (CHMP7-1), 37.6% (CHMP7-3) and 19.8% in the VPS4 knockdown.

There was a concomitant increase in the proportion of micronuclei invaded by ER microtubules, showing a change in the composition of the micronuclear chromatin and confirming disruption of the micronuclear envelope. In control cells, 32.2% of micronuclei are ER-invaded in the interphase cell population (Figure 5.11e). Following CHMP7 knockdown, this increased significantly to 49.5% (CHMP7-1) and 45.0% (CHMP7-3) of micronuclei. Forty-eight hours after VPS4 knockdown, 65.1% of micronuclei display this phenotype.

Together, these observations display a loss of micronuclear compartmentalisation and integrity upon the loss of ESCRT-III nuclear-related function. Interestingly, this mirrors the finding in Chapter 3, whereby nuclei are shown to lose compartmentalisation more frequently following CHMP7 knockdown, as marked by the mislocalisation of PML bodies into the cytoplasm.

5.2.12 A link between CHMP7 and DNA damage in micronuclei

In order to examine the relationship between CHMP7 and micronuclei generated by a known mechanism, breakage of DNA through induction of DNA damage, HeLa cells were treated with a measured dose of UVC radiation. Cells were fixed at various timepoints from the time of irradiation, and stained to show CHMP7 and a marker of DNA damage, phosphorylated histone H2AX (γ H2AX).

UV irradiation causes a significant increase in the number of micronuclei per cell from 16 hours post-irradiation onwards (Figure 5.12d). It has been shown that UV-induced micronuclei are primarily acentric fragments, formed due to chromosome double-strand

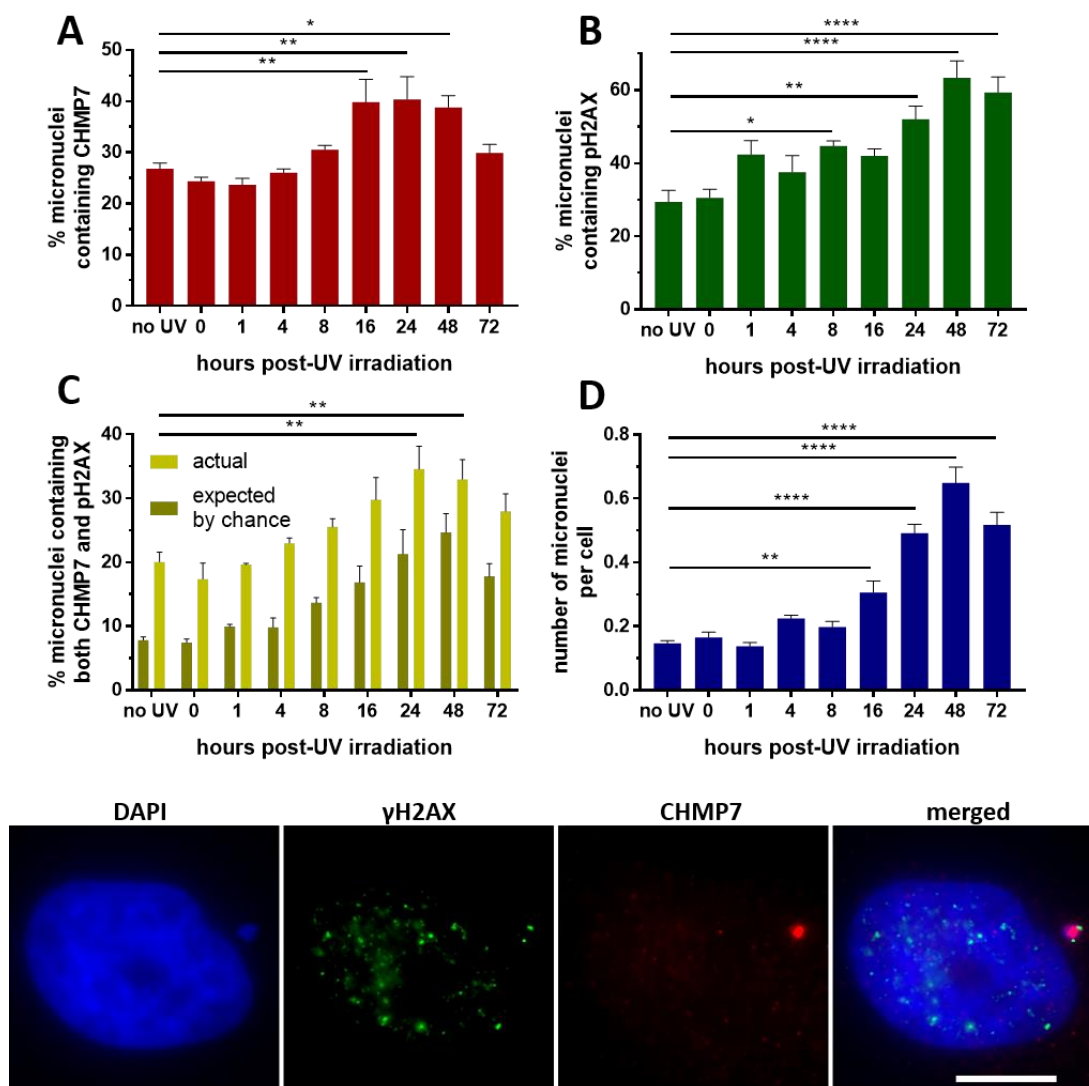


Figure 5.12. Scoring of HeLa cells for CHMP7 and γ H2AX micronuclear foci

HeLa cells were treated with a 10mJ/cm² dose of UV irradiation, and fixed at various timepoints following treatment, alongside a non-irradiated control. The cells were stained using the immunofluorescence protocol with mouse-derived anti- γ H2AX antibody, rabbit-derived anti-CHMP7 antibody and DAPI. Micronuclei were scored for presence of **a**) CHMP7 and **b**) γ H2AX foci, with a micronucleus containing at least one foci being considered as positive (400 micronuclei per treatment). The percentage of micronuclei positive for both PH2AX and CHMP7 are shown in **(c)**. The number of micronuclei per cell is shown in **(d)**. Averages and standard error of three repeats are shown. Results were analysed using a one-way ANOVA with Dunnett's *post hoc* test. **e**) Localisation of CHMP7 and γ H2AX within a single micronucleus. Scale bar represents 10µm.

breaks caused by single-strand DNA lesions remaining unrepaired upon S-phase entry (Wischermann *et al.*, 2008); therefore, UVC treatment represents an appropriate approach to dissect the relationship between DNA integrity in micronuclei and the presence of ESCRT-III.

Interestingly, UV irradiation causes an increase in the proportion of CHMP7-positive micronuclei, from a baseline of 26.8% in the non-irradiated control to a maximum of 40.3% 24 hours post-irradiation (Figure 5.12a). There is a significant difference in the percentage of CHMP7-positive micronuclei at the 16, 24 and 48 hour time points after irradiation when compared to non-irradiated cells. As expected, the percentage of micronuclei which contain γ H2AX foci increases following UV irradiation, with the 8, 24, 48 and 72 hour time points showing significantly increased proportions of γ H2AX micronuclei when compared to controls (Figure 5.12b).

Based on the percentage of micronuclei that are CHMP7-positive, and the percentage that are γ H2AX positive, the proportion of micronuclei which are expected to contain both markers if there is no association between them is shown in Figure 5.12c. The actual percentage of cells which are both CHMP7 and γ H2AX-positive is also shown, which appears consistently higher than would be expected if the two markers were independently marking micronuclei, showing that CHMP7 localises preferentially with micronuclei containing unresolved DNA damage. Figure 5.12e shows localisation of CHMP7 and γ H2AX to the same micronucleus, representing the cooccurrence of the two markers without colocalisation.

These results show that the proportion of micronuclei positive for CHMP7 increases upon induction of DNA damage, implying that CHMP7 is recruited to more of the newly formed micronuclei. Additionally, under all conditions, including the no-UV control, CHMP7 localises with γ H2AX more frequently than would be expected by chance, suggesting an association between micronuclei containing unresolved DNA damage and CHMP7.

5.2.13 CHMP7 forms bridge structures in untreated HeLa, HeLa M and U2OS cells

Upon observing CHMP7 subcellular localisation by immunofluorescence, cells show filamentous formations of CHMP7, such as those shown in Figure 5.13b. Cleasby (PhD thesis, 2013) observed 13.7% of VPS4-depleted HeLa M cells associated with these structures 72 hours following siRNA transfection, however their occurrence rate in untreated cells or in other cell lines is not known.

Therefore, HeLa, HeLa M and U2OS cells were treated with either NT-control or VPS4 siRNA for 48 hours before being fixed and stained to show CHMP7 and α -tubulin to delineate cell boundaries. In control cells, 2.5% (HeLa), 3.2% (HeLa M) and 1.8% (U2OS) of cells were associated with these structures, rising in VPS4-depleted cells to 8.1% (HeLa), 10.1% (HeLa M) and 8.3% (U2OS; Figure 5.13a). The structures observed in VPS4 depleted cells were frequently brighter than in control cells, showing multiple filaments which fork and appear to be associated with multiple nuclei, such as those seen in the VPS4 knockdown panel of Figure 5.13b. This demonstrates that while CHMP7 filaments occur in a small proportion of control cells, the VPS4 knockdown causes an increase in their frequency, suggesting that the function of the ESCRT-III machinery is linked to these structures.

5.2.14 ESCRT-III components localise at bridge structures when CHMP7 is present

The localisation of CHMP4B and CHMP1B to CHMP7 bridge structures was scored across CHMP7 and VPS4 single and combination knockdown HeLa cells. CHMP4B frequently localises to CHMP7 bridges, at a rate of 82.2% in control cells and 98.9% in VPS4-depleted cells (Figure 5.14a) CHMP1B localises to approximately half (47.3%) of CHMP7 bridge structures, increasing to 82.2% in VPS4-depleted cells. As seen previously at CHMP7 nuclear foci and micronuclei, the depletion of CHMP7 is sufficient to prevent the formation of

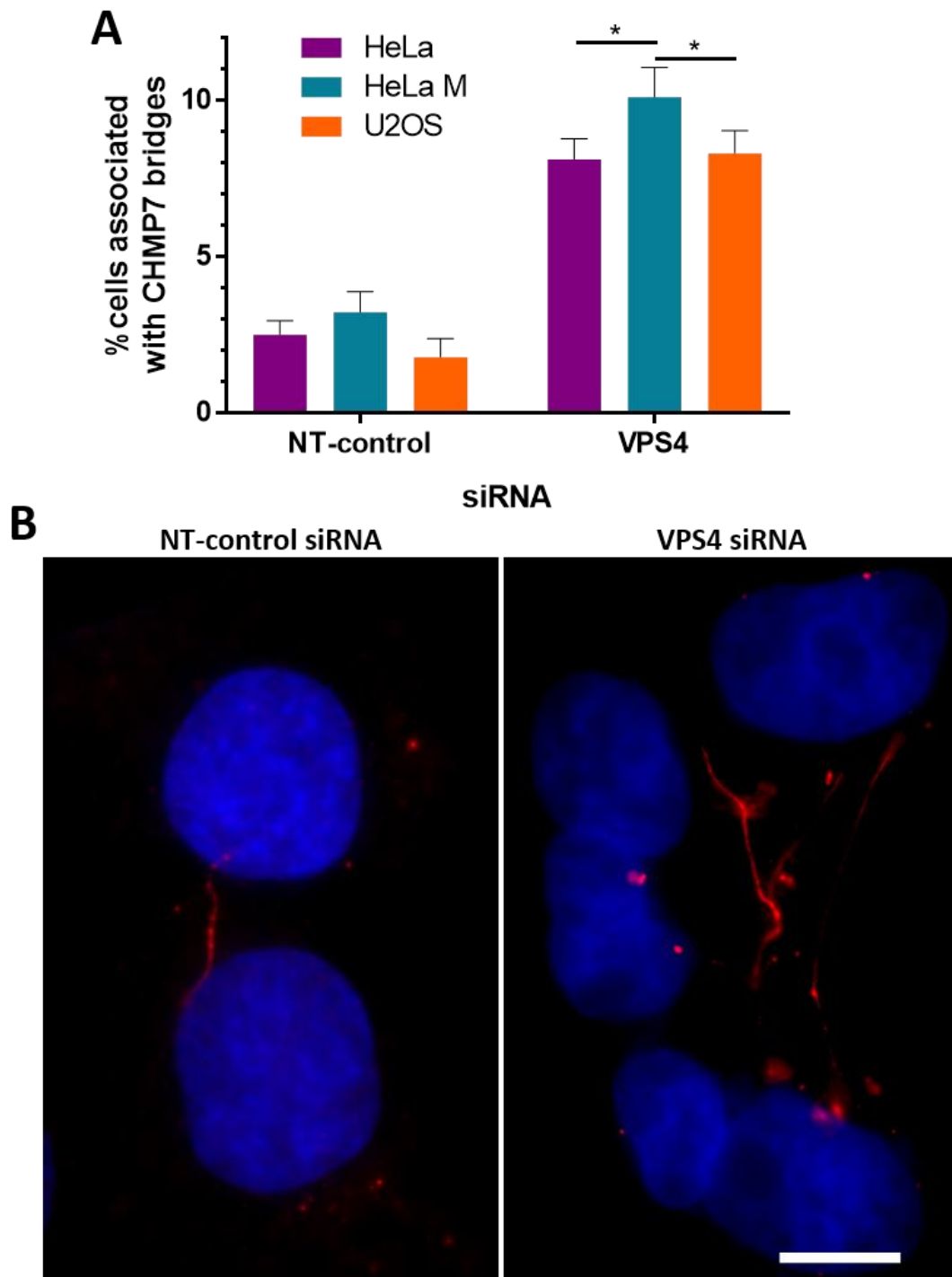


Figure 5.13. CHMP7 forms filamentous structures in various cell lines in control and VPS4-depleted cells

a) Cells were treated for 48h with siRNA, stained to show CHMP7 and DAPI antibody and scored for association with at least one CHMP7 filament structure (minimum 200 cells were scored). Averages and standard error of three independent repeats are shown. Results were analysed using a two-way ANOVA with Sidak's *post hoc* test. **b)** Images showing examples of CHMP7 structures formed in control and VPS4-depleted HeLa cells. Scale bar represents 10 μ m.

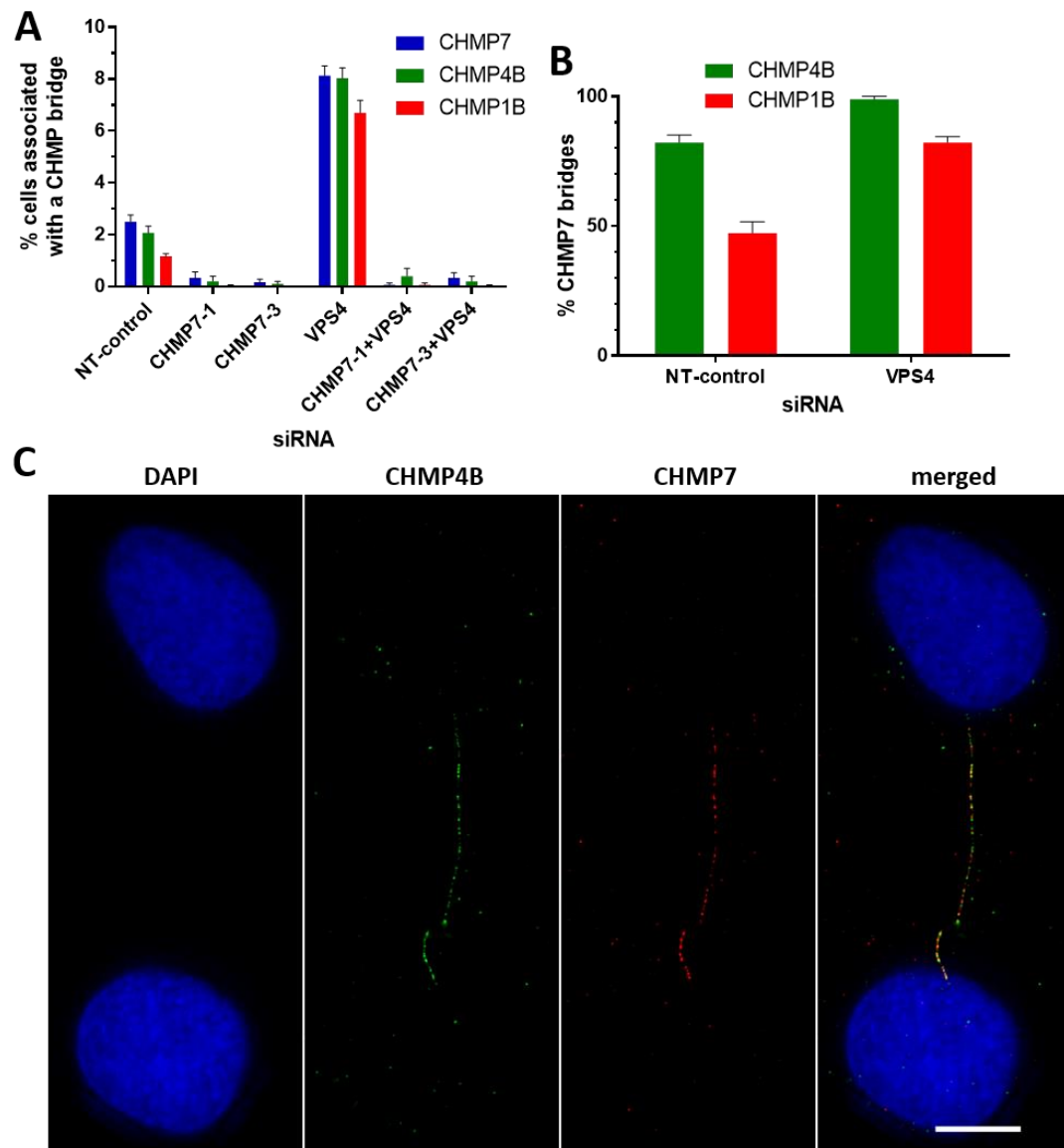


Figure 5.14. ESCRT-III components localise at bridge structures when CHMP7 is present

a) HeLa cells were treated for 48h with siRNA and stained to show CHMP7, CHMP1B or CHMP4B and DAPI. The number of bridges structures observed for each CHMP were scored (minimum 500 cells per condition). Results were analysed using a two-way ANOVA with Dunnett's *post hoc* test, with all knockdowns significantly different to the NT-control for CHMP7 ($p < 0.0001$), CHMP4 ($p < 0.0001$), and CHMP1B ($p < 0.01$). **b)** Filamentous bridge structures identified by the presence of CHMP7 were scored for the presence of either CHMP4B or CHMP1B (100 bridges scored per treatment). Averages and standard error of three independent repeats are shown. **c)** Image showing the localisation of CHMP4B on a CHMP7 structure in a control HeLa cell. Scale bar represents 10 μ m.

CHMP4B or CHMP1B-staining bridge structures (Figure 5.14b), indicating its key role at this structure in addition to those previously determined. The CHMP proteins show some, but not exact, colocalisation with each other, with the protein exhibiting a “beads on a string” conformation (Figure 5.14c) which may suggest that the CHMP7 is localising to a pre-existing cellular feature.

5.2.15 CHMP bridges associate with nuclear material

CHMP7 filaments frequently appear to connect two nuclei, or link nuclei and micronuclei structures. CHMP7 bridges were classified based on their relationship (as shown in the table in Figure 5.15a) to nuclear material in control and VPS4-depleted HeLa cells (Figure 5.15a), in order to characterise the nature of these structures. The majority (56.5%) of structures in control cells bridge two nuclei, with smaller proportions bridging a nucleus and micronucleus, or two micronuclei (8.7% and 2.5% respectively). A number of the structures (11.2%) appear to originate and terminate from two regions of the same nucleus. CHMP7 filaments which originate at a nuclear structure but are not associated with chromatin at the other end account for 12.4% of CHMP7 structures in control cells. A small number of more complex associations include those bridges which link multiple nuclei or micronuclei, an example of which is shown in Figure 5.15b. Approximately 7.5% of CHMP7 filaments do not appear to connect with a nuclear body, however, these always occur between two nuclei, though not showing clear attachment to either.

Owing to the propensity of CHMP7 structures to connect nuclei and micronuclei, they will be referred to as bridges, with those spanning the complete distance between two nuclei referred to as continuous, in contrast to those between two nuclei which are broken (Figure 5.15c). VPS4 depletion demonstrates a significantly higher proportion of broken bridges (39.9%) compared to control cells (27.6%), though more bridges are found in the knockdown overall (Figure 5.15d). Continuous bridges found in VPS4-depleted cells were longer (38.3 μ m)

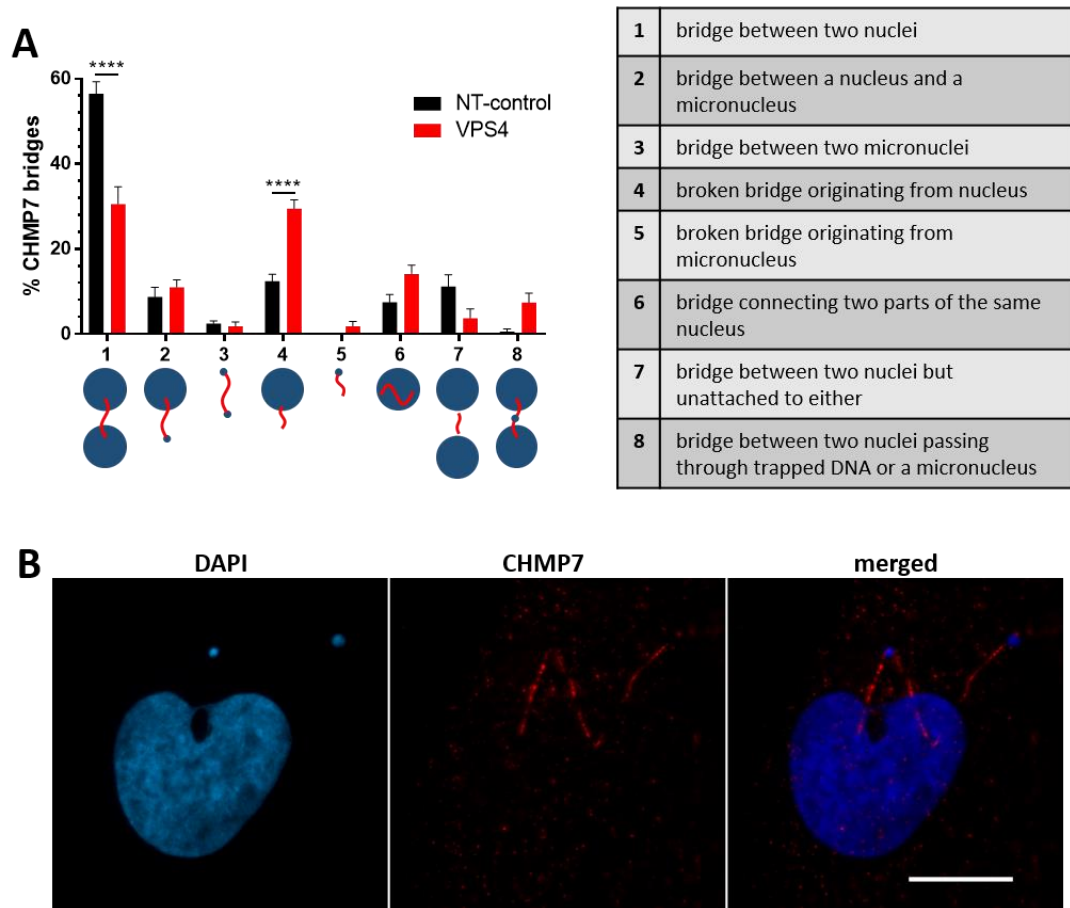


Figure 5.15. CHMP7 bridges connect nuclear structures

a) CHMP7 filament structures were classified based on their relationship to nuclear structures (50 bridges per knockdown were scored). Averages and standard error of three independent repeats are shown. Results were analysed using a two-way ANOVA with Sidak's *post hoc* test, **b)** Image of a single CHMP7 bridge connecting one primary nucleus and two micronuclei in a control HeLa cell. Scale bar represents 10 μ m.

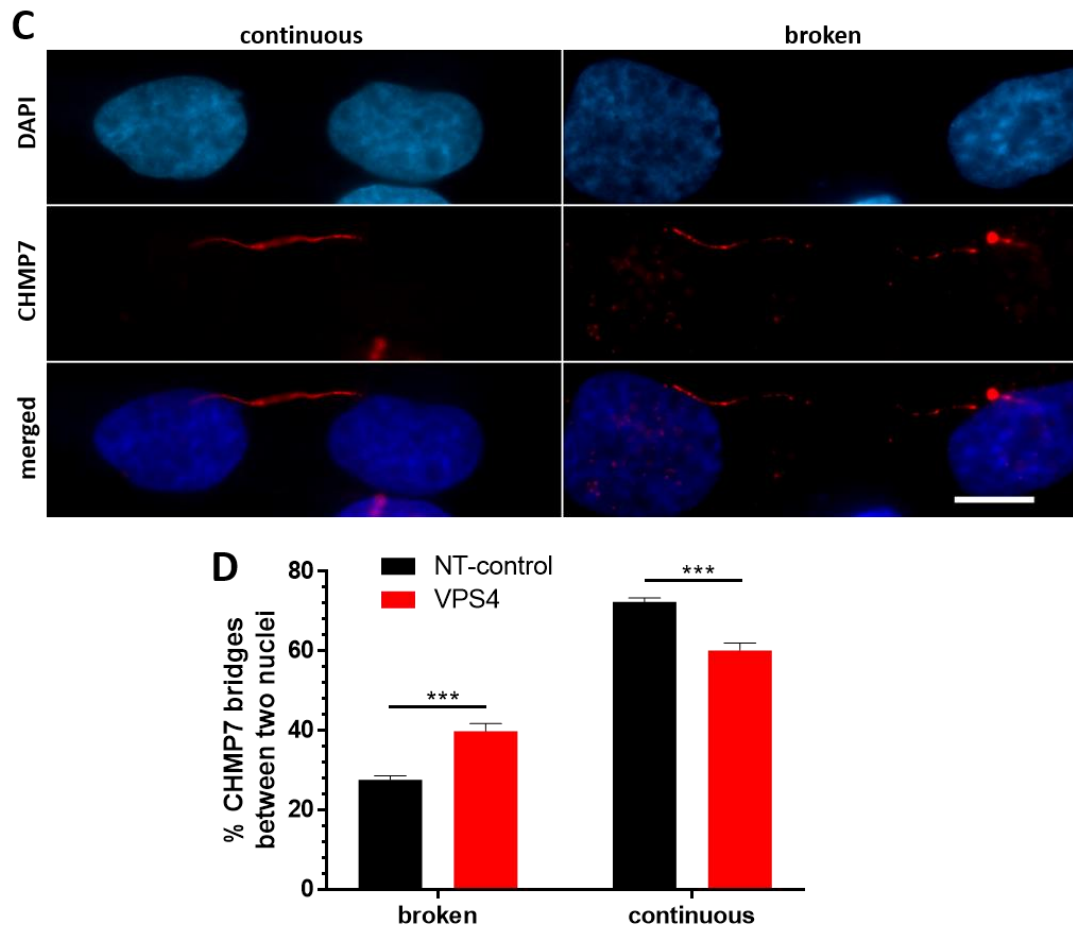


Figure 5.15. (continued)

c) Examples of continuous or broken CHMP7 internuclear bridges. Scale bar represents 10 μ m. **d)** HeLa cells were treated for 48h with siRNA and stained to show CHMP7 and DAPI. Bridges between two nuclei were scored as either intact, indicating a continuous bridge between the nuclei, or broken (50 bridges were scored per condition). Averages and standard error of three independent repeats are shown. Results were analysed using a two-way ANOVA with Sidak's *post hoc* test.

than in control cells (21.3 μ m), suggesting a persistence of these structures as nuclei migrate apart during interphase.

5.2.16 CHMP7 does not localise to BLM ultrafine anaphase bridges

CHMP7 bridges connect chromatin structures, and sometimes contain trapped DNA or micronuclei in between two nuclei, which would suggest a link with mitotic segregation of DNA. The fact that these structures do not display staining with DAPI points to the possibility that the CHMP7 is associated with ultrafine DNA bridges. Ultrafine bridges are DNA structures which are too thin to be stained with nuclear dyes such as DAPI or Hoechst, but have been shown to associate with helicases such as BLM and PICH, which function to resolve the bridge.

Immunofluorescence experiments were carried out to co-stain HeLa cells to show BLM helicase and CHMP7. The ultrafine bridges marked by the BLM helicase antibody become apparent during anaphase, and are no longer observed after the telophase stage of mitosis (Figure 5.16a and Figure 5.16c). BLM ultrafine bridges are common in normal human cells and resolve prior to cytokinesis (Chan *et al.*, 2007) and were commonly observed in untreated HeLa cells, with 61% of fixed anaphase cells and 12% of telophase cells displaying at least one BLM bridge structure. The presence of BLM helicase at an ultrafine bridge shows that the contained DNA is actively being processed for resolution and proper segregation, avoiding the formation of a persistent chromosome bridge which interferes with completion of cytokinesis (Chan and Hickson, 2011). Across these scored bridges, none were observed to colocalise with a CHMP7 bridge.

5.2.17 Development of CHMP7 bridges in mitosis

Since CHMP7 bridges connect two nuclei, it was hypothesised that these bridges originate in mitosis. Mitotic cells were scored for the presence of CHMP7 bridges connecting the segregating nuclei across anaphase, telophase, and cytokinesis. No CHMP7 bridges were

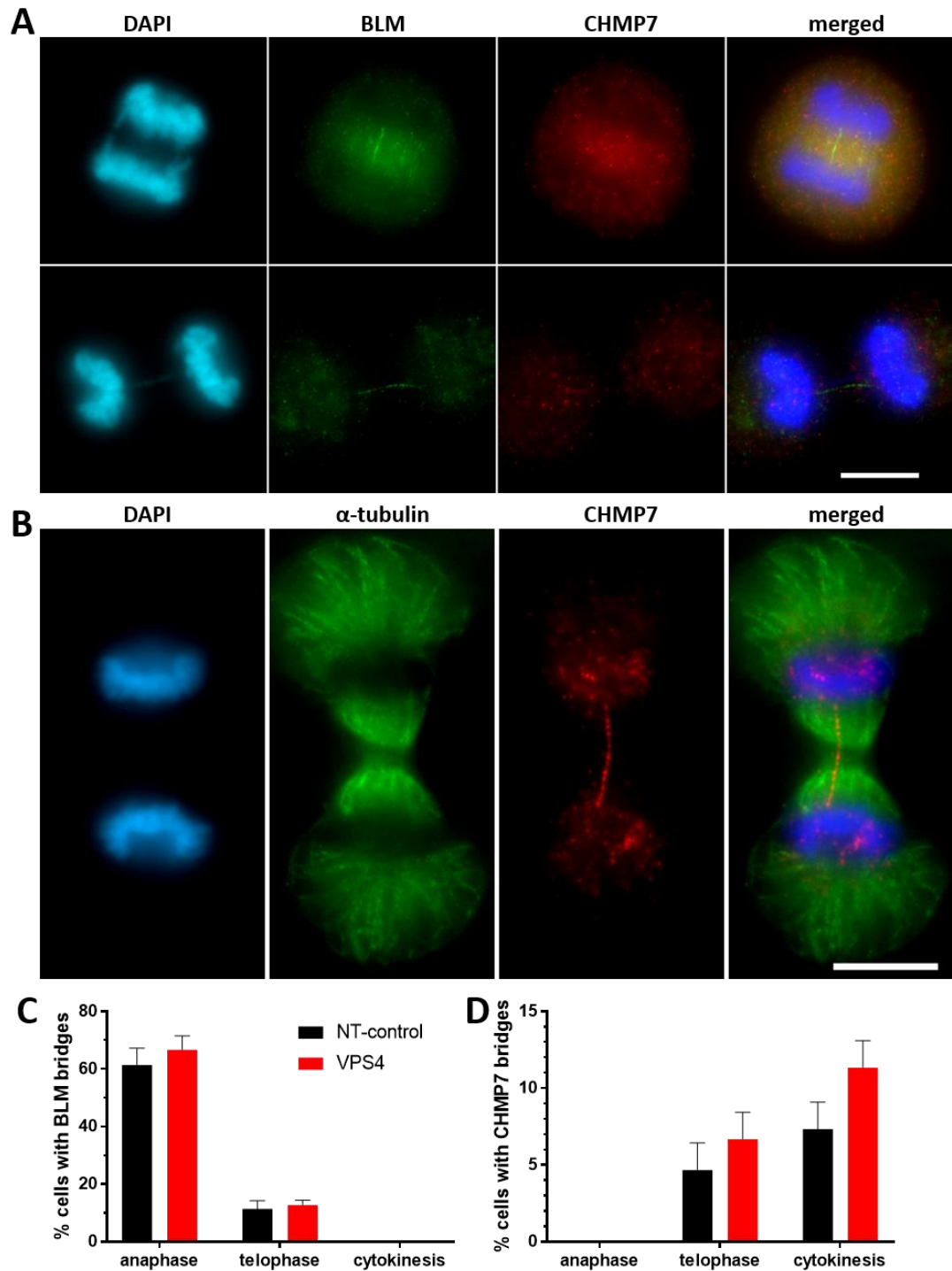


Figure 5.16. CHMP7 bridges do not correspond to anaphase BLM bridges, but appear later in mitosis

a) HeLa cells were stained to show CHMP7, BLM and DAPI. Example of BLM anaphase bridges which lack association with CHMP7. **b)** HeLa cells were stained to show CHMP7, α -tubulin and DAPI. An example of a telophase cell containing an internuclear CHMP7 bridge. Scale bars represent 10 μ m. HeLa cells were treated with siRNA for 48 hours, before being scored for the of either **c)** BLM or **d)** CHMP7 bridges in anaphase, telophase, and cytokinesis (60 cells were scored per condition). Averages and standard error of three independent repeats are shown.

observed in anaphase, however they emerge as mitosis progresses, with to 4.7% in telophase and 7.3% of cytokinetic cells in the control population (Figure 5.16d). The depletion of VPS4 causes an increase in the number of CHMP7 bridges in anaphase (to 6.7%) and cytokinesis (11.3%). These changes are not significant compared to the control condition, however, this may be influenced by the small number of mitotic cells scored. These results imply that CHMP7 bridges are formed in mitosis in telophase and cytokinesis. CHMP7 bridges are observed in telophase, concurrently with the presence of ESCRT-III localisation to telophase chromatin, with the bridge passing through a constricting cleavage furrow (Figure 5.16b). This is consistent with the observed recruitment of CHMP7 and CHMP4B to chromatin at telophase in HeLa, HeLa M and U2OS (Chapter 4).

5.2.18 CHMP7 bridges occur in multinucleated, cytokinetic, and separated cells

Interphase CHMP7 bridges were analysed to observe the nature of cells in which nuclei connected by a CHMP7 bridge are present. The cytoskeleton and shape of cells was visualised using α -tubulin. CHMP7 bridges in control and VPS4-depleted cells were classified based on their occurrence between two nuclei within a multinucleated cell, in two cytoskeletally separate cells, or passing through a midbody structure in a cytokinetic cell (Figure 5.17a and Figure 5.17b).

The effect of the VPS4 knockdown is to prevent the completion of cytokinesis, eventually leading to reversion of a cytokinetic cell into a multinucleated cell. This explains the significant increase in both cytokinetic and multinucleated cells containing CHMP7 bridges following VPS4 depletion. The majority (66.1%) of control cells have bridges connecting nuclei in two cells which have separated cytoskeletons and appear to be completely detached. These cells are likely to be G1 cells connected by a stable intercellular channel, which occur when the NoCut checkpoint, activated by DNA passing through the midbody,

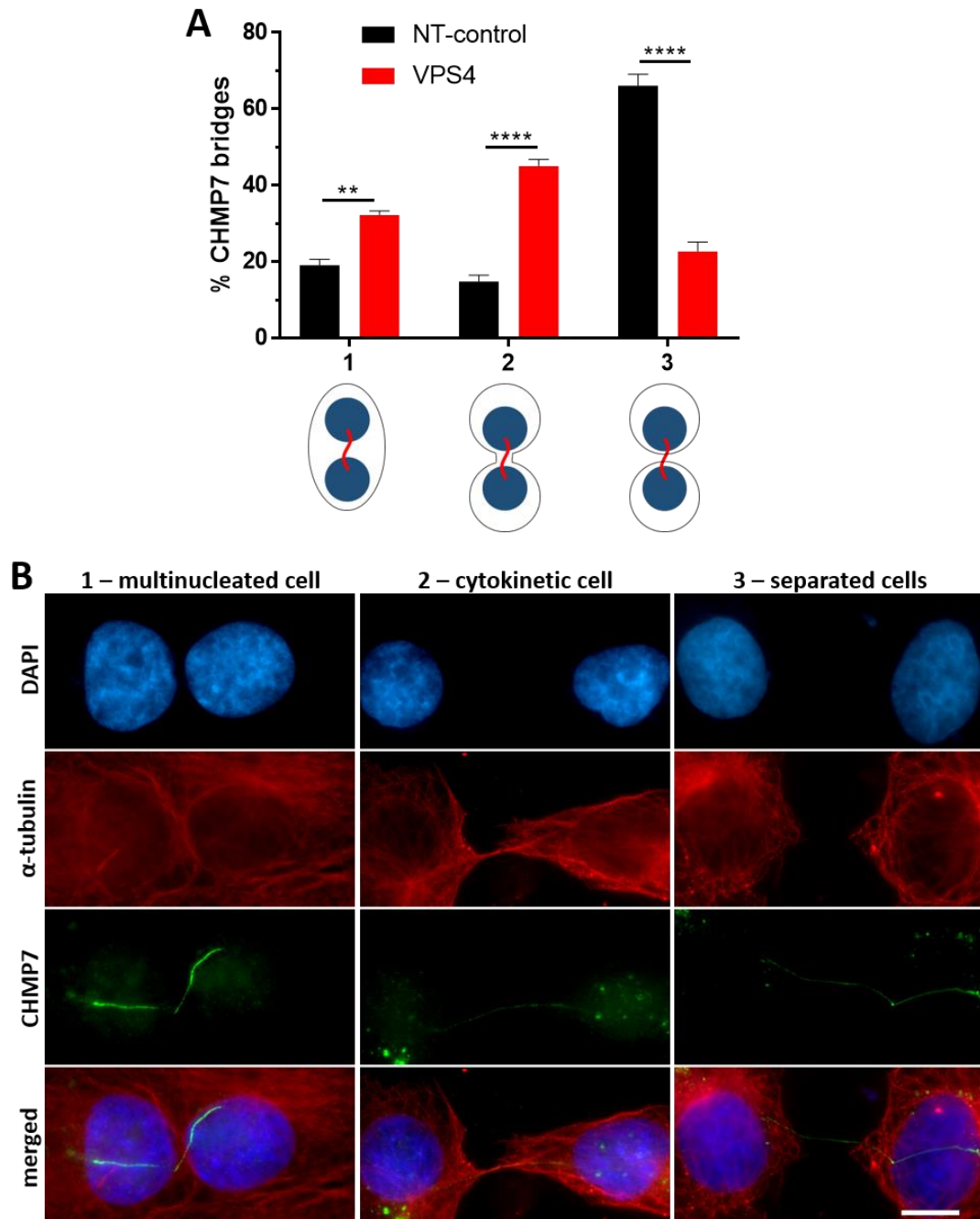


Figure 5.17. Occurrence of CHMP7 bridges at different cell stages

HeLa cells were treated for 48h with siRNA and stained to show CHMP7, α -tubulin and DAPI. **a)** Cells containing CHMP7 filament structures were classified as either connecting nuclei within the same cell (multinucleated), passing through the midbody of a dividing cell (cytokinetic), or connecting nuclei in two apparently separate cells (separated) and 50 bridges were scored per knockdown. Averages and standard error of three independent repeats are shown. Results were analysed using a two-way ANOVA with Sidak's *post hoc* test. **b)** Examples of CHMP7 bridges occurring in multinucleated, cytokinetic and separated cells. Scale bar represents 10 μ m.

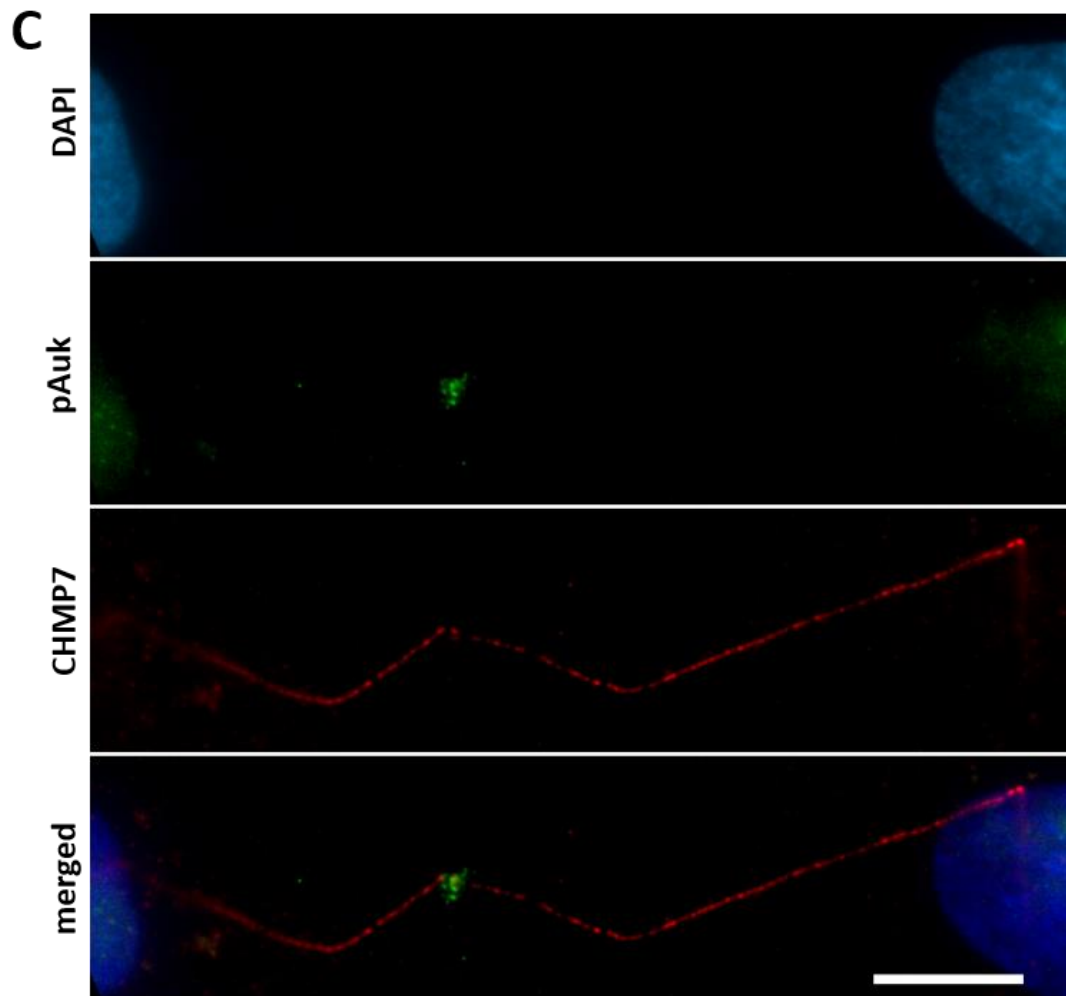


Figure 5.17. (continued)

c) HeLa cell stained to show CHMP7, phosphorylated Aurora kinase (pAuk) and DAPI. The internuclear CHMP7 bridge passes through activated pAuk, demonstrating an active NoCut checkpoint delaying cytokinetic abscission. Scoring of CHMP7 bridges showed that 35/38 (92.1%) were associated with a patch of activated Aurora kinase.

maintains abscission delay for many hours (Steigemann *et al.*, 2009). This prevents either severing of the DNA bridge or formation of a multinucleated cell, both of which are deleterious events for genomic integrity.

A marker of a stable intercellular channel is the presence of activated (phosphorylated) Aurora kinase (pAuk). Therefore, in order to confirm the hypothesis that CHMP7 bridges pass through stable intercellular channels, HeLa cells were stained to show pAuk and CHMP7 (Figure 5.17c). Of 38 scored CHMP7 bridges, 35 showed visible signs of pAuk associated somewhere along the length of the bridge. This indicates that CHMP7 bridges mark persistent nuclear material passing through cells connected due to incomplete or delayed cytokinetic scission.

Taken together, this suggests that the persistent presence of the CHMP7 bridge leads either to furrow ingression and collapse of cytokinesis into a multinucleated cell, or persistence of an intercellular bridge following the disassembly of midbody microtubules, leading to a stable intercellular bridge.

5.2.19 Nuclear membrane assembles on CHMP7 internuclear bridges

CHMP7 bridges show association with DNA structures, and may show the presence of trapped or micronucleated DNA between two nuclei, however the portion of the bridge stained with CHMP7 does not stain positively for DAPI. Therefore, if a chromosome bridge containing DNA is present, it is so thin as to be undetectable by DAPI under the current microscopy conditions. In order to detect possible ultrafine chromosome bridges, an antibody against LAP2 was used, a technique previously used by Steigemann *et al.* (2009; Figure 5.18c).

CHMP7 bridges between two nuclei were scored for the presence of LAP2 along the length of the bridge in both control and VPS4-depleted cells (Figure 5.18a). In both conditions the

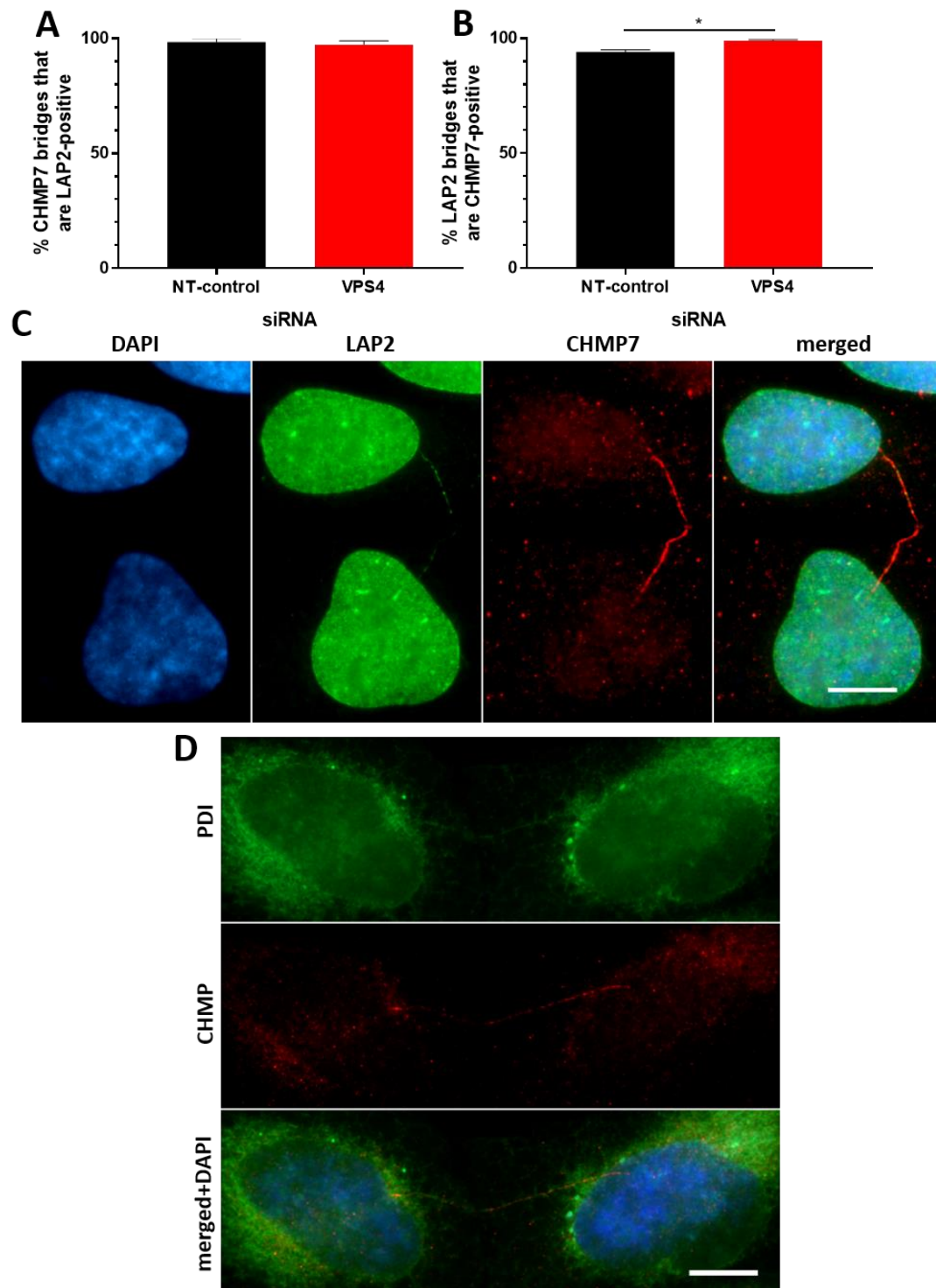


Figure 5.18. Nuclear envelope assembly around CHMP7 internuclear bridges

HeLa cells were treated for 48h with siRNA and stained to show CHMP7, LAP2 and DAPI. **a)** CHMP7 bridges were scored for the presence of LAP2 along the length of the bridge (50 bridges were scored per condition). **b)** CHMP7 bridges were scored for the presence of LAP2 along the length of the bridge (75 bridges were scored per condition). Averages and standard error of three independent repeats are shown. Results were analysed using an unpaired, two-tailed *t*-test. **c)** Example of colocalisation of LAP2 and CHMP7 to the same internuclear structure. **d)** Example of colocalisation of PDI and CHMP7 to the same internuclear structure. Scale bars represent 10 μ m.

majority of CHMP7 bridges were positive for LAP2 – 98.5% and 97.3% for control and VPS4-depleted cells respectively. Scoring was also carried out on LAP2 bridges, in order to determine the prevalence of CHMP7 recruitment to these known nuclear envelope-containing structures (Figure 5.18b). In control cells, CHMP7 localised to 94.0% of these structures, rising to 98.9% in VPS4-depleted cells. This suggests that the presence of CHMP7 is regular and persistent at these bridges in control cells despite the availability of VPS4 to carry out ESCRT-III activity and disassembly.

In an additional experiment, CHMP7 bridges were co-stained with the membrane-staining protein PDI (Figure 5.18d). Of 40 CHMP7 bridges scored for the presence of PDI along the length of the bridge, 24 displayed association with membrane along the structure, concurring with the observation that membrane has been recruited to, and spread across, the DNA structure.

5.2.20 Other nuclear envelope components are not present at CHMP7 bridges

Since the nuclear envelope is present on these CHMP7-positive nuclear structures, it was examined whether other components of the nuclear envelope, nuclear lamina and nuclear pore complexes, are present. Internuclear Lamin B bridges were observed to associate with substantial DAPI staining along at least part of the bridges structure, indicating the presence of chromatin, and deformation of the nuclear morphology into a teardrop shape (Figure 5.19a, right panel). Lamin B-defined bridges were rarely observed (Figure 5.20), particularly in control cells, where they were observed in 0.4% of cells. CHMP7 bridges were scored for the presence of nuclear lamina as indicated by Lamin B staining, either along the full length of the bridge, or along part of the length of the bridge, as shown in Figure 5.19a.

No CHMP7 bridges displayed an intact nuclear lamina along the full length of the structure. However, 15.6% of bridges in control cells and 18.9% in VPS4-depleted cells display both

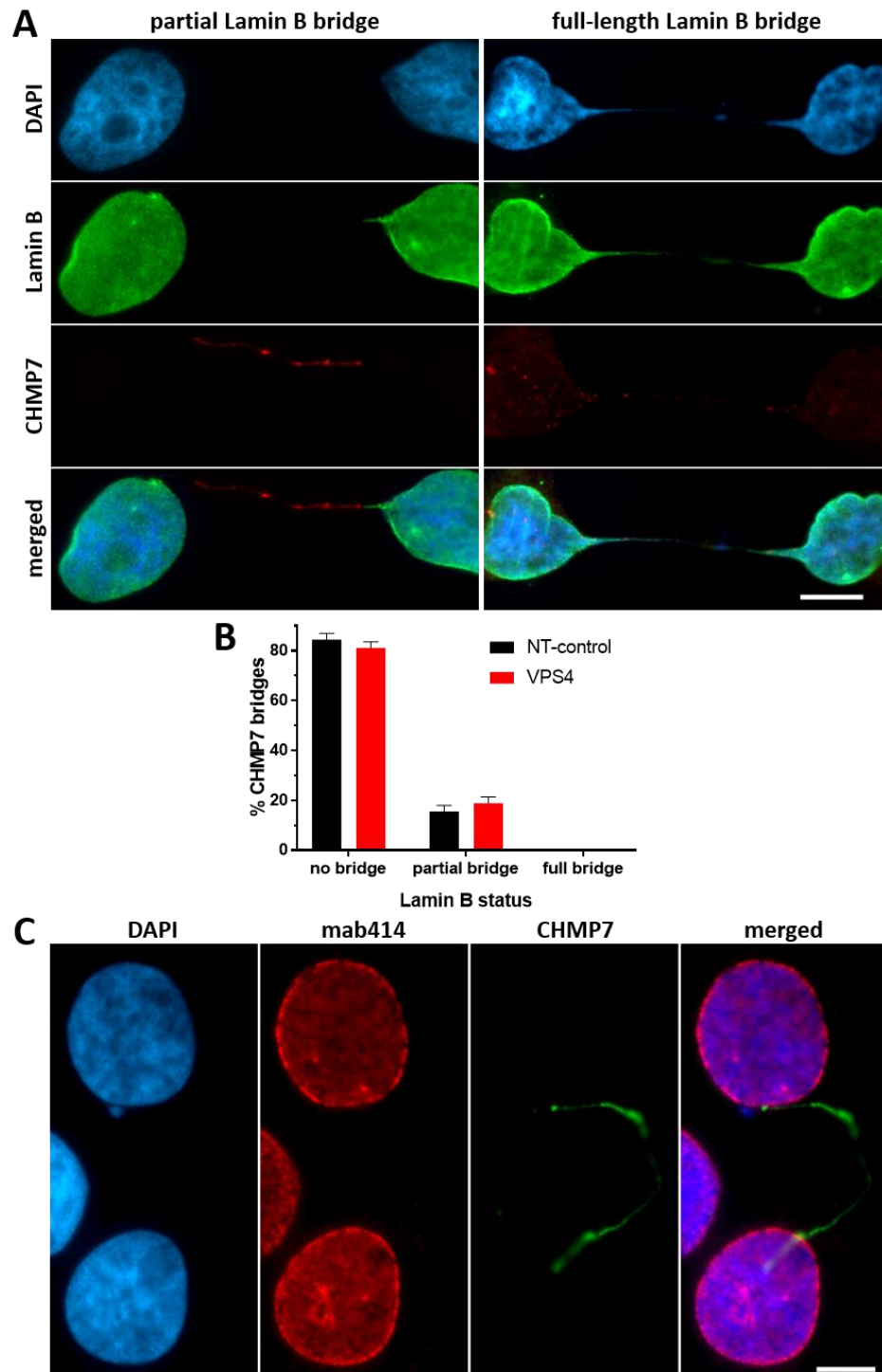


Figure 5.19. Lamin B and mab414 are absent from CHMP7 nuclear bridges

HeLa cells were treated for 48h with siRNA and stained to show CHMP7, Lamin B and DAPI. **a)** Examples of Lamin B extending partially or fully along an internuclear bridge are shown. **b)** CHMP7 bridges were scored for the presence of Lamin B along part or all of the length a CHMP7-positive bridge in HeLa cells treated with either NT-control or VPS4 siRNA for 48 hours (60 bridges were scored per condition). Averages and standard error of three independent repeats are shown. **c)** HeLa cells were stained to show CHMP7, mab414 (NPCs) and DAPI. An example of a CHMP7 bridge lacking localisation of nuclear pore complexes is shown. Scale bar represents 10 μ m.

regions of CHMP7 localisation and Lamin B on the same bridge structure (Figure 5.19b). A representative image of the relationship between Lamin B and CHMP7 on a bridge is shown in Figure 5.19a (left panel), demonstrating that the two markers are found mutually exclusively on the bridge. Nuclear lamina extends from the main body of the nucleus partway along the bridge, and at the point at which it disappears, CHMP7 continues the bridge structure, with this occurring at both ends of the bridge.

Nuclear pore complexes as visualised using mab414 and RANBP2 antibody as described previously were never observed forming bridges between nuclei, preventing scoring of this component alongside CHMP7, and showing that a complete nuclear envelope is not formed on internuclear bridges (Figure 5.19c).

5.2.21 The prevalence of bridges in ESCRT-III knockdown cells

In order to determine the effect of impairment of ESCRT-III recruitment or activity (via CHMP7 and VPS4 depletion, respectively) on the formation of internuclear bridges, various markers were used to score nuclear-nuclear structures in HeLa cells following 48 hour knockdowns (Figure 5.20).

The number of cells associated with a LAP2 bridge were scored across control, CHMP7 and VPS4 knockdown cells. In control cells, 2.6% of cells are associated with a LAP2 bridge. CHMP7 knockdown significantly decreases this to 0.3% (CHMP7-1) and 0.2% (CHMP7-3), however, VPS4 causes an increase in LAP2 bridges to 7.3%. Lamin B-staining internuclear bridges are unaffected by CHMP7 knockdown, however, knockdown of VPS4 causes an increase in these bridges from a control level of 0.6% of cells to 2.7%.

The presence of a chromatin bridge between two nuclei can be scored if the bridge stains along its entire length for DAPI, and if the nucleus is pulled into a teardrop shape, showing tension in the chromatin. DAPI-staining bridges mirrored the presence of Lamin B bridges, with CHMP7 knockdown having no effect, but VPS4 depletion causing an increase in bridges

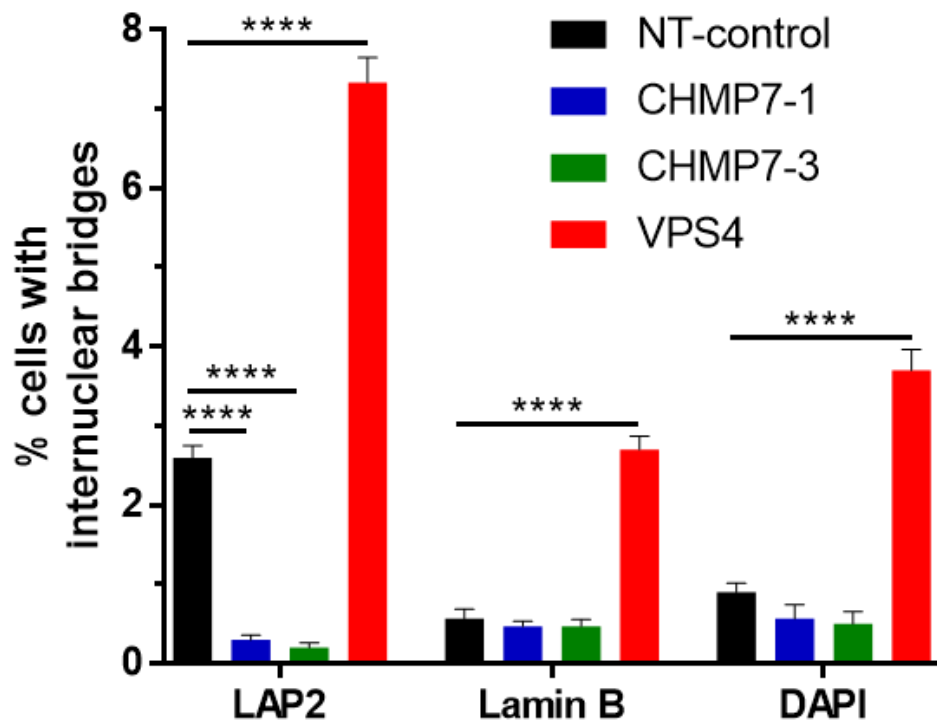


Figure 5.20. The effect of ESCRT-III impairment on the prevalence of internuclear bridges

HeLa cells were treated for 48h with siRNA and stained to show DAPI alongside either LAP2 or Lamin B. Cells were scored for the presence of bridges defined by either LAP2, Lamin B or DAPI (a minimum of 300 cells were scored per condition). Averages and standard error of three independent repeats are shown. Results were analysed using a two-way ANOVA with Dunnett's *post hoc* test.

from 0.5% of cells in the control population compared to 3.7% in the VPS4-depleted condition. CHMP7 depletion has no apparent effect on the frequency of chromatin bridges.

5.3 Discussion

ESCRT-III is present at nuclear anomalies associated with chromosomal instability and genotoxic events. These micronuclei and chromosome bridge structures are indicative of genome damage commonly found in cancers or contributing to the risk of cancer development through loss, gain or breakage of DNA.

This chapter has shown that CHMP7 and the ESCRT-III complex accumulate on micronuclei and chromosome bridges in control cells, with CHMP7 being essential for the subsequent recruitment of ESCRT-III proteins. This correlates with the pattern seen at the reforming nuclear envelope in mitosis and at nuclear foci in VPS4-depleted cells, and represents another aspect of the role for the nuclear ESCRT-III complex.

5.3.1 CHMP7 relationship with micronuclei

CHMP7 was found to localise to a subset of micronuclei, characterised by lack of an organised nuclear envelope, including lack or discontinuity of nuclear lamina, and reduced or absent nuclear pore complex insertion. In addition, these micronuclei had universally lost nucleocytoplasmic compartmentalisation in control cells. Approximately 70% of these micronuclei showed extensive invasion of ER membrane into the micronuclear chromatin, a phenomenon associated with an irreversible collapse of nuclear integrity hatch(Hatch *et al.*, 2013). CHMP7-positive micronuclei were found to be smaller in diameter on average compared to CHMP7-negative cells. CHMP7-positive micronuclei were also more likely to contain chromosome fragments (73%) as opposed to a whole chromosome in control cells in which approximately 50% of all micronuclei were found to contain whole chromosomes.

The loss of CHMP7 also displayed changes in micronuclear number and composition. CHMP7 knockdown resulted in an increase in micronucleated cells from a baseline of 12% to between 25-30% 48 hours post-knockdown. Following the loss of CHMP7, there was a slight decrease in the number of whole chromosome micronuclei. However, there were significant

differences in the composition of micronuclei, resulting in increases in lamina and NPC-defective micronuclei. Ruptured micronuclei, indicated by loss of soluble protein, and collapsed micronuclei, indicated by invasion of ER membrane, are both increased significantly upon CHMP7 knockdown.

5.3.2 CHMP7 recruitment to micronuclei

The process of reformation of a micronuclear envelope is not well understood, however, Hatch *et al.* (2013) demonstrate that almost 100% of micronuclei in U2OS cells show successful nucleocytoplasmic compartmentalisation upon exit from mitosis. Therefore, they must have a sealed nuclear membrane, a process which requires annular fusion events. Approximately 82% of VPS4-depleted HeLa cell nuclei display CHMP7 foci in interphase, due to the effect of the knockdown, which prevents disassembly of the ESCRT-III complex. It is possible that the CHMP7/ESCRT-III system is similarly required to establish an intact nuclear envelope at micronuclei, which may account for the prevalence of ESCRT-III-positive micronuclei in VPS4-depleted cells, which stands at approximately 60%. While this would account for the high proportion of CHMP7-positive micronuclei following VPS4 knockdown, CHMP7 is also found commonly associated with micronuclei in control cells, at a rate of approximately 26%.

Another hypothesis contends that CHMP7 plays a role in the formation of micronuclei, and is therefore present at newly formed micronuclei, remaining associated following their generation. In support of this hypothesis, it has been shown CHMP7 is present at chromosome bridges, from which micronuclei may be derived. In the only study of its kind, Huang *et al.* (2011) used live cell imaging of HeLa cells to observe the mechanisms of micronuclei formation, in which they determined that only approximately 9.2% of micronuclei were derived from breakage of chromosome bridges, which alone is too few to account for these CHMP7-positive micronuclei. This hypothesis would suggest that CHMP7

is already associated with micronuclei prior to their rupture, and that CHMP7-positive micronuclei are more likely to possess a defective nuclear lamina and therefore undergo micronuclear collapse. It has been suggested that micronuclei derived from chromosome bridges are lamin-negative (Okamoto *et al.*, 2012). However, this hypothesis is not supported by the CHMP7 knockdown data, which demonstrates an increase in micronuclei formation upon depletion of either CHMP7 or VPS4. In the absence of live cell imaging, it is not possible to determine whether CHMP7 is localised to micronuclei prior to their collapse, however, the current data suggests that this is unlikely.

5.3.3 A role for CHMP7 and ESCRT-III in micronuclear integrity

This thesis has shown the importance of ESCRT-III for maintenance of nuclear and genomic integrity at primary nuclei of cells. As demonstrated in this chapter through the detection of PARP1 soluble nuclear protein, micronuclei are particularly prone to nuclear envelope ruptures, which occurs in approximately 44% of micronuclei in interphase control HeLa cells. CHMP7 was found almost exclusively localised to micronuclei lacking PARP1, which suggests a specific association with these ruptured structures. The increase in ruptured micronuclei following CHMP7 or VPS4 knockdown also suggests that in the absence of the ESCRT-III activity, this process can still occur. Interestingly, repair of ruptured micronuclei and re-accumulation of soluble nuclear proteins has been observed in U2OS cells (Hatch *et al.*, 2013), though only a fraction of ruptured micronuclei (approximately 10%) had regained compartmentalisation by the onset of mitosis.

Taken together, these data propose a role for CHMP7/ESCRT-III at ruptured micronuclei, and allows us to hypothesise that ESCRT-III could work to seal the nuclear envelope and restore micronuclear integrity (Figure 5.21). Micronuclear collapse contributes to their dysfunction, with DNA damage (γ H2AX accumulation) arising as a result of nuclear envelope rupture, with

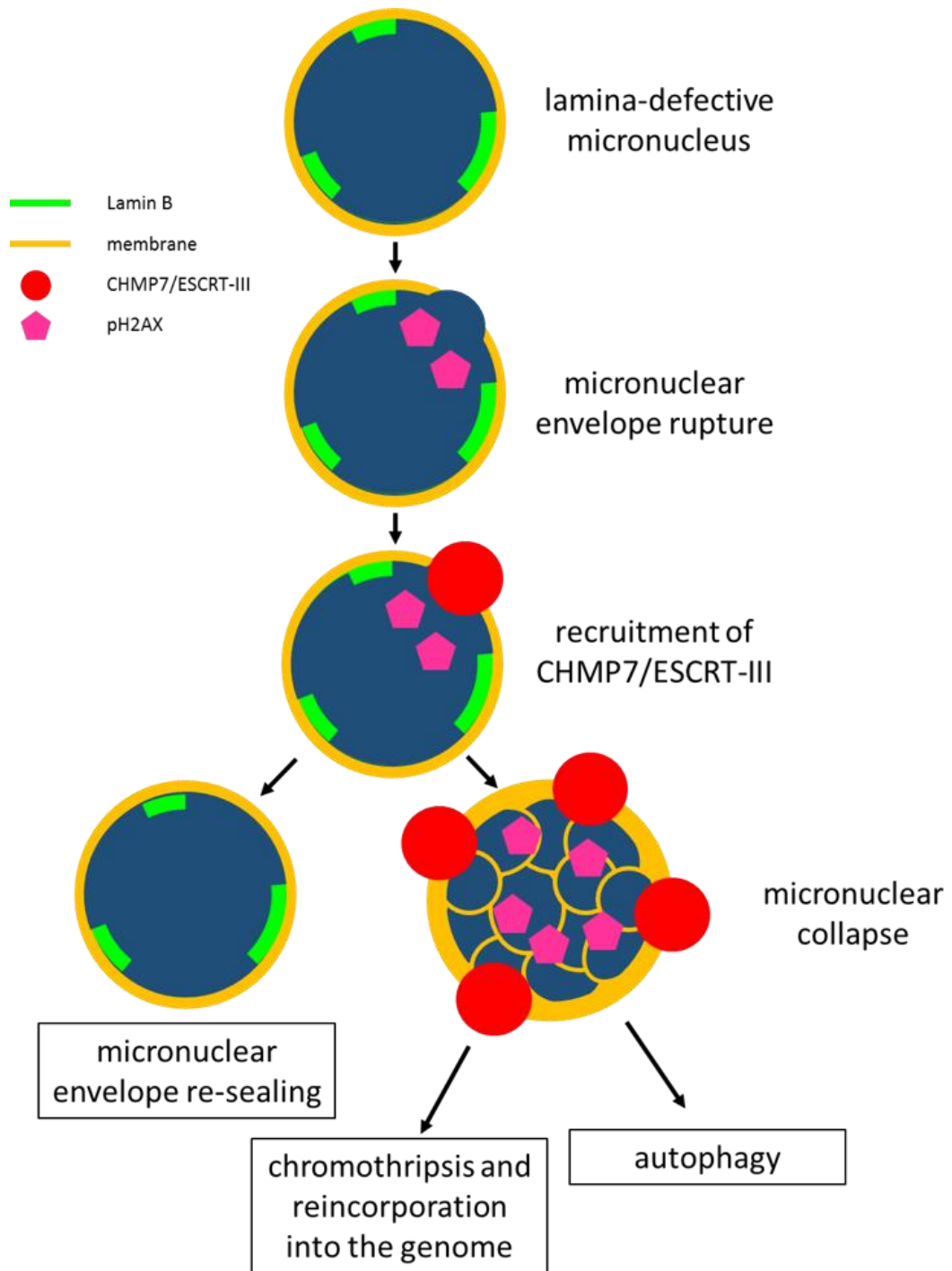


Figure 5.21. Model for the relationship between CHMP7/ESCRT-III and micronuclei

Diagram proposing a model for the recruitment and function of CHMP7/ESCRT-III to micronuclei.

consequences related to failed DNA replication and aneuploidy, as well as chromothripsis and persistent genomic instability. In U2OS cells as studied by Hatch *et al.* (2013), intact micronuclei rejoin the primary nucleus following the subsequent mitosis approximately 70% of the time, and disrupted micronuclei were also reincorporated at the significant rate of over 50%. Therefore, a mechanism for protecting the DNA contained within chromosomal micronuclei is plausible, to allow for the possibility of successful reincorporation of undamaged DNA into the primary nucleus in a subsequent mitosis, or to avoid chromosome shattering and rearrangement.

5.3.4 A role for CHMP7/ESCRT-III in micronuclear collapse

Another hypothesis for CHMP7/ESCRT-III function at micronuclei relates to micronuclear collapse, and the significant changes which occur in the membrane content of these micronuclei. Following nuclear rupture, micronuclear chromatin shows condensation and infiltration of ER tubule structures. This process appears to be irreversible, and it is difficult to imagine how an intact micronucleus could be recovered from this collapsed structure. In this chapter it has been shown that nearly 100% of micronuclei which showed PDI-positive structures within the chromatin are positive for CHMP7 accumulation. This suggests that CHMP7/ESCRT-III localisation at micronuclei persists past the point at which it is possible to restore their compartmentalisation and repair the nuclear membrane. While very little is known about the mechanism by which ER tubules invade micronuclear chromatin, it is clear that it requires remodelling of both the nuclear and ER membranes, potentially involving the action of the ESCRT-III complex (Figure 5.21).

However, CHMP7 or VPS4 depletion results in an increased proportion of micronuclei which are positive for ER membrane invasion, indicating that this process is still able to proceed in their absence. It should be noted that this does not preclude ESCRT-III activity at ER

membrane invasion of chromatin, but does rule out a CHMP7-dependent mechanism of doing so.

5.3.5 A role for CHMP7/ESCRT-III in autophagic degradation of micronuclei

The known links between ESCRTs and autophagy are summarised in Section 1.2.3, which determine that the fusion of autophagosomes and lysosomes may be ESCRT-III dependent. Since the start of this study, localisation of CHMP4B has been observed at micronuclei by Sagona *et al.* (2014), who also suggest a relationship between ESCRT-III and autophagy at micronuclei. This link is based on a mutation of CHMP4B which is known to cause cataracts, which also reduces its localisation to micronuclei, hypothesising that CHMP4B localisation to micronuclei is required for micronuclear degradation. Localisation of CHMP4B to micronuclei found adjacent to lysosomal markers was observed in HeLa cells. However, this observation was not quantified, and no evidence is given for colocalisation of micronuclei or chromatin with lysosome or autophagosome markers.

Thus far, autophagic degradation of micronuclei has been documented in one study by Rello-Varona *et al.* (2012). U2OS cells were treated with cell cycle blocker to increase the frequency of micronuclei and autophagic marker (GFP-LC3), and therefore do not represent normal cells. Under these conditions, 2-5% of micronuclei were adjacent to of colocalising with the autophagic marker. An unquantified subset of these were said to be localised with LAMP2 lysosomal protein. These “autophagic micronuclei” demonstrate discontinuous Lamin B staining and high levels of γ H2AX staining.

Based on the known evidence it is likely that only a small proportion of micronuclei undergo autophagic degradation, however it is possible that may be a role for ESCRT-III (Figure 5.21). This chapter shows that upon CHMP7 knockdown, the number of micronuclei increases, which may indicate loss of a micronuclear degradation pathway.

Micronuclei associated with autophagic markers invariably contain strong signals of DNA damage (γ H2AX; Rello-Varona *et al.*, 2012) indicating that severely damaged micronuclei are targeted for degradation, although the mechanism by which this is detected is not certain. While CHMP7 is localised more frequently to γ H2AX-positive micronuclei than would be expected by chance, this could be accounted for by CHMP7 recruitment to ruptured or collapsed micronuclei likely to accrue DNA damage. CHMP7 does not show exclusive localisation to γ H2AX-positive micronuclei, and indeed a significant proportion of micronuclei containing DNA damage do not stain positively for CHMP7.

5.3.6 The relationship between CHMP7 and chromosome bridges

The presence of a CHMP7 bridge or filament structure within or between cells is not an uncommon event, occurring in approximately 2-3% of control HeLa, HeLa M and U2OS cells, and in 8-10% of VPS4-depleted cells. In control HeLa cells, 82% of CHMP7 bridges display CHMP4B staining, and 47% display CHMP1B staining, with accumulation of these ESCRT-III proteins evident upon VPS4 depletion. CHMP7 depletion abrogates formation of CHMP7, CHMP4B and CHMP1B-defined bridge structures. These findings correlate well with CHMP7/ESCRT-III structures found in this study at micronuclei, in mitosis and on VPS4-depleted interphase cells.

The findings that the majority of CHMP7 filaments link nuclear material support the central hypothesis that ESCRT-III has a role at aberrant nuclear structures. The finding that 77% of filaments in control cells occur between two nuclei suggests a mitotic origin for the bridges. This model is also supported by scoring of mitotic cells, demonstrating the appearance of bridges between daughter nuclei in telophase at a rate of 4.7%, and in cytokinesis in 7.3% of cells. This proportion exceeds the number of CHMP7 bridge-containing cells found in the general cell population, indicating that a subset of the bridges formed in mitosis disappear as the cell continues through interphase.

5.3.7 Formation of CHMP7 bridges

It seems reasonable to hypothesise that CHMP7 localises to bridges formed from chromatid-chromatid catenations, either due to incomplete resolution centromeric cohesion or due to incomplete replication intermediates. These bridges form ultrafine bridges between nuclei which cannot be detected by DAPI staining, which corresponds with the type of structures with which CHMP7 is observed to localise. Ultrafine bridges are a common occurrence in anaphase, however, many are resolved successfully by BLM and PICH helicases prior to telophase (Chan *et al.*, 2007; this study). As the cell enters telophase, ESCRT-III aids in the reformation and sealing of the nuclear envelope, however the presence of a DNA bridge prevents the formation of a sealed nuclear envelope around the entire nucleus (Steigemann *et al.*, 2009).

A model for the formation of CHMP7/ESCRT-III bridges is shown in Figure 5.22a. This demonstrates the localisation of CHMP7/ESCRT-III to chromosome bridges connecting the two daughter nuclei. ESCRT-III plays a key role in sealing the nuclear membrane around the nuclear material at the end of mitosis, however, the presence of a DNA bridge would prevent the complete compartmentalisation of the chromatin and formation of a continuous nuclear envelope. Steigemann *et al.* (2009) demonstrated assembly of nuclear membrane around ultrafine chromosome bridges, and this study shows that bridges displaying INM protein LAP2 stain positively for CHMP7. Therefore, it is hypothesised that ESCRT-III aids in the formation of this nuclear membrane around the bridge DNA, hence its appearance (as shown in this chapter) towards the end of mitosis, in an attempt to compartmentalise chromatin fully despite the presence of the bridge.

5.3.8 A proposed role for CHMP7 bridges in the NoCut pathway

Following the formation of nuclear envelope around the chromosome bridge, CHMP7 appear to persist on the structures, instead of being recycled as would be expected following

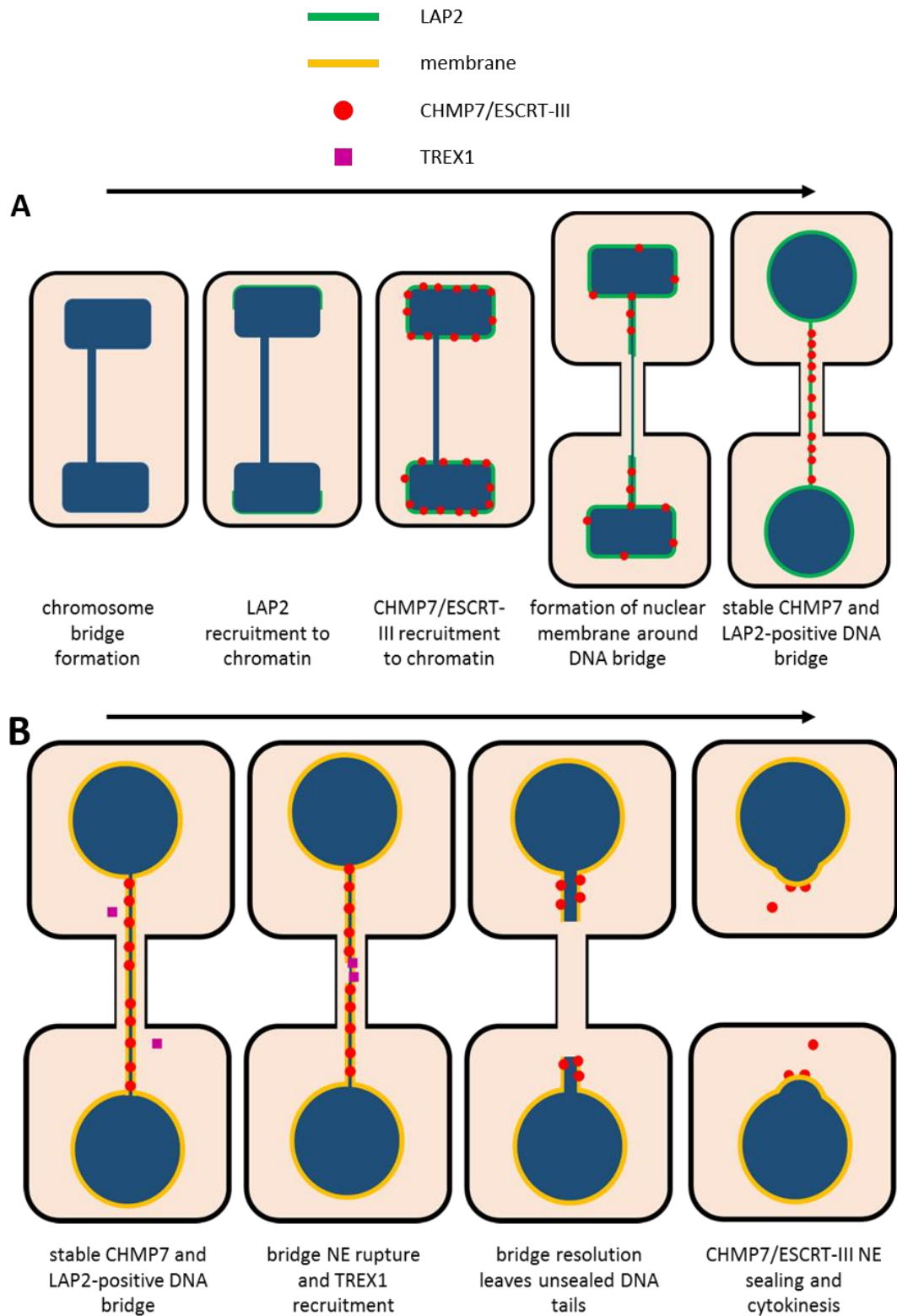


Figure 5.22. Model for the relationship between CHMP7/ESCRT-III and chromosome bridges

a) Diagram proposing a model for the formation of CHMP7 internuclear bridges. **b)** Diagram proposing a model for resolution of stable CHMP7 bridges.

completion of ESCRT-III function. The continued presence of CHMP7 on chromosome bridges may be partially explained by the activation of the Aurora B-mediated NoCut checkpoint, which results in the retention of VPS4 through binding to the ANCHR protein, thus preventing its access to the ESCRT-III midbody complex to catalyse abscission (Thoresen *et al.*, 2014). However, while VPS4 can be excluded from the midbody region, it seems implausible that VPS4 cannot interact with ESCRT-III along the full length of the chromosome bridge.

The ESCRT-III complex is necessary for the completion of cell abscission, and as previously discussed (Section 1.3.5), a specific isoform of CHMP4, CHMP4C, plays a key role in the NoCut mechanism of abscission delay to protect genomic integrity (Carlton *et al.*, 2012). The NoCut checkpoint results in the continued activation of Aurora B kinase when DNA passes through the midbody, however the mechanism by which DNA is sensed is unknown. CHMP7 and CHMP4 are known to be able to interact with each other (Horii *et al.*, 2006). It can be hypothesised that the presence of CHMP7 along the length of chromosome bridges allows it to act as a “signalling platform” for interaction with CHMP4C and activation of the NoCut checkpoint.

CHMP4C is found at nearly 100% of LAP2 positive bridges, colocalising with activated Aurora B in a patch at the approximate midpoint of the bridge, whereas isoforms CHMP4A and CHMP4B were found only at approximately 40% of bridges (Carlton *et al.*, 2012). It has been shown in this chapter that CHMP7 bridges frequently intersect a persistent patch of activated Aurora B kinase. Therefore, there is a correlative relationship between the presence of LAP2 bridges, which have been shown here to stain positively for CHMP7 at rates nearing 100%, and an active NoCut checkpoint along these bridges, indicated by the presence of both Aurora B and CHMP4C.

Additionally, CHMP4C depletion results in faster resolution of LAP2 bridges by circumventing the activation of the NoCut checkpoint. If CHMP7 is necessary for activation of the NoCut

checkpoint, this may explain the surprising reduction in LAP2 bridges observed upon CHMP7 knockdown. The prevention of the NoCut checkpoint delay by depletion of CHMP4C results in increased γ H2AX due to the deregulation of abscission resulting in more aberrant DNA bridge breakage (Carlton *et al.*, 2012). As shown in Chapter 3, the depletion of CHMP7 also results in increased DNA damage as marked by γ H2AX, although there are a number of other potential explanations for the CHMP7 knockdown-mediated increase.

Taken together, these findings may suggest a role for CHMP7 as a marker of chromosome bridges, allowing for a potential role in the activation of the NoCut checkpoint in order to protect genomic integrity. It would be interesting in future to fully explore the origin of CHMP7-positive bridges, potentially through generation of specific classes of chromosome bridges and observation of CHMP7 localisation in live cells.

5.3.9 A potential role for CHMP7/ESCRT-III in chromosome bridge resolution

Recently, a method for resolving persistent chromosome bridges with nuclease activity has been observed, functioning on chromosome bridges which possess a nuclear envelope continuous with that of both daughter nuclei (Maciejowski *et al.*, 2015). This mechanism requires transient rupture of the nuclear envelope on the bridge, allowing accumulation of the TREX1 nuclease, followed by RPA localisation to bridges, which indicates the presence of single strand DNA. Resolution occurs on these bridges at 3-20 hours following anaphase in 85% RPE-1 cells, resulting in reincorporation of the bridge DNA into each daughter nucleus, around which a sealed nuclear envelope forms. It is possible that ESCRT-III action at the nuclear envelope may be required for this process, in order to repair the nuclear envelope following the rupture and regain nuclear integrity (Figure 5.22b).

An interesting phenomenon has been observed in *Drosophila* cells which may be relevant (Karg *et al.*, 2015) in which closing of the nuclear envelope in a specific region is delayed to

allow for inclusion of lagging chromatin and acentric fragments into the primary nucleus. A gap in the nuclear envelope is maintained through Aurora B kinase activation, with an overall effect of safeguarding genomic stability and reducing the number of chromosome bridges and micronuclei generated. If such a mechanism exists in humans it is possible that CHMP7/ESCRT-III is part of a system which regulates the timing of nuclear envelope sealing, possibly linked to the NoCut mechanism.

Chapter Six

Discussion

Contents

	Page
6.1 Key findings	242
6.2 Recent research into CHMP7 and ESCRT-III	245
6.2.1 CHMP7 and ESCRT-III in mitosis	245
6.2.2 CHMP7 and ESCRT-III at nuclear ruptures	246
6.2.3 CHMP7 structure and function in relation to the nuclear envelope	247
6.2.4 CHMP7 and nuclear pore complexes	248
6.3 Future work	250
6.3.1 CHMP7 as a target for cancer therapy	251

6.1 Key findings

The work described in this thesis has shown for the first time that CHMP7 is key to cell function, with CHMP7 depletion causing a wide range of nuclear and mitotic defects which lead to cell cycle arrest and eventual cell death. Chapter 3 uniquely demonstrates the toxicity of the CHMP7 depletion across different cell lines, due to the inability of CHMP7-depleted cells to form an intact, organised nuclear envelope, and interestingly reveals some differences in phenotype between the cell lines observed.

Chapter 4 explores the cause of nuclear defects caused by CHMP7 depletion, through the examination of ESCRT-III foci which form in the absence of VPS4, and through observing, uniquely, the localisation of endogenous CHMP7 protein to the nuclear envelope in mitosis and interphase. At this point it was possible to put forward a role for CHMP7 as an essential protein for the recruitment of ESCRT-III to the reforming nuclear envelope in telophase. This was based on a number of findings. Firstly, the consequences of CHMP7 loss shown in Chapter 3, whereby CHMP7-depleted cells increasingly lost nucleocytoplasmic compartmentalisation, herniated and extruded DNA through lamin holes, and failed to organise centrosomal and nuclear pore complex association with the nuclear envelope. Secondly, localisation studies between CHMP7 and various nuclear envelope components and membrane demonstrated timing and location of CHMP7 at the newly reforming nuclear envelope. Furthermore, the observation of the persistence of ESCRT-III complexes at nuclear envelope holes into interphase in VPS4-depleted cells, with ESCRT-III unable to complete its membrane remodelling function. Consequently, genomic integrity was compromised following both impairment of ESCRT-III function (VPS4 depletion) and impairment of ESCRT-III recruitment (CHMP7 depletion).

Additionally, the novel finding that endogenous CHMP7 localises to the nuclear envelope in untreated interphase cells implies a consistent membrane-associated pool of the protein,

and a potential function at the interphase nuclear envelope. This phenotype was assumed to relate to interphase nuclear membrane remodelling, which may occur due to nuclear budding or rupture. A tagged form of the poorly characterised N-terminal of the protein demonstrated the potential role of this domain, showing localisation to the telophase nuclear envelope independently of the endogenous full length protein. Therefore, a role was hypothesised for the N-terminal domain which incorporates its apparently nuclear-specific role alongside the ESCRT-III complex.

Chapter 5 shows observation the formation of inter-nuclear CHMP7 bridges, mostly connecting nuclear material via an apparently chromatin-free structure which does not stain positively for DAPI. The finding that these structures arise as mitosis progresses, pass through midbodies in cytokinetic cells and correspond to staining of nuclear envelope protein LAP2, which marks out chromosome bridges. The presence of INM protein LAP2 indicates the assembly of nuclear envelope on this DNA structure, however the absence of Lamin B indicates an incomplete envelope, indicating that CHMP7 may be present as part of a delayed, aberrant nuclear envelope formation on nuclear chromatin. This is supported by the fact that those bridges with a visible nuclear lamina lack CHMP7 localisation. It is hypothesised that CHMP7 and ESCRT-III may play a role in the resolution of these structures, in their role as membrane remodelling and sealing machinery.

Finally, Chapter 5 elucidates the common relationship between cancer cell micronuclei and a CHMP7-dependent ESCRT-III complex. CHMP7 localises almost exclusively to micronuclei with aberrant nuclear lamina, which also display an enrichment of LAP2 and loss of nucleocytoplasmic compartmentalisation. Additionally, CHMP7 localises with micronuclei which have undergone an irreversible collapse of integrity, being invaded by ER membrane and containing condensed chromatin more likely to display DNA damage marker γ H2AX. The potential roles for ESCRT-III at micronuclei are shown in Figure 5.21.

It has clearly been shown here that CHMP7 is a consistent marker of damaged nuclear envelope at both the primary nucleus and aberrant nuclear structures. CHMP7 and ESCRT-III are found at regions of loss of nuclear integrity, in combination with lamina holes or absence, and carries out membrane remodelling which, when impaired, leads to consistent nuclear and mitotic defects related the loss of nuclear envelope integrity.

6.2 Recent research into CHMP7 and ESCRT-III

Since the beginning of this project, research into nuclear roles for the ESCRT-III complex has become a topic of great interest, with a number of key findings in this thesis confirmed and complemented using different methods and published by various research groups.

6.2.1 CHMP7 and ESCRT-III in mitosis

This thesis has presented data showing the transient, punctate localisation of CHMP7 to the rim of chromatin in daughter nuclei during late anaphase/telophase. A role for the ESCRT-III in nuclear envelope sealing at the end of mitosis has recently been confirmed through a different route by (Olmos *et al.*, 2015), using observation and depletion of CHMP2A, CHMP3 and CHMP4B. In this new study, endogenous CHMP2A and CHMP2B were observed to localise to daughter nuclei in telophase HeLa cells, the depletion of which resulted in similar nuclear defects and loss of compartmentalisation as documented in Chapter 3 of this thesis. An interaction between CHMP2A and UFD1 of the p97/UFD1/Npl4 complex (discussed in Section 4.1.3 due to its role in nuclear membrane remodelling in NE reformation) was mapped, and suggested as the mode of CHMP2A, and therefore ESCRT-III recruitment to the nuclear envelope.

The role of ESCRT-III in nuclear envelope sealing at mitosis was also determined independently by Vietri *et al.* (2015), in which CHMP4B was observed at telophase chromatin, also in HeLa cells. CHMP1A/B, CHMP2A, CHMP3, CHMP4A/B and IST1 were all observed localising around the reforming daughter nuclei. CHMP1A and CHMP4B localisation was shown to occur independently of the presence of DNA and upstream regulators of ESCRT-III such as ESCRT-0, TSG101 and CEP55. The key finding of this paper was the action of ESCRT-III at sites of spindle microtubule intersection with the nuclear envelope. As occurs at the cytokinetic midbody, CHMP1B appears to recruit spastin in order to sever the spindle connection to chromosomes in order to allow for nuclear envelope sealing. The authors

reported CHMP7 as essential for recruitment of ESCRT-III at mitotic chromatin. However, this assertion was based on abrogation of CHMP4B-eGFP recruitment in 19 cells depleted of CHMP7, and without any further context of testing on this subunit.

6.2.2 CHMP7 and ESCRT-III at nuclear ruptures

An additional role for CHMP7 and ESCRT-III has been confirmed at the interphase nuclear envelope in cancer cells. The growth of cancer *in vivo* often progresses to a metastatic step, in which cancer cells spread from their initial location to invade other tissues. This can mean that cells are forced to infiltrate through small intercellular gaps, placing mechanical strain on the cell. While cytoplasm is highly malleable, the nucleus is a relatively large and rigid structure, meaning that it is squeezed and deformed by the pressure of the tight interstitial space. This distortion can cause nuclear integrity to be compromised, resulting in damaged nuclei which lose their shape through chromatin herniation, or even result in loss of compartmentalisation through rupture of the nuclear envelope (Wolf *et al.*, 2013). Nuclear fragmentation can occur through physical pinching and DNA double-strand breaks, and in these cells, micronuclei with markers of loss of nuclear envelope integrity are significantly increased (Denais *et al.*, 2016).

Significant progress on the role of CHMP7 at interphase nuclear membranes has been made very recently by Denais *et al.* (2016). It has been shown that CHMP4B and VPS4B localise transiently at sites of nuclear membrane damage, induced directly by laser damage, or indirectly through cellular constriction. Depletion of CHMP7, as well as CHMP2A, increased significantly the time for compartmentalisation between the nucleus and cytoplasm to be re-established following ruptures. The recruitment of ESCRT-III to ruptures by CHMP7 to re-seal NE holes provides a robust defence against repeated nuclear rupture, with 90% of cells surviving following repeated induction of rupture. This is of significance in cancerous tumours, in which metastasizing cells frequently must migrate through small spaces to

spread, and are able to deal with constriction-induced rupture through the combined function of ESCRT-III membrane repair and DNA damage repair pathways. Targeting these mechanisms of cell survival may specifically target these cells.

These ruptures were transient, indicating the presence of an effective repair mechanism for the nuclear envelope. Within a few minutes of the rupture, tagged lamin A was observed accumulating at the site of membrane damage, which persisted at a high level for hours beyond the time of rupture, a phenomenon called by Denais *et al.*, (2016) "lamin scars". CHMP4B and VPS4B were observed to form foci at these sites, also within minutes of injuries caused by migration through small pores or specific laser insults. Observation by super-resolution microscopy determined ESCRT-III complexes were formed, independently of the presence of microtubules. Given the key role of CHMP7 in recruiting ESCRT-III at the mitotic nuclear envelope, the authors observed that upon CHMP7 or CHMP2A depletion, the time it took for the nucleus to be repaired, and compartmentalisation to be restored, was significantly increased, showing a role here for CHMP7 as a recruiter of the ESCRT-III complex.

The presence of this repair mechanism allowed more than 90% cells to maintain viability even after multiple nuclear ruptures. The loss of ESCRT-III function alone did not impair cell survival, but its inhibition alongside DNA repair pathways resulted in vastly increased occurrence of cell death. A potential opportunity for cancer treatment in the future may therefore combine inhibitors of the DNA damage response alongside targeting the ESCRT-III-dependent nuclear repair pathway.

6.2.3 CHMP7 structure and function in relation to the nuclear envelope

While the N-terminal domain of CHMP7 was previously uncharacterised in terms of structure and function, this thesis has indicated the importance of the N-terminal domain of the protein. By removing the CHMP domain, it was possible to observe the localisation of the

protein more clearly, in the absence of protein aggregation and puncta formation, such as that seen in the overexpression of the full-length protein (Figure 4.22). The N-terminal half of the protein alone localised to the nuclear envelope in both interphase and mitosis, and localised to perinuclear structures during interphase that resemble the endoplasmic reticular network. However, visualisation of the ER alongside the HA-CHMP7-NT construct was not achieved, which would confirm this finding.

A recent paper has functionally analysed the N-terminal half of CHMP7, demonstrating the ability of this domain to insert a loop into lipid membranes (Olmos *et al.*, 2016). It is also determined that GFP-CHMP7 demonstrates persistent localisation to the endoplasmic reticulum throughout the cell cycle, becoming concentrated around the region of the nuclear envelope during late mitosis.

This ability to localise to the ER, and consequently the outer nuclear membrane, in combination with the recently determined interaction of CHMP7 with LEM (LAP2-Emerin-MAN1) protein LEM2 (Gu *et al.*, 2017), which is found in the inner nuclear membrane, may explain the specificity of CHMP7 for recruitment of ESCRT-III to the nuclear envelope. A hypothesis for the method by which an INM protein can interact with an ONM protein is shown in Figure 4.26, whereby continuity of these two membranes occurs at a nuclear envelope hole, allowing their interaction. However, instead of LAP2 as the proposed interaction partner of CHMP7, LEM2 is a more likely candidate for this role based on this new data.

6.2.4 CHMP7 and nuclear pore complexes

Chapter 3 demonstrates aberration of nuclear pore complex organisation and localisation following CHMP7 depletion across all tested cell lines. Interestingly, depletion of CHMP2A and CHMP2B carried out by Olmos *et al.* (2015) demonstrated no decrease in intensity of NPC staining, concluding no effect of ESCRT-III depletion on NPC incorporation into the

nuclear envelope. These data also confirmed our observations that CHMP7 plays a specific role in mislocalisation of nuclear pore complexes to the cytoplasm, possibly into annulate lamellae, which are organelles composed up of stacked ER membrane sheets. Moreover, nuclear pore complexes are pre-assembled at membranes of annulate lamellae, which have been observed to incorporate into interphase nuclei in patches as part of nuclear membrane expansion during cell growth in *Drosophila* blastoderm embryos (Hampoelz *et al.*, 2016).

This again implies a key role for CHMP7 in ensuring insertion or organisation of nuclear pore complexes, although the mechanism by which NPC insertion at occurs it is still not clear. A role for Chm7 (the yeast homologue of CHMP7) in conjunction with Heh1, a yeast LEM protein, in nuclear pore complex surveillance and quality control has been recently shown by Webster *et al.* (2016). The results shown here may represent the first evidence of a role for CHMP7, possibly in conjunction with the ESCRT-III complex, in nuclear pore complex quality control and insertion in human cells.

6.3 Future work

It appears that CHMP7 loss may drive cell death by multiple mechanisms, including aberrant mitosis and loss of nuclear envelope integrity and function. Therefore, to dissect the interplay between the various abnormalities observed and cellular processes affected, a starting point for future studies should address the cause of the loss of centrosome cohesion in CHMP7-depleted interphase cells. It will also be important to determine why the cell lines in which premature centrosome separation and nuclear-centrosome linker function were observed, HeLa and U2OS, demonstrated different phenotypes in response to CHMP7 depletion. In the context of the other results presented in this thesis, these data support an indirect effect of CHMP7 depletion on centrosome cohesion, via loss of nuclear envelope integrity, rather than an active role in maintaining centrosome anchoring. As discussed in Section 3.3.1, new preliminary results (Dr N Flores-Rodriguez) demonstrate an increase in multipolar mitoses deriving from fragmenting spindle poles following CHMP7 depletion.

The interaction of CHMP7 and ESCRT-III with micronuclei and chromosome bridges is a new area which requires much more investigation. The mechanism by which DNA is sensed passing through the cleavage furrow is unknown, however it is known that such bridges activate the NoCut abscission checkpoint, which is modulated through the CPC and CHMP4C. Activation of the checkpoint is relayed to the cytokinetic ESCRT-III complex, causing delay of ESCRT-III resolution. Understanding the mechanisms of CHMP7 at the nuclear envelope of the bridge in relation to the abscission checkpoint will clarify this important question, and allow further understanding of its physiological relevance and role in genome instability and tumourigenesis.

The ability to observe and image live cells will also allow us to determine more clearly the origin of micronuclei and bridges to which CHMP7 localise, and determine at which point in their formation or collapse/resolution CHMP7 and ESCRT-III localise to these structures. It

will also allow us to determine the fate of these micronuclei and bridges following CHMP7 localisation, and thus determine more clearly the role of ESCRT-III.

6.3.1 CHMP7 as a target for cancer therapy

One of the most interesting application of the work presented in this thesis is the potential for targeting CHMP7 to develop new therapeutic approaches in cancer treatment. Metastatic cancer cells appear to rely heavily on the ability of ESCRT-III to repair the frequent nuclear ruptures which occur as part of their migration (Denais *et al.*, 2016; Raab *et al.*, 2016). Targeting the ability of cancer cells to repair themselves following migration through tissues may specifically affect invasive and metastatic cells, which rely on NE repair to a greater extent than normal cells which are not exposed to such extracellular pressures.

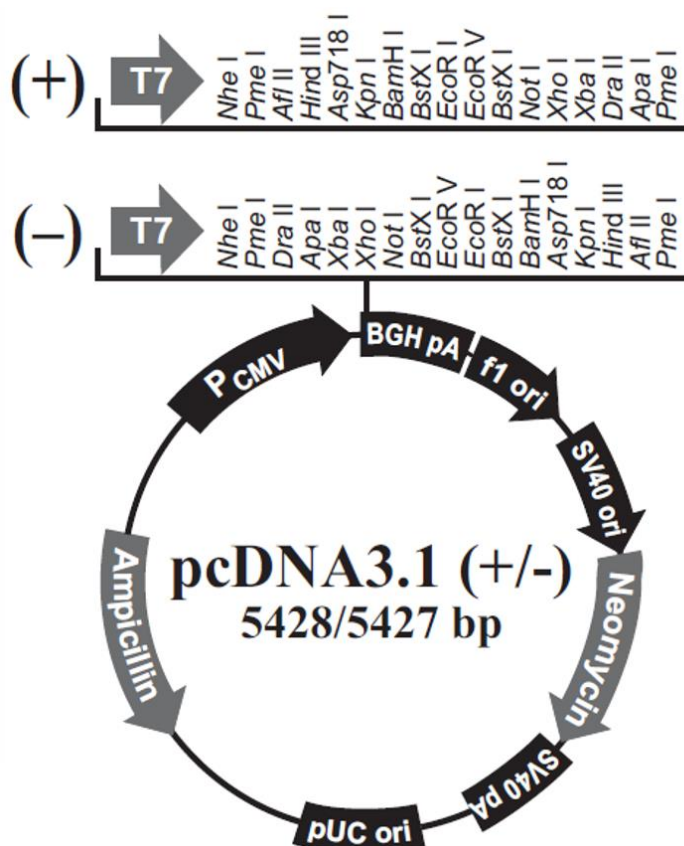
Both of the above papers demonstrate that neither abolishing the NE repair (through either CHMP3 depletion or dominant-negative VPS4 expression) or DNA damage repair systems alone caused significant cell death, indicating a need for a combined approach. This could be achieved through utilising current therapies which target DNA damage repair, or by targeting CHMP7 – as the toxicity of its depletion alone has been demonstrated in this thesis. Based on findings from this study and present research, it appears that targeting of CHMP7 function could allow the nuclear function of ESCRT-III to be specifically abrogated, without affecting the other key activities of ESCRT-III, if this were found to be a desirable approach to treating cancerous cells.

Appendix 1

Vector and cloning site map – pcDNA 3.1+

Vector and cloning maps obtained from ThermoFisher.

pcDNA 3.1+ catalogue number: V79020



```

          enhancer region (3' end)
689  CATTGACGTC AATGGGAGTT TGTTTTGGCA CCAAATCAA CGGGACTTTC CAAATGTCC
          CAAT
749  TAACAACTCC GCCCATTGA CGCAAATGGG CGGTAGGCGT GTACGGTGGG AGGTCTATAT
          3' end of hCMV
          putative transcriptional start
809  AAGCAGAGCT CTCTGGCTAA CTAGAGAACC CACTGCTTAC TGGCTTATCG AAATTAATAC
T7 promoter/primer binding site
869  GACTCACTAT AGGGAGACCC AAGCTGGGCTA GCGTTTAAAC TTAAGCTTGG TACCGAGCTC
          BamH I
          BstX I* EcoR I
          EcoR V
          BstX I* Not I Xho I
929  GGATCCACTA GTCCAGTGTG GTGGAATTCT GCAGATATCC AGCACAGTGG CGGCCGCTCG
          Xba I
          Apa I Pme I
          pcDNA3.1/BGH reverse priming site
989  AGTCTAGAGG GCCCGTTTAA ACCCGCTGAT CAGCCTCGAC TGTGCCTTCT AGTTGCCAGC
1049 CATCTGTTGT TTGCCCTCC CCGTGCCTT CCTTGACCCT GGAAGGTGCC ACTCCACTG
          BGH poly (A) site
1109 TCCTTTCCTA ATAAAATGAG GAAATTGCAT
    
```

CHMP7 HA-tagged constructs

RESTRICTION SITE-START CODON-HA-TAG-STOP CODON-CHMP7

Full-length CHMP7 PCR primer

5' - CTC GTC GGA TCC ATG TAT CCG TAT GAT GTG CCG GAT TAT
GCC TGG TCC CCG GAG CGG GAG - 3'

5' - CTC GTC GAA TTC CTA CAA TGG CTT TAG AGT CGG - 3'

N-terminal half CHMP7 PCR primers

5' - CTC GTC GGA TCC ATG TAT CCG TAT GAT GTG CCG GAT TAT
GCC TGG TCC CCG GAG CGG GAG - 3'

5' - CTC GTC GAA TTC CTA CCC TCG GGC AAA CTT CAC - 3'

HA-tagged full length CHMP7 construct

RESTRICTION SITE-START CODON-HA-TAG-CHMP7 CDS-STOP CODON-RESTRICTION SITE

DNA sequence

GGATCCATGTATCCATATGATGTTCCAGATTATGCTTGGTCCCCGGAGCGGGAGGC
CGAGGCCCCAGCCGGGGGAGACCCGGCGGGCCTTCTGCCCCCCGAGTGGGAGGAGG
ACGAGGAGCGCATGTCTTCTGTTCTCCGCTTTCAAGAGGAGTCGCGAGGTGAAC
AGCACCGACTGGGACAGCAAGATGGGCTTCTGGGCGCCGTTGGTGCTGAGCCACAG
CCGCCGCCAGGGGGTGGTGCGCCTGCGTCTGCGGGACTTGCAGGAGGCCCTTTCAGC
GCAAGGGGAGCGTCCCGCTGGGGCTGGCCACGGTGCTGCAGGACCTGCTGCGTCGA
GGGAGCTGCAGCGGGAGTCAGACTTCATGGCCAGTGTAGACAGCAGCTGGATCTC
CTGGGGGGTGGGGTCTTCTGCTGAAGCCTCTCAAGTGGACTCTTTCTAACATGC
TGGGAGATAATAAGGTTCCAGCTGAGGAGGTCCTTGTGCTGTGGAGCTGTTGAAG
GAAAAGGCTGAGGAGGTGTATCGTCTGTATCAGAACTCGCCCCTCTCCTCCCACCC
CGTGGTGGCCCTGTCAGAGCTCAGCACCTCTGTGCTAACTCCTGCCAGATGAGA
GGACCTTCTACTTGGTGTTGCTGCAGCTGCAGAAGGAGAAGAGGGTCACAGTCCTC
GAGCAGAACGGGAGAAAGATTGTGAAGTTTGCCCCGAGGGCCACGTGCCAAGGTCTC
TCCAGTCAATGACGTAGATGTTGGGGTGTACCAGCTGATGCAGAGTGAACAGCTTC
TCTCACGCAAAGTGGAGTCCTTATCCCAGGAAGCAGAGAGGTGTAAAGAAGAAGCC
CGCCGGGCATGCCGAGCAGGAAAGAAGCAGCTGGCACTGAGGTCTCTCAAGGCCAA
GCAACGGACAGAGAAGCGCATCGAGGCCTTGCATGCCAAGCTGGACACTGTTCAAG
GCATCCTGGACCGGATCTATGCCTCCAGACAGATCAGATGGTTTTTAACGCCTAC
CAGGCTGGGGTAGGAGCACTCAAACCTCCATGAAGGATGTCACAGTGGAGAAGGC
AGAGAGCCTCGTGGATCAGATCCAAGAGCTCTGTGACACCCAGGATGAAGTTTTCTC
AGACTCTGGCTGGTGGGGTAACAAATGGCTTAGATTTTGACAGTGAAGAACTGGAG
AAGGAATTGGACATCCTCCTTCAGGATAACCACCAAGAACCTTTGGATCTGCCTGA
CAACCCCGCAATAGGCATTTTACCAACAGCGTGCCTAACCCCTAGGATCTCAGATG

CTGAACTTGAAGCTGAACTTGAGAACTGTCCTTATCAGAGGGAGGTTTGGTCCCAAGCA
GTAAATCTCCAAAAGGCAATTGGAACCGACTCTAAAGCCATTG**TAGGAATC**

Protein sequence

GSMYPYDVPDYAWSPEREAEAPAGGDPAGLLPPEWEEDEERMSFLFSAFKRSREVN
STDWDSKMGFWAPLVLSHSRRQGVVRLRLRDLQEAFQRKGSVPLGLATVLQDLLRR
GELQRESDFMASVDSSWISWGVGVFLKPLKWTLSNMLGDNKVPAAEVLVAVELLK
EKAEEVYRLYQNSPLSSHPPVVALSELSTLCANSCPDERTFYLVLLQLQKEKRVTVL
EQNGEKIVKFARGPRAKVPVNDVDVGVYQLMQSEQLLSRKVESLSQEAERCKEEA
RRACRAGKKQLALRSLKAKQRTEKRIEALHAKLDTVQGILDRIYASQTDQMVFNAY
QAGVGALKLSMKDVTVEKAESLVDQIQELCDTQDEVSQTLAGGVVNTGLDFDSEELE
KELDILLQDTTKEPLDLPNPNRHRFTNSVNPRI SDAELEAELEKLSLSEGGLVP
SSKSPKRQLEPTLKPL**-EF**

HA-tagged N-terminal CHMP7 construct (amino acids 1-226)

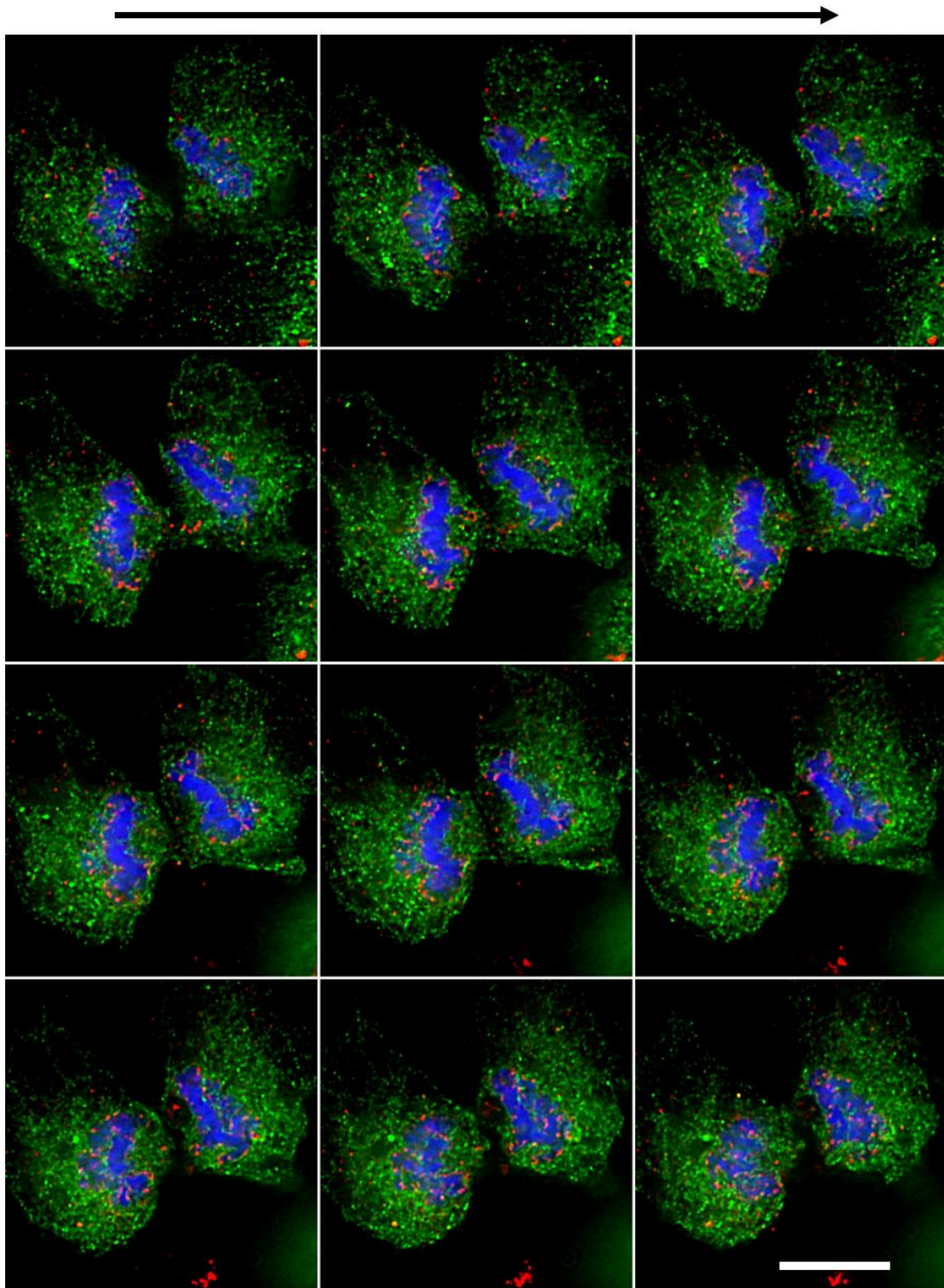
DNA sequence

GGATCCATGTTATCCATATGATGTTCCAGATTATGCTTGGTCCCCGGAGCGGGAGGC
CGAGGCCCCAGCCGGGGGAGACCCGGCGGGCCCTTCTGCCCCCGAGTGGGAGGAGG
ACGAGGAGCGCATGTCCTTCTGTTCTCCGCTTTC AAGAGGAGTCGCGAGGTGAAC
AGCACCGACTGGGACAGCAAGATGGGCTTCTGGGCGCCGTTGGTGCTGAGCCACAG
CCGCCGCCAGGGGGTGGTGCGCCTGCGTCTGCGGGACTTGCAGGAGGCCTTTCAGC
GCAAGGGGAGCGTCCCGCTGGGGCTGGCCACGGTGCTGCAGGACCTGCTGCGTCTGA
GGGAGCTGCAGCGGGAGTCAGACTTCATGGCCAGTGTAGACAGCAGCTGGATCTC
CTGGGGGGTTGGGGTCTTCTGCTGAAGCCTCTCAAGTGGACTCTTCTAACATGC
TGGGAGATAATAAGGTTCCAGCTGAGGAGGTCCTTGTGCGTGTGGAGCTGTTGAAG
GAAAAGGCTGAGGAGGTGTATCGTCTGTATCAGAACTCGCCCCTCTCCTCCCACCC
CGTGGTGGCCCTGTCAGAGCTCAGCACCCCTCTGTGCTAACTCCTGCCCAGATGAGA
GGACCTTCTACTTGGTGTGCTGCAGCTGCAGAAGGAGAAGGGGTCACAGTCCTC
GAGCAGAACGGGAGAAGATTGTGAAGTTTGGCCGAGG**TAGGAATC**

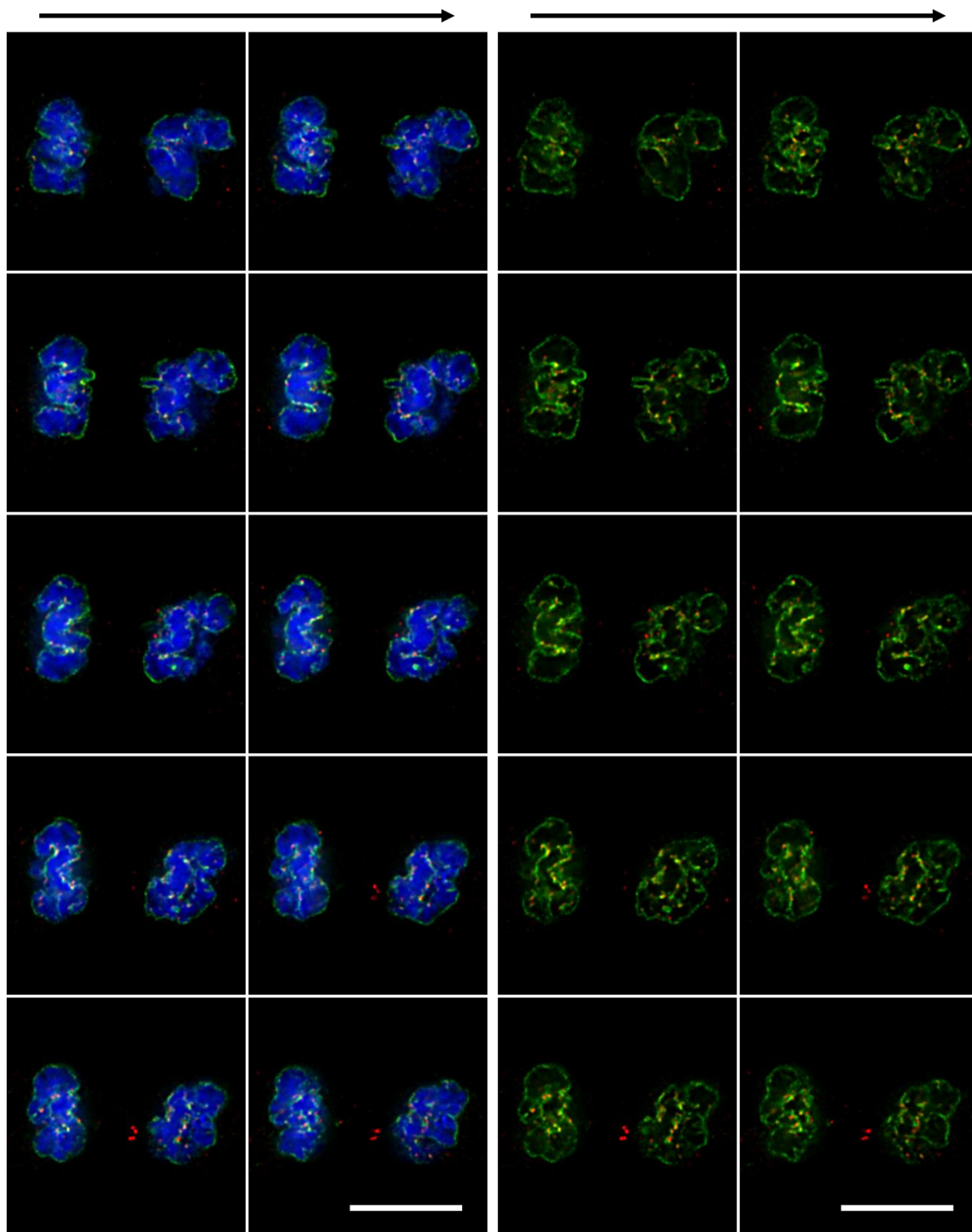
Protein sequence

GSMYPYDVPDYAWSPEREAEAPAGGDPAGLLPPEWEEDEERMSFLFSAFKRSREVN
STDWDSKMGFWAPLVLSHSRRQGVVRLRLRDLQEAFQRKGSVPLGLATVLQDLLRR
GELQRESDFMASVDSSWISWGVGVFLKPLKWTLSNMLGDNKVPAAEVLVAVELLK
EKAEEVYRLYQNSPLSSHPPVVALSELSTLCANSCPDERTFYLVLLQLQKEKRVTVL
EQNGEKIVKFARG**-EF**

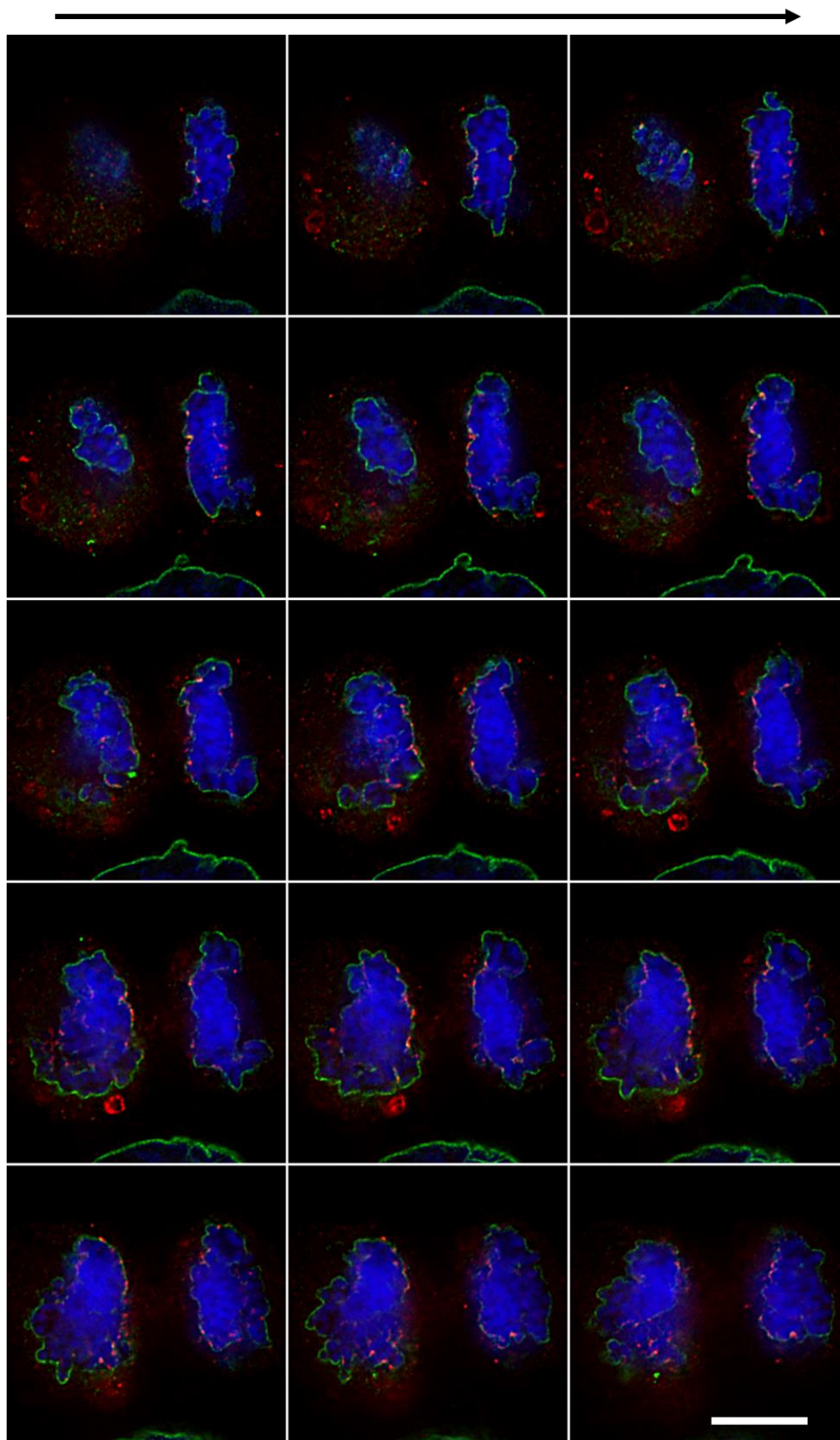
Appendix 2



Appendix 2a - Deconvolved image taken on Deltavision microscope showing juxtapposition of CHMP7 (red) and PDI (green) with chromatin (DAPI, blue) staining in telophase U2OS cell. Slices are spaced 0.2 μ m apart. Scale bar represents 10 μ m.



Appendix 2b - Deconvolved image taken on Deltavision microscope showing juxtaposition of CHMP7 (red) and LAP2 (green) with chromatin (DAPI, blue) staining in telophase U2OS cell. Slices are spaced 0.3 μ m apart. Scale bar represents 10 μ m. Right panel omits the DAPI channel.



Appendix 2c - Deconvolved image taken on Deltavision microscope showing juxtapposition of CHMP7 (red) and Lamin B (green) with chromatin (DAPI, blue) staining in telophase U2OS cell. Slices are spaced 0.2 μ m apart. Scale bar represents 10 μ m.

References

Chapter 1 and Chapter 2

- Adell MAY, Vogel GF, Pakdel M, Müller M, Lindner H, Hess MW, and Teis D. (2014). Coordinated binding of Vps4 to ESCRT-III drives membrane neck constriction during MVB vesicle formation. *Journal of Cell Biology*, 205 (1), 33–49.
- Agromayor M, and Martin-Serrano J. (2006). Interaction of AMSH with ESCRT-III and deubiquitination of endosomal cargo. *Journal of Biological Chemistry*, 281 (32), 23083–23091.
- Azmi I, Davies B, Dimaano C, Payne J, Eckert D, Babst M, and Katzmann DJ. (2006). Recycling of ESCRTs by the AAA-ATPase Vps4 is regulated by a conserved VSL region in Vta 1. *Journal of Cell Biology*, 172 (5), 705–717.
- Babst M, Katzmann DJ, Estepa-Sabal EJ, Meerloo T, and Emr SD. (2002a). ESCRT-III: An Endosome-Associated Heterooligomeric Protein Complex Required for MVB Sorting. *Developmental Cell*, 3 (2), 271–282.
- Babst M, Katzmann DJ, Snyder WB, Wendland B, and Emr SD. (2002b). Endosome-associated complex, ESCRT-II, recruits transport machinery for protein sorting at the multivesicular body. *Developmental Cell*, 3 (2), 283–289.
- Babst M, Wendland B, Estepa EJ, and Emr SD. (1998). The Vps4p AAA ATPase regulates membrane association of a Vps protein complex required for normal endosome function. *EMBO Journal*, 17 (11), 2982–2993.
- Bajorek M, Morita E, Skalicky JJ, Morham SG, Babst M, and Sundquist WI. (2009a). Biochemical analyses of human IST1 and its function in cytokinesis. *Molecular Biology of the Cell*, 20 (5), 1360–73.
- Bajorek M, Schubert HL, McCullough J, Langelier C, Debra M, Stubblefield WB, Uter NT, Myszka DG, Christopher P, and Sundquist WI. (2010). NIH Public Access. *Nature Structural & Molecular Biology*, 16 (7), 754–762.
- Bajorek M, Schubert HL, McCullough J, Langelier C, Eckert DM, Stubblefield W-MB, Uter NT, Myszka DG, Hill CP, and Sundquist WI. (2009b). Structural basis for ESCRT-III protein autoinhibition. *Nature Structural and Molecular Biology*, 16 (7), 754–62.
- Barlin JN, Jelinic P, Olvera N, Bogomolny F, Bisogna M, Dao F, Barakat RR, Chi DS, and Levine DA. (2013). Validated gene targets associated with curatively treated advanced serous ovarian carcinoma. *Gynecologic Oncology*, 128 (3), 512–517.
- Bastos RN, and Barr FA. (2010). Plk1 negatively regulates Cep55 recruitment to the midbody to ensure orderly abscission. *Journal of Cell Biology*, 191 (4), 751–760.
- Berg TO, Fengsrud M, Stromhaug P, Berg T, and Seglen P. (1998). Evidence for Fusion of Autophagosomes With Both Early and Late Endosomes. *Journal of Biological Chemistry*, 273 (34), 21883–92.

- Bishop N, and Woodman P. (2001). TSG101/Mammalian VPS23 and Mammalian VPS28 Interact Directly and Are Recruited to VPS4-induced Endosomes. *Journal of Biological Chemistry*, 276 (15), 11735–11742.
- Bobrie A, Colombo M, Krumeich S, Raposo G, and Théry C. (2012). Diverse subpopulations of vesicles secreted by different intracellular mechanisms are present in exosome preparations obtained by differential ultracentrifugation. *Journal of Extracellular Vesicles*, 1, 18397.
- Carlton JG, and Martin-Serrano J. (2007). Parallels between cytokinesis and retroviral budding: a role for the ESCRT machinery. *Science*, 316 (5833), 1908–12.
- Carlton JG, Caballe A, Agromayor M, Kloc M, and Martin-Serrano J. (2012). ESCRT-III governs the Aurora B-mediated abscission checkpoint through CHMP4C. *Science*, 336 (6078), 220–5.
- Chen D, Wilkinson CRM, Watt S, Penkett CJ, Toone WM, Jones N, and Bähler J. (2007). High-Resolution Crystal Structure and In Vivo Function of a Kinesin-2 Homologue in *Giardia intestinalis*. *Molecular Biology of the Cell*, 19 (1), 308–317. Adell MAY, Vogel GF, Pakdel M, Müller M, Lindner H, Hess MW, and Teis D. (2014). Coordinated binding of Vps4 to ESCRT-III drives membrane neck constriction during MVB vesicle formation. *Journal of Cell Biology*, 205 (1), 33–49.
- Agromayor M, and Martin-Serrano J. (2006). Interaction of AMSH with ESCRT-III and deubiquitination of endosomal cargo. *Journal of Biological Chemistry*, 281 (32), 23083–23091.
- Azmi I, Davies B, Dimaano C, Payne J, Eckert D, Babst M, and Katzmann DJ. (2006). Recycling of ESCRTs by the AAA-ATPase Vps4 is regulated by a conserved VSL region in Vta 1. *Journal of Cell Biology*, 172 (5), 705–717.
- Babst M, Katzmann DJ, Estepa-Sabal EJ, Meerloo T, and Emr SD. (2002a). ESCRT-III: An Endosome-Associated Heterooligomeric Protein Complex Required for MVB Sorting. *Developmental Cell*, 3 (2), 271–282.
- Babst M, Katzmann DJ, Snyder WB, Wendland B, and Emr SD. (2002b). Endosome-associated complex, ESCRT-II, recruits transport machinery for protein sorting at the multivesicular body. *Developmental Cell*, 3 (2), 283–289.
- Babst M, Wendland B, Estepa EJ, and Emr SD. (1998). The Vps4p AAA ATPase regulates membrane association of a Vps protein complex required for normal endosome function. *EMBO Journal*, 17 (11), 2982–2993.
- Bajorek M, Morita E, Skalicky JJ, Morham SG, Babst M, and Sundquist WI. (2009a). Biochemical analyses of human IST1 and its function in cytokinesis. *Molecular Biology of the Cell*, 20 (5), 1360–73.
- Bajorek M, Schubert HL, Mccullough J, Langelier C, Debra M, Stubblefield WB, Uter NT, Myszka DG, Christopher P, and Sundquist WI. (2010). NIH Public Access. *Nature Structural & Molecular Biology*, 16 (7), 754–762.

- Bajorek M, Schubert HL, McCullough J, Langelier C, Eckert DM, Stubblefield W-MB, Uter NT, Myszka DG, Hill CP, and Sundquist WI. (2009b). Structural basis for ESCRT-III protein autoinhibition. *Nature Structural and Molecular Biology*, *16* (7), 754–62.
- Barlin JN, Jelinic P, Olvera N, Bogomolny F, Bisogna M, Dao F, Barakat RR, Chi DS, and Levine DA. (2013). Validated gene targets associated with curatively treated advanced serous ovarian carcinoma. *Gynecologic Oncology*, *128* (3), 512–517.
- Bastos RN, and Barr FA. (2010). Plk1 negatively regulates Cep55 recruitment to the midbody to ensure orderly abscission. *Journal of Cell Biology*, *191* (4), 751–760.
- Berg TO, Fengsrud M, Stromhaug P, Berg T, and Seglen P. (1998). Evidence for Fusion of Autophagosomes With Both Early and Late Endosomes. *Journal of Biological Chemistry*, *273* (34), 21883–92.
- Bishop N, and Woodman P. (2001). TSG101/Mammalian VPS23 and Mammalian VPS28 Interact Directly and Are Recruited to VPS4-induced Endosomes. *Journal of Biological Chemistry*, *276* (15), 11735–11742.
- Bobrie A, Colombo M, Krumeich S, Raposo G, and Théry C. (2012). Diverse subpopulations of vesicles secreted by different intracellular mechanisms are present in exosome preparations obtained by differential ultracentrifugation. *Journal of Extracellular Vesicles*, *1*, 18397.
- Carlton JG, and Martin-Serrano J. (2007). Parallels between cytokinesis and retroviral budding: a role for the ESCRT machinery. *Science*, *316* (5833), 1908–12.
- Carlton JG, Caballe A, Agromayor M, Kloc M, and Martin-Serrano J. (2012). ESCRT-III governs the Aurora B-mediated abscission checkpoint through CHMP4C. *Science*, *336* (6078), 220–5.
- Chen D, Wilkinson CRM, Watt S, Penkett CJ, Toone WM, Jones N, and Bähler J. (2007). High-Resolution Crystal Structure and In Vivo Function of a Kinesin-2 Homologue in *Giardia intestinalis*. *Molecular Biology of the Cell*, *19* (1), 308–317.
- Cimini D, Moree B, Canman JC, and Salmon ED. (2003). Merotelic kinetochore orientation occurs frequently during early mitosis in mammalian tissue cells and error correction is achieved by two different mechanisms. *Journal of Cell Science*, *116* (20), 4213–4225.
- Cleasby, A (2013) Investigating the role of a novel nuclear ESCRT-III assembly (PhD Thesis, University of Sheffield).
- Colombo M, Moita C, van Niel G, Kowal J, Vigneron J, Benaroch P, Manel N, Moita LF, Théry C, Raposo G, et al. (2013). Analysis of ESCRT functions in exosome biogenesis, composition and secretion highlights the heterogeneity of extracellular vesicles. *Journal of Cell Science*, *126* (24), 5553–65.
- Dudek SM, Chiang ET, Camp SM, Guo Y, Zhao J, Brown ME, Singleton PA, Wang L, Desai A, Arce FT, et al. (2010). Abl tyrosine kinase phosphorylates nonmuscle Myosin light chain kinase to regulate endothelial barrier function. *Molecular Biology of the Cell*, *21* (22), 4042–4056.

- Elia N, Fabrikant G, Kozlov MM, and Lippincott-Schwartz J. (2012). Computational model of cytokinetic abscission driven by ESCRT-III polymerization and remodeling. *Biophysical Journal*, 102 (10), 2309–2320.
- Fenech M, Chang WP, Kirsch-Volders M, Holland N, Bonassi S, and Zeiger E. (2003). HUMN project: Detailed description of the scoring criteria for the cytokinesis-block micronucleus assay using isolated human lymphocyte cultures. *Mutation Research - Genetic Toxicology and Environmental Mutagenesis*, 534 (1–2), 65–75.
- Feng Z, Hensley L, McKnight KL, Hu F, Madden V, Ping L, Jeong S, Walker C, Lanford R, and Lemon SM. (2013). A pathogenic picornavirus acquires an envelope by hijacking cellular membranes. *Nature*, 496 (7445), 367–371.
- Francis N, Kingston R, and Woodcock C. (2004). Chromatin Compaction by a Polycomb Group Protein Complex. *Science*, 306 (5701), 1574–1577.
- Fyfe I, Schuh AL, Edwardson JM, and Audhya A. (2011). Association of the endosomal sorting complex ESCRT-II with the Vps20 subunit of ESCRT-III generates a curvature-sensitive complex capable of nucleating ESCRT-III filaments. *Journal of Biological Chemistry*, 286 (39), 34262–34270.
- Ghazi-Tabatabai S, Saksena S, Short JM, Pobbati A V., Veprintsev DB, Crowther RA, Emr SD, Egelman EH, and Williams RL. (2008). Structure and Disassembly of Filaments Formed by the ESCRT-III Subunit Vps24. *Structure*, 16 (9), 1345–1356.
- Gisselsson D, Pettersson L, Höglund M, Heidenblad M, Gorunova L, Wiegant J, Mertens F, Dal Cin P, Mitelman F, and Mandahl N. (2000). Chromosomal breakage-fusion-bridge events cause genetic intratumor heterogeneity. *Proceedings of the National Academy of Sciences*, 97 (10), 5357–62.
- Glotzer M. (2004). Cleavage furrow positioning. *Journal of Cell Biology*, 164 (3), 347–351.
- Hanson PI, Roth R, Lin Y, and Heuser JE. (2008). Plasma membrane deformation by circular arrays of ESCRT-III protein filaments. *Journal of Cell Biology*, 180 (2), 389–402.
- Härtel T, and Schwille P. (2014). ESCRT-III mediated cell division in *Sulfolobus acidocaldarius* - A reconstitution perspective. *Frontiers in Microbiology*, 4 (5), 257.
- Hartmann C, Chami M, Zachariae U, de Groot BL, Engel A, and Grütter MG. (2008). Vacuolar Protein Sorting: Two Different Functional States of the AAA-ATPase Vps4p. *Journal of Molecular Biology*, 377 (2), 352–363.
- Hill CP, and Babst M. (2012). Structure and function of the membrane deformation AAA ATPase Vps4. *Biochimica et Biophysica Acta - Molecular Cell Research*, 1823 (1), 172–181.
- Horii M, Shibata H, Kobayashi R, Katoh K, Yorikawa C, Yasuda J, and Maki M. (2006). CHMP7, a novel ESCRT-III-related protein, associates with CHMP4b and functions in the endosomal sorting pathway. *The Biochemical Journal*, 400 (1), 23–32.
- Howard TL, Stauffer DR, Degnin CR, and Hollenberg SM. (2001). CHMP1 functions as a

- member of a newly defined family of vesicle trafficking proteins. *Journal of Cell Science*, 114 (13), 2395–2404.
- Im YJ, and Hurley JH. (2009). Integrated structural model and membrane targeting mechanism of the human ESCRT-II complex. *Developmental Cell*, 14 (6), 902–913.
- Jimenez AJ, Maiuri P, Lafaurie-Janvore J, Divoux S, Piel M, and Perez F. (2014). ESCRT Machinery Is Required for Plasma Membrane Repair. *Science*, 343 (6174), 1247136.
- Katoh K, Shibata H, Hatta K, and Maki M. (2004). CHMP4b is a major binding partner of the ALG-2-interacting protein Alix among the three CHMP4 isoforms. *Archives of Biochemistry and Biophysics*, 421 (1), 159–165.
- Kelley LA, and Sternberg MJE. (2009). Protein structure prediction on the Web: a case study using the Phyre server. *Nature Protocols*, 4 (3), 363–371.
- Kirkin V, McEwan DG, Novak I, and Dikic I. (2009). A Role for Ubiquitin in Selective Autophagy. *Molecular Cell*, 34 (3), 259–269.
- Lafaurie-Janvore J, Maiuri P, Wang I, Pinot M, Manneville J-B, Betz T, Balland M, and Piel M. (2013). ESCRT-III Assembly and Cytokinetic Abcission Are Induced by Tension Release in the Intercellular Bridge. *Science*, 339 (6127), 1625–1629.
- Landsberg MJ, Vajjhala PR, Rothnagel R, Munn AL, and Hankamer B. (2009). Three-Dimensional Structure of AAA ATPase Vps4: Advancing Structural Insights into the Mechanisms of Endosomal Sorting and Enveloped Virus Budding. *Structure*, 17 (3), 427–437.
- Langelier C, von Schwedler UK, Fisher RD, De Domenico I, White PL, Hill CP, Kaplan J, Ward D, and Sundquist WI. (2006). Human ESCRT-II complex and its role in human immunodeficiency virus type 1 release. *Journal of Virology*, 80 (19), 9465–9480.
- Lata S, Roessle M, Solomons J, Jamin M, Gottlinger HG, Svergun DI, and Weissenhorn W. (2008). Structural Basis for Autoinhibition of ESCRT-III CHMP3. *Journal of Molecular Biology*, 378 (4), 816–825.
- Lee HH, Elia N, Ghirlando R, Lippincott-schwartz J, and Hurley H. (2009a). NIH Public Access. *Science*, 322 (5901), 576–580.
- Lee JA, Liu L, and Gao FB. (2009b). Autophagy defects contribute to neurodegeneration induced by dysfunctional ESCRT-III. *Autophagy*, 5 (7), 1070–1072.
- Li J, Belogortseva N, Porter D, and Park M. (2008). Chmp1A functions as a novel tumor suppressor gene in human embryonic kidney and ductal pancreatic tumor cells. *Cell Cycle*, 7 (18), 2886–2893.
- Lindås A-C, Karlsson EA, Lindgren MT, Ettema TJG, and Bernander R. (2008). A unique cell division machinery in the Archaea. *Proceedings of the National Academy of Sciences*, 105 (48), 18942–6.
- Lini Y, Kimpler LA, Naismith T V., Lauer JM, and Hanson PI. (2005). Interaction of the

- mammalian Endosomal Sorting Complex Required for Transport (ESCRT) III protein hSnf7-1 with itself, membranes, and the AAA + ATPase SKD1. *Journal of Biological Chemistry*, 280 (13), 12799–12809.
- Lottridge JM, Flannery AR, Vincelli JL, and Stevens TH. (2006). Vta1p and Vps46p regulate the membrane association and ATPase activity of Vps4p at the yeast multivesicular body. *Proceedings of the National Academy of Sciences*, 103 (16), 6202–7.
- Manohar S, Harlow M, Nguyen H, Li J, Hankins GR, and Park M. (2011). Chromatin modifying protein 1A (Chmp1A) of the endosomal sorting complex required for transport (ESCRT)-III family activates ataxia telangiectasia mutated (ATM) for PanC-1 cell growth inhibition. *Cell Cycle*, 10 (15), 2529–2539.
- McCullough J, Fisher RD, Whitby FG, Sundquist WI, and Hill CP. (2008). ALIX-CHMP4 interactions in the human ESCRT pathway. *Proceedings of the National Academy of Sciences*, 105 (22), 7687–7691.
- Mizushima N, Levine B, Cuervo AM, and Klionsky DJ. (2008). Autophagy fights disease through cellular self-digestion. *Nature*, 451 (7182), 1069–75.
- Mochida GH, Ganesh VS, de Michelena MI, Dias H, Atabay KD, Kathrein KL, Huang H-T, Hill RS, Felie JM, Rakiec D, et al. (2012). CHMP1A encodes an essential regulator of BMI1-INK4A in cerebellar development. *Nature Genetics*, 44 (11), 1260–4.
- Monroe N, Han H, Gonciarz MD, Eckert DM, Karren MA, Whitby FG, Sundquist WI, and Hill CP. (2014). The oligomeric state of the active Vps4 AAA ATPase. *Journal of Molecular Biology*, 426 (3), 510–525.
- Mora-Bermúdez F, Gerlich D, and Ellenberg J. (2007). Maximal chromosome compaction occurs by axial shortening in anaphase and depends on Aurora kinase. *Nature Cell Biology*, 9 (7), 822–831.
- Morita E, Colf LA, Karren MA, Sandrin V, Rodesch CK, and Sundquist WI. (2010). Human ESCRT-III and VPS4 proteins are required for centrosome and spindle maintenance. *Proceedings of the National Academy of Sciences*, 107 (29), 12889–94.
- Morita E, Sandrin V, Chung H-Y, Morham SG, Gygi SP, Rodesch CK, and Sundquist WI. (2007). Human ESCRT and ALIX proteins interact with proteins of the midbody and function in cytokinesis. *The EMBO Journal*, 26 (19), 4215–27.
- Musacchio A, and Hardwick KG. (2002). The spindle checkpoint: structural insights into dynamic signalling. *Nature Reviews Molecular Cell Biology*, 3 (10), 731–741.
- Muzioł T, Pineda-Molina E, Ravelli RB, Zamborlini A, Usami Y, Göttlinger H, and Weissenhorn W. (2006). Structural Basis for Budding by the ESCRT-III Factor CHMP3. *Developmental Cell*, 10 (6), 821–830.
- Nakatogawa H, Suzuki K, Kamada Y, and Ohsumi Y. (2009). Dynamics and diversity in autophagy mechanisms: lessons from yeast. *Nature Reviews Molecular Cell Biology*, 10 (7), 458–467.

- Nanba K, and Toyooka S. (2008). The allelic distribution of a single nucleotide polymorphism in the PDCD5 gene locus of Japanese non-small cell lung cancer patients. *Molecular Medicine Reports*, 1 (5), 667–671.
- Nickerson DP, West M, and Odorizzi G. (2006). Did2 coordinates Vps4-mediated dissociation of ESCRT-III from endosomes. *Journal of Cell Biology*, 175 (5), 715–720.
- Norden C, Mendoza M, Dobbelaere J, Kotwaliwale C V., Biggins S, and Barral Y. (2006). The NoCut Pathway Links Completion of Cytokinesis to Spindle Midzone Function to Prevent Chromosome Breakage. *Cell*, 125 (1), 85–98.
- Oshima R, Hasegawa T, Tamai K, Sugeno N, Yoshida S, Kobayashi J, Kikuchi A, Baba T, Futatsugi A, Sato I, et al. (2016). ESCRT-0 dysfunction compromises autophagic degradation of protein aggregates and facilitates ER stress-mediated neurodegeneration via apoptotic and necroptotic pathways. *Scientific Reports*, 6 (April), 24997.
- Parkinson N, Ince PG, Smith MO, Highley R, Skibinski G, Andersen PM, Morrison KE, Pall HS, Hardiman O, Collinge J, et al. (2006). ALS phenotypes with mutations in CHMP2B (charged multivesicular body protein 2B). *Neurology*, 67 (6), 1074–1077.
- Peck JW, Bowden ET, and Burbelo PD. (2004). Structure and function of human Vps20 and Snf7 proteins. *The Biochemical Journal*, 377 (3), 693–700.
- Pharoah PDP, Tsai Y-Y, Ramus SJ, Phelan CM, Goode EL, Lawrenson K, Buckley M, Fridley BL, Tyrer JP, Shen H, et al. (2013). GWAS meta-analysis and replication identifies three new susceptibility loci for ovarian cancer. *Nature Genetics*, 45 (4), 362–70, 370–2.
- Pornillos O, Higginson DS, Stray KM, Fisher RD, Garrus JE, Payne M, He GP, Wang HE, Morham SG, and Sundquist WI. (2003). HIV Gag mimics the Tsg101-recruiting activity of the human Hrs protein. *Journal of Cell Biology*, 162 (3), 425–434.
- Raymond CK, I H-S, Vater CA, and Stevens TH. (1992). Morphological classification of the yeast vacuolar protein sorting mutants: evidence for a prevacuolar compartment in class E VPS mutants. *Molecular Biology of the Cell*, 3 (12), 1389–1402.
- Roll-Mecak A, and Vale RD. (2008). Structural basis of microtubule severing by the hereditary spastic paraplegia protein spastin. *Nature*, 451 (7176), 363–367.
- Rusten TE, and Stenmark H. (2009). How do ESCRT proteins control autophagy? *Journal of Cell Science*, 122 (13), 2179–2183.
- Saksena S, Wahlman J, Teis D, Johnson AE, and Emr SD. (2009). Functional Reconstitution of ESCRT-III Assembly and Disassembly. *Cell*, 136 (1), 97–109.
- Samson RY, and Bell SD. (2009). Ancient ESCRTs and the evolution of binary fission. *Trends in Microbiology*, 17 (11), 507–513.
- Samson RY, Obita T, Freund SM, and Williams RL. (2014). A Role for the ESCRT System in Cell Division in Archaea. *Science*, 322 (5908), 1710–1713.

- Scheffer LL, Sreetama SC, Sharma N, Medikayala S, Brown KJ, Defour A, and Jaiswal JK. (2014). Mechanism of Ca²⁺-triggered ESCRT assembly and regulation of cell membrane repair. *Nature Communications*, 5, 5646.
- Scheuring S, Röhrich R a, Schöning-Burkhardt B, Beyer A, Müller S, Abts HF, and Köhler K. (2001). Mammalian cells express two VPS4 proteins both of which are involved in intracellular protein trafficking. *Journal of Molecular Biology*, 312 (3), 469–80.
- Scott A, Chung H-Y, Gonciarz-Swiatek M, Hill GC, Whitby FG, Gaspar J, Holton JM, Viswanathan R, Ghaffarian S, Hill CP, et al. (2005). Structural and mechanistic studies of VPS4 proteins. *The EMBO Journal*, 24 (20), 3658–69.
- Shi T, Dong Y, Li J, Gao P, Fu D, and Ma D. (2010). High-throughput screening identifies CHMP4A associated with hypoxia-inducible factor 1. *Life Sciences*, 87 (19–22), 604–608.
- Shiels A, Bennett TM, Knopf HLS, Yamada K, Yoshiura K, Niikawa N, Shim S, and Hanson PI. (2007). CHMP4B, a novel gene for autosomal dominant cataracts linked to chromosome 20q. *American Journal of Human Genetics*, 81 (3), 596–606.
- Shim S, Kimpler LA, and Hanson PI. (2007). Structure/function analysis of four core ESCRT-III proteins reveals common regulatory role for extreme C-terminal domain. *Traffic*, 8 (8), 1068–1079.
- Skibinski G, Parkinson NJ, Brown JM, Chakrabarti L, Lloyd SL, Hummerich H, Nielsen JE, Hodges JR, Spillantini MG, Thusgaard T, et al. (2005). Mutations in the endosomal ESCRTIII-complex subunit CHMP2B in frontotemporal dementia. *Nature Genetics*, 37 (8), 806–808.
- Slater R, and Bishop NE. (2006). Genetic structure and evolution of the Vps25 family, a yeast ESCRT-II component. *BMC Evolutionary Biology*, 6 (59), 59.
- Spitzer C, Schellmann S, Sabovljevic A, Shahriari M, Keshavaiah C, Bechtold N, Herzog M, Müller S, Hanisch F-G, and Hülkamp M. (2006). The Arabidopsis elch mutant reveals functions of an ESCRT component in cytokinesis. *Development*, 133 (23), 4679–4689.
- Stauffer DR, Howard TL, Nyun T, and Hollenberg SM. (2001). CHMP1 is a novel nuclear matrix protein affecting chromatin structure and cell-cycle progression. *Journal of Cell Science*, 114 (13), 2383–2393.
- Steigemann P, Wurzenberger C, Schmitz MHA, Held M, Guizetti J, Maar S, and Gerlich DW. (2009). Aurora B-Mediated Abscission Checkpoint Protects against Tetraploidization. *Cell*, 136 (3), 473–484.
- Tada K, Susumu H, Sakuno T, and Watanabe Y. (2011). Condensin association with histone H2A shapes mitotic chromosomes. *Nature*, 474 (7352), 477–483.
- Teichmann M, Dumay-Odelot H, and Fribourg S. (2012). Structural and functional aspects of winged-helix domains at the core of transcription initiation complexes. *Transcription*, 3 (1), 2–7.
- Teis D, Saksena S, and Emr SD. (2008). Ordered Assembly of the ESCRT-III Complex on

- Endosomes Is Required to Sequester Cargo during MVB Formation. *Developmental Cell*, 15 (4), 578–589.
- Uhlen M, Fagerberg L, Hallstrom BM, Lindskog C, Oksvold P, Mardinoglu A, Sivertsson A, Kampf C, Sjostedt E, Asplund A, et al. (2015). Tissue-based map of the human proteome. *Science*, 347 (6220), 1260419–1260419.
- Vajjhala PR, Nguyen CH, Landsberg MJ, Kistler C, Gan AL, King GF, Hankamer B, and Munn AL. (2008). The Vps4 C-terminal helix is a critical determinant for assembly and ATPase activity and has elements conserved in other members of the meiotic clade of AAA ATPases. *FEBS Journal*, 275 (7), 1427–1449.
- Wernimont AK, and Weissenhorn W. (2004). Crystal structure of subunit VPS25 of the endosomal trafficking complex ESCRT-II. *BMC Structural Biology*, 4 (1), 10.
- White SR, and Lauring B. (2007). AAA+ ATPases: Achieving diversity of function with conserved machinery. *Traffic*, 8 (12), 1657–1667.
- Wollert T, Wunder C, Lippincott-schwartz J, Hurley JHJH, and H J. (2009a). Membrane scission by the ESCRT-III complex. *Nature*, 458 (7235), 172–7.
- Wollert T, Yang D, Ren X, Lee HH, Im YJ, and Hurley JH. (2009b). The ESCRT machinery at a glance. *Journal of Cell Science*, 122 (13), 2163–2166.
- Xie W, Li L, and Cohen SN. (1998). Cell cycle-dependent subcellular localization of the TSG101 protein and mitotic and nuclear abnormalities associated with TSG101 deficiency. *Proceedings of the National Academy of Sciences*, 95 (4), 1595–600.
- Yang D, Rismanchi N, Renvoisé B, Lippincott-Schwartz J, Blackstone C, and Hurley JH. (2008). Structural basis for midbody targeting of spastin by the ESCRT-III protein CHMP1B. *Nature Structural & Molecular Biology*, 15 (12), 1278–86.
- Yang M, Coppens I, Wormsley S, Baevova P, Hoppe HC, and Joiner KA. (2004). The Plasmodium falciparum Vps4 homolog mediates multivesicular body formation. *Journal of Cell Science*, 117 (17), 3831–8.
- Yorikawa C, Shibata H, Waguri S, Hatta K, Horii M, Katoh K, Kobayashi T, Uchiyama Y, and Maki M. (2005). Human CHMP6, a myristoylated ESCRT-III protein, interacts directly with an ESCRT-II component EAP20 and regulates endosomal cargo sorting. *The Biochemical Journal*, 387 (1), 17–26.
- Yoshitake Y, Howard TL, Christian JL, and Hollenberg SM. (1999). Misexpression of Polycomb-group proteins in Xenopus alters anterior neural development and represses neural target genes. *Developmental Biology*, 215 (2), 375–87.
- You Z, Xin Y, Liu Y, Sun J, Zhou G, Gao H, Xu P, Chen Y, Chen G, Zhang L, et al. (2012). Chmp1A acts as a tumor suppressor gene that inhibits proliferation of renal cell carcinoma. *Cancer Letters*, 319 (2), 190–196.
- Yu X, Harris SL, and Levine AJ. (2006). The regulation of exosome secretion: A novel function of the p53 protein. *Cancer Research*, 66 (9), 4795–4801.

- Yu X, Riley T, and Levine AJ. (2009). The regulation of the endosomal compartment by p53 the tumor suppressor gene. *FEBS Journal*, 276 (8), 2201–2212.
- Yu Z, Gonciarz MD, Sundquist WI, Hill CP, and Jensen GJ. (2008). Cryo-EM Structure of Dodecameric Vps4p and Its 2:1 Complex with Vta1p. *Journal of Molecular Biology*, 377 (2), 364–377.
- Zamborlini A, Usami Y, Radoshitzky SR, Popova E, Palu G, and Göttlinger H. (2006). Release of autoinhibition converts ESCRT-III components into potent inhibitors of HIV-1 budding. *Proceedings of the National Academy of Sciences*, 103 (50), 19140–5.
- Zhang X, Shaw A, Bates PA, Newman RH, Gowen B, Orlova E, Gorman MA, Kondo H, Dokurno P, Lally J, et al. (2000). Structure of the AAA ATPase p97. *Molecular Cell*, 6 (6), 1473–1484.
- Cimini D, Moree B, Canman JC, and Salmon ED. (2003). Merotelic kinetochore orientation occurs frequently during early mitosis in mammalian tissue cells and error correction is achieved by two different mechanisms. *Journal of Cell Science*, 116 (20), 4213–4225.
- Cleasby, A (2013) Investigating the role of a novel nuclear ESCRT-III assembly (PhD Thesis, University of Sheffield).
- Colombo M, Moita C, van Niel G, Kowal J, Vigneron J, Benaroch P, Manel N, Moita LF, Théry C, Raposo G, et al. (2013). Analysis of ESCRT functions in exosome biogenesis, composition and secretion highlights the heterogeneity of extracellular vesicles. *Journal of Cell Science*, 126 (24), 5553–65.
- Dudek SM, Chiang ET, Camp SM, Guo Y, Zhao J, Brown ME, Singleton PA, Wang L, Desai A, Arce FT, et al. (2010). Abl tyrosine kinase phosphorylates nonmuscle Myosin light chain kinase to regulate endothelial barrier function. *Molecular Biology of the Cell*, 21 (22), 4042–4056.
- Elia N, Fabrikant G, Kozlov MM, and Lippincott-Schwartz J. (2012). Computational model of cytokinetic abscission driven by ESCRT-III polymerization and remodeling. *Biophysical Journal*, 102 (10), 2309–2320.
- Feng Z, Hensley L, McKnight KL, Hu F, Madden V, Ping L, Jeong S, Walker C, Lanford R, and Lemon SM. (2013). A pathogenic picornavirus acquires an envelope by hijacking cellular membranes. *Nature*, 496 (7445), 367–371.
- Francis N, Kingston R, and Woodcock C. (2004). Chromatin Compaction by a Polycomb Group Protein Complex. *Science*, 306 (5701), 1574–1577.
- Fyfe I, Schuh AL, Edwardson JM, and Audhya A. (2011). Association of the endosomal sorting complex ESCRT-II with the Vps20 subunit of ESCRT-III generates a curvature-sensitive complex capable of nucleating ESCRT-III filaments. *Journal of Biological Chemistry*, 286 (39), 34262–34270.
- Ghazi-Tabatabai S, Saksena S, Short JM, Pobbati A V., Veprintsev DB, Crowther RA, Emr SD,

- Egelman EH, and Williams RL. (2008). Structure and Disassembly of Filaments Formed by the ESCRT-III Subunit Vps24. *Structure*, 16 (9), 1345–1356.
- Gisselsson D, Pettersson L, Höglund M, Heidenblad M, Gorunova L, Wiegant J, Mertens F, Dal Cin P, Mitelman F, and Mandahl N. (2000). Chromosomal breakage-fusion-bridge events cause genetic intratumor heterogeneity. *Proceedings of the National Academy of Sciences*, 97 (10), 5357–62.
- Glotzer M. (2004). Cleavage furrow positioning. *Journal of Cell Biology*, 164 (3), 347–351.
- Hanson PI, Roth R, Lin Y, and Heuser JE. (2008). Plasma membrane deformation by circular arrays of ESCRT-III protein filaments. *Journal of Cell Biology*, 180 (2), 389–402.
- Härtel T, and Schwille P. (2014). ESCRT-III mediated cell division in *Sulfolobus acidocaldarius* - A reconstitution perspective. *Frontiers in Microbiology*, 4 (5), 257.
- Hartmann C, Chami M, Zachariae U, de Groot BL, Engel A, and Grütter MG. (2008). Vacuolar Protein Sorting: Two Different Functional States of the AAA-ATPase Vps4p. *Journal of Molecular Biology*, 377 (2), 352–363.
- Hill CP, and Babst M. (2012). Structure and function of the membrane deformation AAA ATPase Vps4. *Biochimica et Biophysica Acta - Molecular Cell Research*, 1823 (1), 172–181.
- Horii M, Shibata H, Kobayashi R, Katoh K, Yorikawa C, Yasuda J, and Maki M. (2006). CHMP7, a novel ESCRT-III-related protein, associates with CHMP4b and functions in the endosomal sorting pathway. *The Biochemical Journal*, 400 (1), 23–32.
- Howard TL, Stauffer DR, Degnin CR, and Hollenberg SM. (2001). CHMP1 functions as a member of a newly defined family of vesicle trafficking proteins. *Journal of Cell Science*, 114 (13), 2395–2404.
- Im YJ, and Hurley JH. (2009). Integrated structural model and membrane targeting mechanism of the human ESCRT-II complex. *Developmental Cell*, 14 (6), 902–913.
- Jimenez AJ, Maiuri P, Lafaurie-Janvère J, Divoux S, Piel M, and Perez F. (2014). ESCRT Machinery Is Required for Plasma Membrane Repair. *Science*, 343 (6174), 1247136.
- Katoh K, Shibata H, Hatta K, and Maki M. (2004). CHMP4b is a major binding partner of the ALG-2-interacting protein Alix among the three CHMP4 isoforms. *Archives of Biochemistry and Biophysics*, 421 (1), 159–165.
- Kelley LA, and Sternberg MJE. (2009). Protein structure prediction on the Web: a case study using the Phyre server. *Nature Protocols*, 4 (3), 363–371.
- Kirkin V, McEwan DG, Novak I, and Dikic I. (2009). A Role for Ubiquitin in Selective Autophagy. *Molecular Cell*, 34 (3), 259–269.
- Lafaurie-Janvère J, Maiuri P, Wang I, Pinot M, Manneville J-B, Betz T, Balland M, and Piel M. (2013). ESCRT-III Assembly and Cytokinetic Abscission Are Induced by Tension Release in the Intercellular Bridge. *Science*, 339 (6127), 1625–1629.

- Landsberg MJ, Vajjhala PR, Rothnagel R, Munn AL, and Hankamer B. (2009). Three-Dimensional Structure of AAA ATPase Vps4: Advancing Structural Insights into the Mechanisms of Endosomal Sorting and Enveloped Virus Budding. *Structure*, 17 (3), 427–437.
- Langelier C, von Schwedler UK, Fisher RD, De Domenico I, White PL, Hill CP, Kaplan J, Ward D, and Sundquist WI. (2006). Human ESCRT-II complex and its role in human immunodeficiency virus type 1 release. *Journal of Virology*, 80 (19), 9465–9480.
- Lata S, Roessle M, Solomons J, Jamin M, Gottlinger HG, Svergun DI, and Weissenhorn W. (2008). Structural Basis for Autoinhibition of ESCRT-III CHMP3. *Journal of Molecular Biology*, 378 (4), 816–825.
- Lee HH, Elia N, Ghirlando R, Lippincott-schwartz J, and Hurley H. (2009a). NIH Public Access. *Science*, 322 (5901), 576–580.
- Lee JA, Liu L, and Gao FB. (2009b). Autophagy defects contribute to neurodegeneration induced by dysfunctional ESCRT-III. *Autophagy*, 5 (7), 1070–1072.
- Li J, Belogortseva N, Porter D, and Park M. (2008). Chmp1A functions as a novel tumor suppressor gene in human embryonic kidney and ductal pancreatic tumor cells. *Cell Cycle*, 7 (18), 2886–2893.
- Lindås A-C, Karlsson EA, Lindgren MT, Ettema TJG, and Bernander R. (2008). A unique cell division machinery in the Archaea. *Proceedings of the National Academy of Sciences*, 105 (48), 18942–6.
- Lini Y, Kimpler LA, Naismith T V., Lauer JM, and Hanson PI. (2005). Interaction of the mammalian Endosomal Sorting Complex Required for Transport (ESCRT) III protein hSnf7-1 with itself, membranes, and the AAA + ATPase SKD1. *Journal of Biological Chemistry*, 280 (13), 12799–12809.
- Lottridge JM, Flannery AR, Vincelli JL, and Stevens TH. (2006). Vta1p and Vps46p regulate the membrane association and ATPase activity of Vps4p at the yeast multivesicular body. *Proceedings of the National Academy of Sciences*, 103 (16), 6202–7.
- Manohar S, Harlow M, Nguyen H, Li J, Hankins GR, and Park M. (2011). Chromatin modifying protein 1A (Chmp1A) of the endosomal sorting complex required for transport (ESCRT)-III family activates ataxia telangiectasia mutated (ATM) for PanC-1 cell growth inhibition. *Cell Cycle*, 10 (15), 2529–2539.
- McCullough J, Fisher RD, Whitby FG, Sundquist WI, and Hill CP. (2008). ALIX-CHMP4 interactions in the human ESCRT pathway. *Proceedings of the National Academy of Sciences*, 105 (22), 7687–7691.
- Mizushima N, Levine B, Cuervo AM, and Klionsky DJ. (2008). Autophagy fights disease through cellular self-digestion. *Nature*, 451 (7182), 1069–75.
- Mochida GH, Ganesh VS, de Michelena MI, Dias H, Atabay KD, Kathrein KL, Huang H-T, Hill RS, Felie JM, Rakiec D, et al. (2012). CHMP1A encodes an essential regulator of BMI1-INK4A in cerebellar development. *Nature Genetics*, 44 (11), 1260–4.

- Monroe N, Han H, Gonciarz MD, Eckert DM, Karren MA, Whitby FG, Sundquist WI, and Hill CP. (2014). The oligomeric state of the active Vps4 AAA ATPase. *Journal of Molecular Biology*, 426 (3), 510–525.
- Mora-Bermúdez F, Gerlich D, and Ellenberg J. (2007). Maximal chromosome compaction occurs by axial shortening in anaphase and depends on Aurora kinase. *Nature Cell Biology*, 9 (7), 822–831.
- Morita E, Colf LA, Karren MA, Sandrin V, Rodesch CK, and Sundquist WI. (2010). Human ESCRT-III and VPS4 proteins are required for centrosome and spindle maintenance. *Proceedings of the National Academy of Sciences*, 107 (29), 12889–94.
- Morita E, Sandrin V, Chung H-Y, Morham SG, Gygi SP, Rodesch CK, and Sundquist WI. (2007). Human ESCRT and ALIX proteins interact with proteins of the midbody and function in cytokinesis. *The EMBO Journal*, 26 (19), 4215–27.
- Musacchio A, and Hardwick KG. (2002). The spindle checkpoint: structural insights into dynamic signalling. *Nature Reviews Molecular Cell Biology*, 3 (10), 731–741.
- Muzioł T, Pineda-Molina E, Ravelli RB, Zamborlini A, Usami Y, Göttlinger H, and Weissenhorn W. (2006). Structural Basis for Budding by the ESCRT-III Factor CHMP3. *Developmental Cell*, 10 (6), 821–830.
- Nakatogawa H, Suzuki K, Kamada Y, and Ohsumi Y. (2009). Dynamics and diversity in autophagy mechanisms: lessons from yeast. *Nature Reviews Molecular Cell Biology*, 10 (7), 458–467.
- Nanba K, and Toyooka S. (2008). The allelic distribution of a single nucleotide polymorphism in the PDCD5 gene locus of Japanese non-small cell lung cancer patients. *Molecular Medicine Reports*, 1 (5), 667–671.
- Nickerson DP, West M, and Odorizzi G. (2006). Did2 coordinates Vps4-mediated dissociation of ESCRT-III from endosomes. *Journal of Cell Biology*, 175 (5), 715–720.
- Norden C, Mendoza M, Dobbelaere J, Kotwaliwale C V., Biggins S, and Barral Y. (2006). The NoCut Pathway Links Completion of Cytokinesis to Spindle Midzone Function to Prevent Chromosome Breakage. *Cell*, 125 (1), 85–98.
- Oshima R, Hasegawa T, Tamai K, Sugeno N, Yoshida S, Kobayashi J, Kikuchi A, Baba T, Futatsugi A, Sato I, et al. (2016). ESCRT-0 dysfunction compromises autophagic degradation of protein aggregates and facilitates ER stress-mediated neurodegeneration via apoptotic and necroptotic pathways. *Scientific Reports*, 6 (April), 24997.
- Parkinson N, Ince PG, Smith MO, Highley R, Skibinski G, Andersen PM, Morrison KE, Pall HS, Hardiman O, Collinge J, et al. (2006). ALS phenotypes with mutations in CHMP2B (charged multivesicular body protein 2B). *Neurology*, 67 (6), 1074–1077.
- Peck JW, Bowden ET, and Burbelo PD. (2004). Structure and function of human Vps20 and Snf7 proteins. *The Biochemical Journal*, 377 (3), 693–700.

- Pharoah PDP, Tsai Y-Y, Ramus SJ, Phelan CM, Goode EL, Lawrenson K, Buckley M, Fridley BL, Tyrer JP, Shen H, et al. (2013). GWAS meta-analysis and replication identifies three new susceptibility loci for ovarian cancer. *Nature Genetics*, 45 (4), 362–70, 370–2.
- Pornillos O, Higginson DS, Stray KM, Fisher RD, Garrus JE, Payne M, He GP, Wang HE, Morham SG, and Sundquist WI. (2003). HIV Gag mimics the Tsg101-recruiting activity of the human Hrs protein. *Journal of Cell Biology*, 162 (3), 425–434.
- Raymond CK, I H-S, Vater CA, and Stevens TH. (1992). Morphological classification of the yeast vacuolar protein sorting mutants: evidence for a prevacuolar compartment in class E VPS mutants. *Molecular Biology of the Cell*, 3 (12), 1389–1402.
- Roll-Mecak A, and Vale RD. (2008). Structural basis of microtubule severing by the hereditary spastic paraplegia protein spastin. *Nature*, 451 (7176), 363–367.
- Rusten TE, and Stenmark H. (2009). How do ESCRT proteins control autophagy? *Journal of Cell Science*, 122 (13), 2179–2183.
- Saksena S, Wahlman J, Teis D, Johnson AE, and Emr SD. (2009). Functional Reconstitution of ESCRT-III Assembly and Disassembly. *Cell*, 136 (1), 97–109.
- Samson RY, and Bell SD. (2009). Ancient ESCRTs and the evolution of binary fission. *Trends in Microbiology*, 17 (11), 507–513.
- Samson RY, Obita T, Freund SM, and Williams RL. (2014). A Role for the ESCRT System in Cell Division in Archaea. *Science*, 322 (5908), 1710–1713.
- Scheffer LL, Sreetama SC, Sharma N, Medikayala S, Brown KJ, Defour A, and Jaiswal JK. (2014). Mechanism of Ca²⁺-triggered ESCRT assembly and regulation of cell membrane repair. *Nature Communications*, 5, 5646.
- Scott A, Chung H-Y, Gonciarz-Swiatek M, Hill GC, Whitby FG, Gaspar J, Holton JM, Viswanathan R, Ghaffarian S, Hill CP, et al. (2005). Structural and mechanistic studies of VPS4 proteins. *The EMBO Journal*, 24 (20), 3658–69.
- Shi T, Dong Y, Li J, Gao P, Fu D, and Ma D. (2010). High-throughput screening identifies CHMP4A associated with hypoxia-inducible factor 1. *Life Sciences*, 87 (19–22), 604–608.
- Shiels A, Bennett TM, Knopf HLS, Yamada K, Yoshiura K, Niikawa N, Shim S, and Hanson PI. (2007). CHMP4B, a novel gene for autosomal dominant cataracts linked to chromosome 20q. *American Journal of Human Genetics*, 81 (3), 596–606.
- Shim S, Kimpler LA, and Hanson PI. (2007). Structure/function analysis of four core ESCRT-III proteins reveals common regulatory role for extreme C-terminal domain. *Traffic*, 8 (8), 1068–1079.
- Skibinski G, Parkinson NJ, Brown JM, Chakrabarti L, Lloyd SL, Hummerich H, Nielsen JE, Hodges JR, Spillantini MG, Thusgaard T, et al. (2005). Mutations in the endosomal ESCRTIII-complex subunit CHMP2B in frontotemporal dementia. *Nature Genetics*, 37 (8), 806–808.

- Slater R, and Bishop NE. (2006). Genetic structure and evolution of the Vps25 family, a yeast ESCRT-II component. *BMC Evolutionary Biology*, 6 (59), 59.
- Spitzer C, Schellmann S, Sabovljevic A, Shahriari M, Keshavaiah C, Bechtold N, Herzog M, Müller S, Hanisch F-G, and Hülskamp M. (2006). The Arabidopsis elc mutant reveals functions of an ESCRT component in cytokinesis. *Development*, 133 (23), 4679–4689.
- Stauffer DR, Howard TL, Nyun T, and Hollenberg SM. (2001). CHMP1 is a novel nuclear matrix protein affecting chromatin structure and cell-cycle progression. *Journal of Cell Science*, 114 (13), 2383–2393.
- Steigemann P, Wurzenberger C, Schmitz MHA, Held M, Guizetti J, Maar S, and Gerlich DW. (2009). Aurora B-Mediated Abscission Checkpoint Protects against Tetraploidization. *Cell*, 136 (3), 473–484.
- Tada K, Susumu H, Sakuno T, and Watanabe Y. (2011). Condensin association with histone H2A shapes mitotic chromosomes. *Nature*, 474 (7352), 477–483.
- Teichmann M, Dumay-Odelot H, and Fribourg S. (2012). Structural and functional aspects of winged-helix domains at the core of transcription initiation complexes. *Transcription*, 3 (1), 2–7.
- Teis D, Saksena S, and Emr SD. (2008). Ordered Assembly of the ESCRT-III Complex on Endosomes Is Required to Sequester Cargo during MVB Formation. *Developmental Cell*, 15 (4), 578–589.
- Uhlen M, Fagerberg L, Hallstrom BM, Lindskog C, Oksvold P, Mardinoglu A, Sivertsson A, Kampf C, Sjostedt E, Asplund A, et al. (2015). Tissue-based map of the human proteome. *Science*, 347 (6220), 1260419–1260419.
- Vajjhala PR, Nguyen CH, Landsberg MJ, Kistler C, Gan AL, King GF, Hankamer B, and Munn AL. (2008). The Vps4 C-terminal helix is a critical determinant for assembly and ATPase activity and has elements conserved in other members of the meiotic clade of AAA ATPases. *FEBS Journal*, 275 (7), 1427–1449.
- Wernimont AK, and Weissenhorn W. (2004). Crystal structure of subunit VPS25 of the endosomal trafficking complex ESCRT-II. *BMC Structural Biology*, 4 (1), 10.
- White SR, and Lauring B. (2007). AAA+ ATPases: Achieving diversity of function with conserved machinery. *Traffic*, 8 (12), 1657–1667.
- Wollert T, Wunder C, Lippincott-schwartz J, Hurley JHJH, and H J. (2009a). Membrane scission by the ESCRT-III complex. *Nature*, 458 (7235), 172–7.
- Wollert T, Yang D, Ren X, Lee HH, Im YJ, and Hurley JH. (2009b). The ESCRT machinery at a glance. *Journal of Cell Science*, 122 (13), 2163–2166.
- Xie W, Li L, and Cohen SN. (1998). Cell cycle-dependent subcellular localization of the TSG101 protein and mitotic and nuclear abnormalities associated with TSG101 deficiency. *Proceedings of the National Academy of Sciences*, 95 (4), 1595–600.

- Yang D, Rismanchi N, Renvoisé B, Lippincott-Schwartz J, Blackstone C, and Hurley JH. (2008). Structural basis for midbody targeting of spastin by the ESCRT-III protein CHMP1B. *Nature Structural & Molecular Biology*, 15 (12), 1278–86.
- Yang M, Coppens I, Wormsley S, Baevova P, Hoppe HC, and Joiner KA. (2004). The *Plasmodium falciparum* Vps4 homolog mediates multivesicular body formation. *Journal of Cell Science*, 117 (17), 3831–8.
- Yorikawa C, Shibata H, Waguri S, Hatta K, Horii M, Katoh K, Kobayashi T, Uchiyama Y, and Maki M. (2005). Human CHMP6, a myristoylated ESCRT-III protein, interacts directly with an ESCRT-II component EAP20 and regulates endosomal cargo sorting. *The Biochemical Journal*, 387 (1), 17–26.
- Yoshitake Y, Howard TL, Christian JL, and Hollenberg SM. (1999). Misexpression of Polycomb-group proteins in *Xenopus* alters anterior neural development and represses neural target genes. *Developmental Biology*, 215 (2), 375–87.
- You Z, Xin Y, Liu Y, Sun J, Zhou G, Gao H, Xu P, Chen Y, Chen G, Zhang L, et al. (2012). Chmp1A acts as a tumor suppressor gene that inhibits proliferation of renal cell carcinoma. *Cancer Letters*, 319 (2), 190–196.
- Yu X, Harris SL, and Levine AJ. (2006). The regulation of exosome secretion: A novel function of the p53 protein. *Cancer Research*, 66 (9), 4795–4801.
- Yu X, Riley T, and Levine AJ. (2009). The regulation of the endosomal compartment by p53 the tumor suppressor gene. *FEBS Journal*, 276 (8), 2201–2212.
- Yu Z, Gonciarz MD, Sundquist WI, Hill CP, and Jensen GJ. (2008). Cryo-EM Structure of Dodecameric Vps4p and Its 2:1 Complex with Vta1p. *Journal of Molecular Biology*, 377 (2), 364–377.
- Zamborlini A, Usami Y, Radoshitzky SR, Popova E, Palu G, and Göttlinger H. (2006). Release of autoinhibition converts ESCRT-III components into potent inhibitors of HIV-1 budding. *Proceedings of the National Academy of Sciences*, 103 (50), 19140–5.
- Zhang X, Shaw A, Bates PA, Newman RH, Gowen B, Orlova E, Gorman MA, Kondo H, Dokurno P, Lally J, et al. (2000). Structure of the AAA ATPase p97. *Molecular Cell*, 6 (6), 1473–1484.

Chapter 3

- Bellodi C, Kindle K, Bernassola F, Dinsdale D, Cossarizza A, Melino G, Heery D, and Salomoni P. (2006). Cytoplasmic function of mutant promyelocytic leukemia (PML) and PML-retinoic acid receptor- α . *Journal of Biological Chemistry*, 281 (20), 14465–14473.
- Broers JL, Ramaekers FC, Bonne G, Yaou RB, and Hutchison CJ. (2006). Nuclear lamins: laminopathies and their role in premature ageing. *Physiological Reviews*, 86 (3), 967–1008.
- Broers JL V, Peeters EAG, Kuijpers HJH, Endert J, Bouten CVC, Oomens CWJ, Baaijens FPT, and Ramaekers FCS. (2004). Decreased mechanical stiffness in LMNA-/- cells is caused by defective nucleo-cytoskeletal integrity: Implications for the development of laminopathies. *Human Molecular Genetics*, 13 (21), 2567–2580.
- Chang W, Worman HJ, and Gundersen GG. (2015). Accessorizing and anchoring the LINC complex for multifunctionality. *Journal of Cell Biology*, 208 (1), 11–22.
- Chen Y-CM, Kappel C, Beaudouin J, Eils R, and Spector DL. (2008). Live cell dynamics of promyelocytic leukemia nuclear bodies upon entry into and exit from mitosis. *Molecular Biology of the Cell*, 19 (7), 3147–62.
- Conduit PT, Wainman A, and Raff JW. (2015). Centrosome function and assembly in animal cells. *Nature Reviews Molecular Cell Biology*, 16 (10), 611–624.
- Dasika GK, Lin SC, Zhao S, Sung P, Tomkinson A, and Lee EY. (1999). DNA damage-induced cell cycle checkpoints and DNA strand break repair in development and tumorigenesis. *Oncogene*, 18 (55), 7883–99.
- Dawlaty MM, Malureanu L, Jeganathan KB, Kao E, Sustmann C, Tahk S, Shuai K, Grosschedl R, and van Deursen JM. (2008). Resolution of sister centromeres requires RanBP2-mediated SUMOylation of topoisomerase II α . *Cell*, 133 (1), 103–115.
- Ganem NJ, and Pellman D. (2012). Linking abnormal mitosis to the acquisition of DNA damage. *Journal of Cell Biology*, 199 (6), 871–881.
- Graser S, Stierhof Y-D, and Nigg EA. (2007). Cep68 and Cep215 (Cdk5rap2) are required for centrosome cohesion. *Journal of Cell Science*, 120 (24), 4321–4331.
- Hampoelz B, Mackmull MT, Machado P, Ronchi P, Bui KH, Schieber N, Santarella-Mellwig R, Necakov A, Andres-Pons A, Philippe JM, et al. (2016). Pre-assembled Nuclear Pores Insert into the Nuclear Envelope during Early Development. *Cell*, 166 (3), 664–678.
- Hatch E, and Hetzer M. (2014). Breaching the nuclear envelope in development and disease. *Journal of Cell Biology*, 205 (2), 133–141.
- Hatch EM, Fischer AH, Deerinck TJ, and Hetzer MW. (2013). Catastrophic Nuclear Envelope Collapse in Cancer Cell Micronuclei. *Cell*, 154 (1)
- Horii M, Shibata H, Kobayashi R, Katoh K, Yorikawa C, Yasuda J, and Maki M. (2006). CHMP7,

- a novel ESCRT-III-related protein, associates with CHMP4b and functions in the endosomal sorting pathway. *The Biochemical Journal*, 400 (1), 23–32.
- Houben F, De Vos WH, Krapels IPC, Coorens M, Kierkels GJJ, Kamps MAF, Verstraeten VLRM, Marcelis CLM, Van Den Wijngaard A, Ramaekers FCS, et al. (2013). Cytoplasmic localization of PML particles in laminopathies. *Histochemistry and Cell Biology*, 139 (1), 119–134.
- Ibarra A, and Hetzer MW. (2015). Nuclear pore proteins and the control of genome functions. *Genes and Development*, 29 (4), 337–349.
- Jia LQ, Osada M, Ishioka C, Gamo M, Ikawa S, Suzuki T, Shimodaira H, Niitani T, Kudo T, Akiyama M, et al. (1997). Screening the p53 status of human cell lines using a yeast functional assay. *Molecular Carcinogenesis*, 19 (4), 243–53.
- Jul-Larsen Å, Grudic A, Bjerkvig R, and Ove Bøe S. (2009). Cell-cycle regulation and dynamics of cytoplasmic compartments containing the promyelocytic leukemia protein and nucleoporins. *Journal of Cell Science*, 122 (8), 1201–1210.
- Lammerding J, Fong LG, Ji JY, Reue K, Stewart CL, Young SG, and Lee RT. (2006). Lamins A and C but not lamin B1 regulate nuclear mechanics. *Journal of Biological Chemistry*, 281 (35), 25768–25780.
- Lara-Gonzalez P, Westhorpe FG, and Taylor SS. (2012). The spindle assembly checkpoint. *Current Biology*, 22 (22), R966–R980.
- Lim S, Quinton RJ, and Ganem NJ. (2016). Nuclear envelope rupture drives genome instability in cancer. *Molecular Biology of the Cell*, 27 (21), 3210–3213.
- Lobrich M, and Jeggo PA. (2007). The impact of a negligent G2/M checkpoint on genomic instability and cancer induction. *Nature Reviews Cancer*, 7 (11), 861–869.
- Maciejowski J, Li Y, Bosco N, Campbell PJ, and De Lange T. (2015). Chromothripsis and Kataegis Induced by Telomere Crisis. *Cell*, 163 (7), 1641–1654.
- Meraldi P, and Nigg EA. (2001). Centrosome cohesion is regulated by a balance of kinase and phosphatase activities. *Journal of Cell Science*, 114 (20), 3749–3757.
- Mikule K, Delaval B, Kaldis P, Jurczyk A, Hergert P, and Doxsey S. (2007). Loss of centrosome integrity induces p38-p53-p21-dependent G1-S arrest. *Nature Cell Biology*, 9 (2), 160–70.
- Morita E, Colf LA, Karren MA, Sandrin V, Rodesch CK, and Sundquist WI. (2010). Human ESCRT-III and VPS4 proteins are required for centrosome and spindle maintenance. *Proceedings of the National Academy of Sciences*, 107 (29), 12889–94.
- Norden C, Mendoza M, Dobbelaere J, Kotwaliwale C V, Biggins S, and Barral Y. (2006). The NoCut Pathway Links Completion of Cytokinesis to Spindle Midzone Function to Prevent Chromosome Breakage. *Cell*, 125 (1), 85–98.
- Panic M, Hata S, Neuner A, and Schiebel E. (2015). The Centrosomal Linker and Microtubules

- Provide Dual Levels of Spatial Coordination of Centrosomes. *PLoS Genetics*, 11 (5)
- Pichler A, Gast A, Seeler JS, Dejean A, and Melchior F. (2002). The nucleoporin RanBP2 has SUMO1 E3 ligase activity. *Cell*, 108 (1), 109–120.
- Polo SE, and Jackson SP. (2011). Dynamics of DNA damage response proteins at DNA breaks: A focus on protein modifications. *Genes and Development*, 25 (5), 409–433.
- Satyanarayana A, Hilton MB, and Kaldis P. (2008). p21 Inhibits Cdk1 in the absence of Cdk2 to maintain the G1/S phase DNA damage checkpoint. *Molecular Biology of the Cell*, 19 (1), 65–77.
- Schreiber KH, and Kennedy BK. (2013). When lamins go bad: Nuclear structure and disease. *Cell*, 152 (6), 1365–1375.
- Tamiello C, Kamps MAF, van den Wijngaard A, Verstraeten VLRM, Baaijens FPT, Broers JL V, and Bouten CVC. (2013). Soft substrates normalize nuclear morphology and prevent nuclear rupture in fibroblasts from a laminopathy patient with compound heterozygous LMNA mutations. *Nucleus*, 4 (1), 61–73.
- Theodoropoulos PA, Polioudaki H, Kostaki O, Derdas SP, Georgoulas V, Dargemont C, and Georgatos SD. (1999). Taxol affects nuclear lamina and pore complex organization and inhibits import of karyophilic proteins into the cell nucleus. *Cancer Research*, 59 (18), 4625–4633.
- Thoresen SB, Campsteijn C, Vietri M, Schink KO, Liestøl K, Andersen JS, Raiborg C, and Stenmark H. (2014). ANCHR mediates Aurora-B-dependent abscission checkpoint control through retention of VPS4. *Nature Cell Biology*, 16 (6), 550–60.
- Vargas JD, Hatch EM, Anderson DJ, and Hetzer MW. (2012). Transient nuclear envelope rupturing during interphase in human cancer cells. *Nucleus*, 3 (1), 88–100.
- De Vos WH, Houben F, Kamps M, Malhas A, Verheyen F, Cox J, Manders EMM, Verstraeten VLRM, Van steensel MAM, Marcelis CLM, et al. (2011). Repetitive disruptions of the nuclear envelope invoke temporary loss of cellular compartmentalization in laminopathies. *Human Molecular Genetics*, 20 (21), 4175–4186.
- Webster BM, Thaller DJ, Jäger J, Ochmann SE, Borah S, Lusk CP, Adell M, Vogel G, Pakdel M, Müller M, et al. (2016). Chm7 and Heh1 collaborate to link nuclear pore complex quality control with nuclear envelope sealing. *The EMBO Journal*, 205 (7170), 695–701.

Chapter 4

- Anderson DJ, and Hetzer MW. (2007). Nuclear envelope formation by chromatin-mediated reorganization of the endoplasmic reticulum. *Nature Cell Biology*, 9 (10), 1160–1166.
- Anderson DJ, Vargas JD, Hsiao JP, and Hetzer MW. (2009). Recruitment of functionally distinct membrane proteins to chromatin mediates nuclear envelope formation in vivo. *Journal of Cell Biology*, 186 (2), 183–191.
- Bernardi R, and Pandolfi PP. (2007). Structure, dynamics and functions of promyelocytic leukaemia nuclear bodies. *Nature Reviews Molecular Cell Biology*, 8 (December), 1007–1016.
- Boisvert F, Hendzel MJ, and Bazett-Jones DP. (2000). Promyelocytic Leukemia (PML) Nuclear Bodies Are Protein Structures that Do Not Accumulate RNA. *Journal of Cell Biology*, 148 (2), 283–292.
- Brand P, Lenser T, and Hemmerich P. (2010). Assembly dynamics of PML nuclear bodies in living cells. *PMC Biophysics*, 3 (1), 3.
- Burke B, and Ellenberg J. (2002). Remodelling the walls of the nucleus. *Nature Reviews Molecular Cell Biology*, 3 (7), 487–497.
- Butler JT, Hall LL, Smith KP, and Lawrence JB. (2009). Changing nuclear landscape and unique PML structures during early epigenetic transitions of human embryonic stem cells. *Journal of Cellular Biochemistry*, 107 (4), 609–614.
- Cleasby, A (2013) Investigating the role of a novel nuclear ESCRT-III assembly (PhD Thesis, University of Sheffield).
- Dellaire G, and Bazett-Jones DP. (2004). PML nuclear bodies: Dynamic sensors of DNA damage and cellular stress. *BioEssays*, 26 (9), 963–977.
- Federico MB, Vallerga MB, Radl A, Paviolo NS, Bocco JL, Di Giorgio M, Soria G, and Gottifredi V. (2016). Chromosomal Integrity after UV Irradiation Requires FANCD2-Mediated Repair of Double Strand Breaks. *PLoS Genetics*, 12 (1)
- Fichtman B, Ramos C, Rasala B, Harel A, and Forbes DJ. (2010). Inner/Outer nuclear membrane fusion in nuclear pore assembly: biochemical demonstration and molecular analysis. *Molecular Biology of the Cell*, 21 (23), 4197–211.
- Güttinger S, Laurell E, and Kutay U. (2009). Orchestrating nuclear envelope disassembly and reassembly during mitosis. *Nature Reviews Molecular Cell Biology*, 10 (3), 178–191.
- Haraguchi T, Kojidani T, Koujin T, Shimi T, Osakada H, Mori C, Yamamoto A, and Hiraoka Y. (2008). Live cell imaging and electron microscopy reveal dynamic processes of BAF-directed nuclear envelope assembly. *Journal of Cell Science*, 121 (15), 2540–2554.
- Horii M, Shibata H, Kobayashi R, Katoh K, Yorikawa C, Yasuda J, and Maki M. (2006). CHMP7, a novel ESCRT-III-related protein, associates with CHMP4b and functions in the

- endosomal sorting pathway. *The Biochemical Journal*, 400 (1), 23–32.
- Lim S, Quinton RJ, and Ganem NJ. (2016). Nuclear envelope rupture drives genome instability in cancer. *Molecular Biology of the Cell*, 27 (21), 3210–3213.
- Luciani JJ, Depetris D, Usson Y, Metzler-Guillemain C, Mignon-Ravix C, Mitchell MJ, Megarbane A, Sarda P, Sirma H, Moncla A, et al. (2006). PML nuclear bodies are highly organised DNA-protein structures with a function in heterochromatin remodelling at the G2 phase. *Journal of Cell Science*, 119 (12), 2518–31.
- Münch S, Weidtkamp-Peters S, Klement K, Grigaravicius P, Monajembashi S, Salomoni P, Pandolfi PP, Weißhart K, and Hemmerich P. (2014). The tumor suppressor PML specifically accumulates at RPA/Rad51-containing DNA damage repair foci but is nonessential for DNA damage-induced fibroblast senescence. *Molecular and Cellular Biology*, 34 (10), 1733–46.
- Rogakou EP, Pilch DR, Orr AH, Ivanova VS, and Bonner WM. (1998). DNA double-stranded breaks induce histone H2AX phosphorylation on serine 139. *Journal of Biological Chemistry*, 273 (10), 5858–5868.
- Salomoni P, and Pandolfi PP. (2002). The role of PML in tumor suppression. *Cell*, 108 (2), 165–170.
- Schellhaus AK, De Magistris P, and Antonin W. (2016). Nuclear Reformation at the End of Mitosis. *Journal of Molecular Biology*, 428 (10), 1962–1985.
- Shemesh T, Klemm RW, Romano FB, Wang S, Vaughan J, Zhuang X, Tukachinsky H, Kozlov MM, and Rapoport TA. (2014). A model for the generation and interconversion of ER morphologies. *Proceedings of the National Academy of Sciences*, 111 (49), E5243–51.
- Uhlen M, Fagerberg L, Hallstrom BM, Lindskog C, Oksvold P, Mardinoglu A, Sivertsson A, Kampf C, Sjostedt E, Asplund A, et al. (2015). Tissue-based map of the human proteome. *Science*, 347 (6220), 1260419–1260419.
- Vietri M, Schink KO, Campsteijn C, Wegner CS, Schultz SW, Christ L, Thoresen SB, Brech A, Raiborg C, and Stenmark H. (2015). Spastin and ESCRT-III coordinate mitotic spindle disassembly and nuclear envelope sealing. *Nature*, 522 (7555), 231–5.
- Walters AD, Bommakanti A, and Cohen-Fix O. (2012). Shaping the nucleus: factors and forces. *Journal of Cellular Biochemistry*, 113 (9), 2813–21.
- Wang S, Romano FB, Field CM, Mitchison TJ, and Rapoport TA. (2013). Multiple mechanisms determine ER network morphology during the cell cycle in *Xenopus* egg extracts. *Journal of Cell Biology*, 203 (5), 801–814.
- Yang S, Kuo C, Bisi JE, and Kim MK. (2002). PML-dependent apoptosis after DNA damage is regulated by the checkpoint kinase hCds1/Chk2. *Nature Cell Biology*, 4 (11), 865–870.

Chapter 5

- Amaral N, Vendrell A, Funaya C, Idrissi F-Z, Maier M, Kumar A, Neurohr G, Colomina N, Torres-Rosell J, Geli M-I, et al. (2016). The Aurora-B-dependent NoCut checkpoint prevents damage of anaphase bridges after DNA replication stress. *Nature Cell Biology*, 18 (5), 516–526.
- Biebricher A, Hirano S, Enzlin JH, Wiechens N, Streicher WW, Huttner D, Wang LHC, Nigg EA, Owen-Hughes T, Liu Y, et al. (2013). PICH: A DNA Translocase Specially Adapted for Processing Anaphase Bridge DNA. *Molecular Cell*, 51 (5), 691–701.
- Carlton JG, Caballe A, Agromayor M, Kloc M, and Martin-Serrano J. (2012). ESCRT-III governs the Aurora B-mediated abscission checkpoint through CHMP4C. *Science*, 336 (6078), 220–5.
- Chan K-L, North PS, and Hickson ID. (2007). BLM is required for faithful chromosome segregation and its localization defines a class of ultrafine anaphase bridges. *The EMBO Journal*, 26 (14), 3397–409.
- Chan KL, and Hickson ID. (2011). New insights into the formation and resolution of ultra-fine anaphase bridges. *Seminars in Cell and Developmental Biology*, 22 (8), 906–912.
- Chan KL, Palmai-Pallag T, Ying S, and Hickson ID. (2009). Replication stress induces sister-chromatid bridging at fragile site loci in mitosis. *Nature Cell Biology*, 11 (6), 753–760.
- Cimini D, Moree B, Canman JC, and Salmon ED. (2003). Merotelic kinetochore orientation occurs frequently during early mitosis in mammalian tissue cells and error correction is achieved by two different mechanisms. *Journal of Cell Science*, 116 (20), 4213–4225.
- Cleasby, A (2013) Investigating the role of a novel nuclear ESCRT-III assembly (PhD Thesis, University of Sheffield).
- Crasta K, Ganem NJ, Dagher R, Lantermann AB, Ivanova E V, Pan Y, Nezi L, Protopopov A, Chowdhury D, and Pellman D. (2012). DNA breaks and chromosome pulverization from errors in mitosis. *Nature*, 482 (7383), 53–8.
- Fenech M, Kirsch-Volders M, Natarajan AT, Surralles J, Crott JW, Parry J, Norppa H, Eastmond DA, Tucker JD, and Thomas P. (2011). Molecular mechanisms of micronucleus, nucleoplasmic bridge and nuclear bud formation in mammalian and human cells. *Mutagenesis*, 26 (1), 125–132.
- Forment J V., Kaidi A, and Jackson SP. (2012). Chromothripsis and cancer: causes and consequences of chromosome shattering. *Nature Reviews Cancer*, 12 (10), 663–70.
- Hatch EM, Fischer AH, Deerinck TJ, and Hetzer MW. (2013). Catastrophic Nuclear Envelope Collapse in Cancer Cell Micronuclei. *Cell*, 154 (1), 47–60.
- Horii M, Shibata H, Kobayashi R, Katoh K, Yorikawa C, Yasuda J, and Maki M. (2006). CHMP7, a novel ESCRT-III-related protein, associates with CHMP4b and functions in the endosomal sorting pathway. *The Biochemical Journal*, 400 (1), 23–32.

- Huang Y, Fenech M, and Shi Q. (2011). Micronucleus formation detected by live-cell imaging. *Mutagenesis*, 26 (1), 133–138.
- Janssen A, van der Burg M, Szuhai K, Kops GJ, and Medema RH. (2011). Chromosome segregation errors as a cause of DNA damage and structural chromosome aberrations. *Science*, 333 (6051), 1895–1898.
- Karg T, Warecki B, and Sullivan W. (2015). Aurora B-mediated localized delays in nuclear envelope formation facilitate inclusion of late-segregating chromosome fragments. *Molecular Biology of the Cell*, 26 (12), 2227–41.
- Ke Y, Huh J-W, Warrington R, Li B, Wu N, Leng M, Zhang J, Ball HL, and Yu H. (2011). PICH and BLM limit histone association with anaphase centromeric DNA threads and promote their resolution. *The EMBO Journal*, 30 (16), 3309–21.
- Maciejowski J, Li Y, Bosco N, Campbell PJ, and De Lange T. (2015). Chromothripsis and Kataegis Induced by Telomere Crisis. *Cell*, 163 (7), 1641–1654.
- Mendoza M, Norden C, Durrer K, Rauter H, Uhlmann F, and Barral Y. (2009). A mechanism for chromosome segregation sensing by the NoCut checkpoint. *Nature Cell Biology*, 11 (4), 477–483.
- Morita E, Colf LA, Karren MA, Sandrin V, Rodesch CK, and Sundquist WI. (2010). Human ESCRT-III and VPS4 proteins are required for centrosome and spindle maintenance. *Proceedings of the National Academy of Sciences*, 107 (29), 12889–94.
- Murai J, Huang SYN, Das BB, Renaud A, Zhang Y, Doroshov JH, Ji J, Takeda S, and Pommier Y. (2012). Trapping of PARP1 and PARP2 by clinical PARP inhibitors. *Cancer Research*, 72 (21), 5588–5599.
- Norppa H, and Falck GCM. (2003). What do human micronuclei contain? *Mutagenesis*, 18 (3), 221–233.
- Okamoto A, Utani KI, and Shimizu N. (2012). DNA replication occurs in all lamina positive micronuclei, but never in lamina negative micronuclei. *Mutagenesis*, 27 (3), 323–327.
- Rello-Varona S, Lissa D, Shen S, Niso-Santano M, Senovilla L, Marino G, Vitale I, Jemaa M, Harper F, Pierron G, et al. (2012). Autophagic removal of micronuclei. *Cell Cycle*, 11 (1), 170–176.
- Rouzeau S, Cordelières FP, Buhagiar-Labarchède G, Hurbain I, Onclercq-Delic R, Gemble S, Magnaghi-Jaulin L, Jaulin C, and Amor-Guéret M. (2012). Bloom’s syndrome and PICH helicases cooperate with topoisomerase II α in centromere disjunction before anaphase. *PLoS ONE*, 7 (4), e33905.
- Sagona AP, Nezis IP, and Stenmark H. (2014). Association of CHMP4B and autophagy with micronuclei: Implications for cataract formation. *BioMed Research International*, 2014, 974393.
- Shi Q, and King RW. (2005). Chromosome nondisjunction yields tetraploid rather than aneuploid cells in human cell lines. *Nature*, 437 (7061), 1038–42.

- Shimizu N, Shimura T, and Tanaka T. (2000). Selective elimination of acentric double minutes from cancer cells through the extrusion of micronuclei. *Mutation Research-Fundamental and Molecular Mechanisms of Mutagenesis*, 448 (1), 81–90.
- Steigemann P, Wurzenberger C, Schmitz MHA, Held M, Guizetti J, Maar S, and Gerlich DW. (2009). Aurora B-Mediated Abscission Checkpoint Protects against Tetraploidization. *Cell*, 136 (3), 473–484.
- Terradas M, Martín M, Tusell L, and Genescà A. (2010). Genetic activities in micronuclei: Is the DNA entrapped in micronuclei lost for the cell? *Mutation Research - Reviews in Mutation Research*, 705 (1), 60–67.
- Thoresen SB, Campsteijn C, Vietri M, Schink KO, Liestøl K, Andersen JS, Raiborg C, and Stenmark H. (2014). ANCHR mediates Aurora-B-dependent abscission checkpoint control through retention of VPS4. *Nature Cell Biology*, 16 (6), 550–60.
- Utani K, Okamoto A, and Shimizu N. (2011). Generation of micronuclei during interphase by coupling between cytoplasmic membrane blebbing and nuclear budding. *PLoS ONE*, 6 (11), e27233.
- Utani KI, Kohno Y, Okamoto A, and Shimizu N. (2010). Emergence of micronuclei and their effects on the fate of cells under replication stress. *PLoS ONE*, 5 (4)
- Wischermann K, Popp S, Moshir S, Scharfetter-Kochanek K, Wlaschek M, de Grujil F, Hartschuh W, Greinert R, Volkmer B, Faust a, et al. (2008). UVA radiation causes DNA strand breaks, chromosomal aberrations and tumorigenic transformation in HaCaT skin keratinocytes. *Oncogene*, 27 (31), 4269–4280.
- Zhang C-Z, Spektor A, Cornils H, Francis JM, Jackson EK, Liu S, Meyerson M, and Pellman D. (2015). Chromothripsis from DNA damage in micronuclei. *Nature*, 522 (7555), 179–184.

Chapter 6

- Denais CM, Gilbert RM, Isermann P, McGregor AL, te Lindert M, Weigelin B, Davidson PM, Friedl P, Wolf K, and Lammerding J. (2016). Nuclear envelope rupture and repair during cancer cell migration. *Science*, 352 (6283), 353–358.
- Gu M, LaJoie D, Chen OS, von Appen A, Ladinsky MS, Redd MJ, Nikolova L, Bjorkman PJ, Sundquist WI, Ullman KS, et al. (2017). LEM2 recruits CHMP7 for ESCRT-mediated nuclear envelope closure in fission yeast and human cells. *Proceedings of the National Academy of Sciences*, 114 (11), 201613916.
- Hampoelz B, Mackmull MT, Machado P, Ronchi P, Bui KH, Schieber N, Santarella-Mellwig R, Necakov A, Andres-Pons A, Philippe JM, et al. (2016). Pre-assembled Nuclear Pores Insert into the Nuclear Envelope during Early Development. *Cell*, 166 (3), 664–678.
- Olmos Y, Hodgson L, Mantell J, Verkade P, and Carlton JG. (2015). ESCRT-III controls nuclear envelope reformation. *Nature*, 522 (7555), 236–9.
- Olmos Y, Perdrix-Rosell A, and Carlton JG. (2016). Membrane Binding by CHMP7 Coordinates

- ESCRT-III-Dependent Nuclear Envelope Reformation. *Current Biology*, 26 (19), 2635–2641.
- Raab M, Gentili M, de Belly H, Thiam H-R, Vargas P, Jimenez AJ, Lautenschlaeger F, Voituriez R, Lennon-Duménil A-M, Manel N, et al. (2016). ESCRT III repairs nuclear envelope ruptures during cell migration to limit DNA damage and cell death. *Science*, 352 (6283), 359–362.
- Vietri M, Schink KO, Campsteijn C, Wegner CS, Schultz SW, Christ L, Thoresen SB, Brech A, Raiborg C, and Stenmark H. (2015). Spastin and ESCRT-III coordinate mitotic spindle disassembly and nuclear envelope sealing. *Nature*, 522 (7555), 231–5.
- Webster BM, Thaller DJ, Jäger J, Ochmann SE, Borah S, Lusk CP, Adell M, Vogel G, Pakdel M, Müller M, et al. (2016). Chm7 and Heh1 collaborate to link nuclear pore complex quality control with nuclear envelope sealing. *The EMBO Journal*, 205 (7170), 695–701.
- Wolf K, te Lindert M, Krause M, Alexander S, te Riet J, Willis AL, Hoffman RM, Figdor CG, Weiss SJ, and Friedl P. (2013). Physical limits of cell migration: Control by ECM space and nuclear deformation and tuning by proteolysis and traction force. *Journal of Cell Biology*, 201 (7), 1069–1084.